Ag-In-Cd CONTROL ROD BEHAVIOR

AND

AEROSOL FORMATION

IN

SEVERE REACTOR ACCIDENTS

by

DAVID ANDREW PETTI

S.B. Massachusetts Institute of Technology
(1983)
S.M. Massachusetts Institute of Technology
(1983)

SUBMITTED TO THE DEPARTMENT OF
NUCLEAR ENGINEERING
IN PARTIAL FULFILLMENT OF THE
REQUIREMENTS FOR THE DEGREE OF

DOCTOR OF SCIENCE

at the

MASSACHUSETTS INSTITUTE OF TECHNOLOGY

DECEMBER 1985

© Massachusetts Institute of Technology 1985

Signature of Author _____
Department of Nuclear Engineering
December 5, 1985

Certified by _____
Dr. Norman C. Rasmussen, Thesis Supervisor
McAfee Professor of Engineering

Certified by _____
Dr. Richard R. Hobbins, Thesis Supervisor
Source Term Coordinator, EG&G, Idaho

Accepted by _____
Dr. Allan F. Henry
Chairman Departmental Graduate Committee

MASSACHUSETTS INSTITUTE
OF TECHNOLOGY

APR 04 1986

LIBRARIES

ARCHIVES

Ag-In-Cd CONTROL ROD BEHAVIOR AND AEROSOL FORMATION IN SEVERE REACTOR ACCIDENTS

by
DAVID PETTI

Submitted to the Department of
Nuclear Engineering on November 25, 1985
in partial fulfillment for the degree of
Doctor of Science In Nuclear Engineering

Abstract

Ag-In-Cd control rod behavior and aerosol formation in severe reactor accidents are examined in an attempt to improve the methodology used to estimate reactor accident source terms.

Four models are incorporated into a code named VAPOR to describe the downward relocation and simultaneous vaporization behavior of the Ag-In-Cd alloy expected after control rod failure in a severe reactor accident. The rod failure model predicts the rate of drainage of molten alloy from the control rod breach. The velocity and film thickness of the alloy as it travels down the outside of the control rod guide tube are calculated by the liquid film model. The mass transfer model estimates the rate of vaporization of Ag, In and Cd from the moving alloy. The zircaloy dissolution model describes the potential chemical interactions between the zircaloy guide tube and the control rod alloy.

The VAPOR code is used to predict the release of Ag, In and Cd vapors expected in Power Burst Facility (PBF) Severe Fuel Damage (SFD) 1-4 experiment. In addition, a sensitivity study is performed. Although Cd is found to be the most volatile constituent of the alloy, all of the calculations predict that the rapid relocation of the alloy down to cooler portions of the core results in a small release for all three control rod alloy vapors.

Potential aerosol formation mechanisms in a severe reactor accident are reviewed. Specifically, models for homogenous, ion-induced, heteromolecular and heterogeneous nucleation are investigated. These models are applied to Ag, Cd and CsI to examine the nucleation behavior of these three potential aerosol sources in a

severe reactor accident and to illustrate the competition among these mechanisms for vapor depletion.

The results indicate that aerosol formation in a severe reactor accident occurs in three stages. In the first stage, ion-induced nucleation causes aerosol generation. During the second stage, ion-induced and heterogeneous nucleation operate as competing pathways for gas-to-particle conversion until sufficient aerosol surface area is generated . In the third stage, ion-induced nucleation ceases and heterogeneous nucleation becomes the dominant mechanism of gas-to-particle conversion until equilibrium is reached. The aerosol size distribution following nucleation is found to depend only on the total number of particles in the system and the volume concentration of aerosols at equilibrium.

Preliminary results from PBF Test SFD 1-4 are presented. The discussion is focused on the control rod and aerosol behavior observed in the experiment. When appropriate, the results of this work are used to suggest plausible scenarios that might explain events that occurred in this high temperature, integral effects experiment.

Conclusions from this work are presented and their impact on source term estimation is assessed.

Thesis Supervisor: Dr. Norman C. Rasmussen

Title: McAfee Professor of Engineering

Thesis Supervisor: Dr. Richard R. Hobbins

Title: Source Term Coordinator, EG&G Idaho

TABLE OF CONTENTS

ABSTRACT 2

DEDICATION 8

ACKNOWLEDGEMENTS 9

1.0 INTRODUCTION 10

1.1 Background 10

1.2 In-vessel Phenomena in Severe Reactor Accidents 11

1.3 Context, Purpose and Structure 13

1.4 References 17

2.0 A REVIEW OF Ag-In-Cd CONTROL ROD BEHAVIOR IN SEVERE REACTOR ACCIDENTS 18

2.1 Description of a PWR Control Rod 18

2.2 Experimental Work 19

2.3 Analytical Work 31

2.4 Motivation for Current Work 34

2.5 References 43

3.0 THE DEVELOPMENT OF A Ag-In-Cd VAPOR RELEASE MODEL 44

3.1 Rod Failure Model 46

3.2 Liquid Film Model 53

3.3 Mass Transfer Model 64

3.4 Zircaloy Dissolution Model 74

3.5 Conservation Equations and Code Details 76

4.0 RESULTS USING THE VAPOR CODE 88
4.1 Study of Control Rod Failure and Liquid Film Behavior 88
4.2 Sensitivity Study 96
4.3 Experimental Prediction for The PBF SFD 1-4 Test 108
4.4 Uncertainties and Limitations of the VAPOR code 112
4.5 References 123
5.0 A REVIEW AND DISCUSSION OF AEROSOL FORMATION MECHANISMS 124
5.1 Introduction 125
5.2 Homogeneous Nucleation: Theory, Limitations and Applications 129
5.3 Ion-induced Nucleation 155
5.4 Heteromolecular Nucleation 157
5.5 Heterogeneous Nucleation 168
5.6 The Kelvin Effect 173
5.7 Summary and Application to the Current Work 182
5.8 References 185
6.0 AEROSOL NUCLEATION BEHAVIOR OF SILVER, CADMIUM AND CESIUM IODIDE 188
6.1 Introduction 188

6.2 Homogeneous Nucleation Results and Discussion 189
6.3 Ion-induced Nucleation Results and Discussion 190
6.4 Heterogeneous Nucleation Results and Discussion 198
6.5 Aerosol Maps 204
6.6 The Effect of Wall Condensation 211
6.7 Conclusions 231
7.0 EQUILIBRIUM AEROSOL PARTICLE SIZE DISTRIBUTION FOLLOWING NUCLEATION 234
7.1 Introduction 234
7.2 Solutions to the Aerosol Transport Equation 235
7.3 Modeling Assumptions 242
7.4 Aerosol Particle Size Distribution and Examples 252
7.5 Conclusions 265
7.6 References 267
8.0 CONTROL ROD AND AEROSOL BEHAVIOR IN PBF TEST SFD 1-4 268
8.1 Introduction 268
8.2 System Design, Instrumentation and Test Procedure.....270
8.3 General Test Results 278

8.4 Control Rod and Aerosol Behavior 290
8.5 Preliminary Conclusions from
PBF Test SFD 1-4 306
8.6 References 308
9.0 SUMMARY AND CONCLUSIONS 309
9.1 Control Rod Behavior 309
9.2 Aerosol Formation 313
9.3 Recommendations for Future Study 318
APPENDIX A -- CALCULATION OF CONTROL ROD INTERNAL
PRESSURE 321
APPENDIX B -- VAPOR CODE 330
APPENDIX C -- COMPILATION OF MATERIALS PROPERTIES ...381
APPENDIX D -- MOMENTUM EQUATION IN THE
LIQUID FILM MODEL 384
APPENDIX E -- AEROMAP CODE 389
APPENDIX F -- RESULTS FROM AEROSOL MONITOR
CALIBRATION 406

DEDICATION

To my parents, Barbara and Guy, my brother, Michael, and my sister, Sandra, for giving me the courage to adhere to my convictions and achieve my goals.

ACKNOWLEDGEMENTS

This work would not have been possible without the help of many people at both EG&G, Idaho and MIT. Special thanks go to my co-advisors Professor Norman C. Rasmussen and Dr. Richard R. Hobbins. Their valuable advice and guidance and more importantly their support and encouragement were inspirational during this research. Dr. Hobbins has helped me integrate the information from the diverse disciplines necessary to do source term research. Professor Rasmussen has made me examine my assumptions and assess the impact my results have on nuclear reactor safety.

On a more personal note, the ski trip Norm and I took in Idaho was a great experience that I will never forget. As an advisor, Norm is not only a mentor but also a friend. His dedication and committment to teaching and research serve as outstanding examples for other faculty. Norm always shows great concern for his students. Having an advisor like Norm has made graduate school more worthwhile.

The careful and thorough reading of the thesis by Professor Richard K. Lester and Dr. Donald Hagrman is greatly appreciated. In addition, the numerous discussions I had with Dr. Hagrman were extremely valuable; he served as a "behind the scenes" advisor and helped me to understand my work in a broader context. Without his input, this work would have suffered. Thanks also goes to Mr. Daniel Osetek, Mr. Michael Carboneau and Mr. Eric Coryell, Dr. Clark Lemon and Dr. Earl Marwil for the stimulating discussions they provided me during this work.

Special thanks to Professor Neil E. Todreas. His excellent teaching has enstilled in me a real love for the fundamentals of nuclear reactor engineering. For that I am eternally grateful.

My sincere gratitude goes to Linda Suter for the many hours she spent typing the manuscript and to Gerry Reilly, Sarah Thompson, Arlene Ackerman and Louise Nelson for their preparation of the figures.

A final thanks to my numerous friends and colleagues at MIT: Ray Coxe, Mike Izenson, Susan Reilly, Joy Maneke, Victor Ianello, Steve Piet, Margarita Crocker, Bob Witt, Susan Cooper, Maureen Psaila, Ko Kato, Ray Gamino, Andy Wolford, Ken Rempe, Marty Plys, Meta Brown, Chris Wilson and Mike Fellows. Together we were able to support each other during the difficult times at MIT. The friendships formed and the memories of the good times we shared will hopefully last forever.

1. INTRODUCTION

1.1 Background

Following the accident at Three Mile Island, questions began to surface within the nuclear community concerning the current technical basis for estimating the radiological consequences of severe reactor accidents. Several scientists called attention to the fact that existing NRC models and Regulatory Guides would have overpredicted the release of radioiodine observed in the TMI accident [1.1]. In addition, reexamination of past nuclear accidents and destructive tests indicated that in the presence of water, only a small fraction of volatile fission products was released to the environment [1.2,1.3]. These observations led several organizations (USNRC, EPRI, ANS, IDCOR, APS) to reassess radionuclide release from postulated severe reactor accidents, also known as the "source term."

A reevaluation of the source term could produce many potential benefits to the nuclear industry. If a factor of ten reduction in the predicted radiological releases from such accidents was technically warranted, then mass evacuation in emergency planning [1.4] would not be required. Licensing and siting requirements for new plants might also be relaxed. Moreover, a reduction in

the estimated radiological source term might well restore public confidence in nuclear power and the understanding gained might impact the design of the next generation of light water reactors.

1.2 In-vessel Phenomena in Severe Reactor Accidents

Knowledge about several complex physical and chemical processes is required to estimate the radiological source term from a severe reactor accident. The important in-vessel phenomena can be grouped into six major categories:

(1) Core thermal hydraulic behavior. Core heatup and uncovery, zircaloy oxidation, and hydrogen generation are the major phenomena that determine the thermal hydraulic conditions in a severe reactor accident. The local core temperatures, flow rates and composition of the H_2O/H_2 mixture are functions of the specific accident sequence.

(2) Core damage phenomena. The potential damage mechanisms that cause loss of the original core geometry are fuel rod ballooning, liquefaction of UO_2 by zircaloy, and the melting and relocation of control rods, structural material, fuel and cladding. The timing of these processes can have an important impact on the time and mode of reactor pressure vessel failure.

(3) Fission product release. Gap release, diffusion through grains, release from liquefied or molten fuel and release due to fuel quench are considered to be the major release mechanisms in a severe reactor accident. Fuel burnup, chemistry, time at

temperature and system pressure are important parameters that affect fission product release.

(4) Nonfission product vapor release. Vaporization of Ag, In, Cd, Sn and Fe from molten control rod and structural materials is the major source of nonfission product vapors in severe reactor accidents. At higher temperatures, UO_2 and Zr vapors may also be generated.

(5) Aerosol generation, deposition and transport. Condensation of hot vapors released from the core will result in the formation of aerosols. These aerosols are transported from the core through the upper plenum and the reactor cooling system into containment. During transport, natural physical processes such as aerosol agglomeration, settling and deposition will result in some fission product and aerosol retention in the accident.

(6) Fission Product and Aerosol Chemistry. Chemical interactions between fission products, core structural materials (zircaloy, stainless steel, control rods, UO_2), coolant, and aerosols can occur which can alter the fission product and aerosol behavior in the accident.

Although these in-vessel phenomena are common to all severe reactor accidents, radiological source term estimates for risk-dominant accident sequences differ. The predicted differences in the fission product and aerosol behavior can in part be attributed to the degree of coupling among the in-vessel phenomena. Hence, an accurate prediction of the timing, magnitude and chemical form(s) of the fission products and aerosols

released in a severe reactor accident requires both mechanistic "phenomenological" models for each of the above processes and an algorithm that integrates all these models into a logical framework to ensure that proper coupling among the various physical and chemical processes is achieved.

1.3 Context, Purpose and Structure

Major improvements have been made in the methodology used to estimate radionuclide release in severe reactor accidents. Despite this fact, uncertainties about basic physical and chemical phenomena still exist. The USNRC and the APS [1.5, 1.6] have identified several technical issues that remain to be addressed in order to reduce the current uncertainty and ensure that the technical data base is complete. The purpose of this work is to examine two of these technical issues: Ag-In-Cd control rod behavior and aerosol formation in severe reactor accidents.

1.3.1 Ag-In-Cd Control Rod Behavior

The role of Ag-In-Cd control rods in severe reactor accidents is currently not well understood. The low melting point of the alloy, the high volatility of Cd and the large quantities of this material in the core

potentially make it a major aerosol source in a severe reactor accident. Control rod aerosols, if present at the time of substantial fission product release, could enhance the transport of fission products into containment as well as influence fission product chemistry in the upper plenum and primary system.

The major goal of this phase of the work is to determine the behavior of Ag-In-Cd control rods in severe reactor accidents. Specifically, effort is concentrated on characterizing the magnitude and timing of Ag, In and Cd vapor release from the core. The results will be compared to the control rod behavior observed in the Power Burst Facility Severe Fuel Damage Test SFD 1-4. This is the only in-pile experiment conducted to date whose purpose is to study the behavior of Ag-In-Cd control rods under realistic accident conditions. The impact of these results on source term estimation will be assessed.

1.3.2 Aerosol Formation

Aerosol formation is not modeled mechanistically in most fission product and aerosol transport codes. The aerosol generation rate and size distribution are either obtained from a semi-empirical correlation or are left as an input in the transport model. This approach could

lead to uncertainties and inaccuracies not only in the prediction of aerosol generation rates but also in the potential interactions between fission products and aerosols in the reactor coolant system.

The major objective of this phase of the work is to review mechanistic models for aerosol formation and assess their importance in severe reactor accidents. The models will be applied to various potential aerosol sources in severe reactor accidents. In addition, the aerosol behavior observed in the PBF SFD 1-4 experiment will be discussed and the impact of these results on source term estimation will be addressed.

The remainder of the work is organized as follows. Section 2 reviews the behavior of Ag-In-Cd control rods in severe reactor accidents. A model to describe Ag, In and Cd vapor release is developed in Section 3 and results are presented in Section 4. Section 5 reviews potential aerosol formation mechanisms in severe reactor accidents. Section 6 examines the nucleation behavior of Ag, Cd and CsI - three potential aerosol sources in a severe reactor accident. The aerosol size distribution immediately following aerosol generation is determined in Section 7. The control rod and aerosol behavior observed in PBF SFD Test 1-4 is discussed in Section 8. Conclusions and recommendations for future study are the

subject of Section 9. Additional details of various analyses are found in Appendices A through F.

1.4 REFERENCES

1.1 Stratton, W.R., Malinauskas, A.P., Campbell, D.O., Letter to USNRC Chairman Ahearne, USNRC, August 14, 1980.

1.2 Morewitz, H.A., "Fission Product and Aerosol Behavior Following Degraded Core Accidents", Nuclear Technology, 53, (2), May 1981, pp. 120-134.

1.3 Vinjamuri, K., A Review of Fission Product Behavior During Past Accidents and Destructive Tests, EGG-TFBP-6026, September 1982.

1.4 Levenson, M. and Rahn, M., "Realistic Estimates of the Consequences of Nuclear Accidents," Nuclear Technology,53, (2), May 1981, pp. 99-110.

1.5 Reassessment of the Technical Bases for Estimating Source Terms, NUREG-0956, Draft July 1985.

1.6 Report to the American Physical Society of the Study Group on Radionuclide Release from Severe Accidents at Nuclear Power Plants, Draft February 1985.

2. A REVIEW OF Ag-In-Cd CONTROL ROD BEHAVIOR IN SEVERE REACTOR ACCIDENTS

Accurately predicting the magnitude and timing of silver, indium and cadmium vapors released during a severe reactor accident is necessary to assess the radiological consequences of the accident. Substantial vaporization of silver, indium and cadmium could result in the formation of aerosols and enhance the transport of fission products into containment. In addition, their presence could influence fission product chemistry in the upper plenum.

This section will review Ag-In-Cd control rod behavior in severe reactor accidents. The geometry of a PWR control rod is presented in Section 2.1. Sections 2.2 and 2.3 review both the experimental work and the current analytic models that are used to describe the behavior of Ag-In-Cd control rods in severe reactor accidents. The motivation for the current work is presented in Section 2.4.

2.1 Description of a PWR Control Rod

Many existing PWRs operate with Ag-In-Cd control rods. The average PWR contains approximately 2800 kg of

Ag-In-Cd alloy in the core which represents 2.8% of the total core mass. The beginning of life composition of the alloy is approximately 80% Ag, 15% In and 5% Cd by weight.

The geometry of a PWR control rod is very similar to a fuel rod. Ingots or pellets of the alloy are stacked and clad in a stainless steel sheath to form the control rod. The gap between the pellets and the clad is backfilled with helium. The stainless steel rod is inserted into a zircaloy guide tube. Clearance exists between the zircaloy guide tube and the stainless steel sheath to allow for cooling water to enter and remove the heat generated by neutron absorption and β-γ heating during operation. There are approximately 16 guide tubes per assembly. A schematic of the geometry is shown in Figure 2.1. The dimensions are shown for a PBF control rod used in Test SFD 1-4.

2.2 Experimental Work

Experiments have been conducted at ORNL [2.1], KFK [2.2, 2.3, 2.4] and AEE Winfrith [2.5] to understand the behavior of Ag-In-Cd control rods in severe reactor accidents. Based on these experiments, the following general observations were made:

Figure 2.1

Schematic of PBF Control Rod (Not to Scale)

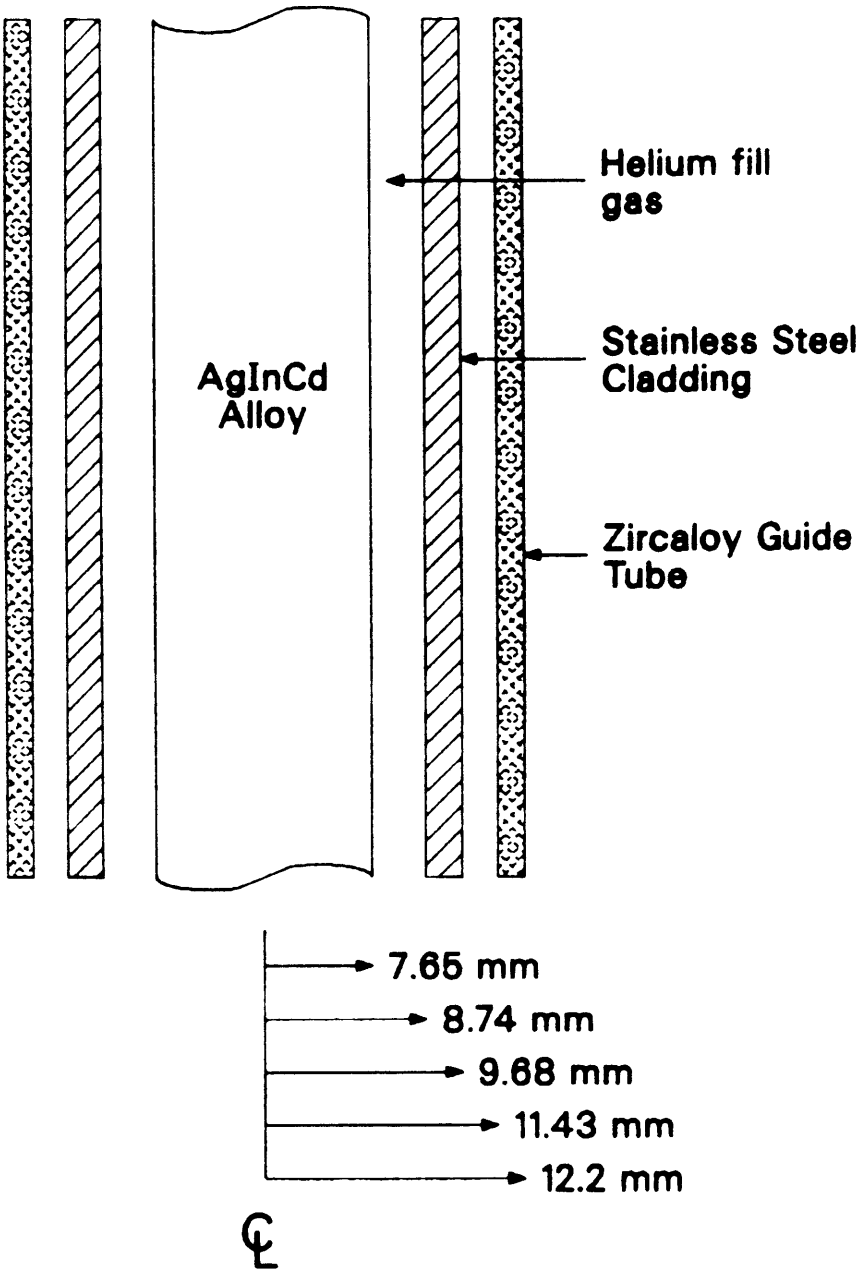

P204-LN85044-1

(1) the Ag-In-Cd alloy melts between 1073 and 1123 K;
(2) at low system pressures and when no zircaloy is present, the control rod fails between 1623 and 1723 K when the stainless steel sheath loses its integrity as it approaches melting;
(3) for low system pressures, failure of control rods with zircaloy guide tubes occurs at 1473 K as a result of thermal expansion, physical contact and chemical interaction between the stainless steel clad and the zircaloy guide tube;
(4) at low ambient pressures, the molten material is forcibly ejected from the control rod because of the high cadmium vapor pressure; and
(5) in the ORNL and KfK tests where zircaloy was present, the molten silver and indium chemically interacted with the zircaloy to form Zr-Ag and Zr-In solutions.

The experiments conducted at ORNL [2.1] were part of the One Kilogram Core Melt Test Program. In these tests, short bundles were heated in a crucible furnace. The vapor/aerosol mixture released from the melt was transported to a collection and measuring system equipped with an aerosol monitor and a series of filters.

In one test, termed CM-14, a bundle of twelve zircaloy clad fuel capsules about 10 cm long and one control rod capsule clad in stainless steel were heated to approximately 2073 K in about 7.5 minutes. Examination of the sample revealed fuel columns standing above a frozen pool of previously molten metals. This final configuration was attributed to chemical

dissolution of the zircaloy by silver and indium. A mass balance after the experiment suggested that 6.5% of the cadmium and 0.35% of the silver were released from the bundle. No other constituents were detected.

In a second test, termed CM-16, a one kilogram sample of core material in a 'mini' fuel bundle geometry was subjected to three equal heating intervals to 2073, 2473 and 2673 K. The masses of silver, indium and cadmium released were measured and the results are shown in Table 2.1. Based on the temporal data, the major release component in the first heating interval up to 2073 K was found to be cadmium whereas silver was the major component at higher temperatures. The investigators concluded that aerosol formation in a severe PWR accident is dominated by the control rod alloy.

Two different sets of experiments have been conducted at Kfk by Hagen [2.2, 2.3]. In the first test, a stainless steel clad control rod was placed in the center of a 3x3 fuel rod bundle. No zircaloy guide tube was used in the test. In this test, the stainless steel sheath containing the molten alloy burst when heated to 1723 K. Parts of the zircaloy fuel cladding were covered with droplets of the molten alloy. The second set of tests, termed the ABS series, used the

TABLE 2.1

RESULTS OF ORNL TEST CM-16

	Mass Released (g)	Release Fraction
Ag	0.07	0.054
In	0.54	0.061
Cd	0.53	0.53

same geometry as the previous test except that the control rod was encapsulated in its own zircaloy guide tube. The purpose of these tests was (1) to determine how the melting of the absorber materials may influence damage mechanisms in a fuel bundle and (2) to determine how the distribution of the control rod alloy influences aerosol generation, fission product release and transport, and the embrittlement of reactor components.

The first three tests in the series, termed ABS-1, ABS-2 and ABS-3, were run at atmospheric pressure to peak temperatures of 2273 K, 1973 K, and 1673 K respectively. The flow rate of steam into the bundle was 2.5×10^{-4} kg/s and the temperature rise rate was approximately 1 K/sec. Based on the results of Test ABS-3, the control rods in all three tests failed at a temperature above 1473 K, most likely due to thermal expansion, contact and chemical interaction between the stainless steel and zircaloy. Eutectics can form between the iron and nickel in the stainless steel and the zircaloy at temperatures as low as 1337 K.

Severe damage occurred in both test ABS-1 and ABS-2. Significant molten material had relocated and solidified at the bottom of the test assembly. In addition, a rubble bed of zircaloy and UO_2 resided at the lower end of the test assembly. It is hypothesized

that the molten alloy had chemically reacted with the zircaloy as it flowed down the rods and refroze at the base. Reasons for the severe damage are a matter of speculation at the moment. Chemical analysis of the debris is planned in the near future. Substantial cadmium vaporization occurred in both tests. Although no formal mass balance has been performed, Hagen believed that roughly all of the cadmium was released.

Since the peak temperature was much lower in Test ABS-3, the damage was much less severe. Control rod failure was identified as a hole in both the stainless steel cladding and the zircaloy guide tube. Other than the holes, both the guide tube and the cladding were intact. Control rod material was found to have flowed down the guide tube and into the bottom corner of the test assembly.

In another experiment, Test ABS-6, Hagen determined the failure temperature of a stainless steel clad control rod in a stainless steel guide tube. The absorber rod failed at approximately 1673 K , which is only 100 K below the melting point of stainless steel. Thus, the failure is most likely a result of internal pressurization of the control rod by cadmium and the helium fill gas in addition to the loss of clad strength as the stainless steel approached its melting point.

In another set of experiments, carried out at the SASCHA facility by Albrecht et. al.[2.4], control rod materials were included with representative amounts of structural materials to form short fuel rods containing UO_2 and simulated fission products. These rods were heated in a crucible to 2673 K. The vapor/aerosol mixture released from the melt was transported to an aerosol cascade impactor and a series of filters to measure the release as a function of time. The results of the experiment, expressed as a percent released, are shown in Table 2.2. Albrecht noted that in those experiments in which silver was present, some of the iodine was in the form of AgI. Thus, it appears that the presence of control rod material might alter the chemical form of the fission products.

Experiments were conducted at AEE Winfrith in England by Mitchell et. al. [2.5] to study the formation of aerosols from the Ag-In-Cd alloy. A sample specimen was heated and the resultant vapor/aerosol mixture was transported to a collection system similar to the other systems mentioned earlier. In two separate experiments, 4 cm segments of unclad alloy (24 g) were heated in an open crucible to 1700 and 1870 K. A mixed deposit of crystals and spherical particles was found on the walls of the collection system. The deposit consisted

TABLE 2.2

SACHA RESULTS

	Percent Released
Ag	75
In	20
Cd	100

primarily of cadmium. The results of the mass balance are shown in Table 2.3.

In a second set of experiments, five samples of the alloy clad in stainless steel were heated to temperatures between 1550 and 1760 K. A significant release of material occurred in all tests. At the time of stainless steel rupture, a high concentration of vapor was released which condensed rapidly to form an aerosol. The results for one test in which a mass balance was performed are shown in Table 2.3. Mitchell et. al. suggested that the extent of aerosol formation and the composition of the aerosol is dependent on the location of clad failure. A break in the side of the clad (which occurred in three of the five experiments) directed the alloy in a vertical direction resulting in material flowing down to the catchpot at the bottom of the crucible. In this case, as shown in Table 2.3, very little silver and indium was airborne and the aerosol was totally cadmium. However, in the remaining two experiments, the stainless steel failed at the top of the sample. This mode of failure resulted in material being ejected toward the sampling system above the crucible. In these two experiments, significant quantities of silver were transported with the cadmium into the collection system. Like the ORNL

TABLE 2.3

AEE WINFRITH RESULTS

		Percent Released		
Unclad	Temperature (K)	Ag	In	Cd
1	1700	10	10	90
2	1800	10	25	99
Clad				
1	1750	0	0	21.6 [a]
		94.76	97.2	75.0 [b]

a. Vapor/aerosol deposit.

b. Debris in catchpot.

investigators, they concluded that the Ag-In-Cd alloy will be a major source of vapor release early in the course of a severe accident. The liquid indium and silver will flow to cooler regions of the core and the cadmium will be the dominant aerosol source.

These out-of-pile experiments have indicated that the Ag-In-Cd alloy would be a dominant aerosol source in a severe reactor accident. The tests have provided valuable information about control rod failure and the potential chemical interactions between the absorber alloy and the zircaloy guide tube. Although the actual results exhibit some scatter, releases in all of the experiments were dominated by Cd, indicating that it is the most volatile constituent of the Ag-In-Cd alloy. The conditions for the experiments were also very similar. All of the experiments were conducted at atmospheric pressure and with the exception of Hagen's ABS tests, were small scale tests in which the alloy was heated in a crucible-like apparatus. However, because these conditions are not representative of those expected in a severe reactor accident, extrapolation of the data is difficult. The impact of these limitations will be discussed in Section 2.4.

2.3 Analytic Work

Work is currently underway to model the release behavior of silver, indium and cadmium in severe reactor accidents. Based on the experiments at ORNL and KfK, Lorenz et. al. [2.6] have developed an interim model for Ag-In-Cd vapor release. They recommend that the following procedure be used

(1) Assume failure of the control rod cladding at T= 1723 K, i.e., when the maximum control volume temperature along the rod reaches this value.
(2) At the time of rod rupture, assume 5% of the Ag, 5% of the In and 50% of the Cd becomes an aerosol in the reactor vessel gas space.
(3) Linearly increase the degree of release as the predicted local core temperature rises, such that as the melting point is reached, 50% of the Ag, 15% of the In and 80% of the Cd in the control volume becomes aerosol.
(4) If the local temperatures are predicted to rise above the melting point (2573 K), the balance of the alloy material should be released as 3073 K is reached.

Wichner [2.7] has performed an analysis to determine the amount of vapor that could exist in the reactor vessel volume (548 m^3) under the condition of chemical equilibrium. He assumed that equilibrium exists between the gas and condensed phase of each specie. The entire core was assumed to be at 2973 K and Raoult's law was assumed to be applicable for the partial pressure of each constituent in the melt. The results are shown in Table 2.4.

TABLE 2.4

RESULTS OF WICHNER'S ANALYSIS

	Mass (Kg)	Release Fraction
Ag	532	0.24
In	242	0.47
Cd	162	1.0

Taig [2.8] has studied vaporization from a liquid surface. The amount of vaporization that can occur is limited by:

(1) transport through the condensed phase;

(2) heterogeneous reaction at the phase boundary; and

(3) transport away from the surface to the gas.

Since the third process was assumed to be the rate limiting process, a mass transfer model was developed to describe the fractional release rate of vapor. Hence,

$$df/dt = (k_m * A * p_v)/(R * T * m_{tot})$$

where

df/dt = fractional release rate (s^{-1}),

k_m = mass transfer coefficient (m/s),

p_v= vapor pressure (Pa),

A = surface area (m^3),

R = gas constant (Pa-m^3/kg-K),

T = temperature (K), and

m_{tot} = total mass of the specie in liquid (kg).

The model was not applied to silver, indium and cadmium release but instead to CsI vaporization from the surface of the fuel and to the vaporization of stainless steel components in the reactor. The results suggested that for certain high pressure/low flow accidents, gas phase

mass transfer will limit the amount of vaporization that can occur.

Powers, at Sandia [2.9], has studied the pressurization of control rods during severe reactor accidents. Correlations were developed from activity data for the liquid binary systems Ag-Cd, Ag-In and In-Cd. Based on these correlations, a model of the vapor pressure behavior of the Ag-In-Cd alloy was developed. His results suggest that treating the alloy as an ideal mixture will only slightly overpredict the vaporization of cadmium from the alloy, yet will yield excessively high vapor pressures of Ag and In. Further results of his work will be discussed in Sections 2.4 and 4.2.

This review of the current analytic work indicates that an adequate model to describe Ag, In and Cd vapor release in severe reactor accidents does not exist. The models are empirical at best and in some cases do not provide any information on the rate of vapor release. Section 2.4 will describe the important phenomena that are needed to predict Ag-In-Cd control rod behavior in severe reactor accidents.

2.4 Motivation for the Current Work

The purpose of this work is to provide an analytic

tool for describing the release of silver, indium and cadmium vapor in a severe reactor accident. The PBF SFD 1-4 experiment will be used to benchmark the tool since it most closely replicates the conditions expected during an accident. The behavior of the control rod material in an integral effects in-pile experiment is quite complex. The out-of-pile experiments were conducted under conditions that are quite different from the experimental conditions for PBF Test SFD 1-4. The different experimental conditions will strongly affect the behavior of the Ag-In-Cd control rods in these different experiments. This section compares the out-of-pile experiments with the in-pile PBF SFD 1-4 experiment and presents calculations to show why it is inappropriate to use existing models to describe control rod behavior in PBF Test SFD 1-4.

System pressure is an important variable in determining the timing and mode of control rod failure. In all of the out-of-pile tests described earlier in which no zircaloy guide tube was used, control rod failure occurred slightly before stainless steel melting as a result of rupture of the stainless steel clad. At the time of rod failure, molten material was forcibly ejected from the rod due to the high cadmium vapor pressure. For those tests in which a zircaloy guide

tube was present, the stainless steel ballooned, contacted the zircaloy and chemically reacted with the zircaloy cladding. This ballooning and bursting mode of control rod failure is a result of the low system pressure used in these experiments. By contrast, the PBF SFD 1-4 test will be conducted at 6.9 MPa (1000 psi). To understand the behavior of the control rod in this high pressure test, a simple isothermal thermodynamic analysis was performed to determine the internal pressure of a PBF control rod as a function of temperature. Details of the analysis are found in Appendix A. (Although axial temperature gradients could exist in the control rod, this simple isothermal analysis can still be used as a conservative estimate as long as the value of the maximum temperature of the rod is used in the argument that follows.) The assumptions used in the analysis are:

(1) each constituent of the alloy obeys Raoult's law;

(2) the rod is backfilled with helium; and

(3) the liquid control rod alloy has a constant density of 8.85 g/cc.

The results, plotted in Figure 2.2, indicate that the total internal pressure in the rod is always below 6.9 MPa (68 atm). As a result, the forcible ejection of

Figure 2.2

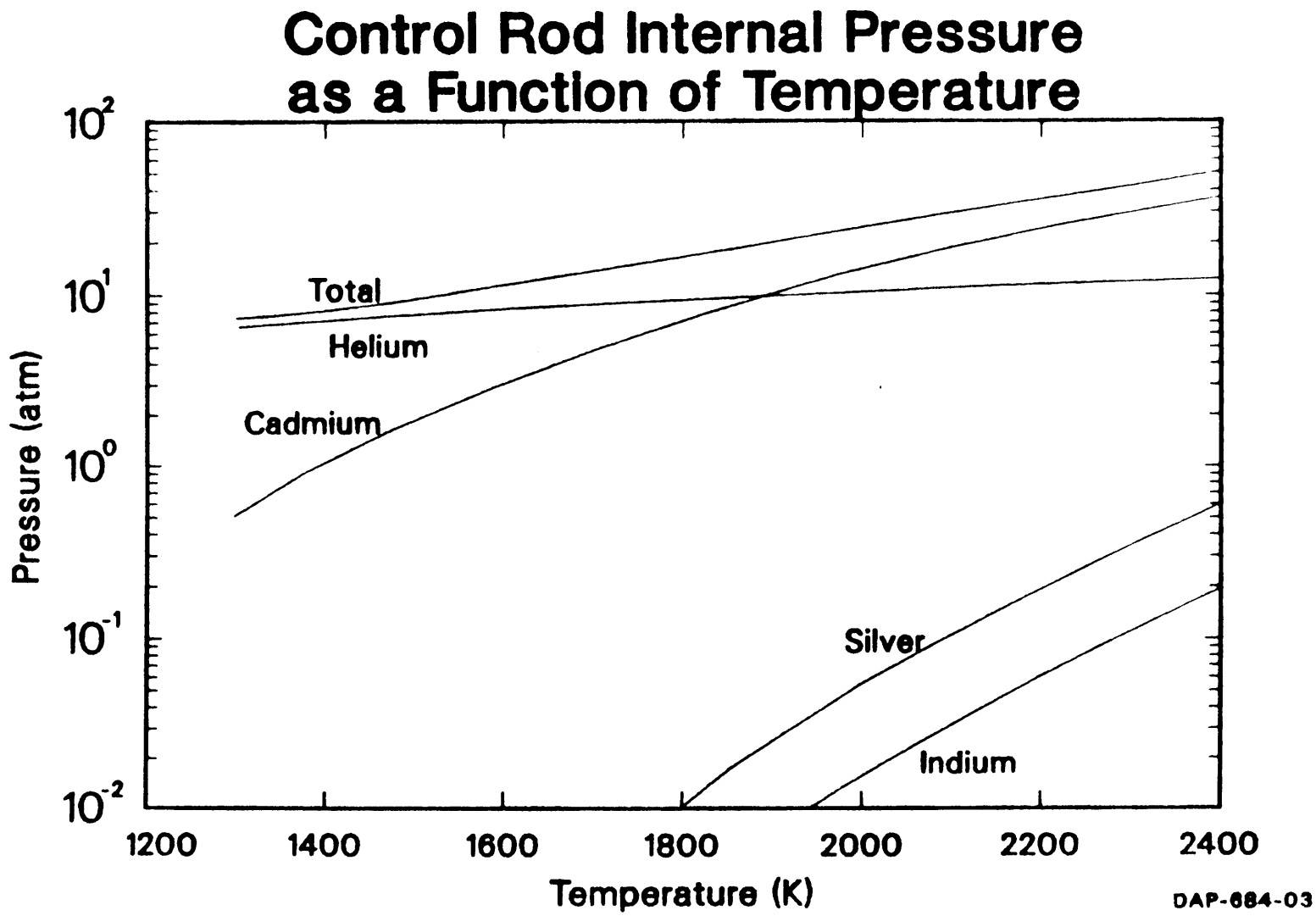
Control Rod Internal Pressure
as a Function of Temperature
Pressure (atm)
10^2
10^1
10^0
10^-1
10^-2
Total
Helium
Cadmium
Silver
Indium
1200
1400
1600
1800
2000
2200
2400
Temperature (K)
DAP-684-03

the molten alloy observed in both the ORNL and KfK tests would not occur at high system pressures. The pressure differential across the rod is negative which prevents rupture of the stainless steel before the melting point is reached. Instead, failure of the control rod would be expected to occur at the melting point of the stainless steel and the molten material would candle down the rod. A similar analysis performed by Powers [2.9] substantiates this conclusion.

Such an analysis is useful when thinking about the differences in control rod behavior in different postulated accident sequences. Based on the out-of-pile experiments, the stainless steel will fail in low pressure accident sequences like a large break or interfacing system LOCA, (i.e., AH and V sequences) at or near 1473 K before melting is reached whereas for high pressure sequences like a transient with loss of off site power and a small break LOCA (i.e., TMLB' and S_2D sequences), failure will occur at stainless steel melting. This effect could be important since the time of rod failure impacts the timing of silver, indium and cadmium vapor release relative to fission product release.

In some of the experiments, the sample capsules or bundles were heated in a crucible. This geometry is

different from the rod-like geometry used in PBF Test SFD 1-4. In the PBF Test SFD 1-4, molten control materials can flow down and refreeze at cooler locations in the rod bundle whereas crucible experiments maintain a pool of molten materials from which vaporization may continue. None of the analytic models presented in Section 2.3 describe this potential downward relocation of the alloy. The surface-to-volume ratio which is important in determining release rates is quite different in the small scale experiments than in the PBF SFD 1-4 experiment. In addition, the geometry will play a crucial role in determining the amount zircaloy dissolved by the control rod alloy. PBF Test SFD 1-4 will provide a realistic rod-like geometry to understand the competition between zircaloy oxidation and dissolution by the alloy. Oxidation of the zircaloy will limit the amount of potential silver and indium reaction. Thus, the large liquefaction of zircaloy observed in some of the out-of-pile experiments might not occur in PBF Test SFD 1-4.

The mechanism governing the release of silver, indium and cadmium vapor in PBF Test SFD 1-4 will be quite different than that observed in the out-of-pile experiments. To understand the vaporization behavior of the alloy for a variety of different system pressures

(and hence accident sequences) a "boiling map" for each constituent was developed. In the primary system, boiling of a constituent in the alloy will occur when the following inequality is satisfied:

$$P_V * Y > P_{sys}$$

where

P_V = vapor pressure of pure liquid (Pa),

Y = mole fraction of constituent in the alloy, and

P_{sys} = system pressure (Pa).

This equation when plotted as a function of system pressure is an hyperbola (see Figure 2.3). For a given system pressure, boiling will occur when the appropriate vapor pressure/mole fraction pair lies above the corresponding system pressure curve.

In the ORNL and KfK tests, since the system was at atmospheric pressure, the temperature of the melt increased above the respective saturation temperatures for Ag, In and Cd. Consequently, the large vapor release was a result of boiling each constituent from the melt. However, in PBF Test SFD 1-4, the physical conditions are different. The high system pressure will raise the saturation temperature of the silver and indium well above the maximum temperature of 2400 K expected in the test. For cadmium, although the saturation temperature

Figure 2.3

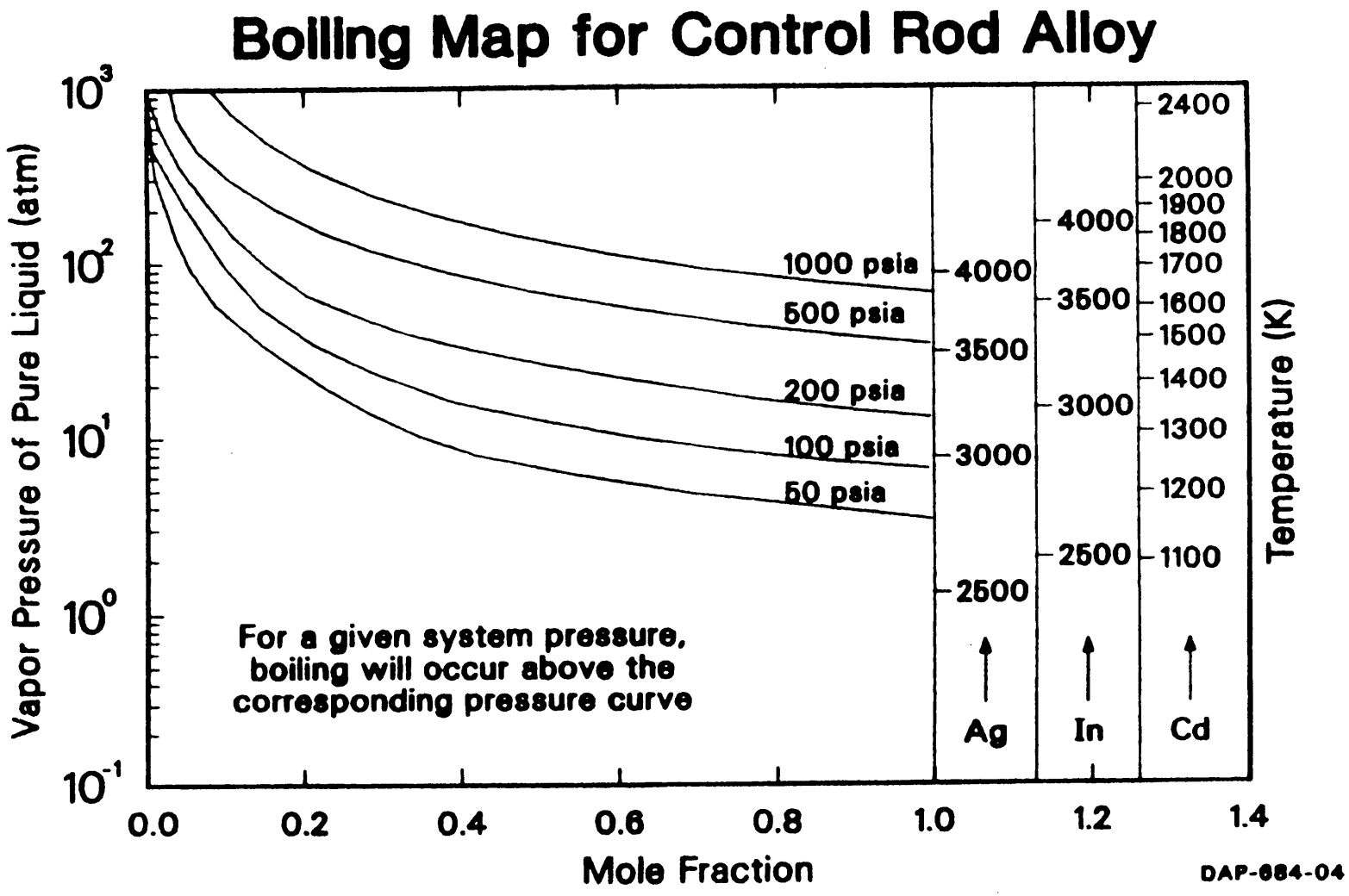
Boiling Map for Control Rod Alloy
Vapor Pressure of Pure Liquid (atm)
10^3
10^2
10^1
10^0
10^-1
1000 psia
500 psia
200 psia
100 psia
50 psia
For a given system pressure, boiling will occur above the corresponding pressure curve
4000
3500
3000
2500
Ag
In
Cd
2400
2000
1900
1800
1700
1600
1500
1400
1300
1200
1100
Temperature (K)
0.0
0.2
0.4
0.6
0.8
1.0
1.2
1.4
Mole Fraction
DAP-684-04

at 6.9 MPa (1000 psi) is below 2400 K, the low mole fraction of cadmium in the melt will preclude boiling of cadmium in the experiment. Thus, for all three components, Raoult's law, system pressure and the maximum temperature in the test combine to limit the possible vapor pressure/mole fraction pairs to a region below the 6.9 MPa (1000 psi) curve. As a result, in PBF Test SFD 1-4, boiling of the Ag, In and Cd will not occur. Instead, the release of Ag, In and Cd in the experiment will be controlled by multicomponent convective mass transfer. Once again, the same conclusion has been obtained by Powers [2.9]. Similar analysis can be performed using the boiling "map" to understand the mechanism controlling the release of silver, indium and cadmium vapor in a variety of accident sequences.

Based on this analysis, it is apparent that existing models which were developed from out-of-pile experiments conducted at low pressure are inappropriate for describing the behavior of Ag, In and Cd vapor release in a high pressure in-pile experiment like PBF Test SFD 1-4. A model to describe the downward relocation and simultaneous vaporization behavior of the alloy is developed in the next section.

2.5 REFERENCES

2.1 Parker, G.W., Creek, G.E., and Sutton, A.L., "Influence of Variable Physical Process Assumptions on Core Melt Aerosol Release," Proceedings of the International Meeting on Thermal Nuclear Reactor Safety, NUREG/CP-0027 Chicago, IL, August 28-September 2, 1982, Vol. 2.

2.2 Hagen, S. et. al., "An Expermental Investigation of the Meltdown Phase of UO_2-Zircaloy Fuel Elements at Non-Cooling," KfK Report 2750, November 1978.

2.3 Personal Communication with L. Sepold, KfK Representative to EG&G, Idaho, June 1985.

2.4 Albrecht, H., "Fission Product Release Program at the SASCHA Facility," BMFT/USNRC Core-Melt Information Exchange Meeting, October 27-28, 1982.

2.5 Mitchell, J.P., Nichols, A.L., and Simpson, J.A.H., "The Characterization of Ag-In-Cd Control Rod Aerosols Generated at Temperatures Below 1900 K," CSNI Specialist Meeting on Nuclear Aerosols in Reactor Safety, Karlsruhe, Germany, September 4-6, 1984.

2.6 Lorenz, R.A., Beahm, E.C. and Wichner, R.P., "Review of Tellurium Release Rates from LWR Fuel Elements and Aerosol Formation from Silver Control Rod Materials," ORNL Informal Letter Report, February 28, 1983.

2.7 Wichner, R.P. and Spence, R.D., Quantity and Nature of LWR Aerosols Produced in the Pressure Vessel During Core Heatup Accidents - A Chemical Equilibrium Estimate, NUREG/CR-3181, March 1984.

2.8 Taig, A.R., "Release and Retention Phenomena in Degraded Cores," ANS Topical Meeting on Fission Product and Source Term Research, Snowbird, UT, July 15-19, 1984.

2.9 Powers, D.A., Behavior of Control Rods During Core Degradation I. Pressurization of Silver-Indium-Cadmium Control Rods, SAND85-0469, Februrary, 1985.

3. THE DEVELOPMENT OF A Ag-In-Cd VAPOR RELEASE MODEL

During a severe reactor accident, the Ag-In-Cd absorber alloy with its melting point at 1073 K is likely to be the first core material to melt. At high system pressures, the molten Ag-In-Cd is expected to remain "bottled" in its stainless steel cladding until steel melting is approached at 1723 K. Because of the chemical interaction between Ag, In and zircaloy, the alloy will penetrate and flow down the outside of the guide tube to cooler portions of the core. A schematic of the physical situation is shown in Figure 3.1. The rod is assumed to fail at the first node that reaches 1723 K. The material then flows out of the break and down the control rod guide tube, during which time mass transfer of Ag, In and Cd into the hydrogen/steam mixture occurs. The rate at which this liquid moves down the guide tube will determine the amount of time that mass transfer can occur in the primary system. A code named VAPOR has been developed to model this behavior.

This section will discuss the four major models in the VAPOR code. The rod failure model will describe the rate at which alloy leaves the control rod housing; the

Figure 3.1

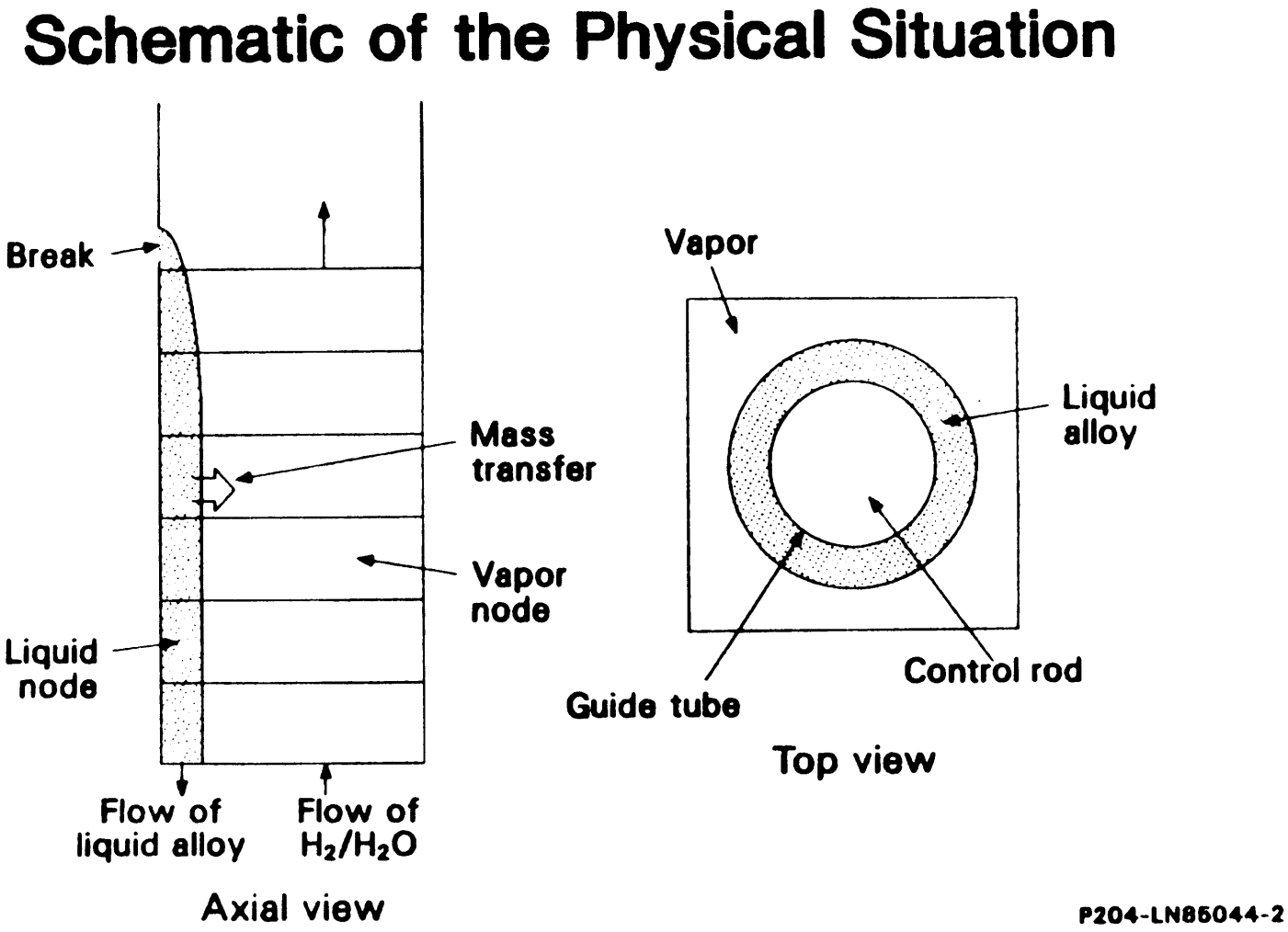
Schematic of the Physical Situation
Break
Mass transfer
Vapor node
Liquid node
Flow of liquid alloy
Flow of H_2/H_2O
Axial view
Vapor
Liquid alloy
Guide tube
Control rod
Top view
P204-LN85044-2

liquid film model will describe the velocity and film thickness of the alloy as it travels down the rod; the mass transfer model will calculate the rate at which Ag In and Cd is transferred from the flowing alloy to the hydrogen/steam mixture; and finally a simple model will be presented to describe the potential dissolution of the zircaloy by the alloy.

3.1 Rod Failure Model

At high system pressures, upon heatup of the control rod, there is insufficient internal pressurization due to alloy vaporization to cause the control rod to rupture. Therefore, the alloy will remain bottled in its stainless steel sheath until 1723 K (the melting point of the stainless steel) is reached. At that time, the failure of the stainless steel allows the molten alloy to come in contact with the zircaloy guide tube. Dissolution of the zircaloy by the Ag and In will cause the alloy to penetrate the guide tube and flow into the primary system. This section will describe the model used to predict the rate at which the alloy exits the failure in the rod.

Sufficient time exists for all axial elevations of the rod to reach the melting point of the alloy (1073 K) before stainless steel melting at the hottest node is

reached. As a result, all of the alloy above the point of failure is assumed to be molten and available for release. The rod is modeled as a control volume consisting of all the nodes above the axial location of failure. The flow of the alloy is considered to be one dimensional from a volume of height h(t), through a break of area A_2, as shown in Figure 3.2.

Both a mass and a momentum balance are needed to determine the behavior of the alloy in the rod. Conservation of mass for the control volume states

$$\frac{d}{dt}(m_{cv}) = -\rho A_2 V_2 \tag{3.1}$$

where

ρ = density of the alloy (kg/m^3),

A_2 = break area (m^2), and

V_2 = velocity at the break (m/s).

The unsteady form of Bernoulli's equation along a streamline between points 1 and 2 is used to determine the velocity at the break. Hence

$$\int_1^2 \rho \frac{\partial V}{\partial t} dS + p_2 + \tfrac{1}{2}\rho V_2^2 = p_1 + \tfrac{1}{2}\rho V_1^2 + \rho g h - K_c \frac{\rho V_2^2}{2} - \left(\frac{fL}{D}\right) \frac{\rho V_1^2}{2} \tag{3.2}$$

Figure 3.2

Control Volume Selection for Rod Failure Model

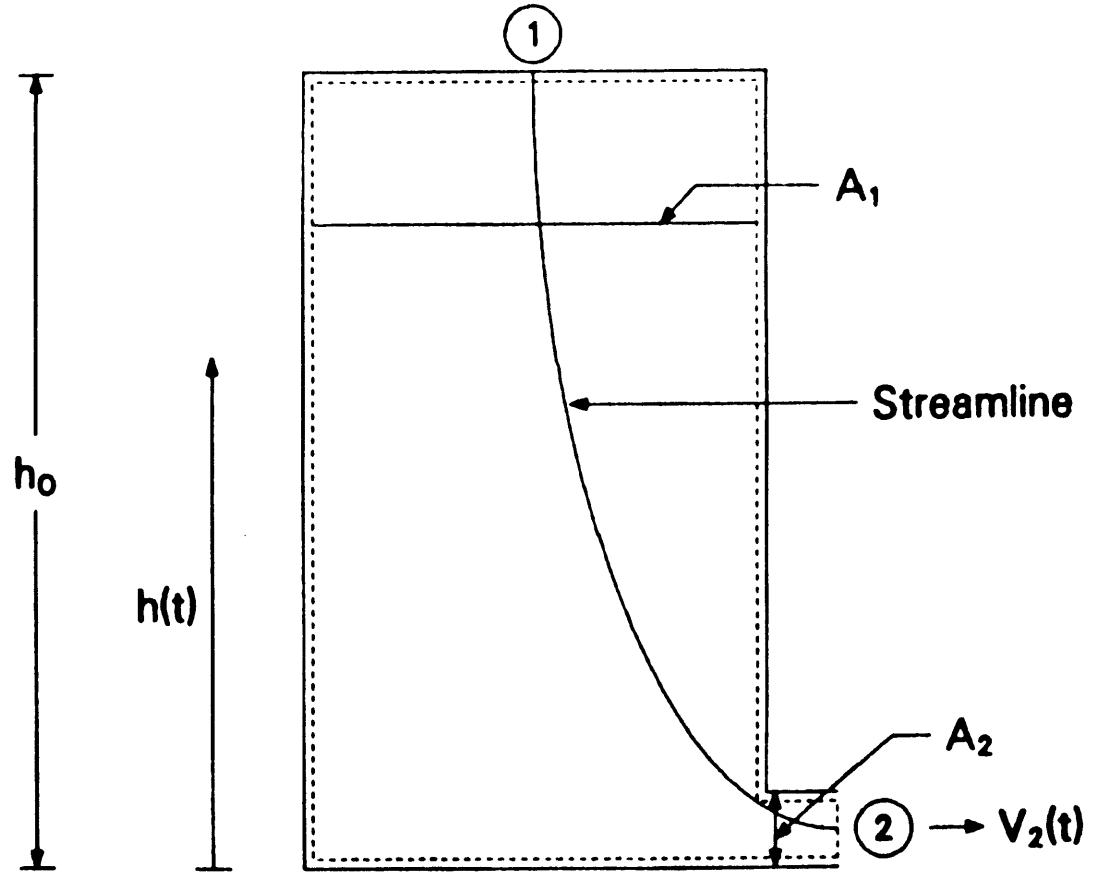

where

ρ = density of the alloy (kg/m^3),

p_2 = pressure at point 2 (Pa),

V_2 = velocity at the break (m/s),

p_1 = pressure at point 1 (Pa),

V_1 = velocity of liquid surface (m/s),

h = height of alloy (m),

g = acceleration due to gravity (m/s^2),

K_c = form loss coefficient due to contraction at the break,

f = dimensionless friction factor,

L = length of the streamline (m),

D = inside diameter of rod (m), and

$\frac{\partial V}{\partial t}$ = acceleration of the liquid alloy (m/s^2).

For cases where the system pressure is high like PBF Test SFD 1-4, the static pressure differential (p_2-p_1) is set equal to zero. In addition, friction in the rod is assumed to be negligible. Thus, Equation (3.2) becomes

$$\int_1^2 \rho \frac{\partial V}{\partial t} dS + \frac{\rho V_2^2}{2} = \frac{\rho V_1^2}{2} + \rho g h - K_c \frac{\rho V_2^2}{2} \qquad (3.3)$$

The form loss coefficient, K_c, is given by [3.1]

$$K_c = \begin{cases} 0.32\ (1 - A_2/A_1) & \text{if } A_2 < 0.4712\ A_1 \\ A_2/A_1 & \text{if } A_2 > 0.4712\ A_1 \end{cases}$$

where

A_2 = area of break (m^2), and

A_1 = crosssectional area of rod (m^2).

The integral in Equation (3.3) can be approximated by

$$\int_1^2 \frac{\partial V}{\partial t}\, ds \cong \frac{dV_1}{dt}\, h$$

Hence, Equation (3.3) becomes

$$h\,\frac{dV_1}{dt} + V_2^2(1 + K_c) - V_1^2 = 2gh \qquad (3.4)$$

Using the following approximations

$$V_1 = \frac{A_2}{A_1}\, V_2 \qquad \text{and} \qquad \frac{dV_1}{dt} = \frac{A_2}{A_1}\ \frac{dV_2}{dt}$$

a simplified form of Equation (3.4) can be developed:

$$\frac{dV_2}{dt} = g\frac{A_1}{A_2} - \frac{V_2^2(1 + K_c - (A_2/A_1)^2)}{2(A_2/A_1)h} \qquad (3.5)$$

Since $m_{cv} = \rho A_1 h$, Equation (3.1) becomes

$$\frac{dh}{dt} = -\frac{A_2}{A_1} V_2 \qquad (3.6)$$

Equations (3.5) and (3.6) are two coupled non-linear differential equations which can be solved to find $V_2(t)$ and $h(t)$. However, to make the analysis simpler and analytically tractable, the temporal acceleration term was neglected, $\frac{dV_2}{dt} = 0$. For small sized holes in which $A_2 << A_1$ this assumption is valid because the small fractional loss rate insures an almost constant gravity head. For large holes where $A_2 \sim A_1$, as will be shown later, drainage is so rapid that a more detailed analysis is not warranted. Equation (3.5) is

then solved exactly for V_2 as a function of h which yields a quasi-steady form of the momentum equation

$$V_2 = \left[\frac{2gh}{1 + K_c - (A_2/A_1)^2}\right]^{\frac{1}{2}} \tag{3.7}$$

Substitution of Equation (3.7) into (3.6) yields

$$\frac{dh}{dt} = -\left[\frac{2g(A_2/A_1)h}{1 + K_c - (A_2/A_1)^2}\right]^{\frac{1}{2}} \tag{3.8}$$

which can be solved analytically. The solution to Equation (3.8) subject to the initial condition that $h(t=0)=h_0$ is

$$h(t) = (\sqrt{h_0} - \frac{\gamma t}{2})^2 \tag{3.9}$$

where

$$\gamma = \left[\frac{2g(A_2/A_1)^2}{1 + K_c - (A_2/A_1)^2}\right]^{\frac{1}{2}}$$

Thus, equations (3.7) and (3.9) describe the velocity of the alloy at the break, V_2,and the height of the resevoir, h, as functions of time. Inspection of these equations reveals that h is quadratic and V_2 is linear in time. A plot of h(t) versus time is given in Figure 3.3. The time at which the resevoir is drained (h=0) is equal to $\frac{2\sqrt{h_0}}{\gamma}$. Figure 3.4 is a plot of the velocity at the break versus time for various area ratios. As can be seen from the figure, if the break area is large, then the time to drain the rod is small.

3.2 Liquid Film Model

Many researchers have studied the behavior of molten material flowing and refreezing in channels. For example, Gasser and Kazimi [3.2] have studied the behavior of molten fuel streaming through the axial shield in an LMFBR. Ishii, Chen and Grolmes [3.3] have studied the motion of molten cladding in fast reactor loss-of-flow accidents. In addition, El-Genk and Moore [3.4] have studied the transient freezing of liquified fuel rod material in a reactivity initiated transient.

In all of these analyses, the transient freezing behavior of the molten material (i.e., the temperature, thickness and velocity of the liquid film) is determined

Figure 3.3

Variation of h with Time

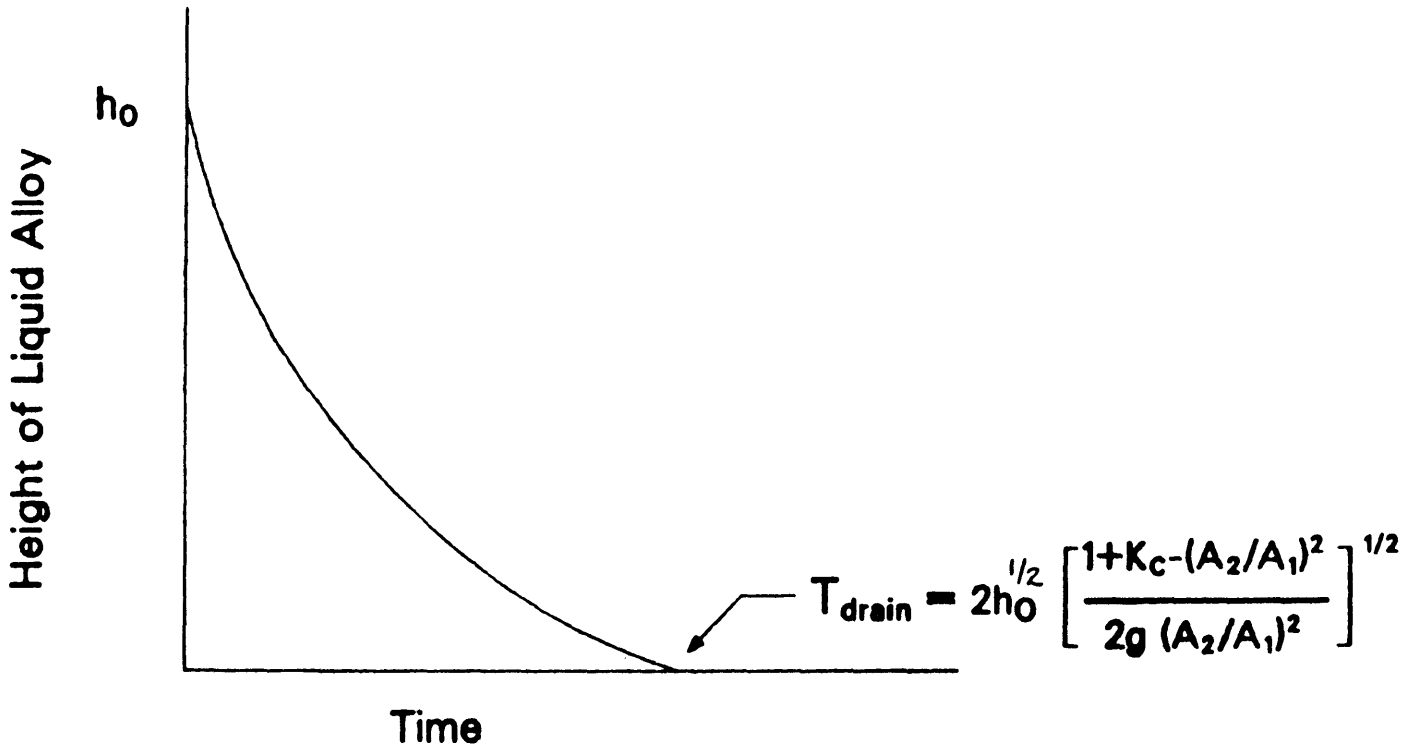

RB50002-4

Figure 3.4

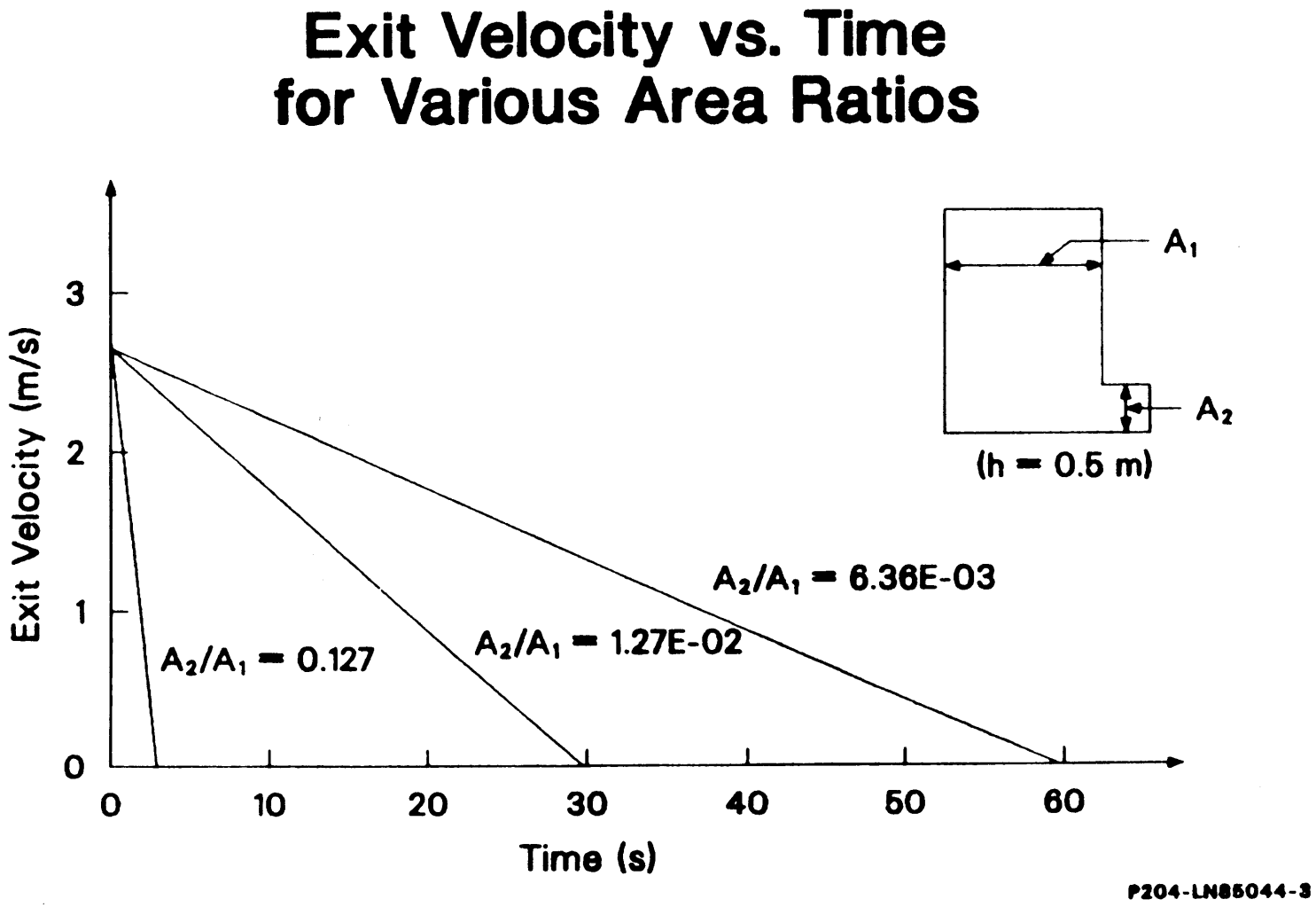
Exit Velocity vs. Time
for Various Area Ratios
Exit Velocity (m/s)
3
2
1
0
0
10
20
30
40
50
60
Time (s)
A1
A2
(h = 0.5 m)
A2/A1 = 6.36E-03
A2/A1 = 1.27E-02
A2/A1 = 0.127
P204-LN85044-3

by local mass, energy and momentum balances. The physical situation for the control rod alloy is different. Since the alloy melts at such a low temperature (1073 K) refreezing will probably not occur until the alloy reaches the bottom of the active fuel length in PBF Test SFD 1-4. (However, if the Ag-In-cd dissolves the zircaloy, the freezing temperature of the resulting solution would be considerably higher than that of Ag-In-Cd.) As a result, a formal energy balance is not developed; the temperature of the alloy is obtained from a thermal hydraulic core heatup code and used as a boundary condition for the problem. It is hypothesized that the behavior of the alloy as it flows down the rod (its thickness and velocity) is not determined by heat transfer but instead by mass transfer into the hydrogen-steam mixture. This idea is used in the development of the following liquid film model. Much of the theory to follow was developed from references on annular two phase flow in water systems such as that of Collier [3.5].

As the liquid alloy exits the break, it flows down the outside of the zircaloy guide tube. At the same time, mass transfer is occuring at the liquid-vapor interface (from the liquid to the vapor) in a countercurrent flow arrangement. The liquid flow is

considered to be annular and one dimensional in the axial direction. In addition, the effects of grid spacers are neglected. The implications of these assumptions are discussed in Section 4.1. Entrainment of the alloy by the vapor is not considered since the velocity of the gas is calculated to be small. The liquid and vapor are divided into a series of nodes. A momentum balance on each liquid node yields

$$\frac{\partial}{\partial t}\int_{vol}\rho\,\underline{V}\,d\,Vol + \iint_{s}\rho\,(\underline{V}\cdot\underline{n})\,dA = \Sigma\vec{F} \qquad (3.10)$$

where the first term represents the temporal acceleration of the fluid, the second term is the momentum convected into and out of the control volume through the surfaces and the right hand side of the equation is the sum of all the forces acting on the volume. In the present analysis the first term is neglected and a quasi-steady solution is sought. Applying the z-component of Equation (3.10) to a single node as shown in Figure 3.5 yields

$$G - \tau_i P_i \Delta z - \tau_w P_w \Delta z = (\dot{m}V)_{out} - (\dot{m}V)_{in} \qquad (3.11)$$

Figure 3.5

Momentum Balance on a Liquid Node*

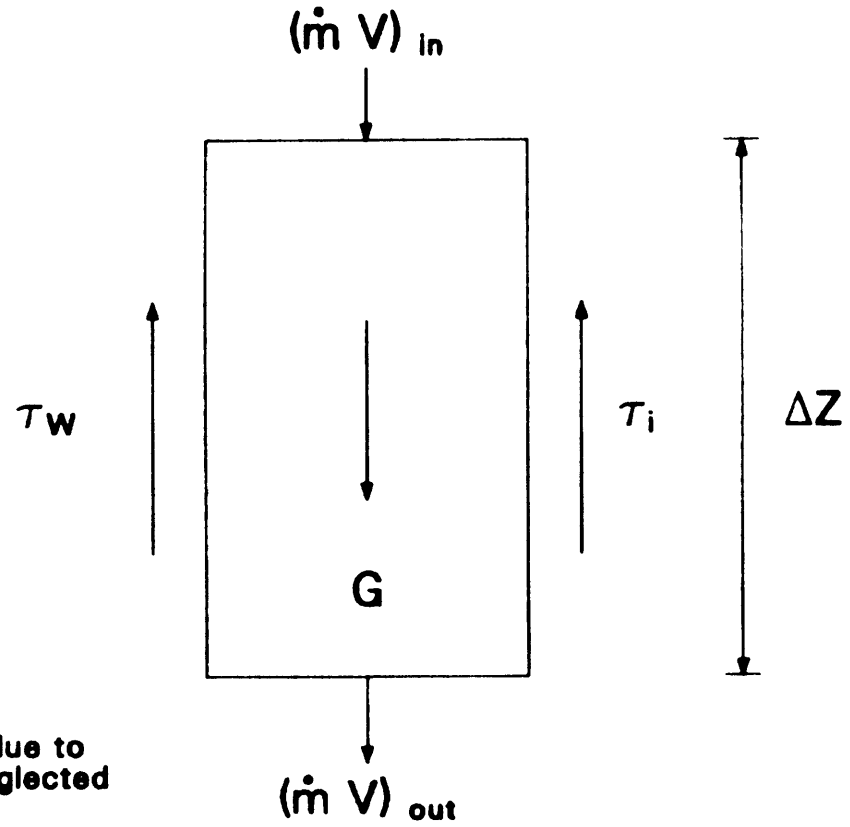

* Radial momentum due to mass transfer is neglected

P204-LN85044-4

where

G = gravity force on the liquid node (N),

τ_i = interfacial shear stress between the liquid and vapor (N/m^2),

P_i = interfacial perimeter over which τ_i acts (m),

τ_w = shear stress due to wall friction (N/m^2),

P_w = wetted perimeter over which τ_w acts (m),

Δz = axial length of the node (m),

$(\dot{m}V)_{out}$ = momentum flux out of the node (N), and

$(\dot{m}V)_{in}$ = momentum flux into the node (N).

The gravity force, interfacial shear force and the wall shear force are given respectively by

$$G = \rho_\ell g \Delta z_j \frac{\pi}{4}[(D + 2\delta_j)^2 - D^2] = \rho \pi D \delta_j g \Delta z_j \qquad (3.12)$$

$$\tau_i P_i \Delta z_j = \frac{f_i \rho_g}{2} (u_g - V_j)^2 \pi (D + 2\delta_j) \Delta z_j \qquad (3.13)$$

$$\tau_w P_w \Delta z_j = f_{w,\ell} \frac{\rho_\ell V_j^2}{2} \pi D \Delta z_j \qquad (3.14)$$

where

g = acceleration due to gravity (m^2/s)

D = diameter of control rod housing (m),

ρ_ℓ = density of the alloy (kg/m^3),

Δz_j = axial length of node j (m),

f_i = dimensionless interfacial friction factor,

u_g = gas velocity (m/s),

δ_j = thickness of node j (m),

V_j = velocity of node j (m/s), and

$f_{w,\ell}$ = dimensionless friction factor due to wall friction.

The interfacial friction factor is given by

$$f_i = f_{w,g}\left(1 + 300 \frac{\delta_j}{D_e}\right) \qquad (3.15)$$

where

$f_{w,g}$ = dimensionless wall friction factor if the gas flowed alone in the channel, and

D_e = equivalent diameter of the channel (m).

The friction factors $f_{w,g}$ and $f_{w,l}$ are evaluated using

$$f = \begin{cases} 16/Re & \text{for laminar flow, and} \quad (3.16a) \\ 0.046/Re^{0.2} & \text{for turbulent flow.} \quad (3.16b) \end{cases}$$

For the liquid alloy, $f_{w,\ell}$ is evaluated using a film Reynold's number which is given by

$$Re = \frac{4\rho_\ell V \delta}{\mu_\ell} \qquad (3.17)$$

where μ_ℓ is the viscosity of the liquid alloy. The transition between laminar and turbulent liquid film flow occurs at roughly Re = 1800. For evaluation of $f_{w,g}$ the Reynold's number is given by

$$Re = \frac{\rho_g u_g D}{\mu_g} \qquad (3.18)$$

where

ρ_g = density of the hydrogen/steam mixture (kg/m^3), and

μ_g = viscosity of the hydrogen/steam mixture (kg/m-s).

The corresponding flow transition for the gas flow occurs at Re = 2200.

The spatial acceleration terms ($\dot{m}V$) are evaluated in the following manner:

A) For the momentum convected into node j,

(1) for the first node (j=1)

$$(\dot{m}V)_{in} = \rho_\ell A_{fail} V_{fail}^2 \tag{3.19}$$

where

ρ_ℓ = alloy density (kg/m^3),

A_{fail} = area of break in the rod (m^2),

V_{fail} = velocity of break (m/s), and

(2) for all other nodes (j >1)

$$(\dot{m}V)_{in} = \rho_{j-1} \pi D \delta_{j-1} V_{j-1}^2 \tag{3.20}$$

where (j-1) refers to the previous node.

B) For the momentum convected out of node j,

$$(\dot{m}V)_{out} = \rho_j \pi D \delta_j V_j^2 \tag{3.21}$$

Substituting all of these terms back into the momentum balance (Equation 3.11), results in an equation which determines the velocity of node j, V_j, as a function of the velocity of the previous node V_{j-1}, the thickness of the node δ_j and the geometry. If the liquid film is laminar, the velocity is a quadratic function and can be solved analytically whereas, for turbulent liquid film flow, no analytic solution is possible. In this case, Newton's method is used to solve for the velocity at the node. Details of the algebra are given in Appendix D.

The thickness of the node, δ_j , is determined by performing a mass balance on each specie to obtain the total mass in a node. Thus, the thickness can be calculated using the equation

$$\delta_j = \sum_{i=1}^{n} m_{i,j} / (\pi \rho_\ell D \Delta z_j) \tag{3.22}$$

where

$m_{i,j}$ = mass of species i in liquid node j (kg).

3.3 Mass Transfer Model

As the alloy travels down the control rod guide tube, the Ag, In and Cd will be vaporizing into the hydrogen-steam mixture. This section will present a model to describe the rate of mass transfer of each specie into the gas flow. Figure 3.6 represents a simplified schematic of the physical situation. The molten control material is visualized as having flowed down the intact portion of the control rod guide tube, covering it completely. A hydrogen-steam mixture flows over the molten material at a bulk temperature of T_∞ while the control material is at a uniform temperature T_{wall}. Since the system pressure is high enough to suppress boiling, the heat and mass transfer aspects can effectively be uncoupled. In addition, chemical reactions between the vapors and the bulk fluid are neglected.

The partial pressure of each constituent (Ag, In and Cd) at the surface can be calculated using Raoult's law. Hence,

Figure 3.6

Simplified Conceptual Picture for Vapor Release Model

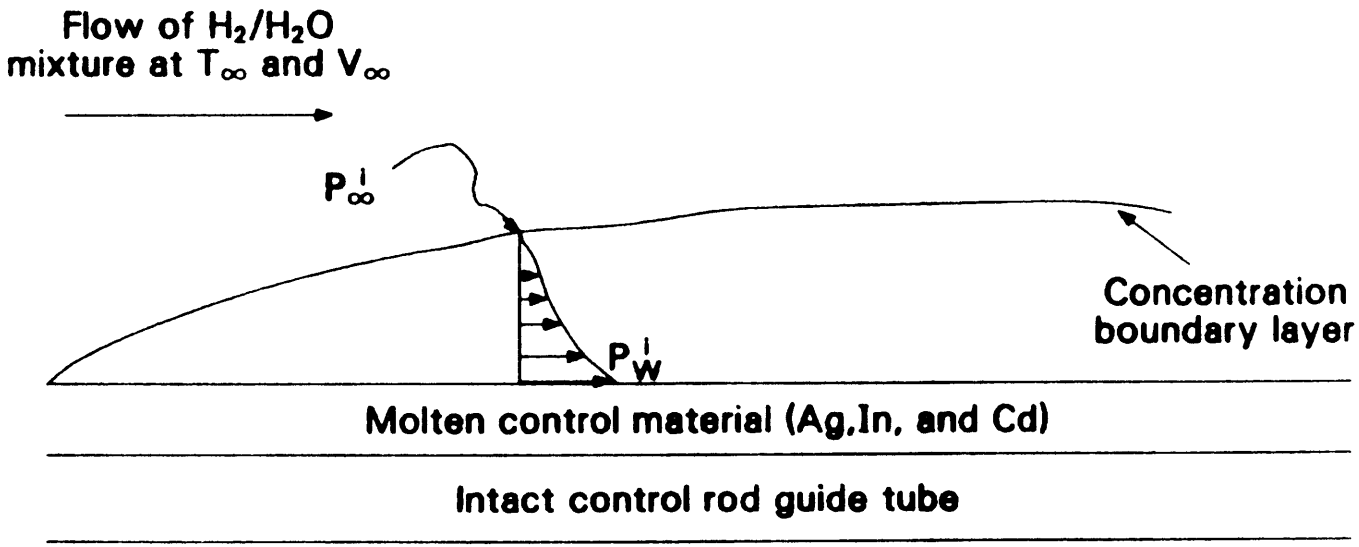

P204-LN85044-5

$$p_i^w = p_i^v (T_{wall}) Y_i \tag{3.23}$$

where

Y_i = mole fraction of specie i in liquid,

$p_i^v(T_{wall})$ = vapor pressure of specie i (Pa),

p_i^w = partial pressure of specie i at the surface (Pa).

The applicability of this assumption will be discussed in Section 4.3. As a result of the flow of H_2/H_2O over the liquid control material, the rate at which the vapors enter the flow stream is determined by the rate of mass transfer through the concentration boundary layer. The absolute molar flux of specie i, $\vec{N}_i^w$, into the flow stream is given by [3.6]

$$\vec{N}_i^w = \vec{J}_i^w + X_i^w \sum_{j=1}^{n} \vec{N}_j^w \tag{3.24}$$

where the first term is the diffusive flux of specie i at the surface due to the partial pressure (concentration) gradient of specie i between the surface and the bulk fluid and the second term is due to the

bulk flow of all the vapors from the surface into the flow stream. Equation (3.24) results in n coupled equations involving the molar flux of all species. Assuming that the absolute molar flux of the hydrogen/steam mixture is zero, Equation (3.24) can be solved for N_i^w, the molar flux of each diffusing species. This yields

$$N_i^w = [J_i^w(1 - \sum_{\substack{j=1 \\ j\neq i}}^{n} X_j^w) + X_i^w \sum_{\substack{j=1 \\ j\neq 1}}^{n} J_j^w]/(1 - \sum_{j=1}^{n} X_j^w) \qquad (3.25a)$$

This mass transfer model is applicable only for cases where the system pressure is high enough to suppress boiling. At low system pressures, the Cd will probably boil and Equation (3.25a) will no longer be valid. To overcome this problem, an assumption has been made that will allow a low pressure case to be considered. If the vapor pressure of any specie at any liquid node during the simulation exceeds the system pressure then the mass transfer is uncoupled and the following equation is used:

$$N_i^w = J_i^w \qquad (3.25b)$$

Thus, in the event of boiling one of the constituents of the alloy, the absolute molar flux is just equated to the diffusive flux. It is understood that convective mass transfer is the wrong mechanism for these conditions and that a boiling mass transfer model should be developed for this case. Nevertheless, uncoupling the mass transfer does allow a low pressure simulation to be considered.

The diffusive flux, J_i^w,(by analogy to the convective heat flux) can be expressed in terms of the partial pressure difference between the liquid surface and the bulk vapor as

$$J_i^w = \frac{h_D}{RT} (p_i^w - p_i^\infty) \qquad (3.26)$$

where

h_D = mass transfer coefficient for specie i (m/s),

p_i^w = partial pressure of specie i at the surface (Pa),

p_i^∞ = partial pressure of specie i in the bulk flow (Pa),

R = gas constant (Pa-m^3/kgmole K), and

T = temperature (K).

The partial pressure in the bulk, p_i^{∞} , is calculated using the mass of specie i in the vapor and the ideal gas law. By using the mass transfer analogy and dimensional analysis, the mass transfer coefficient, h_D, is found to be a function of Reynolds number, Schmidt number and the geometry. Sample correlations are found in Table 3.1. The Schmidt number, Sc, is

$$Sc_i = \mu/\bar{\rho}D_i$$

and

μ = mixture viscosity (kg/m-s),

$\bar{\rho}$ = mixture density (kg/m^3),and

D_i = diffusion coefficient of specie i in bulk fluid (m^2/s).

The viscosity of the hydrogen-steam mixture is calculated using a result from kinetic theory [3.6]:

$$\mu = \frac{X_1\mu_1}{X_1 + X_2\phi_{21}} + \frac{X_2\mu_2}{X_1\phi_{21} + X_2} \qquad (3.27)$$

TABLE 3.1

MASS TRANSFER CORRELATIONS

(1) Flow in tubes of diameter d

$2000 < Re < 35000$ (turbulent flow)

$$h_D = 0.023(D/d)Re^{0.83}Sc^{0.44}$$

$Re < 2000$ (laminar flow)

$$h_D = 3.56(D/d)$$

(2) Flow over a flat plate of length L

$Re_L < 10^5$ (laminar)

$$h_D = (D/L)(Re_L)^{1/2}Sc^{1/3}$$

$Re_L > 10^5$ (turbulent)

$$h_D = 0.037(D/L)(Re_L)^{0.8}Sc^{1/3}$$

where, in general,

$$\phi_{ij} = \frac{1}{\sqrt{8}} \left(1 + \frac{M_i}{M_j}\right)^{-\frac{1}{2}} \left[1 + \left(\frac{\mu_i}{\mu_j}\right)^{\frac{1}{2}} \left(\frac{M_j}{M_i}\right)^{\frac{1}{2}}\right]^2 \qquad (3.28)$$

and

M_i = molecular weight (kg/kgmole), and

μ_i = viscosity (kg/m-s).

The density of the mixture is given by

$$\bar{\rho} = \rho_1 M_1 + \rho_2 M_2 \qquad (3.29)$$

where

$\bar{\rho}$ = mixture density (kg/m^3),

ρ_i = density (kgmole/m^3), and

M_i = molecular weight (kg/kgmole).

For the case of multicomponent mass transfer, where the rate of mass transfer is low, binary diffusion coefficients may be used to describe the diffusion of each metallic vapor in the gas stream. Diffusion coefficients are calculated using the Chapman Eskong relationship [3.6]

$$D_{AB} = 1.858 \times 10^{-3} T^{3} \frac{[(M_A+M_B)/(M_A M_B)]^{\frac{1}{2}}}{P\sigma_{AB}^{2}\Omega_D} \qquad (3.30)$$

where

D_{AB} = binary diffusion coefficient for specie A in fluid B (m^2/s),

T = temperature (K),

P = pressure (atm),

σ_{AB} = characteristic length (A), and

Ω_D = diffusion collision integral.

The values of σ_{AB} and Ω_D are given by [3.7]

$$\sigma_{AB} = (\sigma_A + \sigma_B)/2 \qquad (3.31)$$

$$\Omega_D = \frac{A}{(T^*)^B} + C\exp(-DT^*) + E\exp(-FT^*) + (G\exp(-HT^*) \qquad (3.32)$$

where

$$T^* = kT/\varepsilon_{AB} \tag{3.33a}$$

and

$$\frac{\varepsilon_{AB}}{k} = \left(\frac{\varepsilon_A}{k} \quad \frac{\varepsilon_B}{k}\right)^{\frac{1}{2}} \tag{3.33b}$$

and A, B, C, D, E, F, G, and H are constants given in Reference [3.7]. Values of ε and σ are based on [3.7]

$$\frac{\varepsilon}{k} = 0.75T_c \quad \text{and} \quad \sigma = \frac{5}{6} V_c^{1/3}$$

where T_c and V_c are the critical temperature and volume respectively in K and cm^3/gmole. Critical properties are taken from Reference 3.8. This equation is for use at low pressures. Large uncertainties may exist for use of this theory at high pressures. Note that for the calculation of D_i, the hydrogen-steam mixture is considered as a single fluid by using the following pseudocritical properties in the above formulas:

$$T_c^* = \sum_i T_{c_i} X_i \qquad (3.34a)$$

$$V_c^* = \sum_i V_{c_i} X_i \qquad (3.34b)$$

$$M_c^* = \sum M_{c_i} X_i \qquad (3.34c)$$

where X_i is the mole fraction of specie i (hydrogen or steam) in the gas mixture.

3.4 Zircaloy Dissolution Model

As the Ag-In-Cd alloy travels down the zircaloy guide tube, chemical interactions between the zircaloy, silver and indium will occur. Eutectics of Zr-Ag and Zr-In are known to form at temperatures as low as 1473 K and 1273 K respectively. The binary phase diagrams, presented in Reference 3.9 suggest that only 10-20% Ag alloying with zircaloy and 10% In alloying with zircaloy

is required for eutectic formation. Since very little is known about the rates of these chemical interactions, modeling these phenomena is difficult. As a result, a preliminary dissolution model has been developed to incorporate these interactions.

The model can be stated as follows:

(1) No eutectic interaction is allowed before the rod material above the point of failure totally drains.
(2) After rod failure, as each node below the point of failure exceeds stainless steel melting (1723 K), all of the alloy on the outside and on the inside of that node is moved onto the outer surface of the node below it.
(3) The calculation continues until all of the nodes have disappeared from the system.
(4) The model does not incorporate the presence of zircaloy in the liquid film flow. As a result, no vapor pressure reduction due to alloying is considered.

Since rod drainage times are quite fast (~5 seconds), the first assumption in the model is reasonable. The model assumes that this chemical attack is only a result of alloy which has melted through the stainless steel. Any alloy already existing on the outer surface of the guide tube does not react with the zircaloy. Although eutectics between Ag, In and Zr will occur 250-350 K below stainless steel melting, the amount of Ag and In on the node surface is usually quite small (~1 g), and not enough to cause complete meltthrough of the zircaloy. In addition, this assumption is made in an

attempt to simulate the behavior of the oxide film that would exist on the surface of the control rod guide tube. The oxide film would prohibit zircaloy dissolution by the absorber alloy on the outside of the guide tube. However, dissolution is allowed within the control rod once the stainless steel clad has melted. This alloying process is assumed to be instantaneous since sufficient quantities of Ag and In are inside the control rod node to dissolve completely the zircaloy guide tube. Limitiations of the zircaloy dissolution model are presented in Section 4.4.

3.5 Conservation Equations and Code Details

A code named VAPOR has been developed which incorporates all of the models described earlier. VAPOR can calculate mass transfer from a moving liquid film to a moving gas stream in countercurrent flow. This countercurrent flow arrangement is modeled as a series of nodes and flow junctions as illustrated in Figure 3.7. This section will present the conservation of mass equations which are used to track each specie, provide a flowchart of the VAPOR code and discuss the structure, input, and output of VAPOR.

Conservation of mass is used to track each specie in each node. Hence for the liquid nodes,

Figure 3.7

Nodal Structure of VAPOR Code

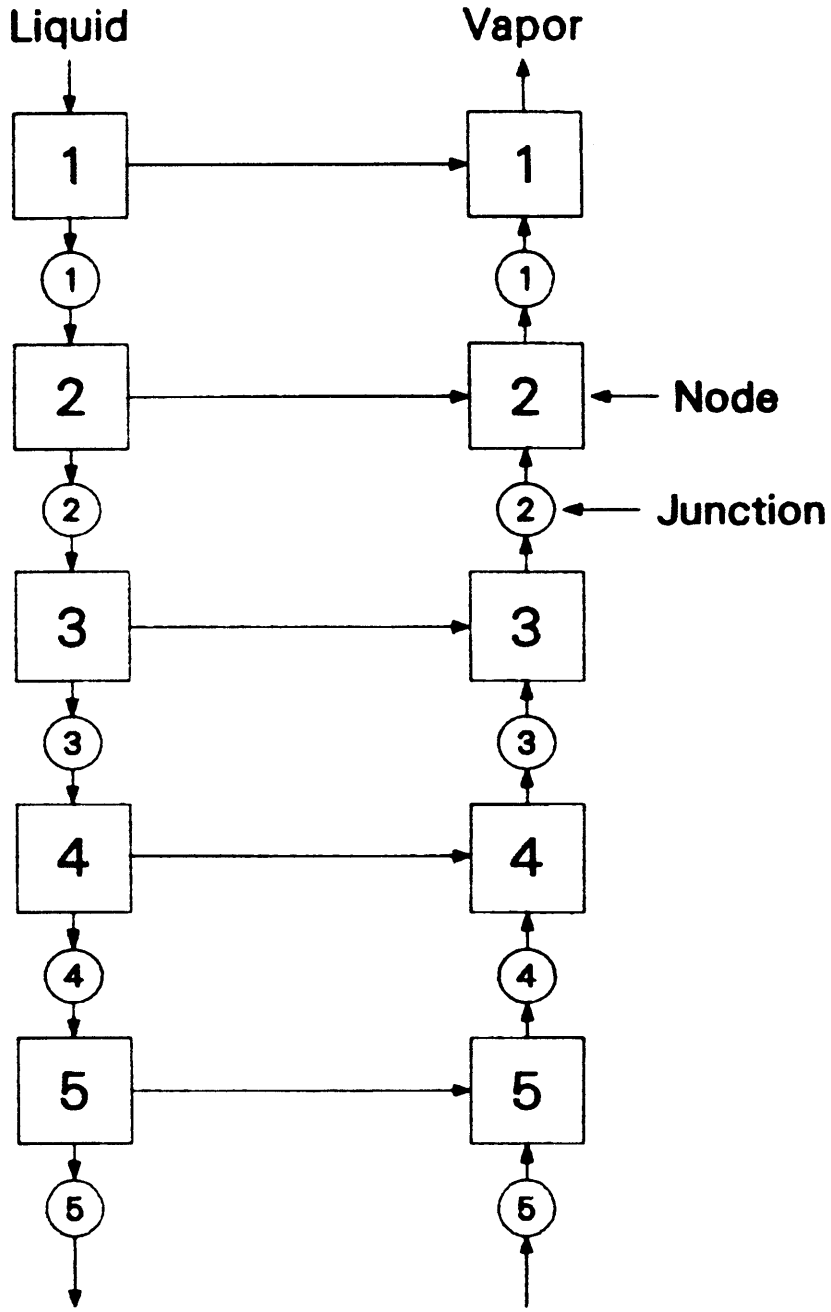

$$\frac{d}{dt}\left(m^{\ell}_{i,j}\right) = \dot{m}_{i,j-1} - \dot{m}_{i,j} - XN_{i,j} \qquad (3.35a)$$

and for the vapor nodes

$$\frac{d}{dt}\left(m^{v}_{i,j}\right) = \dot{m}_{i,j} - \dot{m}_{i,j-1} + XN_{i,j} \qquad (3.35b)$$

where

$m^{\ell}_{i,j}$ = mass of specie i in liquid node j (kg)

$m^{v}_{i,j}$ = mass of specie i in vapor node j (kg),

$\dot{m}_{i,j}$ = flow rate of specie i at junction j (kg/s),

$\dot{m}_{i,j-1}$ = flow rate of specie i at junction j-1 (kg/s), and

$XN_{i,j}$ = rate of mass transfer of specie i across the interface from the liquid to the vapor at node j (kg/s).

Because of the countercurrent flow scheme used, the flow of liquid at junction j is based on the velocity at the jth node, whereas, for the vapor, flow at junction j is based on the velocity at node j+1.

For the very first liquid node, the flow of liquid

exiting the break in the control rod is calculated using

$$\dot{m}_{i,break} = w_i \rho A_{fail} V_{fail} \tag{3.36}$$

where

$\dot{m}_{i,break}$ = flow rate of specie i leaving the break (kg/s),

w_i = weight fraction of specie i in the rod,

ρ = density of alloy (kg/m^3),

A_{fail} = area of hole in the rod (m^2), and

V_{fail} = velocity at the break, calculated using the rod failure model (m/s).

The liquid flow rates of each specie at each subsequent junction are calculated using

$$\dot{m}_{i,j} = \frac{V_j}{\Delta z_j} m^{\ell}_{i,j} \tag{3.37}$$

where

V_j = velocity of film at node j determined by the liquid film model (m/s),

Δz_j = axial length of node j (m), and

$m_{i,j}$ = mass of specie i in liquid node j (kg).

The flow rates of each specie at each vapor junction are calculated in a slightly different way. The hydrogen and steam flow rates at each junction and the pressure at each node are left as input to VAPOR. VAPOR assumes that each node is at constant pressure throughout the transient. For a given vapor node volume, the ideal gas law states that the total number of moles in the volume is given by

$$n = \frac{pV}{RT} \tag{3.38}$$

The time derivative of Equation (3.38), assuming constant pressure and volume is

$$\frac{\partial n}{\partial t} = -\left(\frac{pV}{RT^2}\right) \frac{dT}{dt} \tag{3.39}$$

Conservation of moles for the node states that

$$\frac{\partial n}{\partial t} = \dot{n}_{in} - \dot{n}_{out} \tag{3.40}$$

where

$\dot{n}_{in}$ = total molar flow of all species into the node (moles/sec), and

$\dot{n}_{out}$ = total molar flow of all species out of the node (moles/sec).

Thus in order for each node to remain isobaric, the total molar flow out of the node, $\dot{n}_{out}$, must be given by

$$\dot{n}_{out} = \dot{n}_{in} - \frac{\partial n}{\partial t} = \dot{n}_{in} + \frac{pV}{RT^2} \frac{dT}{dt} \qquad (3.41)$$

where

$\dot{n}_{in}$ = total molar flow into the volume due to both mass transfer from the liquid film and flow from the adjacent node (moles/s),

V = node volume (m^3),

p = pressure (Pa),

R = gas constant (Pa-m^3/kgmole K),

T = temperature (K), and

$\frac{dT}{dt}$ = local rate of increase of temperature in the volume (K/s).

Thus, Equation (3.41) takes into account both the addition of new vapor into the node and the thermal expansion of the vapor in the node when calculating $\dot{n}_{out}$. The mass flow rate for each specie is then calculated using a donor cell approach,

$$\dot{m}_{i,j-1} = MW_i X_{i,j}^{bulk} \dot{n}_{out} \qquad (3.42)$$

where

$\dot{m}_{i,j-1}$ = flow rate of specie i at junction j-1 (kg/s),

MW_i = molecular weight of specie i (kg/kgmole),

$X_{i,j}^{bulk}$ = mole fraction of specie i in vapor node j, and

$\dot{n}_{out}$ = total molar flow out of node (moles/s).

A slight discrepancy develops when hydrogen and steam flow rates that were calculated assuming no other species were present in the vapor field are used as input to VAPOR. In actual fact, in order to keep constant pressure, those flows would have to change slightly to accomodate the addition of Ag, In and Cd into the gas stream. This is an inherent problem because the control rod vapor release behavior is uncoupled from the overall core thermal hydraulic behavior in this analysis. Implementation of such an

uncoupled approach without appropriate feedback, although justifiable because of its computational simplicity may result in problems such as that described above.

A flowchart of the VAPOR code is shown in Figure 3.8. The code is structured into three main blocks or subprograms: the initialization block, the thermal hydraulic block and the differential equation block. The initialization block reads in all of the code thermal hydraulic input and initializes all the variables. Specifically, VAPOR initializes the mass of hydrogen and steam in each vapor node, seeds the outer surface of the control rod with a small amount of liquid alloy and calculates the initial velocity of the alloy at the break. The seeding allows the liquid film model to work somewhat easier since it does not have to handle the movement of the alloy front as it initially travels down the rod. The thermal hydraulic block of the code calculates thermal hydraulic and transport parameters such as diffusion coefficients, the viscosity and density of the alloy and the hydrogen/steam mixture, Reynolds number of the flow, Schmidt number and the mass transfer coefficients at each node. The differential equation block uses the models described earlier to calculate the flows at all the junctions and set up the

Figure 3.8

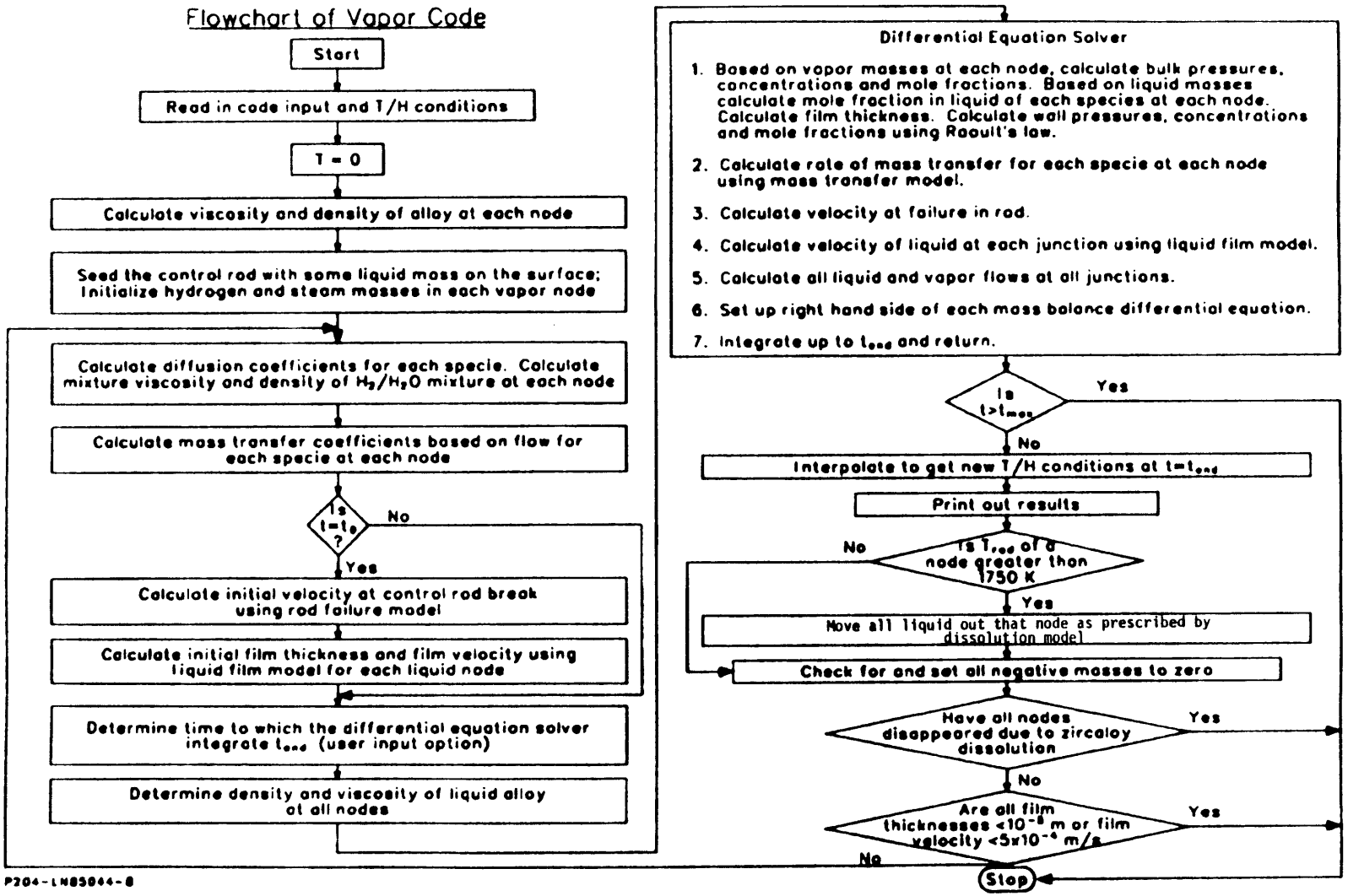
Flowchart of Vapor Code
Start
Read in code input and T/H conditions
T = 0
Calculate viscosity and density of alloy at each node
Seed the control rod with some liquid mass on the surface; Initialize hydrogen and steam masses in each vapor node
Calculate diffusion coefficients for each specie. Calculate mixture viscosity and density of H_2/H_2O mixture at each node
Calculate mass transfer coefficients based on flow for each specie at each node
Is $t=t_0$?
No
Yes
Calculate initial velocity at control rod break using rod failure model
Calculate initial film thickness and film velocity using liquid film model for each liquid node
Determine time to which the differential equation solver integrate t_{end} (user input option)
Determine density and viscosity of liquid alloy at all nodes
Differential Equation Solver
1. Based on vapor masses at each node, calculate bulk pressures, concentrations and mole fractions. Based on liquid masses calculate mole fraction in liquid of each species at each node. Calculate film thickness. Calculate wall pressures, concentrations and mole fractions using Raoult's law.
2. Calculate rate of mass transfer for each specie at each node using mass transfer model.
3. Calculate velocity at failure in rod.
4. Calculate velocity of liquid at each junction using liquid film model.
5. Calculate all liquid and vapor flows at all junctions.
6. Set up right hand side of each mass balance differential equation.
7. Integrate up to t_{end} and return.
Is $t>t_{max}$
Yes
No
Interpolate to get new T/H conditions at $t=t_{end}$
Print out results
No
Is T_{end} of a node greater than 1750 K
Yes
Move all liquid out that node as prescribed by dissolution model
Check for and set all negative masses to zero
Have all nodes disappeared due to zircaloy dissolution
Yes
No
Are all film thicknesses $<10^{-8}$ m or film velocity $<5\times10^{-4}$ m/s
Yes
No
Stop
P204-LN85044-8

right hand side of the mass conservation equations. This result is then fed to the differential equation solver which performs the integration. Upon return from the differential equation solver, VAPOR checks to see if a liquid node has reached stainless steel melting (1723 K). If it has, then, as prescribed by the zircaloy dissolution model, the liquid alloy inside and on the outer surface of the rod at that node is moved to the node beneath it. The analysis is terminated when one of the following conditions are met:

(1) the maximum simulation time, as input by the user, is exceeded.(t_{max} is usually set as the last time point in the thermal hydraulic input);
(2) all nodes beneath the point of rod failure have been liquefied;
(3) the film thickness at all nodes is less than 10^{-5}m (Since seeding the control rod initially resulted in a film thickness on the order of 10^{-4}m such a termination criteria seemed reasonable.); or
(4) the film velocity at all nodes is less 5.0×10^{-4} m/s.

VAPOR can handle up to 10 liquid nodes and 10 vapor nodes with 6 species in the vapor and 4 species in the liquid. Mass balances are performed on each specie in each volume. This yields a maximum of 10*6 + 10*4 = 100 coupled non-linear differential equations. The stiffness of these coupled equations warranted the use of a stiff differential equation solver which was available on the EG&G, Idaho computer system.

The code thermal hydraulic inputs are the wall and gas temperatures at each node, and the flows of hydrogen and steam in the vapor as functions of time. Other user defined inputs include the size of the failure of the control rod, the initial height of the molten alloy reservoir and other relevant geometry such as rod diameter, gas flow area and vapor node volume. The code outputs are the masses, flowrates, liquid film velocity, film thickness and the partial pressure of each species at each node. The most important of these output parameters is the flow out of the top vapor node since this is the vapor source term to the upper plenum which is needed in aerosol calculations. Results of using VAPOR and limitations of the code are presented in the next section. A code listing, sample input and output are found in Appendix B. A table of the material properties needed in the VAPOR code is presented in Appendix C.

3.6 REFERENCES

3.1 White, F.M., Fluid Mechanics, McGraw-Hill, Inc., 1979.

3.2 Gasser, R.D. and Kazimi, M.S., "A Study of Post-Accident Molten Fuel Downward Streaming Through the Axial Shield in the Liquid Metal Fast Breeder Reactor," Nuclear Technology, 33, May 1977.

3.3 Ishii, M., Chen, W.L. and Grolmes, M.A., "Molten Clad Motion Model for Fast Reactor Loss-of-Flow Accidents," Nuclear Science and Engineering , 60, 1976, pp. 435-451.

3.4 El-Genk, M.S. and Moore, R.L., "Transient Debris Freezing and Potential Wall Melting During a Severe Reactivity Initiated Accident Experiment," Nuclear Technology, 53, June 1981, pp. 354-373.

3.5 Collier, J.G., Convective Boiling and Condensation, McGraw-Hill, New York, 1981.

3.6 Bird, R.B., Stewart, W.E. and Lightfoot, E.N., Transport Phenomena, Wiley and Sons, New York, 1960.

3.7 Read, R.C., Praunitz, J.M., and Sherwood, J.M., The Properties of Liquids and Gases, McGraw-Hill, New York, 1977.

3.8 Gates, D. and Thodos, G., "The Critical Constants of the Elements," AIChE Journal, 6, (1), pp. 50-54, March 1960.

3.9 Cronenburg, A.W., Review of Ag-In-Cd Control Rod Behavior Under Class IX Accident Conditions and Model Development, ESA/LANL-104, July 1982.

4. RESULTS USING THE VAPOR CODE

The VAPOR code has been run to investigate the interaction between the physical models used to describe Ag, In and Cd vapor release in a severe reactor accident. This section discusses the results of three sets of simulations. First, a study was performed to understand the dynamic behavior of the liquid film as it travels down the rod. Second, a sensitivity study was conducted to determine those parameters in the VAPOR code which most affect the release of Ag, In and Cd. VAPOR was then run to obtain an experimental prediction of the release of Ag, In and Cd vapor in the PBF SFD 1-4 experiment. This section concludes with a discussion of the uncertainties and limitations of the VAPOR code.

4.1 Study of Control Rod Failure and Liquid Film Behavior

The total release of control rod vapor in a severe reactor accident depends on the rate of downward relocation of the Ag-In-Cd alloy to cooler portions of the core. The purpose of this study is to understand the behavior of the alloy as it leaves the control rod and travels down the outside of the guide tube. The rod

failure model and the liquid film model presented in Section 3 imply that the size of the hole in the control rod, A_{fail}, is the parameter which has the most influence on alloy dynamics. The area of the failure in the control rod is somewhat difficult to determine exactly. Because of the chemical interactions between the zircaloy, silver and indium, the hole size would probably increase during drainage. As a result, it is a natural variable to study parametrically. Three different hole sizes were used in the study: $10^{-6}m^2$, $10^{-5}m^2$ and $10^{-4}m^2$. These holes correspond to circles of about 1 mm, 3 mm and 1 cm in diameter.

A two second simulation was run to determine how the film thickness and velocity vary with changes in A_{fail}. The geometry for this parametric study consisted of a 0.8 m long control rod guide tube (see Figure 3.1) in its own flow channel. A constant 50/50 molar mixture of hydrogen and steam at 6.9 MPa (1000 psi) flowed over the guide tube surface. Control rod failure was assumed to occur 0.5 m from the top of the rod. As a result, three axial nodes (each of length 0.1 m) were used in the calculation with three species in the liquid (Ag, In and Cd) and five species in the vapor (Ag, In, Cd, H_2, and H_20). Additional details of the geometry and thermal hydraulic conditions are

presented in Table 4.1.

As shown in Figures 4.1 and 4.2, the film thickness, δ, and the velocity, V_1, at node 1 show large variations with changes in A_{fail}. (Plots of V and δ for nodes 2 and 3 show similar behavior except at slightly later times. Hence for brevity, the results are not plotted.) These large variations can be explained by examining the control rod drainage time as a function of hole size. Hole sizes of 10^{-6}, 10^{-5}, and 10^{-4} m^2 result in rod drainage times of approximately 60, 5 and 0.5 seconds respectively. For the large size hole ($10^{-4}m^2$), inertial effects that were neglected in the rod failure model (dV/dt = 0) would tend to increase the drainage time slightly. Nevertheless, very rapid drainage predicted for the large hole causes a very rapid release of the liquid alloy. As a result, the film thickness plotted in Figure 4.1 increases very rapidly in a delta function fashion. However, since no more alloy is exiting the break after 0.5 seconds, the film thickness and velocity at node 1 decrease as the liquid flows by gravity down the rod. For the rod with the small hole (10^{-6} m^2), since the rod drainage time (30 sec) is much longer than the simulation time (2 sec), the mass flux of material leaving the break is almost constant. Hence, a gradual

TABLE 4.1
GEOMETRTY AND THERMAL HYDRAULIC INPUT
FOR LIQUID FILM STUDY

Parameter	Value
Flow area, A_{flow}	4.72e-05 m^2 [a]
Axial length of node, ΔZ	1.00e-01 m
Volume of node, V	4.72e-06 m^3
Surface area of liquid node, SA	3.85e-03 m^2
Equivalent diameter, D_e	4.91e-02 m
Rod outer diameter, D_{rod}	1.22e-02 m
Rod inner diameter, D_{in}	1.14e-02 m
Initial height of alloy above the break, h_0	5.00e-01 m
Time step	1.00e-01 s
Rod and Coolant Temperatures	
Rod Node 1	Linearly increase at a rate of 50 K/s from 1800 to 1910 K
Coolant Node 1	T_{rod} Node 1 + 10 K
Rod Node 2	T_{rod} Node 1 + 20 K
Coolant Node 2	T_{cool} Node 1 - 20 K
Rod Node 3	T_{rod} Node 1 - 40 K
Coolant Node 3	T_{cool} Node 1 - 40 K
Flow of H_2	1.04e-03 g/s
Flow of H_2O	9.38e-03 g/s

a. means 4.72 x 10^{-5} m^2

Figure 4.1

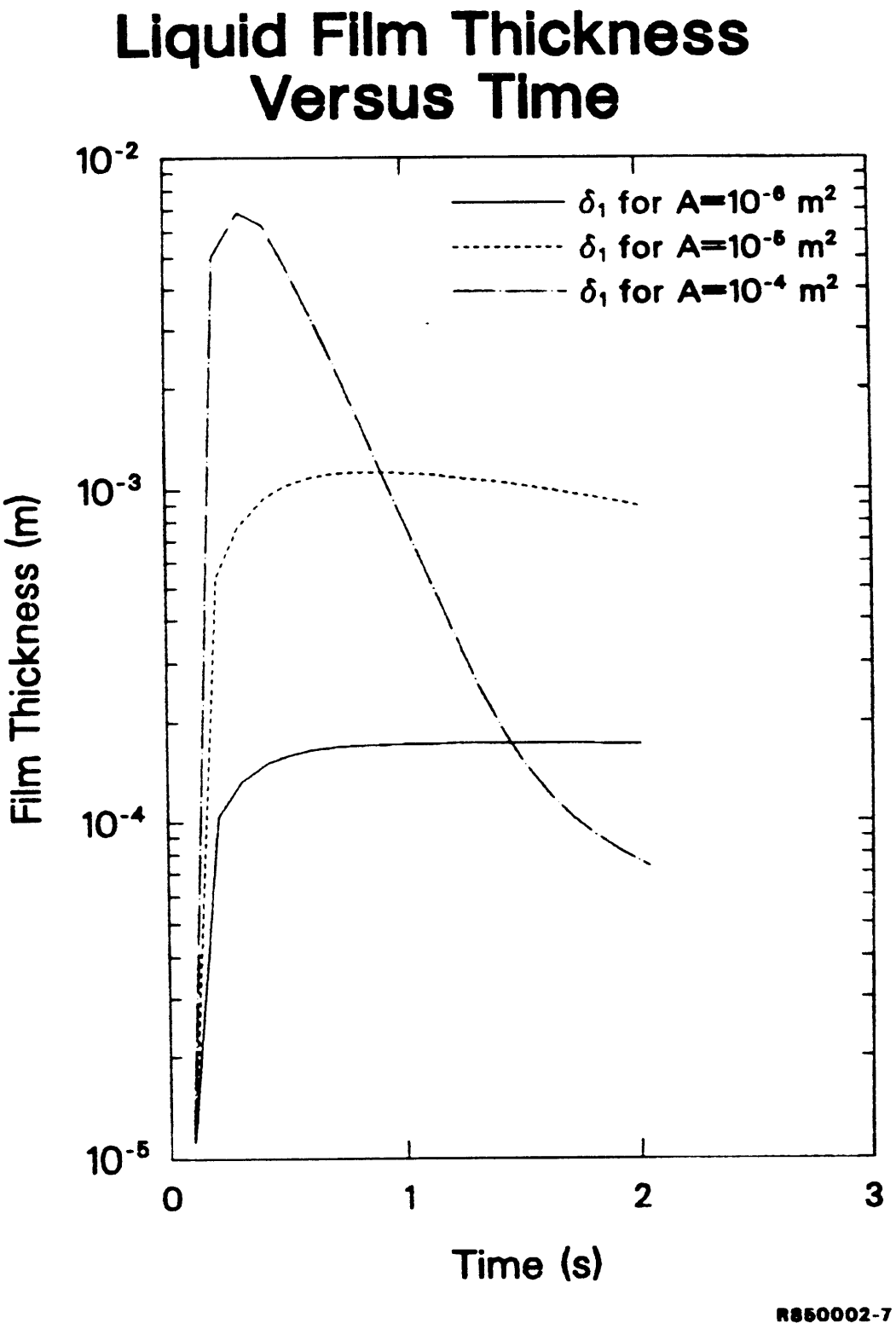
Liquid Film Thickness Versus Time
10^{-2}
10^{-3}
10^{-4}
10^{-5}
Film Thickness (m)
δ_1 for A=10^{-6} m^2
δ_1 for A=10^{-5} m^2
δ_1 for A=10^{-4} m^2
0
1
2
3
Time (s)
R850002-7

Figure 4.2

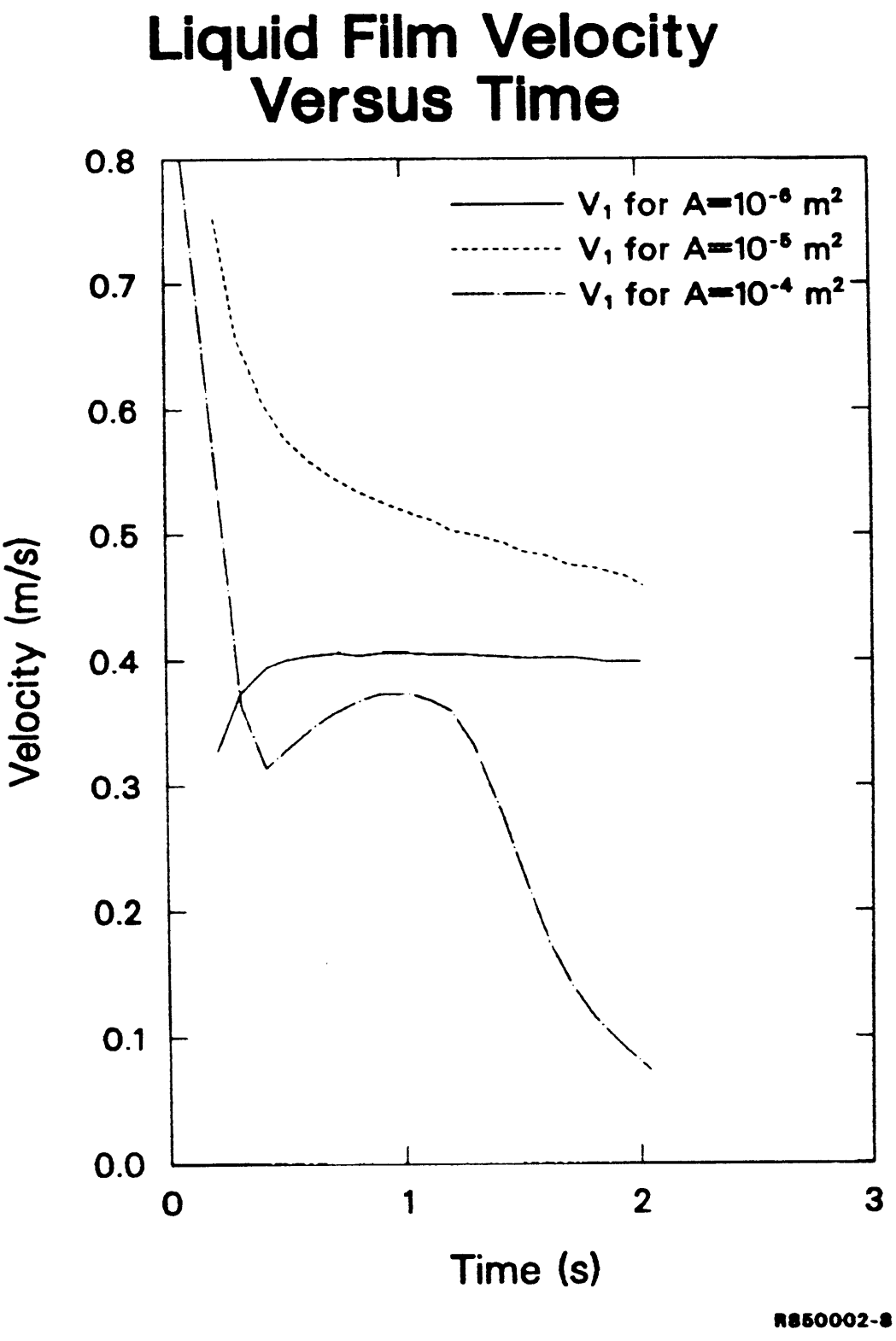
Liquid Film Velocity Versus Time
0.8
0.7
0.6
0.5
0.4
0.3
0.2
0.1
0.0
Velocity (m/s)
0
1
2
3
Time (s)
V1 for A=10-6 m2
V1 for A=10-5 m2
V1 for A=10-4 m2
R850002-8

buildup in both film thickness and velocity is observed and a quasi-steady state is obtained. For the 10^{-5} m^2 size failure, since the drainage time is on the order of the simulation time, the results fall between the previous two extremes. The rapid increase in film thickness and the large initial velocity are attributed to buildup of material in the node from the break. However, since less and less material leaves the break each second, the velocity begins to decrease. Beyond 1.2 seconds, more material is exiting the node as a result of gravity than is being supplied from the break which causes the film thickness of the alloy to decrease.

The difference in the dynamic behavior of the alloy in the three cases can be generalized by examining the time scale for drainage relative to the simulation time. In all cases, the behavior of the alloy can be described by a buildup phase in which material from the break flows onto the rod and a drainage phase in which gravity causes the alloy to run down the rod. Initially, the buildup phase will dominate the alloy behavior. This will be followed by a period of time in which both buildup and drainage are occuring at roughly the same rate. Neither process dominates during this transition phase. Rather, the alloy dynamics are determined by a

superposition of these two processes. At later times, the drainage phase will dominate the alloy behavior.

The rate at which buildup and drainage occur and the timing of each phase are functions of the hole size. For large sized holes, rapid drainage causes the alloy dynamics to change continuously. Buildup and drainage occur very rapidly and very close together in time. For small sized holes, buildup and drainage occur much more slowly and dominate at distinctly different times. The two phases are separated by a quasi-steady period in which the buildup and drainage balance. For drainage times on the order of 5 seconds, the buildup phase is fast but not quite as rapid as the large size hole case. Although the film thickness levels off, it difficult to define a quasi-steady state since the velocity is continually decreasing with time. By the end of the simulation, the drainage phase is just starting to dominate as evidenced by the decrease in film thickness. Had the simulation continued for ten seconds, then alloy behavior similar to the case of the large size hole would have been observed, except that the time scale would have been longer and the rate of buildup and drainage would have been less. Thus, the results of this study suggest that the area of the hole in the control rod determines the time constant and the magnitude of

the buildup and drainage behavior in the liquid film system.

4.2 Sensitivity Study

The VAPOR code was used to conduct a sensitivity study to determine the effect that certain key variables and assumptions have on the release of Ag, In and Cd in severe reactor accidents. Specifically, the release of these control rod vapors was thought to be most sensitive to system pressure and system flow. Moreover, these variables were selected because the effect of changes in them could be correlated most directly to different accident sequences in LWRs.

The test matrix shown in Table 4.2 lists the high and low values of system pressure and system flow that were used in the sensitivity study. Based on this 2x2 matrix, four different cases could be considered:

(1) a high pressure/high flow simulation (HPHF),

(2) a high pressure/low flow simulation (HPLF),

(3) a low pressure/high flow simulation (LPHF),and

(4) a low pressure/low flow simulation (LPLF).

In addition to these parameters, the Cd vapor release was thought to be very sensitive to the assumption that the partial pressure of cadmium at the liquid surface

TABLE 4.2

TEST MATRIX FOR SENSITIVITY STUDY

Variable	High Value	Low Value
System Pressure	1000 psi	250 psi
System Flow	1.5 g/s H_2O	0.3 g/s H_2O
	0.1667 g/s H_2	0.0333 g/s H_2

obeyed Raoult's law. Thus, another case was added to the sensitivity study. This simulation was run at high pressure and low flow. However, to test the sensitivity to Raoult's law, the partial pressure of Cd was calculated using

$$P_{Cd} = P_{Cd} * Y * 10$$

In other words, for this case, cadmium would artifically exert a partial pressure at the surface of the liquid ten times greater than that predicted by Raoult's law. Each simulation in the sensitivity study lasted for twenty seconds. The geometry of the control rod and the core nodalization were similar to that used in the liquid film study. Details of the geometry and thermal hydraulic input are presented in Table 4.3.

The effects that system flow and pressure have on vapor release can be better understood by examining the following simple model. A liquid vaporizes into a volume of size Y m^3. The concentration of the vapor at the liquid surface is maintained at C_0 kg/m^3. A carrier gas flows over the liquid surface and transports the vapor out of the volume at a rate of Q m^3/s. Initially, the carrier gas contains no vapor.

A mass balance on the vapor in the volume yields

TABLE 4.3
GEOMETRTY AND THERMAL HYDRAULIC INPUT
FOR SENSITIVITY STUDY

Parameter	Value
Flow area, A_{flow}	8.46e-04 m^2 [a]
Axial length of node, ΔZ	1.00e-01 m
Volume of node, V	8.46e-05 m^3
Surface area of liquid node, SA	3.83e-03 m^2
Equivalent diameter, D_e	1.13e-02 m
Rod outer diameter, D_{rod}	1.22e-02 m
Rod inner diameter, D_{in}	1.14e-02 m
Area of hole, A_{fail}	1.00e-05 m^2
Initial height of alloy above the break, h_0	5.00e-01 m
Time step	1.00 s
Rod and Coolant Temperatures	
Rod Node 1	Linearly increase at a rate of 5 K/s from 1800 to 1910 K
Coolant Node 1	T_{rod} Node 1 + 10 K
Rod Node 2	T_{rod} Node 1 + 20 K
Coolant Node 2	T_{cool} Node 1 - 20 K
Rod Node 3	T_{rod} Node 1 - 40 K
Coolant Node 3	T_{cool} Node 1 - 40 K

a. means 8.46 x 10^{-4} m^2

$$Y \frac{dC}{dt} = h_D S(C_0 - C) - CQ \qquad (4.1)$$

where

C = concentration of vapor in volume (kg/m^3),

C_0 = concentration of vapor at the liquid surface (kg/m^3),

h_D = mass transfer coefficient (m/s),

S = surface area of liquid (m^2),

Y = volume (m^3), and

Q = volumetric flow rate (m^3/s).

Equation (4.1) indicates that the concentration of vapor in the volume, C, is determined by a balance between the rate of diffusion into the volume and the rate of convection out of the volume. Integration of Equation (4.1) subject to the initial condition $C = 0$ at $t = 0$ gives

$$\frac{C}{C_0} = \frac{h_D S}{h_D S + Q} \left(1 - \exp\left(-\frac{h_D S + Q}{Y} t\right)\right) \qquad (4.2)$$

If rate coefficients for diffusion and convection, a_1

and a_2, are defined to be

$$a_1 = \frac{h_D S}{V} \qquad \text{and} \qquad a_2 = \frac{Q}{V}$$

then Equation (4.2) becomes

$$\frac{C}{C_0} = \frac{a_1}{a_1+a_2} \left[1 - \exp(-(a_1+a_2)t)\right] \tag{4.3}$$

The release rate of vapor out of the volume is then given by

$$R = CQ = C_0 V \frac{a_1 a_2}{a_1+a_2} \left(1 - \exp(-(a_1+a_2)t)\right) \tag{4.4}$$

In steady state, this expression becomes

$$R_{SS} = C_0 V \left(\frac{a_1 a_2}{a_1+a_2} \right) = \frac{C_0}{\frac{1}{h_D S} + \frac{1}{Q}} = \frac{C_0}{A} \tag{4.5}$$

The effect of changes in the rate of diffusion and

convection on the release of vapor can now be assessed. As seen in Equation (4.5), the release rate is defined as the vapor surface concentration, C_0, divided by an effective rate coefficient, A. This result is exactly analogous to the flow of electricity in the electric circuit. The release rate can be thought of as the electric current and the concentration C_0 is comparable to the potential difference. As a result, the effective rate coefficient represents the overall resistance to mass transfer. The diffusional resistance ($1/h_DS$) and the resistance due to convection out of the volume ($1/Q$) operate in series to determine the overall resistance.

When the rate of convection is much greater than the rate of diffusion ($a_2 >> a_1$), the release rate is insensitive to flow and is controlled totally by diffusion, i.e.,

$$R = C_0 h_d S \tag{4.6}$$

However, if diffusion from the surface greatly exceeds convection out of the volume ($a_1 >> a_2$) then the vapor release rate is independent of the rate of diffusion and is controlled entirely by convection. Hence,

$$R = C_0 Q \qquad (4.7)$$

When neither process is dominant, the result falls between these two extremes as given by Equation (4.5).

This simple model can be used to explain the results of this sensitivity study. As shown in Table 4.4, an increase in system flow causes an increase in the cadmium release. The increased flow convects more vapor out of the volume. In addition, the flow increase reduces the vapor concentration in the volume which causes the rate of mass transfer to increase. However, since diffusion and convection operate in series, the integrated release of Cd only increases by a factor of 1.2 when system flow increases by a factor of 5. Thus, the vapor release is not very sensitive to system flow.

The integrated release is much more sensitive to system pressure than system flow. A factor of 4 decrease in pressure produces a factor of 3 increase in the cadmium release. Two effects account for this behavior. First, since diffusion coefficients vary inversely with pressure, the rate of diffusion is higher at low pressure than at high pressure. Second, the absolute molar flux from the liquid surface increases as pressure decreases. The molar flux of specie i is

TABLE 4.4

CADMIUM RESULTS FROM THE SENSITIVITY STUDY

	High Flow	Low Flow
High Pressure	2.319 %	2.253 %
Low Pressure	7.570 %	7.157 %

High Pressure/Low Flow with change in Raoult's Law = 24.8 %.

proportional to x_i^w, the mole fraction of specie i at the liquid surface. As a result, for a given partial pressure at the liquid surface, the mole fraction and therefore the molar flux are larger at low pressure than at high pressure. Both of these effects result in larger vaporization rates at low pressure and hence larger releases. Once again, the non-linear sensitivity indicates that convection and diffusion operate in series.

The release of cadmium is very sensitive to the assumption that the alloy obeys Raoult's law. Artificially increasing the partial pressure of Cd at the liquid surface by a factor of 10 results in a factor of 10 increase in the integrated release. In light of the linear behavior exhibited here, a more detailed discussion of the appropriateness of the Raoult's law assumption is needed.

Raoult's law is basically a statement about the interactions between various constituents in a solution. If the various constituents in a solution or liquid alloy obey Raoult's law, then there is an attraction between the constituents which results in a vapor pressure reduction over the liquid. However, not all solutions obey Raoult's law. In fact, intermolecular forces within a liquid may cause strong

deviations from Raoult's law by factors ranging from 10^{-5} to 10^{2} [4.1]. In addition, Raoult's law is more likely to be valid when trying to predict the vapor pressure behavior of those constituents that make up a large fraction of the solution. Hence, the small mole fraction of Cd in the alloy (5 wt. %) suggests that cadmium could exhibit deviations from Raoult's law.

Powers [4.2] has also examined the validity of modeling the alloy as ideal. Based on experimental data from the three binary systems Ag-In, Cd-In and Ag-Cd, Powers has formulated a model for the ternary Ag-In-Cd system. His results indicate that Raoult's law can be used to describe the vapor pressure behavior of cadmium over the alloy. However, the model used by Powers considers only pairwise interactions between each constituent in the alloy. Ternary interactions are not accounted for. It is difficult to judge the importance of ternary interactions in the alloy. Thus, although the assumption of ideality appears reasonable, until an experiment is conducted to determine the vapor pressure behavior of the alloy, the Raoult's law assumption continues to be one of the largest uncertainties in the VAPOR model.

This sensitivity study has also shown that the release of Ag, In and Cd vapor is quite small. At

1000 psi, only 2% of the Cd is released; at 250 psi 7% is released. Since the Ag and In are much less volatile than Cd, their release is much less than 1%. The major reason for these low release values is that most of the alloy is flowing down the rod rapidly and leaving the system as liquid. Thus, although the release rate of Cd vapor is high (0.06 - 0.1 g/s), the residence time of the alloy in the system is small, usually less than one minute. The rapid relocation of the control rod alloy down to cooler portions of the core results in a small release of the alloy vapors at high pressure.

As a result of this sensitivity study, the following conclusions can be drawn.

(1) System pressure is an important variable which affects the release of Ag, In and Cd in severe reactor accidents. In low pressure accident sequences, like V and AH, the vapor release will be greater than the release for high pressure sequences like S_2D and TMLB'.
(2) System flow is not an important variable in the overall release process.
(3) The release of Cd is very sensitive to the assumption that the alloy vapor pressure behavior can be described by Raoult's law. Experimental work needs to be done to determine if the assumption is valid.
(4) The rapid relocation of the alloy down the rod to cooler portions of the core results in a small residence time (typically less than a minute) for the alloy in the system and hence a small vapor source term, as long as impedements like grid spacers do not significantly delay the alloy flow.

4.3 Experimental Prediction of the PBF SFD 1-4 Test

The VAPOR code has been run to estimate the release of Ag, In and Cd vapor in the PBF SFD 1-4 experiment. The PBF SFD 1-4 experiment is the last in a series of tests conducted by EG&G Idaho at the Power Burst Facility (PBF). The purpose of these tests is to understand fuel behavior as well as fission product release, deposition and transport, and hydrogen generation under severely degraded conditions. A more complete description of the test is found in Section 8. Additional details of the experiment are found in Reference 4.3

The thermal hydraulic input needed to run the VAPOR code was provided by SCDAP (Severe Core Damage Analysis Package) experimental predictions of the SFD 1-4 experiment [4.4]. Specifically, the VAPOR code requires the control rod and bulk coolant temperatures, the bundle average flows of hydrogen and steam and the rate of addition and depletion of hydrogen and steam in the bundle as functions of axial elevation and time. SCDAP provides thermal hydraulic output for the whole transient. However, only a limited portion of the output is needed for the VAPOR calculation. All thermal hydraulic input to VAPOR begins at 8065.5 seconds, the time at which the first control rod axial node reaches

stainless steel melting (1723 K), and ends at 8188 seconds. This corresponds to 50 time channels of output from SCDAP which is the maximum amount of input VAPOR can handle. This is not a limitation, however, since most of the control rod dynamics should be finished by 8188 seconds.

The geometry of the PBF bundle shown in Figure 4.3 is needed as input to the VAPOR code. The analysis assumes quarter core symmetry. As a result, all flow input is scaled down by 0.25. Since SCDAP predicts stainless steel melting at node 4, (halfway up the rod) the three axial nodes (each 0.125 m long) below this elevation were used in the analysis. Details of the input to the VAPOR code are shown in Table 4.5.

Since SCDAP does not currently model axial heat conduction in the control rods, it was felt that the predictions of large axial temperature gradients in the control rod were somewhat unrealistic. Hence, two different cases were considered for analysis. Case 1 used all the thermal hydraulic output "as is" from SCDAP. For Case 2, the control rod temperatures were changed to smooth out the unrealistic axial temperature gradients predicted by SCDAP. The temperature at node 4 was unchanged. The following estimates were used for the remaining three nodes:

Figure 4.3

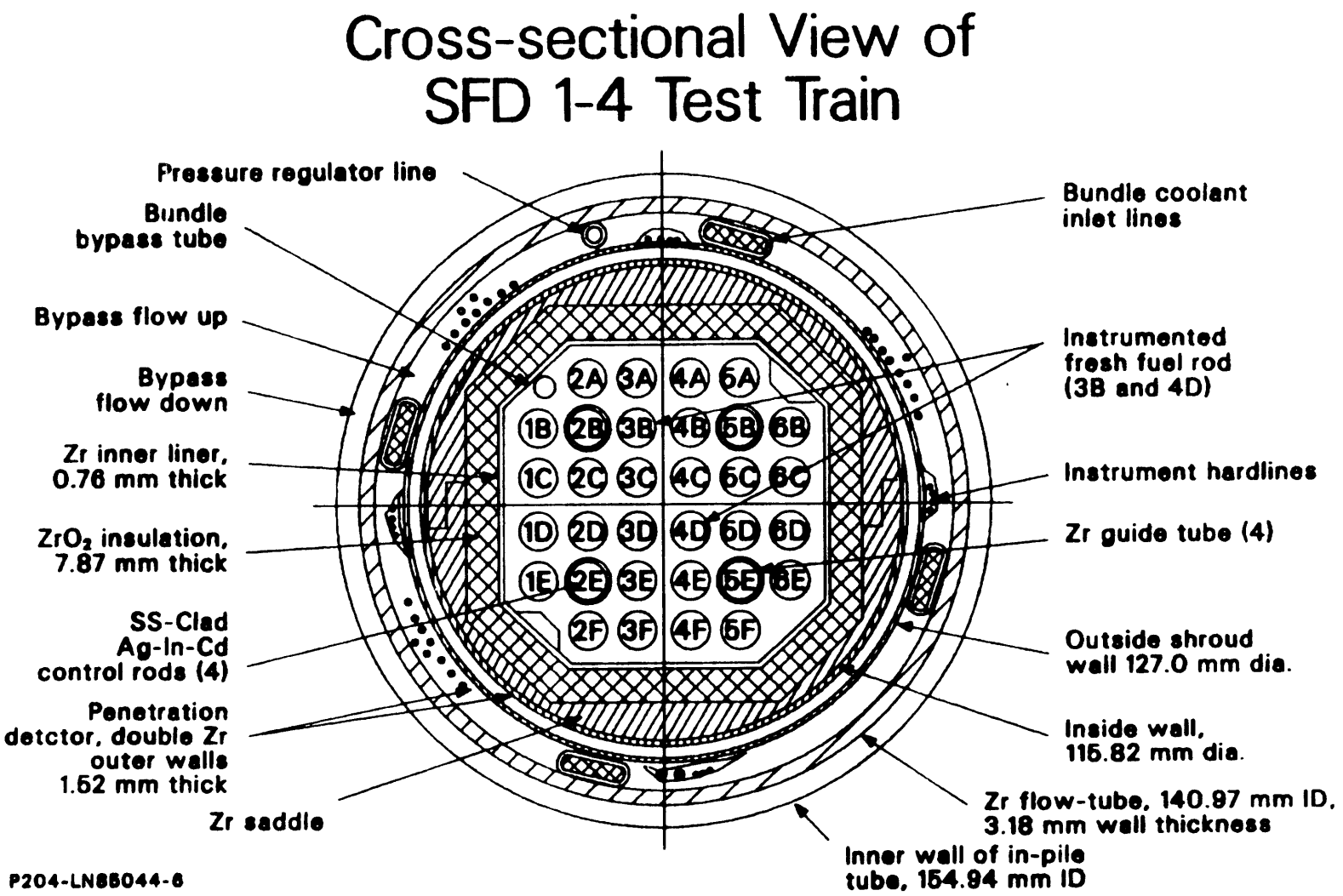
Cross-sectional View of
SFD 1-4 Test Train
Pressure regulator line
Bundle
bypass tube
Bypass flow up
Bypass
flow down
Zr inner liner,
0.76 mm thick
ZrO_2 insulation,
7.87 mm thick
SS-Clad
Ag-In-Cd
control rods (4)
Penetration
detctor, double Zr
outer walls
1.52 mm thick
Zr saddle
Bundle coolant
inlet lines
Instrumented
fresh fuel rod
(3B and 4D)
Instrument hardlines
Zr guide tube (4)
Outside shroud
wall 127.0 mm dia.
Inside wall,
115.82 mm dia.
Zr flow-tube, 140.97 mm ID,
3.18 mm wall thickness
Inner wall of in-pile
tube, 154.94 mm ID
2A 3A 4A 5A
1B 2B 3B 4B 5B 6B
1C 2C 3C 4C 5C 6C
1D 2D 3D 4D 5D 6D
1E 2E 3E 4E 5E 6E
2F 3F 4F 5F
P204-LN85044-6

TABLE 4.5
PBF TEST SFD 1-4 GEOMETRICAL INPUT TO THE VAPOR CODE

Parameter	Value
Flow area, A_{flow}	8.46e-04 m^2 [a]
Axial length of node, ΔZ	1.25e-01 m
Volume of node, V	1.06e-04 m^3
Surface area of liquid node, SA	4.81e-03 m^2
Equivalent diameter, D_e	1.13e-02 m
Rod outer diameter, D_{rod}	1.22e-02 m
Rod inner diameter [b], D_{in}	8.74e-03 m
Area of hole, A_{fail}	1.00e-05 m^2
Initial height of alloy above the break [c], h_0	4.66e-01 m

a. means 8.46×10^{-4} m^2
b. This is the inner diameter of the stainless steel clad. It is assumed that on melting the alloy will fill the gap.
c. This initial height reflects the fact that the alloy has relocated somewhat on melting. Thus h_0 is not equal to 0.5 m.

TCROD(Node 3)= TCROD(Node 4) - 100 K,

TCROD(Node 2)= TCROD(Node 4) - 200 K, and

TCROD(Node 1)= TCROD(Node 4) - 300 K.

These temperatures should provide a more realistic estimate of the release of Ag, In and Cd vapor.

The Ag, In and Cd release rate predictions for Cases 1 and 2 are shown in Figures 4.4 and 4.5. Note that these are release rates per rod and should be multiplied by 4 to obtain total release rates from the bundle. The low integrated releases in Table 4.6 are due to three factors:

(1) the release is occuring before the expected peak temperature (2400 K) of the transient is reached;
(2) mass transfer is less at high pressure since diffusion coefficients decrease as pressure increases; and
(3) since the relocation of the alloy down to cooler portions of the rod and into the lower plenum is quite rapid, the residence time for the alloy in the system is small.

The large control rod axial temperature gradients that are predicted by SCDAP and used in the Case 1 analysis are unrealistic because the calculation neglected the effect of axial conduction. As a result, the releases from the Case 2 analysis should be used as a best estimate source term.

4.4 Uncertainties and Limitations of the VAPOR Code

Sources of uncertainty in each of the four models

Figure 4.4

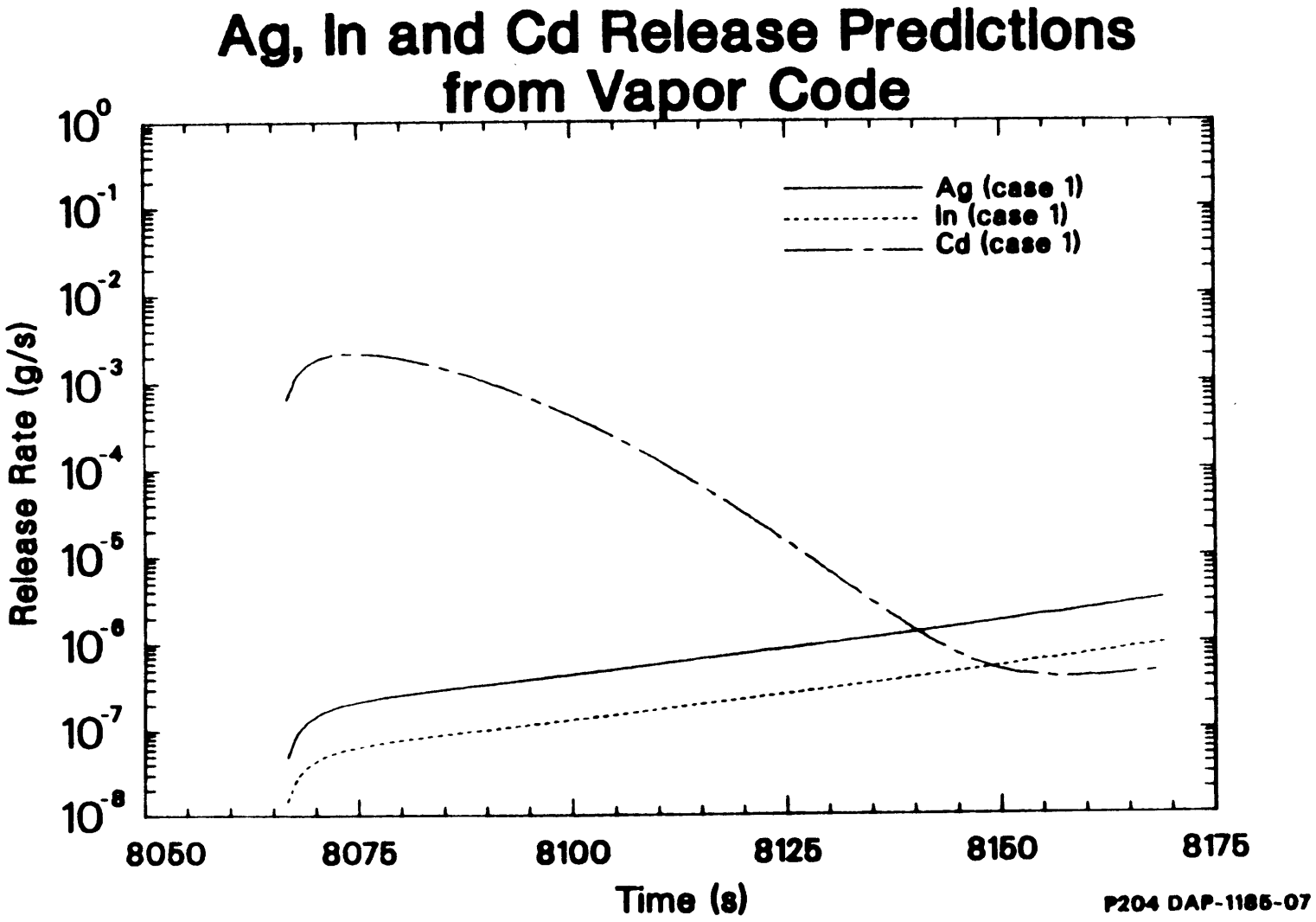

(Note: Time corresponds to SCDAP results in reference 4.4)

Figure 4.5

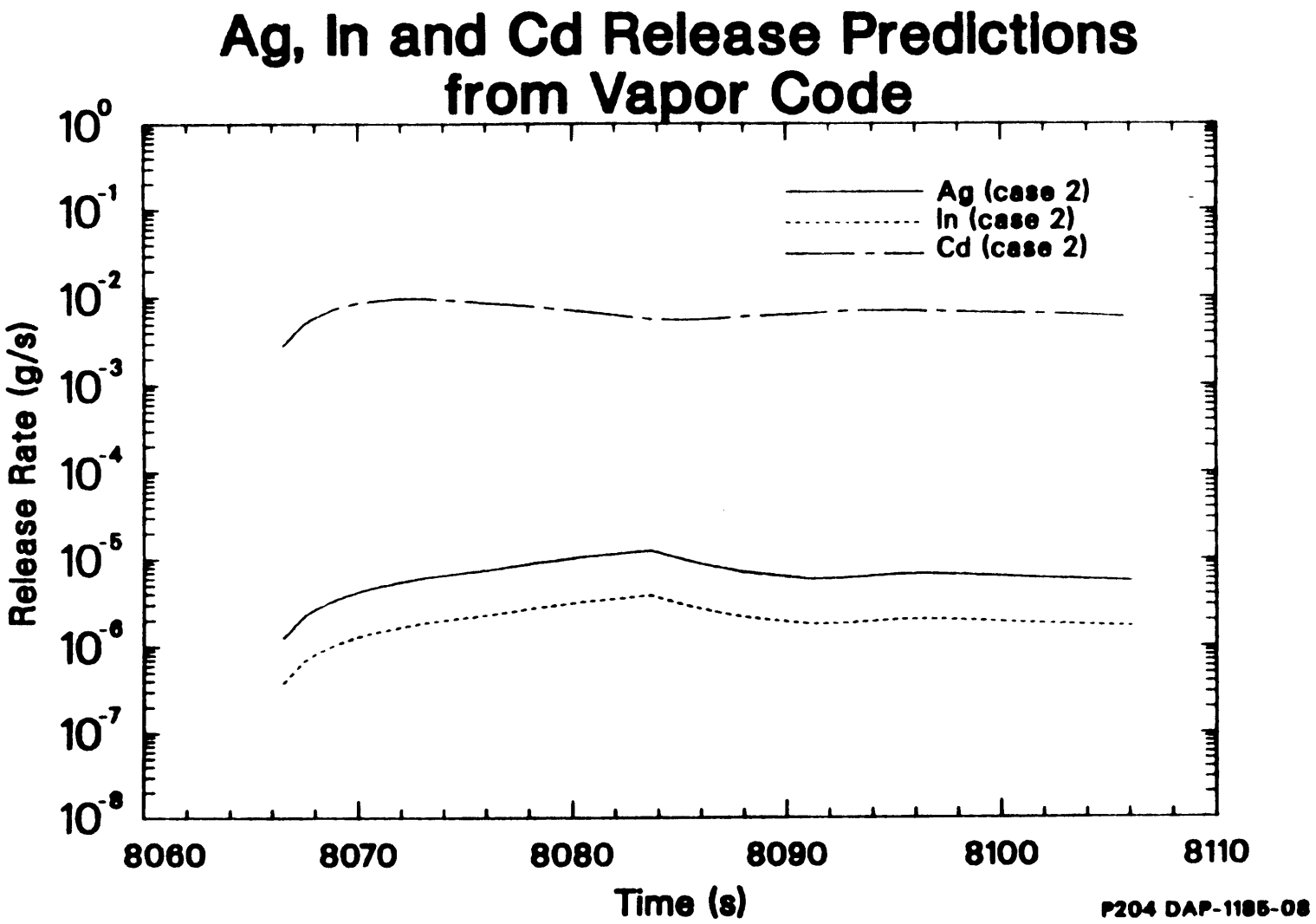

(Note: Time corresponds to SCDAP results in reference 4.4)

TABLE 4.6

INTEGRATED RELEASE PREDICTIONS OF

AG, IN AND CD

FOR PBF TEST SFD 1-4

	Percent Released	
	Case 1	Case 2
Ag	2.28e-05[a]	5.87e-05
In	4.64e-05	9.54e-05
Cd	2.24e-01	1.235

a. means 2.28×10^{-5}

used in the VAPOR code arise both from the use of simple engineering models to describe complex physical processes and from a lack of information about basic physical properties. The purpose of this section is to present the major sources of uncertainty in each of the models, to suggest areas where improvement is needed, and to discuss the limitations of the VAPOR code imposed by the modeling assumptions.

In the rod failure model, the size of the hole in the control rod guide tube, A_{fail}, is unknown and probably will increase as a function of time because of the dissolution of zircaloy by Ag and In. As shown in Section 4.1, the hole size has a major impact on the dynamics of the liquid alloy as it travels down the outer surface of the guide tube. Fortunately, since a reasonable value of 10^{-5} m^2 for the size of the hole could be obtained using engineering judgement, this source of uncertainty was judged to small compared to others in the VAPOR code.

Since the VAPOR code was developed primarily for predicting the release of control rod vapors in a high system pressure environment, the rod failure model does not describe the bursting behavior of the guide tube expected a low system pressures. The inclusion of a model to describe the bursting of the rod and the

subsequent dispersal of the alloy as well as the additional vaporization would increase the versatility of the code.

The physical properties used to calculate the thickness and velocity of the liquid film are subject to uncertainty. The values used for the viscosity and density of the Ag-In-Cd alloy are not temperature dependent. The viscosity of the alloy, given in Appendix C, is that of pure silver at its melting point. Very little data exist for the viscosity of molten indium and cadmium. Moreover, it is not clear how to estimate the viscosity of the ternary alloy even if the viscosity of each component is known. However, since the alloy is mainly composed of silver, the value used in VAPOR seems reasonable. Once again, these uncertainties were judged to be small in comparison to others present in the model.

The liquid film model assumes that the alloy covers the total surface of the control rod guide. Although such an assumption appears reasonable and is used in many core meltdown models, it is only an approximation. The melting and relocation of the alloy is inherently a two dimensional problem. The thickness and velocity of the alloy will vary both axially and azimuthally. Providing an accurate description of this complex

behavior is very difficult. However, the azimuthal symmetry assumption results in a conservative estimate of the release of Ag, In and Cd vapor since it produces the largest surface-to-volume ratio for the alloy as it travels down the rod. In addition, the effect that grid spacers would have on the downward relocation and vaporization behavior of the alloy has not been modeled. The grid spacers could delay the downward flow of the alloy. Moreover, they might retain some of the alloy and act as a surface from which additional vaporization could occur.

The major uncertainties in the mass transfer model deal with accurately describing the rate of vaporization of the alloy as it travels down the control rod guide tube. In laminar flow, the rate of mass transfer is directly proportional to the diffusion coefficient. Currently, the mass transfer model assumes that the diffusion coefficient of a specie varies inversely with pressure. This behavior, as predicted by Chapman-Eskong theory, is valid only at low pressures. Reference 4.5 states that insufficient data exist at high pressure to give a definitive recommendation on how to resolve the problem. At most, using the inverse pressure relationship would result in a factor of two uncertainty in the estimate of the diffusion coefficient. In

addition, the alloy is currently modeled as an ideal solution. As discussed in Section 4.2, the validity of this assumption is open to question. The sensitivity study suggests that the release of Cd is very sensitive to the vapor pressure at the surface of the alloy. Thus, the overall effect of these two uncertainties is to increase the rate of vaporization of all three species from the alloy, possibly by a factor of two to ten. Clearly, this is one of the major sources of uncertainty in the release of Ag, In and Cd vapor.

The last major source of uncertainty is attributed to the zircaloy dissolution model. Modeling the degradation behavior of the control rod alloy below the point of failure is very difficult because little is known about the rates of chemical interaction between the Ag, In, stainless steel and zircaloy. If zircaloy is dissolved by Ag and In, then the freezing point of the solution would be considerably higher than that of Ag-In-Cd. As a result, the material would tend to freeze earlier and at higher positions on the rod than pure Ag-In-Cd. On the other hand, since eutectics can form between zircaloy and stainless steel as low as 1337 K, alloying between the zircaloy and stainless steel at locations below the initial failure could occur at temperatures below the 1773 K value used in the zircaloy

dissolution model. This effect would tend to accelerate destruction of the control rod. In addition, the inhibiting effect that a ZrO_2 layer on the surface of the cladding has on the potential chemical reaction is unknown at this time. All of these interactions could affect the timing and the extent of control rod degradation and vapor release in a severe reactor accident. As a result, the dissolution model can only be considered empirical at best. Additional information about the potential chemical interactions needs to be obtained to reduce the uncertainty associated with the degradation behavior of the lower intact portion of the control rod.

The VAPOR code was developed to model Ag, In and Cd vapor release from the PBF SFD 1-4 experiment. The test had some unique features which allowed some simplifying assumptions to be made. However, as a result, the code has certain limitations which impact its potential application to severe LWR accidents. The current formulation of the VAPOR code does not use an energy balance to determine the temperature of the alloy as it travels down the rod. Instead, the alloy is assumed to reach the local temperature of the guide tube instantaneously. In addition, since the entire length of the control rod is assumed to be above the freezing

point of the alloy and changes in the alloy freezing behavior due to zircaloy dissolution are neglected, no refreezing is modeled. This approach was adopted for computational simplicity since a proper energy balance on the alloy would require detailed modeling of the oxidation of the guide tubes, axial conduction in the alloy and boiloff of the coolant. This level of detail could only be provided by a core heatup code like SCDAP and hence was beyond the scope of this work. Moreover, such detail was not required to model control rod behavior in PBF Test SFD 1-4.

This uncoupled approach may be inappropriate to predict the release of Ag, In and Cd vapor in a severe reactor accident. At the time the control rod fails in a power reactor the lower portion of the core could be below the melting point of the alloy and might be covered with water. As a result, an explicit energy balance for the alloy would be needed to model its refreezing as it travels down the rod. It is recommended that the VAPOR code be integrated into a core heatup code like SCDAP in order to model these potential interactions.

After control rod failure, the Ag-In-Cd alloy is expected to relocate rapidly to cooler portions of the core where it is will refreeze and cease to be a vapor

source. The behavior of the control rod alloy after substantial core degradation has occurred is not very well known and hence is not modeled in VAPOR. The complex changes in core geometry after melting of core material make it difficult to predict the potential interaction between the hot molten core material and the refrozen alloy. Incorporating the VAPOR code into SCDAP would allow some investigation of the potential interactions between molten core material and control rod alloy.

The purpose of this section was to discuss uncertainties and limitations of the VAPOR code in an attempt to indicate the type of improvements that are needed to make the code more versatile. Despite its limitations, the VAPOR code is a simple yet mechanistic attempt to describe Ag, In and Cd vapor release in a severe reactor accident. It provides an excellent framework upon which some of the changes described above can be implemented.

4.5 REFERENCES

4.1 Wichner, R.P. and Spence, R.D., Quantity and Nature of LWR Aerosols Produced in the Pressure Vessel During Core Heatup Accidents - A Chemical Equilibrium Estimate, NUREG/CR 3181.

4.2 Powers, D.A., Behavior of Control Rods During Core Degradation I. Pressurization of Silver-Indium-Cadmium Control Rods, SAND85-0469, February, 1985.

4.3 Martinson, Z.R., PBF Severe Fuel Damage Test SFD 1-3 and 1-4 Experimental Operating Specifications, July 1984.

4.4 Gasparini, M., PBF Severe Fuel Damage Test Series Test SFD 1-4 Experiment Prediction, July 1984.

4.5 Read, R.C., Praunitz, J.M., and Sherwood, J.M., The Properties of Liquids and Gases, McGraw-Hill, New York, 1977.

5. A REVIEW AND DISCUSSION OF AEROSOL FORMATION MECHANISMS

During a severe reactor accident, overheating of the core would cause the release of fission products, the vaporization of control rod material and the melting of zircaloy and UO_2. The hot vapors produced by these processes would condense in the relatively cool upper plenum of an LWR and form aerosols. This section will review mechanistic models for aerosol formation and discuss their importance in severe reactor accidents.

A qualitative description of the vapor/aerosol system as well as an introduction to several definitions needed to understand aerosol formation is provided in Section 5.1. Section 5.2 reviews the classical theory of homogeneous nucleation, investigates a few of the assumptions inherent in the theory and discusses various engineering applications. The next three sections, Sections 5.3, 5.4, and 5.5, present descriptions of ion-induced nucleation, heteromolecular nucleation and heterogeneous nucleation. In Section 5.6, new expressions for the Kelvin effect are derived to predict the vapor pressure behavior of the aerosol in different physical environments. Section 5.7 summarizes the

results of this review and discusses the goals for the current work.

5.1 Introduction

The term saturation is used to describe the physical state of a pure vapor. The saturation ratio is defined as the ratio of the vapor pressure to the equilibrium vapor pressure. Hence, a vapor is saturated ($S = 1$) when its vapor pressure is equal to its equilibrium vapor pressure at a given temperature, subsaturated ($S < 1$) when the vapor pressure is less than the equlibrium vapor pressure or supersaturated ($S > 1$) if the vapor pressure exceeds the equilibrium vapor pressure. In the presence of its liquid or solid phase, a vapor will condense whenever it is supersaturated. However, in the absence of preexisting nucleation sites, significant supersaturation is required before the vapor will condense. Such a phase change occurs via the production of small droplets or aerosols. The process is termed nucleation. Nucleation is used in two different contexts in aerosol physics to describe the condensation behavior of a vapor. The formation of small particles or aerosols from a supersaturated vapor is termed homogeneous nucleation, whereas the condensation of vapor onto preexisting aerosols is classified as

heterogeneous nucleation.

Nucleation is a physico-chemical transition that occurs on the molecular level. As will be discussed later, rates of aerosol formation can be calculated by using macroscopic properties of the system. However, insight about the transition from the vapor to the aerosol can be gained by understanding the physical state of the system at a microscopic level. Figure 5.1 is a schematic of the various physical states of the vapor-aerosol system.

A vapor is defined as a collection of monomers or single molecules in the gas phase. These monomers undergo collisions to form dimers, trimers and other small clusters of n-mers by a series of monomer/n-mer reactions. These collisions cause an n-mer to either grow to size n+1 by condensation of a monomer or to shrink to an (n-1)-mer by monomer evaporation from the cluster. If the number of monomers in the cluster is large (n>100), then the cluster can be defined as an aerosol. In the limit, as the size of the aerosol grows very large, a bulk liquid (or solid) is formed.

Determining the physical properties of the components of the vapor-aerosol system is not easy. Although the monomer vapor can be described using bulk thermodynamic gas properites and the appropriate

Figure 5.1

The Vapor-Aerosol-Liquid System

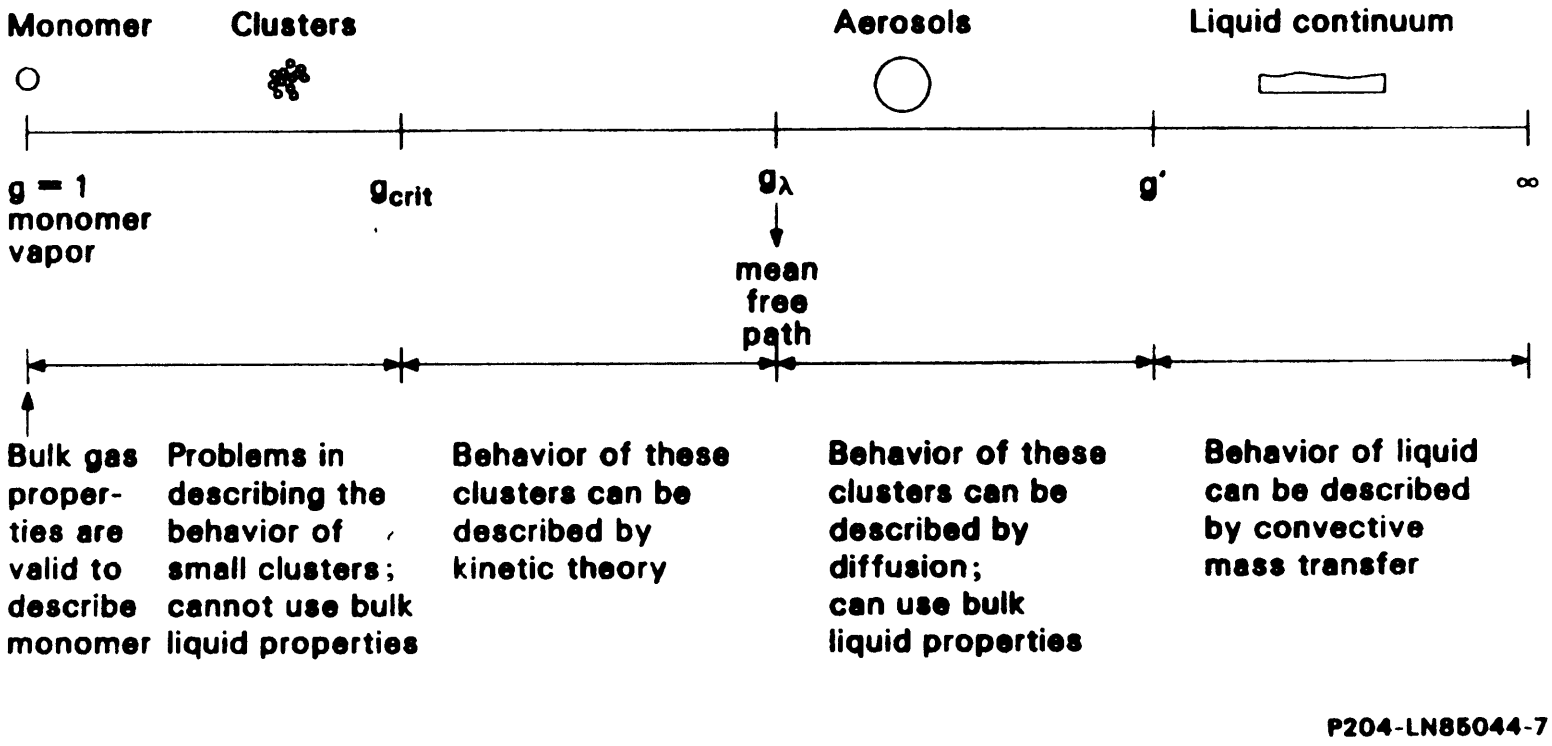

equation of state, and large aerosols can be described using bulk liquid properties such as surface tension and density, controversy exists over the correct model to use to describe the physical behavior of clusters between these two extremes. Several investigators [5.1, 5.2, 5.3, 5.4] have suggested that it is invalid to use the thermodynamic properties of a bulk liquid to describe the behavior of small clusters (up to 100 atoms in size). The collisions between these small clusters and monomers are perhaps more aptly described by statistical mechanics or kinetic theory. To date, no satisfactory resolution has been found. Moreover, the exact 'critical' cluster size, g_{crit}, above which the assumption about the use of bulk liquid properties is valid is not well defined. Nevertheless, bulk liquid properties are commonly used to describe small clusters. This assumption is one of the major liabilities in nucleation theory.

Moreover, the physical laws which govern the behavior of clusters are determined by the cluster size. Kinetic theory can be used to describe the growth rate of a cluster whose size is above the critical value, g_{crit}, but smaller than the mean free path in the system. For clusters or aerosols larger than the mean free path, the behavior and growth of aerosols is

best described using diffusion theory and bulk liquid properties. However, describing the growth of clusters below g_{crit} is difficult because bulk liquid properties are inappropriate in this size range. It is important to have a good physical picture of this size spectrum in order to understand aerosol formation, growth and depletion, as well as some of the assumptions inherent in the formulation that follows.

5.2 Homogeneous Nucleation: Theory, Limitations and Applications

5.2.1 Classical Becker-Doring Theory

During the past sixty years, many researchers have studied the theory of homogeneous nucleation. The approach presented here is taken mainly from the work of McGraw and Marlow [5.5]. In classical nucleation theory, a particle free vapor is allowed to undergo a series of monomer reactions with clusters. These clusters exist as a result of van der Waals forces between the vapor molecules and change with time through either monomer evaporation or condensation. Cluster-cluster reactions are neglected because the concentration of clusters is usually much smaller than the monomer concentration. Thus the net flux of

clusters of size g transforming to size g+1, J(g,g+1), is simply given by the difference between the condensation and evaporation rates, i.e.,

$$J(g,g+1) = \beta_g S_g c_g - \gamma_{g+1} S_{g+1} c_{g+1} \qquad (5.1)$$

where β_g is the monomer absorption or condensation coefficient per unit surface area of a cluster of size g, s_g is the surface area of cluster g, γ_{g+1} is the evaporation coefficient per unit surface area and c_{g+1} is the concentration of g size clusters.

The absorption coefficient, β_g , is given by [5.3]

$$\beta_g = \alpha \eta_g p/(2\pi m k T_g)^{\frac{1}{2}} \qquad (5.2)$$

where α is the sticking coefficient, η_g is a factor to correct for growth controlled by diffusion rather than by kinetic theory, m is the mass of the monomer, T_g is the cluster temperature and p is the pressure of the vapor. The sticking coefficient reflects the fact that not all monomers that condense will actually adhere to the cluster. Most analyses assume $\alpha = 1$, since it is

quite difficult to obtain an accurate theoretical estimate of the value of α. The coefficient η_g is given by

$$\eta_g = \frac{1}{1 + (\frac{r_g}{D})[kT/2\pi m]^{\frac{1}{2}}} \qquad (5.3)$$

Omberg and Olander [5.3] note that for small drop radii, r_g, this equation reduces to the standard Hertz-Knudsen equation whereas for large drop radii, the condensation coefficient reduces to the solution for mass transfer from a sphere.

The evaporation coefficent is determined from the theory of microscopic reversibility [5.6] which states that at equilibrium every forward process has to be matched by its corresponding reverse process. Thus, the net flux, J(g,g+1), must vanish. Hence,

$$\beta_g S_g c_g^e = \gamma_{g+1} S_{g+1} C_g^e \qquad (5.4)$$

where c_g^e is the concentration of g size clusters at equilibrium. Substituting for the evaporation coefficient, γ_{g+1}, the net flux can be written as

$$J(g,g+1) = \beta_g c_g^e S_g \left[\frac{c_g}{c_g^e} - \frac{c_{g+1}}{c_{g+1}^e} \right] \qquad (5.5a)$$

$$= p(g)[u(g) - u(g+1)] \qquad (5.5b)$$

where

$$p(g) = \beta_g S_g c_g^e$$

$$u(g) = c_g / c_g^e$$

The equilibrium distribution of clusters, c_g^e, is determined by thermodynamic considerations to be of the form [5.5]

$$c_g^e = c_1^e \exp(-\Delta G_0(g)/kT) \qquad (5.6)$$

where c_1^e is the monomer concentration (= p/kT). The free energy of formation of a cluster of size g from the vapor, $\Delta G_0(g)$, is determined by a balance between the surface tension energy of the drop and the free energy change in the condensation process [5.5]. Thus,

$$\Delta G_0(g) = 4\pi \left(\frac{3V_1}{4\pi}\right)^{2/3} g^{2/3} \sigma - gkT\ell nS \qquad (5.7)$$

where S is the supersaturation ratio, σ is the surface tension and V_1 is the atomic volume. Now, since

$$g = \frac{\rho N_A}{A} \left(\frac{4}{3}\pi r_g^3\right) \quad \text{and} \quad V_1 = \frac{A}{\rho N_A}$$

Equation (5.7) with a little rearrangement can be written as a function of radius to yield [5.7]

$$\Delta G_0(r) = 4\pi r^2 \sigma - \frac{4}{3}\pi r^3 \rho_\ell R_V T \ell n S \tag{5.8}$$

As shown in Figure 5.2, for $S > 1$, this equation exhibits a maximum at a value of

$$r^* = \frac{2\sigma}{\rho_\ell R_V T \ell n S} \tag{5.9}$$

Equation (5.8) and Figure 5.2 illustrate an important point about homogeneous nucleation. In a supersaturated vapor, competition between the free energy released in the condensation process and the surface energy required to form the aerosol results in a

Figure 5.2

Free Energy of Formation, ΔG_o, for Homogeneous Nucleation

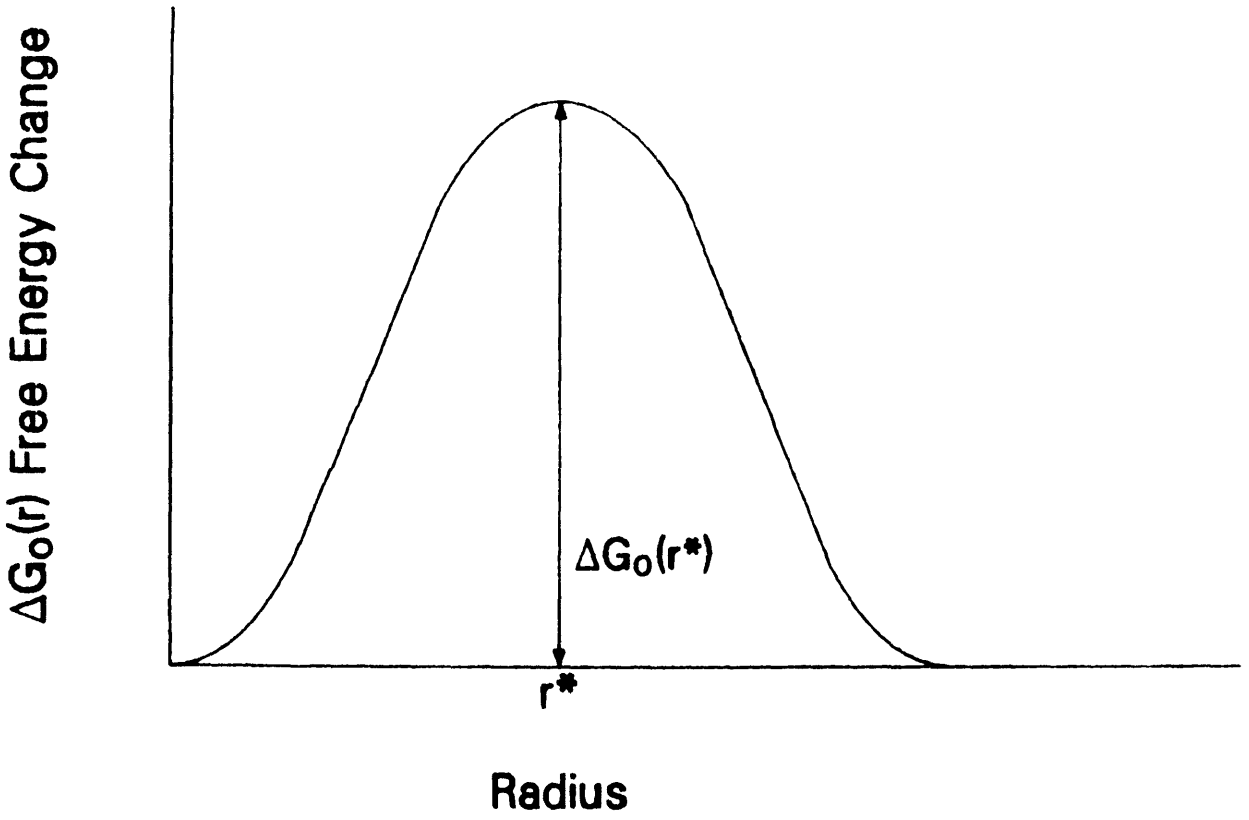

free energy barrier that the molecular clusters must overcome to form stable clusters of $r > r^*$. As will be shown in Section 5.6, r^* is defined as the critical radius at which the rates of evaporation and condensation are equal. Clusters less than r* are unstable and will evaporate whereas clusters greater than r^* will grow due to condensation.

Equation (5.6) suggests that molecular clusters can exist in equilibrium with vapor. However, in the strictest sense, this result is valid only for a subsaturated or saturated vapor. The absence of a driving force - the condensation term in Equation (5.7) - precludes a saturated vapor from undergoing homogeneous nucleation. No net growth of clusters occurs since the rates of condensation and evaporation are equal.

If a vapor is supersaturated, the existence of an equilibrium distribution is subject to question. Clusters of size $r < r^*$ cannot exist in equilibrium with a supersaturated vapor since the rate of evaporation exceeds the rate of condensation. In addition, Equation (5.6) suggests an exponential increase in the concentration of clusters greater than radius r^*. This result is clearly unphysical and is overcome in most analyses by truncating the distribution

at $R \sim 2r^*$ ($G \sim 2g^*$). Only clusters of radius r^* are thermodynamically stable in the presence of a supersaturated vapor because at this size the rate of evaporation and condensation are equal. Despite these arguments, justification of the physical existence of the equilibrium cluster distribution is made by arguing that if the distribution exists for a saturated or subsaturated vapor then it must surely exist for a supersaturated vapor since an increase in supersaturation causes both the concentration of clusters and the collision rate between single molecules and clusters to increase [5.7].

The existence of the distribution is not required to describe the phase transition. The net fluxes are defined only in terms of a non-equilibrium cluster concentration c_g. However, since the equilibrium distribution is used to define both the evaporation coefficient and as will be shown later the non-equilibrium cluster concentration, c_g, Equation (5.6) can be thought of as a mathematical relationship that is needed in the derivation that follows.

A mass balance for size g clusters can now be written as

$$\frac{dc_g}{dt} = J(g-1,g) - J(g,g+1) \qquad (5.10a)$$

$$= p(g-1)[u(g-1)-u(g)] - p(g)[u(g)-u(g+1)] \qquad (5.10b)$$

Classical nucleation theory looks for the steady state solution of Equation (5.10a) subject to the following conditions

$$c_1/c_1^e = u(1) = 1$$
$$c_G/c_G^e = u(G) = 0$$

The first boundary condition states that the monomer concentration is constant and equal to the equilibrium concentration. The second boundary condition in g space, known as the 'Szilard boundary condition' [5.8] assumes that aerosols larger than size G ($G \sim 2g^*$) are removed from the system and hence their concentration is zero.

At steady state, the net fluxes are found to be independent of size, i.e.,

$$J= J(g-1,g) = J(g,g+1) = p(g)[u(g)-u(g+1)] \qquad (5.11)$$

By dividing both sides of Equation (5.5a) by p(g) and summing from g=1 to g=G-1, Equation (5.11) becomes

$$J = \left[\sum_{g=1}^{G-1} \frac{1}{p(g)} \right]^{-1} \tag{5.12}$$

which is the exact expression for the rate of homogeneous nucleation of a vapor. By summing Equation (5.11) from g to G-1 and using the results of Equation (5.12), an expression can be obtained for the cluster concentration, c_g. Thus,

$$c_g = c_g^e \left[\sum_{k=g}^{G-1} \frac{1}{p(k)} \Big/ \sum_{k=1}^{G-1} 1/p(k) \right] \tag{5.13}$$

Equations (5.12) and (5.13) are the exact Becker-Doring expressions for the steady state nucleation rate and cluster distribution respectively.

The form of these equations make them cumbersome to apply in engineering applications where aerosol formation is a small part of a much larger analysis problem. No closed form solution exists for the cluster

concentration, c_g. This result is not critical,however, since the cluster concentration is not used in most analyses. It is more important to be able to obtain a closed form solution for J since it represent not only the steady state flux of clusters through g-space but also the net flux of new particles exiting the growth chain at size G. It is this latter interpretation that is required in most aerosol/engineering analyses.

Thus, a more convenient form of Equation (5.12) is obtained by (1) substituting the equilibrium cluster distribution, c_g^e , (Equation 5.6), and the value of the condensation coefficient β_g (with α and η_g =1) (Equation 5.2) into Equation (5.12), (2) converting the sum to an integral, (3) expanding it about its maximum value and evaluating the integral. The final result is [5.7]

$$J_{HMG} = \left(\frac{p_v(T_v)}{kT_v} \right)^2 \left(\frac{2\sigma m}{\pi} \right)^{\frac{1}{2}} \frac{S^2}{\rho_\ell} \exp\left(- \frac{4\pi}{3} \frac{\sigma r^{*2}}{kT_v} \right) \qquad (5.14)$$

This is the classical Becker-Doring (B-D) result for homogeneous nucleation in terms of macroscopic parameters such as m, the mass of an atom of the vapor,

S, the supersaturation ratio, ρ_ℓ , the liquid density and σ , the surface tension.

As stated above, Equation (5.14) can be used to describe the steady state flux of clusters of any size from g = 2 to g = G. However, since the term "nucleation rate" is used to refer specifically to the net rate at which clusters exceed the thermodynamically stable critical cluster size r^* [5.5], r^* is commonly refered to as the radius of formation and J_{HMG} is considered to be the corresponding rate of homogeneous nucleation of aerosols of size r^*. With this interpretation, Equation (5.14) can then be used as the generation rate of new aerosols of size r^* in an aerosol transport analysis and sizes less than r^* can be neglected. This alternative interpretation of Equations (5.12) and (5.14) represents a difference in terminology and not a lack of understanding of the physical phenomena.

5.2.2 Critical Examination of B-D Theory

Before discussing some of the engineering applications of nucleation theory, it is instructive to list a few of the assumptions inherent in the Becker-Doring treatment and to review the work of others who have examined the effect of these assumptions on the

rate of homogeneous nucleation.

The basic assumptions inherent in the B-D theory are

(1) The free energy of formation of a cluster is comprised of the free energy change due to condensation and the surface tension energy of the drop;
(2) Initially the system consists of a particle free vapor;
(3) The growth of a cluster is controlled by monomer addition alone;
(4) The system is infinite in extent in the sense that no walls exist;
(5) The monomer concentration is constant in time (u(1)=1);
(6) Large drops of size G are removed from the system. (Szilard boundary condition, u(G)=0);
(7) The solution is for steady state;
(8) Bulk liquid properties are applicable to small clusters; and
(9) The analysis assumes a single component, inert system.

Lothe and Pound [5.4] suggest that important statistical mechanical contributions to the free energy of formation of clusters were neglected in the Becker-Doring formulation. They consider three additional components to the free energy of formation of clusters. These are:

(1) the free energy of separating a group of g molecules from a larger ensemble, ΔG_s ,

$$\Delta G_s = \frac{kT\ell n(2\pi g)}{2} + T_s \qquad (5.15)$$

where s is the molecular entropy of the liquid;

(2) the translational free energy of the cluster, $\Delta G_{E,t}$,

$$\Delta G_{E,t} = -kT\ell n[(2\pi mkT)^{3/2} v/k^3] \qquad (5.16)$$

where m is the molecular mass and v is the molecular volume of the cluster at pressure p and temperature T; and

(3) the rotational free energy of the cluster, $\Delta G_{E,r}$,

$$\Delta G_{E,r} = -kT\ell n[(2kT)^{3/2} (\pi I^3)^{\frac{1}{2}} /\hbar^3] \qquad (5.17)$$

where I is the moment of inertia of a spherical droplet and $\hbar = \frac{h}{2\pi}$. Lothe and Pound then conclude that the term ΔG_0 in the classical equation should be replaced by $\Delta G^* = \Delta G_0 + \Delta G_s + \Delta G_{E,t} + \Delta G_{E,r}$. However, it is interesting to note that since the last three terms are insensitive to size the critical radius of nucleation, r* , is unaffected by this change and is still given by

Equation (5.8). The result of this change is a factor, Γ, termed the Lothe-Pound (L-P) correction factor [5.1] given by

$$\Gamma = (IkT)^{3/2}\left(\frac{kT}{\rho}\right)\left(\frac{g^*}{\pi^2}\right)(2\pi mkT)^{3/2}\exp(-S/k)/\hbar^6 \qquad (5.18)$$

which should be multiplied by the classical nucleation rate expression (with ΔG_0 replaced by ΔG^*). When Lothe and Pound applied their correction factor to water vapor nucleation data, they obtain nucleation rates which are a factor of 10^{17} higher than would be predicted using the classical theory.

The Lothe-Pound theory disagrees with much of the early data obtained from cloud chamber experiments. Feder et. al. [5.2] suggest that the discrepancy is a result of using bulk liquid surface tension to describe the surface tension of small clusters (< 100 atoms) which form at nucleation. Their analysis indicates that agreement between data and the L-P theory can be restored if the surface tension is increased by 15% or if the pre-exponential term in the nucleation rate could be decreased by approximately 10^{15}. This later suggestion would roughly correspond to using classical

B-D theory instead of L-P theory.

It should be noted that the aerosol community is still debating the merits of these two theories. Most analyses, that this researcher has seen, have used B-D theory basically because it predicts the early cloud chamber data much better than L-P theory. Kolar-Anic and Balescu [5.8] point out that the experimental nucleation data fall into two distinct categories: cloud chamber data which are best predicted by B-D theory and supersonic nozzle data which tend to confirm L-P theory. It has been proposed [5.9] that agreement with a given theory depends on the fluid. Nucleation rates of regular nonpolar vapors agree with the L-P theory whereas fluids having hydrogen bonding or rod-shaped molecules are better predicted using B-D theory.

The second assumption of a particle free vapor implies that there is no preexisting aerosol to scavenge the monomer. In most real world systems, significant impurities exist which would tend to promote heterogeneous nucleation onto preexisting condensation nuclei. McGraw and Marlow [5.5] as well as Gelbard and Seinfeld [5.11] have studied the effect of a preexisting aerosol on homogeneous nucleation. McGraw and Marlow found that departures from classical nucleation theory occur at very low equilibrium vapor pressures

($< 10^{-5}$ torr) whereas at higher pressures, the classical expression is found to be a good approximation. Gelbard and Seinfeld, however, found that when account is made for the presence of particles much larger than the critical size r*, the rate of homogeneous nucleation is less than predicted by classical theory. This is to be expected since the surface area provided by the preexisting aerosol allows for condensation which is not accounted for in the classical formulation. Their results suggest that at a given vapor pressure and preexisting aerosol surface area, a higher supersaturation is required to sustain a given nucleation rate than in a particle free system. The difference in the conclusions of these two groups of researchers may be attributed to differences in the actual surface area of the aerosols introduced into their respective calculations. If more aerosol surface area is exposed to the vapor, then less homogeneous nucleation is expected to occur. Thus it appears that an accurate account of the preexisting aerosol distribution needs to be obtained to properly model vapor nucleation.

Gelbard and Seinfeld [5.11] have examined the third assumption that growth is controlled by monomer addition. The rate equations developed earlier do not

account for processes like cluster-cluster agglomeration. Reference [5.1] points out that some researchers have assumed that the probability of a cluster interacting with another cluster is small. Yet, Gelbard and Seinfeld suggest that classical nucleation theory may be incorrect in predicting the nucleation rate since cluster-cluster agglomeration is not accounted for in the formulation. McGraw and Marlow [5.5] suggest that in multicomponent systems, cluster removal could be quite important especially for long nucleation times. If the time scale for nucleation is long then many of the other aerosol depletion mechanisms (i.e., agglomeration, depletion, settling) also need to be considered in parallel with nucleation condensation and evaporation. It is only by considering all of these rate processes simultaneously that the behavior of the system will be correctly understood.

Omberg and Olander [5.3] have pointed out that classical theory assumes that the system is in essence an infinite medium. There is no convective flow component to remove aerosols from the system. In addition, although not mentioned by Omberg and Olander, condensation on walls is also not accounted for in the classical formulation. Certainly if a preexisting aerosol will affect the rate of homogeneous nucleation,

the additional surface area introduced by wall might also have an effect. In most engineering systems, the effects of cold walls and bulk flow need to be assessed.

Becker-Doring theory also has two assumptions inherent in the boundary conditions used to obtain a solution. The boundary condition u(1)=1 implies that the monomer concentration is constant. The effects of a variable source rate and depletion due to nucleation or condensation on walls is not considered in the theory. This condition may however be valid as long as the time dependent aerosol behavior is modeled with appropriate time step control.

Kolar-Anic and Balescu [5.8] have studied the effect of the so called "Szilard boundary condition" (u(G)=0) on the nucleation rate. They suggest that the classical physical picture is incorrect. In the classical physical picture, every cluster which grows to a size G is removed from the system, broken down into G separate molecules and enters the system once more as monomer. They conclude that this circular behavior is inappropriate and instead that the 'flow' of matter from vapor to clusters to liquid is unidirectional.

As a result, they propose that the system should be considered as having two reservoirs. The first of these would provide monomer at a constant rate and at the end

of the chain the second reservoir would remove clusters of size G at a constant rate. The constant removal rate of G size clusters is not the same as u(G)= 0. Instead, a constant removal rate implies a constant value of u(G) in steady state. As a result, a series of steady states can exist depending on the particular removal rate. Furthermore, they claim that the particular value of u(G) (ratio of G size clusters at steady state to those at equilibrium) is a measure of the distance any given steady state system is from equilibrium.

Their analysis suggests that the resulting steady state cluster distribution is a function of the removal rate or the distance from equilibrium. They postulate that the discrepancy between some of the experimental data and the B-D and L-P theories might be explained by the fact that in the experiments u(G) was not equal to zero but instead took on a finite value. As a result, each experiment may have obtained a different steady state solution and thus the discrepancy may just be a measure of the distance from equilibrium.

Feder et. al. [5.2], McGraw and Marlow [5.5] and Reference [5.1] have investigated the steady state assumption employed in classical nucleation theory. All of these authors calculate a time constant associated with nucleation. McGraw and Marlow were concerned with

studying the relative time scales over which nucleation and other processes like cluster condensation take place. Both Feder et. al. and Reference [5.1] remark that the many researchers who have investigated the time to reach steady state agree that in usual experimental situations the time period to build up a steady state distribution of clusters is of the order of 10^{-7} seconds and thus the effect is insignificant.

Almost all of the references cited thus far have noted the inadequacy of using bulk liquid properties to describe small clusters less than 100 atoms. Lothe and Pound [5.4] and Feder et. al [5.2] suggest that the use of bulk liquid properties may be why the L-P theory is not in agreement with some of the experiemental data. Reference [5.1] remarks that some work has been done to modify the surface tension to account for a low radius of curvature. However, this correction is not applicable for some of the high curvatures encountered in small clusters. At the present time there is no real theory to deal with the problem. Nevertheless, the approximation is commonly made.

Katz and Donohue [5.6] have studied the effect of nucleation with simultaneous chemical reaction. They modify the classical conservation equation to account for transition due to chemical reaction. Their results

show that the rate of surface reaction can significantly increase the rate of nucleation. Chemical nucleation is self-catalytic. Condensation occurs more rapidly because the clusters serve as chemical reaction sites which help deplete the monomer faster than with no chemical reaction. As a result, nucleation can occur at a lower supersaturation than predicted by the classical theory alone. Although this effect might be quite important, it is difficult to obtain good kinetic rate data at high temperatures for some reactions.

The classical Becker-Doring theory of nucleation derives an expression for the rate of aerosol formation in the absence of all other aerosol processes. Using such a quasi-steady expressions in the general aerosol transport equation may be inappropriate to predict aerosol formation if strong coupling exists between the various aerosol processes. The results of this section suggest that many of the subtle assumptions in classical B-D theory should not be overlooked since they may be incorrect. Nevertheless, because of the complexity of the problem in many real world applications the quasi-steady rate expression (Equation 5.14) is used to predict aerosol formation.

5.2.3 Engineering Applications

Nucleation theory is used to solve many problems encountered in engineering. This section presents some of the applications of nucleation theory in such fields as chemical engineering, magneto-hydrodynamics (MHD) and nuclear engineering. The purpose of this section is to illustrate the role of nucleation in these analyses and to indicate that reasonable results can be obtained using the macroscopic nucleation rate predicted by Becker-Doring theory.

Hill et. al. [5.10] have studied the condensation of metal vapors in rapid expansion nozzles that could be expected in the turbines of liquid-metal-cooled nuclear space vehicles. They developed a model to predict the incidence of homogeneous nucleation in a nozzle and found that although mercury is very reluctant to condense, vapors of sodium, potassium and rubidium condense very easily. The local degree of supersaturation was obtained assuming an isentropic expansion through the nozzle. The subsequent growth of the nucleated droplets was calculated and the effect on the pressure and temperature of the vapor as it passed through the nozzle was determined.

Rossner and Epstein [5.12, 5.13] and Rosner [5.14] have studied the enhancement of diffusion limited

vaporization rates due to homogeneous nucleation of vapor in the thermal boundary layer. In their work, hot material on a wall is vaporizing by mass transfer into a cold fluid. The decrease in temperature through the boundary layer results in a rapid decrease in the local equlibrium vapor pressure (because of the exponential variation of equilibrium vapor pressure with temperature.) When the equilibrium vapor pressure falls far enough below the partial pressure of the diffusing species at some point in the thermal boundary layer, homogeneous nucleation occurs. This nucleation further steepens the actual partial pressure gradient of the diffusing species and thus enhances the mass transfer rate into the bulk fluid. They developed a supersaturation criterion to determine the local value of the partial pressure in the thermal boundary layer required for nucleation. However, to implement their model, a knowledge of the critical nucleation rate, J_{crit}, must be known a priori in order to determine where in the boundary layer the nucleation will occur. Epstein and Rosner found that nucleation rates in the boundary layer were on the order of 10^{10} - 10^{17} particles/cc-s instead of the common critical value of 1 particle/cc-s which is used to define critical superaturation in cloud chambers. Epstein and Rosner

[5.13] have also suggested that their work can be used to predict the onset of incipient fog formation within boundary layers near cool surfaces. Such an effect is important when large temperature gradients exist between the bulk gas and the wall. Generally much higher temperature gradients are required for metal vapors than for water vapors.

Omberg and Olander [5.3] have developed a similar model for predicting the effect of condensation in the boundary layer on mass transfer from a rotating disk. An Eulerian approach is used to model the behavior of the vapor and aerosols in a series of fixed control volumes in the flow field. Convective and diffusive terms are incorporated into the steady-state droplet balance equations. An excellent review of nucleation theory is also provided.

Kennedy et. al [5.7] have performed an analysis to determine the formation and growth of primary aerosol particles following the mixing of molten UO_2 fuel and argon in a simulated hypothetical core disruptive accident (HCDA) in an LMFBR. Kennedy models the mixing of the hot fuel with the cool gas and subsequently predicts the rate of homogeneous nucleation using classical Becker-Doring theory. Droplet growth equations are coupled to mass and energy balances on the

vapor and liquid drops to determine the behavior of the system. Results are used to try to predict the primary aerosol distribution found from ORNL experiments. Their model was able to predict the low range of the particle size distribution observed in the tests but could not reproduce the larger end of the size spectrum.

Im and Ahluwalia [5.15] have studied nucleation and subsequent aerosol and vapor deposition of slag and seed in MHD components. Their analysis includes homogeneous and heterogeneous nucleation, and aerosol agglomeration as well as gas phase equilibrium chemistry. Im and Ahluwalia [5.16] have recently modified their MHD model to be able to handle aerosol transport in severe LWR accidents. Their aerosol code, named RAFT (Reactor Aerosol Formation and Transport) includes all of the effects mentioned above. Potential aerosol sources include Ag, Cd, CsI, CsOH and Te. Although the code is proprietary, their published results for the TREAT STEP experiments [5.16] suggest that CsI homogeneously nucleates and the other volative species condense onto this CsI seed.

Despite it limitations, homogeneous nulceation has been a beneficial tool to predict aerosol generation in a wide variety of engineering systems.

5.3 Ion-induced Nucleation

During a severe reactor accident, the high radiation levels in the core will cause substantial ionization of the hydrogen and steam. As a result, a phenomenon like nucleation on ions which is relatively unimportant in such processes as cloud formation where ion densities are low may be quite important in the aerosol formation process. A remark on terminology is needed here. In most of the aerosol literature, ion-induced nucleation is a specific type of heterogeneous nucleation mechanism. However, because of its importance in severe reactor accidents, ion-induced nucleation will be classified as a separate mechanism of aerosol formation throughout this document. The term heterogeneous nucleation will be used exclusively to describe vapor condensation onto a preexisting aerosol.

Several investigators have studied nucleation onto gaseous ions. A brief review of the classical theory is present in Reference [5.1]. Russell [5.17] has rederived the classical expression and extended the Lothe-Pound approach for the case of ion-induced nucleation. The theory behind ion-induced nucleation, presented here, parallels that of the classical B-D theory for homogeneous nucleation. The ions act as condensation sites for the supersaturated vapor. The

free energy change in the condensation process is given by [5.17]

$$\Delta G_0(r_k) = 4\pi\sigma(r_k^2 - r_a^2) - \frac{4\pi}{3V_m}(r_k^3 - r_a^3)kT\ell nS \qquad (5.19)$$
$$-(1 - \frac{1}{\varepsilon})\frac{e^2}{8\pi\varepsilon_0}(\frac{1}{r_k} - \frac{1}{r_a})$$

where

ε = dielectric constant of condensing species,

V_m = molecular volume of species,

σ = surface tension,

e = charge of the electron,

and r_k and r_a are roots of

$$\frac{\partial(\Delta G(r))}{\partial r} = -kT\ell nS + \frac{2\sigma V_m}{r} - \frac{e^2 V_m}{8\pi r^4(4\pi\varepsilon_0)}(1-\frac{1}{\varepsilon}) = 0 \qquad (5.20)$$

corresponding to the largest and smallest values of the free energy. As can be seen from Equation (5.19), the presence of the ions is to introduce another term into the free energy balance. This term accounts for the electrical attraction between the ions and the vapor and is thus another driving force for the nucleation process. A plot of Equation (5.19) is shown in

Figure 5.3. The curve for the free energy change looks similar to that for homogeneous nucleation. A free energy barrier, centered at r_k, exists due to the competition between the condensation term (kTlnS) and the surface tension term ($4\pi r^2\sigma$) in Equation (5.19).

Once r_k and ra have been determined from Equation (5.20), the rate of nucleation of the vapor as a result of ions, J_{ion}, can be calculated using

$$J_{ION} = \frac{4\pi r_k^2 p_v(T_v)}{(2\pi mkT)^{\frac{1}{2}}} \left[\frac{4\pi\sigma r_k^2 - (1-\varepsilon^{-1})(e^2/8\pi\varepsilon_0 r_k)}{9\pi kTn_k}\right]^{\frac{1}{2}} N_a \exp(-\Delta G_0(r)/kT) \quad (5.21)$$

where

n_k = number of atoms in a cluster of radius k,and

N_a = number of ions/volume.

5.4 Heteromolecular Nucleation

The previous models of aerosol formation consider each vapor to exist and nucleate independently of all the other vapors in the volume. No explicit chemical interaction was considered. During a severe reactor accident, however, many vapors will be released from the core simultaneously due to the release of fission products and the melting of control material, structural

Figure 5.3

Free Energy of Formation, ΔG_o, for Ion Nucleation

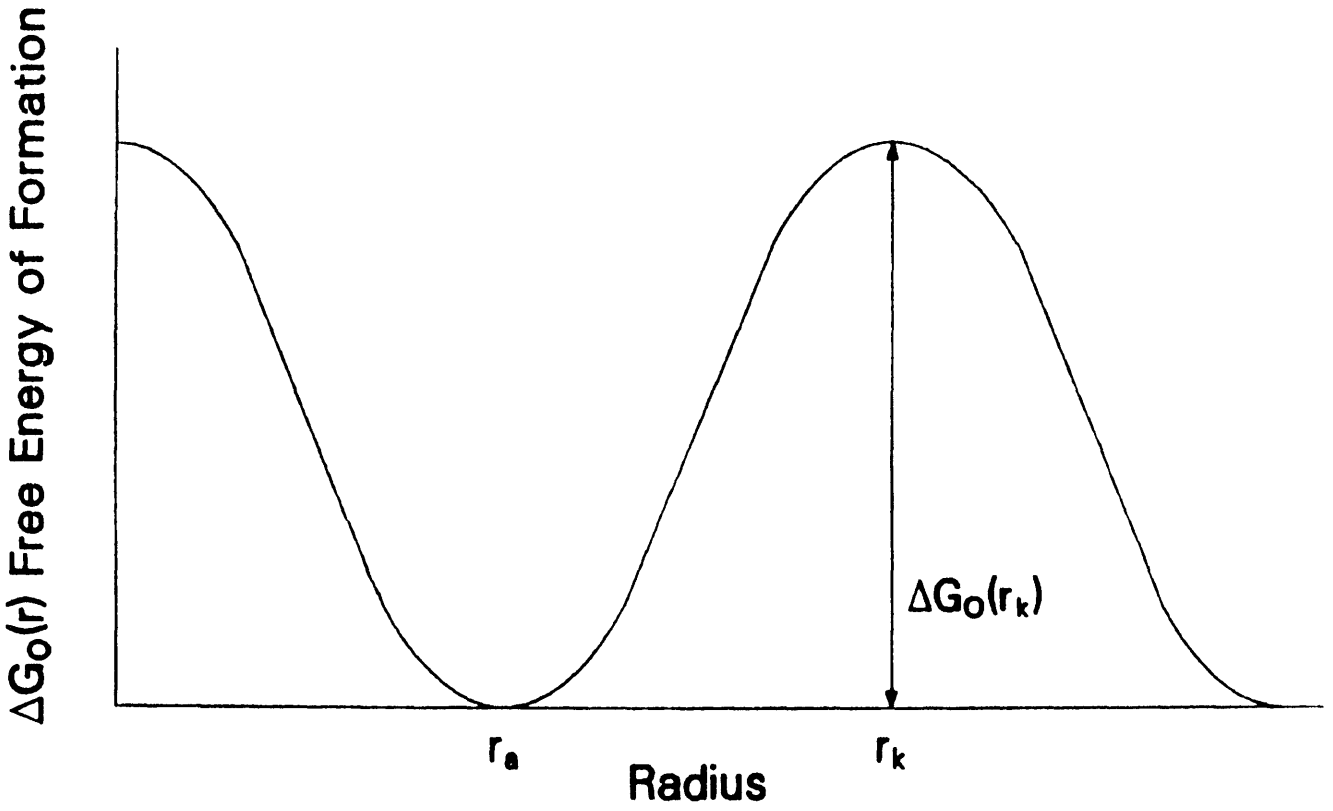

R850002-10

material, cladding and fuel. As a result, the nucleation behavior of the vapors is a function of the chemical potential of all the species in the system. This section will review the previous work concerning nucleation in multicomponent systems and discuss the thermodynamics of heteromolecular nucleation.

Very little work has been done to date on the nucleation of multicomponent systems of vapors. Hidy [5.18] reviewed the work of Reiss [5.19] and Mirabel and Katz [5.20] on binary homogeneous nucleation. Reiss studied the kinetics of binary nucleation and developed a theory that closely parallels the classical treatment of homogeneous nucleation of a pure vapor. Mirabel and Katz used the theory of binary nucleation developed by Reiss to predict the nucleation behavior of gaseous mixtures of $H_2SO_4 + H_2O$ and $HNO_3 + H_2O$ for various relative humidities and acid vapor activities. They also developed a generalized version of the Kelvin effect which included the composition dependence of the surface tension of a binary mixture.

To date, as far as this author knows, no work has been done to extend the formulation of binary nucleation to a multicomponent system. Such a formulation, although easy on paper, is quite difficult to implement. An examination of the thermodynamics of the

system is presented next in an attempt to highlight the difficulties of predicting aerosol formation in multicomponent systems like the core and upper plenum of a nuclear reactor in a severe accident. Wherever possible, analogies to the single component nucleation case are drawn.

By analogy with single component nucleation, the change in free energy of the multicomponent system is given by

$$\Delta G(n_i) = 4\pi r^2 \sigma + \sum_{i=1}^{n} n_i(\mu_{\ell,i} - \mu_{g,i}) \qquad (5.22)$$

where

σ = surface tension of the drop (N/m),

$\mu_{\ell,i}$ = chemical potential of liquid phase of specie i (J/kgmole),

$\mu_{g,i}$ = chemical potential of vapor phase of specie i (J/kgmole), and

n_i = number of moles of specie i in the vapor.

The free energy of the system, $\Delta G(n_i)$, is minimized by requiring

$$\frac{\partial \Delta G(n_i)}{\partial n_i} = 0$$

for all i. Hence the first derivatives become

$$(\mu_{\ell,i} - \mu_{g,i}) + \frac{2\sigma\bar{V}_i}{r} - \frac{3\bar{V}}{r}(1-X_i^*)\frac{d\sigma}{dX_i}\Bigg|_{\substack{\text{all} \\ X\neq X_i}} \qquad (5.23)$$

where

$\bar{V}_i$ = partial molar volume of specie (m^3/kgmole),

X_i^* = mole fraction of specie i in liquid drop,

$\bar{V}$ = total volume of drop (m^3)= $\sum_i n_i \bar{V}_i$, and

$d\sigma/dX_i$ describes the variation of the surface tension of the drop with mole fraction of specie i. This results in i equations to determine i-1 mole fractions (X_1^* ,X_2^* , ... X_{i-3}^*,... X_i^*) and the radius of formation r* . Thus, in heteromolecular nucleation, the aerosol that is formed is a mixture of species defined by their respective mole fractions. The critical radius is given by

$$\frac{4}{3}\pi r^{*3} = \sum_i \bar{V}_i \qquad (5.24)$$

Although, the first derivatives can be written down analytically, trying to calculate the critical

concentrations, X_i is difficult. The partial molar volume, $\bar{V}_i$, and the change in chemical potential for each specie needs to be determined before a prediction of the heteromolecular nucleation rate can be made.

The partial molar volume of each specie is given by [5.21]

$$\bar{V}_i = V_i + RT \left. \frac{\partial (\ell n \gamma_i)}{\partial p} \right|_{T,X} \tag{5.25}$$

where

V_i = partial molar volume of the pure component (m^3/kgmole).

γ_i = activity coefficient of specie i in solution, and

p = pressure (Pa).

In general, the change in chemical potential of the vapor is given by

$$\mu_{\ell,i} - \mu_{g,i} = -RT\ell n \frac{p_i}{p_{i,sol}} = -RT\ell n \eta_i \tag{5.26}$$

where

p_i = vapor pressure of specie i in vapor (Pa),

$p_{i,sol}$ = vapor pressure of specie i in a solution of

composition (X_1^* ,X_2^* ,...X_{i-3}^*,...X_i^*) (Pa), and

η_i = pseudo-supersaturation of specie i in the multicomponent system (not the classical definition of supersaturation of a pure vapor),

R = gas constant (Pa-m^3/kgmole K), and

T = temperature (K).

This pseudo-supersaturation η_i can be rewritten as

$$\eta_i = \frac{p_i}{p_{i,sol}} = \frac{p_i}{p_{i,\phi}} \left(\frac{p_{i,\phi}}{p_{i,sol}}\right) \tag{5.27}$$

where $p_{i,\phi}$ is the vapor pressure of the pure component. The ratio of the vapor pressure in solution, $p_{i,sol}$, to the pure component vapor pressure is given by

$$\frac{p_{i,sol}}{p_{i,\phi}} = \gamma_i X_i \tag{5.28}$$

where

γ_i = activity coefficient of specie i, and

X_i = mole fraction of specie i in solution.

If γ_i= 1, then the solution is termed ideal and it obeys

Raoult's law. The activity coefficient is intended to describe deviations of the vapor pressure behavior of a solution from ideality. For a multicomponent system, the pseudo-supersaturation, η_i, is then related to the pure component supersaturation, S_i, by

$$\eta_i = \frac{S_i}{\gamma_i X_i} \tag{5.29}$$

Thus, Equation (5.26) can be rewritten as

$$\mu_{\ell,i} - \mu_{g,i} = - RT\ell nS_i + RT\ell n\gamma_i + RT\ell nX_i \tag{5.30}$$

Summing over all species yields the free energy change due to condensation of all the vapors

$$\Sigma n_i(\mu_{\ell,i} - \mu_{g,i}) = RTN(\sum_i X_i \ell nX_i + \sum_i X_i \ell n\gamma_i) - RTN \Sigma X_i \ell nS_i \tag{5.31}$$

where $N = \sum_i n_i$. The second term in Equation (5.31) is just the free energy change if each

specie were to condense or nucleate separately. The first term is the partial molar free energy change due to mixing, denoted by ΔG^M, and accounts for the free energy change when the vapors condense to form a droplet of liquid solution. The mixing term can be either positive or negative depending on the values of the activity coefficients. Positive changes in ΔG^M mean that energy was expended to form the solution; conversely, negative changes in ΔG^M are the result of energy being released in the formation of the solution.

Using the above formulations, the overall free energy change can be written in a form similar to single component homogeneous nucleation as

$$\Delta G(r) = 4\pi r^2\sigma - NRT \sum_i X_i \ell n \eta_i \qquad (5.32)$$

Rewriting the free energy due to condensation in terms of a system supersaturation, S', yields

$$\Delta G(r) = 4\pi r^2\sigma - NRT \ell n\, S' \qquad (5.33)$$

where

$$S' = \prod_i \eta_i^{X_i} = \prod_i \left(\frac{S_i}{\gamma_i X_i} \right)^{X_i}$$

or

$$\ell n S' = \sum_i \left(X_i \ell n S_i - X_i \ell n X_i - X_i \ell n \gamma_i \right)$$

In addition, since

$$N = \frac{4\pi r^3}{3\bar{\nu}} \tag{5.34}$$

and $\bar{\nu}$ is the molar volume of the drop (m^3/kgmole), Equation (5.33) can be written as

$$\Delta G(r) = 4\pi r^2 \sigma - \frac{4}{3} \pi r^3 \frac{RT}{\bar{\nu}} \ell n S' \tag{5.35}$$

which is identical in form to the single component nucleation case except for $\bar{\nu}$ and S'. Thus by analogy, the radius of formation, r^*, is given by

$$r^* = \frac{2\sigma\bar{\nu}}{kT \ell n S'} \tag{5.36}$$

and the free energy at r* is

$$\Delta G(r^*) = \frac{16 \pi \sigma^3 \bar{v}^2}{3(RT \ell n S')^2} \qquad (5.37)$$

Thus, the simple concepts developed in homogeneous nucleation of a pure vapor can be used to understand the more complex case of heteromolecular nucleation of a multicomponent system of vapors.

Examination of the thermodynamics of such a multicomponent system reveals that in general, the vapor pressure and partial molar volume are functions of the activity coefficient. The activity coefficient of a constituent in a solution is a function of the temperature and composition of the solution. The values of the activity coefficient are usually determined experimentally. This is the major drawback of the multicomponent approach. In many cases, such as severe accidents, little is known about the values of the activity coefficients in the complex solutions that are expected to form. Many experiments would have to be performed to determine these values. In addition, the variation of the surface tension with composition is

unknown. The value of both the surface tension and the rate of change of surface tension with respect to composition ($d\sigma/dX_i$) need to be known. At present, obtaining reliable surface tension data for some of the materials that will be present in a severe accident is difficult. Thus, although the free energy of the system can be described analytically, finding values of the activity coefficients for this complex system make it almost impossible to implement such a theory. Nevertheless, this formulation has provided some insight into the complicated nature of the problem.

5.5 Heterogeneous Nucleation

Heterogeneous nucleation is not technically a method of aerosol formation. Rather, it is a method by which a preexisting aerosol grows due to vapor condensation. However, to consider only homogeneous and ion-induced nucleation without examining heterogeneous nucleation would lead to an incomplete understanding of gas-to-particle conversion. Once aerosol concentrations are high, heterogeneous nucleation will become the major mechanism for gas-to-particle conversion. Thus, the condensation of vapor onto an aerosol and its subsequent growth needs to be modeled if a proper understanding of the vapor-aerosol system is to be obtained.

The rate of heterogeneous nucleation is a function of the size of the aerosol particle. For aerosol particles much less than the mean free path of the carrier gas, the rate of condensation is determined by kinetic theory to be [5.22, 5.23]

$$J_{kin} = \frac{p-p_d}{(2\pi mkT)^{\frac{1}{2}}} \frac{MW}{N_A} N(d_p) \pi d_p^2 \qquad (5.38)$$

where

J_{kin} = mass condensation rate per unit volume (kg/m^3-s),

p = partial pressure of vapor (Pa),

p_d = vapor pressure at the aerosol surface (Pa),

MW = molecular weight of the vapor (kg/kgmole),

N_A = Avagardro's number (atoms/kgmole),

m = mass of an atom of vapor (kg),

k = Boltzman's constant (J/K),

T = temperature (K),

d_p = particle diameter (m), and

$N(d_p)$ = number of aerosol particles of size dp per unit volume (particles/m^3).

Although the vapor pressure for a pure liquid is only a function of temperature, for aerosol particles less that

0.1 μm, the vapor pressure at the surface of the aerosol is also a function of the curvature of the surface. This is known as the Kelvin effect [5.22]. A more detailed discussion of this phenomenon is presented in Section 5.6. Hence,

$$p_d = p_v(T)K \tag{5.39}$$

and K is given by

$$K = \exp\left(\frac{4\sigma V_m}{d_p kT}\right) \tag{5.40}$$

where

$p_v(T)$ = vapor pressure of pure liquid (Pa),

σ = surface tension (N/m),

d_p = diameter of aerosol particle (m), and

V_m = molecular volume (m^3/atom).

In addition, since the partial pressure of the vapor can be expressed as $p = s * p_v(T_v)$, Equation (5.38) can be rewritten as

$$J_{kin} = \frac{p_v(T_v)}{(2\pi mkT)^{\frac{1}{2}}} (S-K) \frac{MW}{N_A} N(d_p)\pi d_p^2 \tag{5.41}$$

For aerosol particles much larger than the mean free path, diffusion controls the rate of heterogeneous nucleation [5.22, 5.23]. Hence,

$$J_{DIFF} = \frac{2\pi d_p D p_v(T_v)}{kT_v} (S-K) \frac{MW}{N_A} N(d_p) \qquad (5.42)$$

where

J_{DIFF} = mass condensation rate per unit volume (kg/m^3-s), and

D = diffusion coefficient of the vapor in the carrier gas (m^2/s),

and all other variables are previously defined.

For small particles, the kinetic theory solution (Equation 5.41) is in error since it predicts rates greater than the theoretical maximum rate of mass transfer into a vaccuum [5.22]. Fuchs developed a model to compensate for this effect which is valid over the entire range of particle size. He assumed that the transport of vapor to the surface was controlled by kinetic theory within a concentric sphere of $d + (4/3)\ \lambda$ where λ is the mean free path of the gas. Beyond this diameter, diffusion controls condensation [5.21]. The Fuchs model is obtained by applying a

correction factor to the diffusion model. The correction factor is given by

$$F = \frac{1 + Kn}{1 + 1.71Kn + 1.33Kn^2} \tag{5.43}$$

where Kn is the Knudsen number. The Knudsen number is given by

$$Kn = 2\lambda/d_p \tag{5.44}$$

where the mean free path, λ , is defined as

$$\lambda = 3\nu\left(\frac{\pi m}{8kT}\right)^{\frac{1}{2}} \tag{5.45}$$

and

ν = kinematic viscosity of the carrier gas (m^2/s), and all other variables are previously defined. For a multicomponent gas mixture, m, the mass of an atom, is calculated using a mole fraction weighted

average of the gas mixture.

For very large aerosols, additional mass transfer occurs because of forced convection of the flow over the surface of the aerosol particle. As a result, an additional correction factor termed the wind effect of aerosols can be formulated. It is given by [5.24]

$$W = 1 + 0.276 Rep^{\frac{1}{2}} Sc^{0.33} \qquad (5.46)$$

where Rep is the Reynolds number based on particle diameter. Thus, a general expression for the rate of heterogeneous nucleation is found by taking the equation for the diffusional rate of condensation onto aerosols (Equation 5.42) and multiplying it by both the Fuchs correction factor, F, and the wind effect, W. Hence,

$$J_{HET} = \frac{2\pi d_p Dp_v(T_v)}{RT_v} (S-K) MWN(d_p) FW \qquad (5.47)$$

5.6 Kelvin Effect

To describe the rate of heterogeneous nucleation of

a vapor onto a preexisting aerosol, it is important to determine the vapor pressure of the specie at the surface of the aerosol. For single component aerosols, less than 0.1 μm in diameter, the vapor pressure is a function of the curvature of the drop. This effect is known as the Kelvin effect. This section will rederive the classical Kelvin relationship for a pure vapor so that two problems with this classical formulation- the case of a vapor in the presence of ions and a multicomponent system of vapors- can be studied and new expressions can be derived.

The Kelvin effect is determined by examining a force balance on the liquid drop and requiring that the drop be in static equilibrium. This requires that the first derivative of the system free energy with respect to radius be equal to zero. The result for the case of homogeneous nucleation of a pure vapor is

$$\frac{\partial \Delta G}{\partial r} = 8\pi r\sigma - \frac{4\pi r^2}{V} RT\ell n \left[\frac{p}{p_v(T_v)}\right] = 0 \qquad (5.48)$$

where

r = radius of aerosol (m),

V = molar volume (m^3/kgmole),

σ = surface tension (N/m),

p = partial pressure of vapor (Pa),

$p_v(T_v)$ = vapor pressure of specie on a flat surface (Pa),

T = temperature (K), and

R = gas constant (Pa-m^3/kgmole-K).

Rearranging Equation (5.46) yields

$$p = p_v \exp\left(\frac{2\sigma V}{rRT}\right) = p_v \exp\left(\frac{4\sigma V_m}{d_p kT}\right) \qquad (5.49)$$

where V_m is the molecular volume (m^3/molecule) and k is Boltzman's constant. Thus, the vapor pressure on the surface of the aerosol is larger than the pure vapor pressure given by the exponent in Equation (5.49). The Kelvin equation can be rewritten as

$$K = \exp\left(\frac{d^* \ell nS}{d_p}\right) \qquad (5.50)$$

where

d^*= diameter of aerosol formed by homogeneous nucleation (m),

d_p = diameter of aerosol particle (m),and

S = supersaturation.

Written in this manner, the physical significance of the Kelvin effect can be understood. The Kelvin effect is a statement about the stability of aerosol particles in a supersaturated vapor. At $r = r^*$, Equation (5.50) has a value of S, the supersaturation. Physically, this implies that the aerosol of size r^* is in equilibrium (no growth or evaporation) because the partial pressure gradient between the vapor and the aerosol as denoted by $S - K$ in Equation (5.47) is zero. Furthermore, the Kelvin effect reveals that particles less than r^* are unstable and will evaporate since $(S - K) < 0$ whereas particles greater than r^* will condense and grow since $(S - K) > 0$. This result is found in many classical aerosol texts.

This classical formulation, however, presents two problems when trying to model the growth of small particles. The first problem is understood by examining Figure 5.4. Consider the case of an aerosol being formed by ion-induced nucleation. As seen in the figure, because of the differences in the free energy of the two systems, the critical radius in an ion environment, r_k, is always less than the corresponding radius in an ion-free environment, r^*. Also plotted in the figure is the Kelvin effect as a function of the

Figure 5.4

Classical Formulation of Kelvin Effect
Problem 1

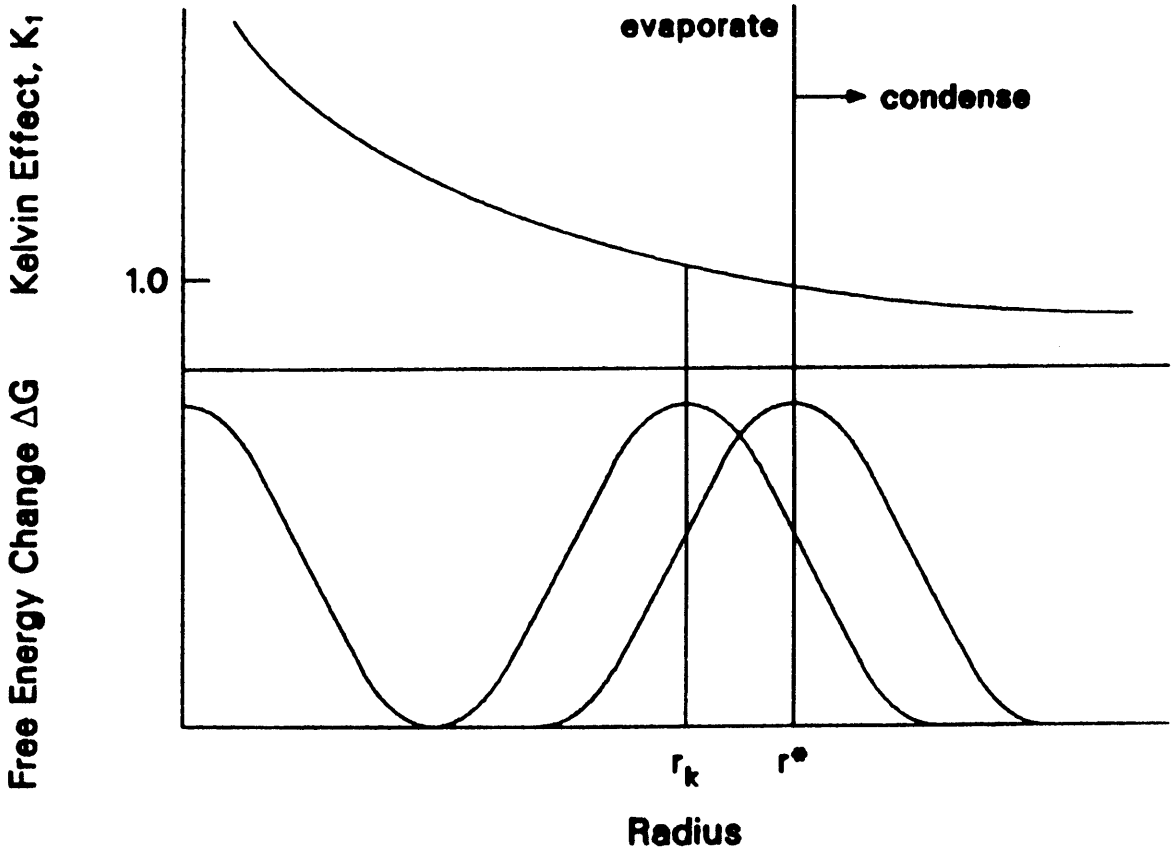

radius of the aerosol particle. As shown in the figure, the Kelvin equation would predict that aerosols formed by ion-induced nucleation would evaporate since $r_K < r^*$. Clearly this is unphysical.

In the presence of ions, Equation (5.49) is not valid since the free energy of the system is altered. As a result, a new Kelvin relationship is needed to describe the vapor pressure behavior of the aerosol in this case. The first derivative of the free energy and thus, the force balance for ion-induced nucleation is

$$\frac{\partial \Delta G}{\partial r} = -kT\ell n \frac{p}{p_v} + \frac{2\sigma V_m}{r} - \frac{e^2 V_m}{8\pi\varepsilon_0 (4\pi r^4)} = 0 \qquad (5.20)$$

Rearranging and exponentiating the logarithm yields

$$p = p_v \exp\left(\frac{2\sigma V_m}{rkT} - \frac{e^2 V_m}{8\pi\varepsilon_0 (4\pi r^4) kT}\right) \qquad (5.51)$$

This is the Kelvin effect for a pure vapor in the presence of ions. Note that the only difference between this result and the ion free vapor result (Equation 5.49) is the second term in the argument of

the exponent. This term accounts for the presence of ions and tends to reduce the vapor pressure at the surface of the aerosol when compared to the ion free result.

The second problem, similar to the first, is understood by examining Figure 5.5. In this case, consider two vapors, for example Cd and CsI, which can nucleate to form aerosols. As shown in the figure, the critical radius of CsI is always larger than for Cd ($r^*_{Cd} < r^*_{CsI}$) due to differences in the surface tension and vapor pressure of the two materials. Thus if Cd is released either in larger quantities or before CsI, it would nucleate first at r^*_{Cd}. As a result, the CsI vapor that is present would see aerosols of size r^*_{Cd} in the system. However, since $r^*_{Cd} < r^*_{CsI}$, the Kelvin effect for CsI would prohibit condensation of CsI onto the aerosol until the radius of the aerosol grew beyond r^*_{CsI} in size. Once again, this situation is not physically correct.

The original Kelvin equation is inapproriate for this situation since it is derived by assuming that each vapor will nucleate separately in the volume. A new relationship based on heteromolecular nucleation is needed. For a multicomponent system of vapors, the free energy minimum of the system is found by calculating the

Figure 5.5

Classical Formulation of Kelvin Effect
Problem 2

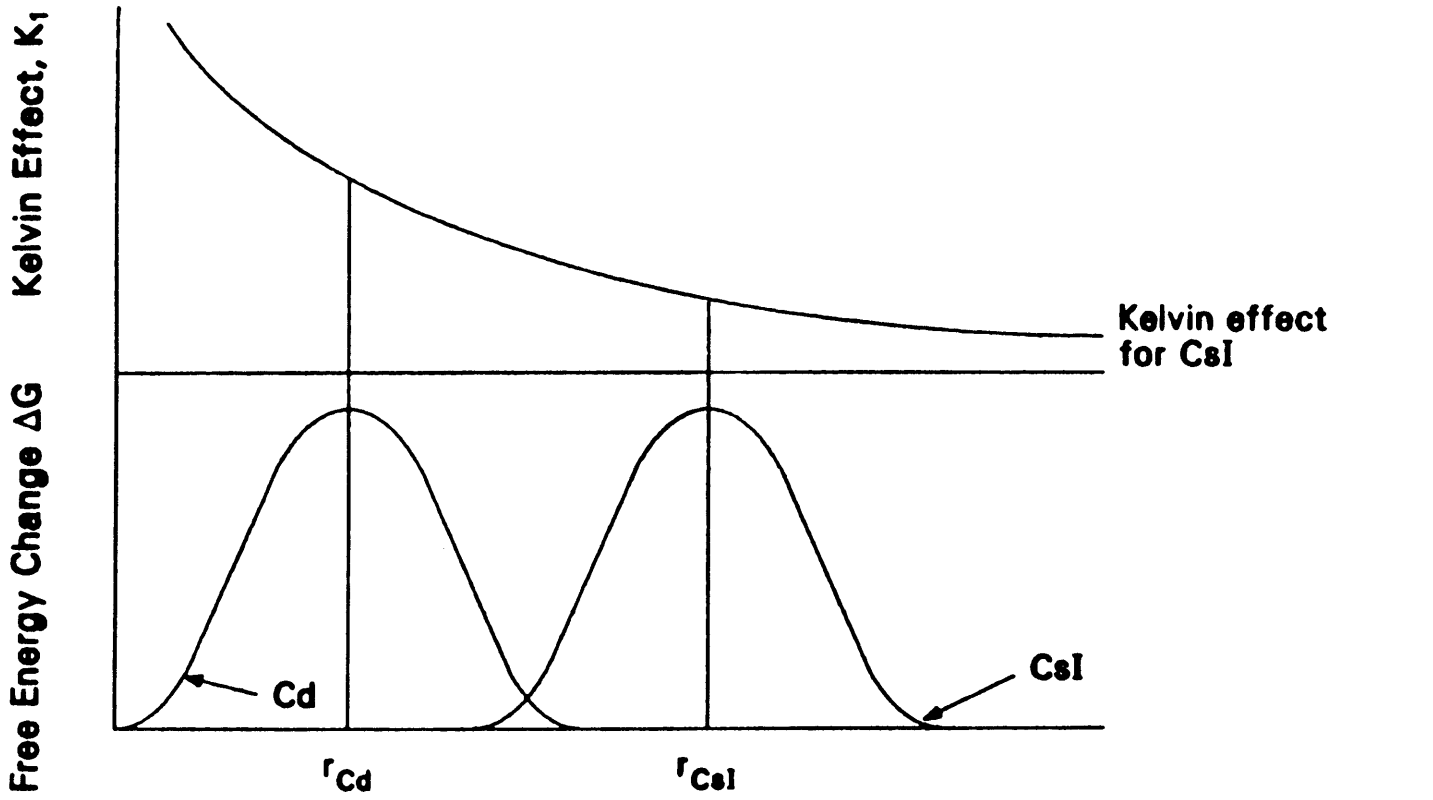

derivative with respect to mole fraction for each specie in the system. Hence,

$$\frac{\partial \Delta G}{\partial n_i} = - RT \ell n \eta_i + \frac{2\sigma \bar{V}_i}{r} - \frac{3\bar{V}}{r} (1-X_i) \frac{d\sigma}{dX_i}\Bigg|_{\substack{\text{all} \\ X \neq X_i}} = 0 \qquad (5.23)$$

where all terms have been defined in Section 5.4. Since $\eta_i = \frac{p_i}{p_{i,\phi} \gamma_i X_i}$, the Kelvin relationship is given by

$$p_i = p_{i,\phi} \gamma_i X_i \exp \left(\frac{2\sigma V_i}{rRT} - \frac{3\bar{V}(1-X_i)}{rRT} \frac{d\sigma}{dX_i} \right) \qquad (5.52)$$

Note that this result differs from the pure vapor result in three respects. First, in the terms multiplying the exponent, the pure component vapor pressure is multiplied by the activity coefficient, γ_i , and the mole fraction, X_i, in the drop. This reflects the fact that the specie is in a solution and its vapor pressure is not necessarily that of the pure component. Second, in the first term of the exponent, the surface tension is not the surface tension of the pure specie but instead is a function of all the species on the

aerosol. Finally, the second term in the exponent accounts for changes in surface tension with respect to composition. This result is a natural extension of the binary result obtained by Mirabel and Katz [5.20]. However,once again application of this result to a multicomponent system is difficult because of the lack of information on activity coefficients and the surface tension of a multicomponent aerosol. Nevertheless, it is presented for completeness.

This section has illustrated that in the presence of ions or in a multicomponent system of vapors the Kelvin effect would have to be modified to predict accurately the vapor pressure behavior at the surface of the aerosol.

5.7 Summary and Application to Current Work

The purpose of this section was to review models for aerosol formation including homogeneous nucleation, ion-induced nucleation, heteromolecular nucleation and heterogeneous nucleation. Certain key results from this review are highlighted below.

(1) With the exception of heterogeneous nucleation, all of the aerosol formation processes studied are characterized by a free energy barrier that must be overcome for nucleation to occur. For homogeneous nucleation, the free energy barrier results from the competition between the energy released in the condensation process and

the surface energy required to form aerosols.

(2) Gas temperature, surface tension, vapor pressure and vapor supersaturation are the key variables needed to describe the rate of aerosol formation.

(3) Although the Becker-Doring theory of homogeneous nucleation has several limitations, it has been applied with relative success to a variety of engineering problems.

(4) The presence of ions in the nucleation environment alters the free energy of the system. The electrical attraction between the ions and vapor provides an additional driving force for nucleation.

(5) The thermodynamics of heteromolecular nucleation requires information about the chemical interactions that occur in the multicomponent system of vapors. Since this information is not well known for vapors produced in a severe reactor accident, this model could not be considered here.

(6) Changes in the nucleation environment such as the presence of ions or a multicomponent system of vapors will alter the overall free energy of the system. As a result, the classical expression for the Kelvin effect must be modified accordingly to predict the vapor pressure behavior at the surface of the aerosol.

Hot vapors released from an overheated reactor core in a severe accident will condense and form aerosols. The ultimate behavior of the vapor/aerosol system is determined by the competition among the nucleation mechanisms reviewed earlier. Based on this review, the following questions can be posed concerning the role of aerosol formation in a severe reactor accident.

(1) Under what conditions will the rate of vapor supersaturation be so great that it cannot be relieved by heterogeneous

nucleation alone and thus cause ion-induced and/or homogeneous nucleation to occur?

(2) What is the effect of ions on the nucleation behavior of the vapor and how effective is ion-induced nucleation in relieving vapor supersaturation?

(3) What is the aerosol particle size distribution following the period of aerosol formation in a severe reactor accident?

The first two questions will be answered in Section 6. Rates of homogeneous, ion-induced and heterogeneous nucleation will be calculated for Ag, Cd and CsI under a variety of conditions. The calculations will determine the nucleation behavior of these three potential aerosol sources expected in the heatup phase of a severe reactor accident. In addition, these rates will be compared to illustrate the competition among these mechanisms and to predict for a given set of conditions the dominant mechanism of gas-to-particle conversion. In Section 7, the aerosol transport equation will be solved to obtain the aerosol particle size distribution following the period of aerosol formation. This systematic study of the aerosol formation process should provide answers to these questions and thereby increase the understanding of fission product and aerosol behavior in severe reactor accidents.

5.8 REFERENCES

5.1 Chalmers, B. (ed.), Condensation and Evaporation, Progress in Materials Science, Vol. 11, MacMillian Co.,New York, 1963, pp. 1-40.

5.2 Feder, J., Russell, K.C., Lothe, J. and Pound, G.M.,"Homogeneous Nucleation and Growth of Droplets", Adv.Physics, 15, 1966, pp. 111-178.

5.3 Omberg, R.P. and Olander, D.R., "Effect of Condensation in the Boundary Layer on Mass Transfer from a Rotating Disk," The Physics of Fluids, 14 (8), pp. 1605-1618, August 1971.

5.4 Lothe, J. and Pound, G.M., "Reconsiderations of Nucleation Theory," J. Chem. Phys., 36 (8), April 1962.

5.5 McGraw, R. and Marlow, W.H., "The Multistate Kinetics of Nucleation in the Presence of an Aerosol", J. Chem. Phys., 78 (5), March 1983.

5.6 Katz, J.L. and Donohue, M.D., "Nucleation with Simultaneous Chemical Reaction", J. Coll. Inter. Sci., 85 (1), January 1982.

5.7 Kennedy, M.F. et. al., Primary Aerosol Particle Size Distribution from Homogeneous Nucleation Condensation and Particle Growth, NUREG-0391, 1977.

5.8 Kolar-Anic, Lj. and Balescu, R., "On the Steady State Solutions of the Kinetics of Homogeneous Nucleation," Chem. Physics, 46, 1980, pp. 281-286.

5.9 Dawson, D.B.. et. al., "Nucleation of Supersaturated Vaporsin Nozzles",J. Chem. Phys., 51,(12), Dec 15, 1969, pp. 5389-5397.

5.10 Hill, P.G., Witting, H. and Demetri, E.P., "Condensation of Metal Vapors During Rapid Expansion," J. Heat Transfer, November 1963.

5.11 Gelbard, F. and Seinfeld, J., "The General Dynamic Equation for Aerosols", J. Coll. Int. Sci., 68 (2), Feb. 1979.

5.12 Epstein, M. and Rosner, D., "Enhancement of Diffusion-Limited Vaporization Rates by

Condensation Within the Thermal Boundary Layer," Int. J. Heat and Mass Transfer, 13, 1970, pp. 1393-1414.

5.13 Rosner, D. and Epstein, M.,"Fog Formation Conditions Near Cool Surfaces," J. Coll. and Int. Sci., 28 (1), September 1968.

5.14 Rosner,D., "Enhancement of Diffusion-Limited Vaporization Rates by Condensation Within the Thermal Boundary Layer," Int. J. Heat and Mass Transfer, 10, 1967, pp. 1267-1279.

5.15 Im, K.H. and Ahluwalia, R.K., "Nucleation of Slag and Seed in MHD Plants," 20th Symposium on Engineering Aspects of MHD, Univ. of Cal. Irvine, June 14-16, 1982.

5.16 Im, K.H. and Ahluwalia, R.K., "RAFT: A Computer Model for Formation and Transport of Fission Product Aerosols in LWR Primary Systems", ANS Topical Meeting on Fission Product Behavior and Source Term Research, Snowbird, Utah, July 15-19, 1984.

5.17 Russell, K.C., "Nucleation on Gaseous Ions," J. Chem.Phys., 5, (4), Feb. 15,1969, pp. 1809-1816 .

5.18 Hidy, G.M., Aerosols: An Industrial and Environmental Science, Academic Press, 1984.

5.19 Reiss, H., "The Kinetics of Phase Transitions in Binary Systems", J. Chem. Phys.,18,(6), June 1950, pp.840-848.

5.20 Mirabel, P. and Katz, J.L., "Binary Homogeneous Nucleation as a Mechanism for the Formation of Aerosols", J. Chem.Phys., 60, (3), February 1, 1974, pp. 1138-1144.

5.21 Smith, J.M. and VanNess, H. C., Introduction to Chemical Engineering Thermodynamics, McGraw-Hill, 1975.

5.22 Hinds, W., Aerosol Technology, Wiley Interscience, New York, 1982.

5.23 Freidlander, S.K., Smoke, Dust and Haze: Fundamentals of Aerosol Science, Wiley Interscience, New York, 1977.

5.24 Davies, C.N., "Evaporation of Airborne Drops", Fundamentals of Aerosol Science, Chapter 3, Wiley Interscience, New York, 1978.

6. AEROSOL NUCLEATION BEHAVIOR OF SILVER, CADMIUM AND CESIUM IODIDE

6.1 Introduction

Several aerosol sources exist in an LWR core during a severe reactor accident. They include:

(1) Ag, In and Cd vapors released from molten absorber material (only for those design with Ag-In-Cd control rods),
(2) CsI and CsOH, the major chemical forms of cesium and iodine in the accident,
(3) Sn released from hot cladding,
(4) Fe and other vapors emitted from hot structural material,
(5) ZrO_2 from oxidized cladding, and
(6) UO_2/Zr vapors from molten fuel/cladding.

The work presented in this section is limited to aerosol sources created in the early stages of the accident before significant fuel melting. As a result, UO_2 vapor is not considered. In addition, ZrO_2 is not considered since its potential contribution was judged to be small in comparison to other aerosol sources in the core.

Examination of the material properties of the remaining aerosol sources suggests that Ag, Cd and CsI would bracket the nucleation behavior of vapors released in a severe accident. Silver is a low vapor pressure material with a very high surface tension characteristic of most metals. Cadmium is very volatile but has a

moderate surface tension. Since cesium iodide is a salt, it has a low surface tension and low vapor pressure.

Section 6.2 presents results for homogeneous nucleation rates of Ag, Cd and CsI using Becker-Doring theory. Ion-induced nucleation rates for the three species are compared with homogeneous nucleation rates in Section 6.3. The rate of heterogeneous nucleation for cadmium is calculated for a wide variety of conditions in Section 6.4. Aerosol maps are developed in Section 6.5 to study the competition among these three mechanisms for depleting vapor and to determine the dominant gas-to-particle conversion mechanism under a variety of conditions. The effect of wall condensation as a competing mechanism for vapor depletion is examined in Section 6.6. Conclusions are drawn in Section 6.7.

6.2 Homogeneous Nucleation Results and Discussion

Controversy still exists over which homogeneous nucleation model should be used to predict aerosol formation rates. However, since all of the studies mentioned in Section 5 that involved metal vapors used the classical Becker-Doring theory, the same approach will be taken here.

Homogeneous nucleation rates for Ag, Cd and CsI were calculated using Equation 5.14. Values of the material properties are found in Appendix C and the results are shown in Figures 6.1 through 6.3. Several observations can be made from these figures:

(1) Whereas water will nucleate at supersaturations slightly greater than one, the supersaturation needed for Ag and Cd to homogeneously nucleate is large. Because the surface tensions of Ag and Cd are about five to ten times that of water, a much larger driving force or supersaturation is needed for Ag and Cd to overcome the free energy barrier; because of its low surface tension, CsI nucleates at much lower supersaturations than Ag or Cd;
(2) As the temperature of the system increases, the supersaturation required to nucleate decreases. Since more thermal energy (~ kT) is available, less supersaturation is needed to produce the same change in state; and
(3) A critical supersaturation, S_{crit}, is needed to initiate nucleation. Above this value, the rate of homogeneous nucleation increases sharply. This behavior is the result of the free energy barrier to spontaneous nucleation that exists. Once the vapor has enough free energy to overcome the barrier either as a result of temperature or supersaturation, homogenous nucleation occurs to reduce the free energy of the system.

6.3 Ion-induced Nucleation Results and Discussion

Ion-induced nulceation rates for Ag, Cd and CsI were calculated using Equation (5.19). The results, superimposed on the homogeneous nucleation predictions,

Figure 6.1

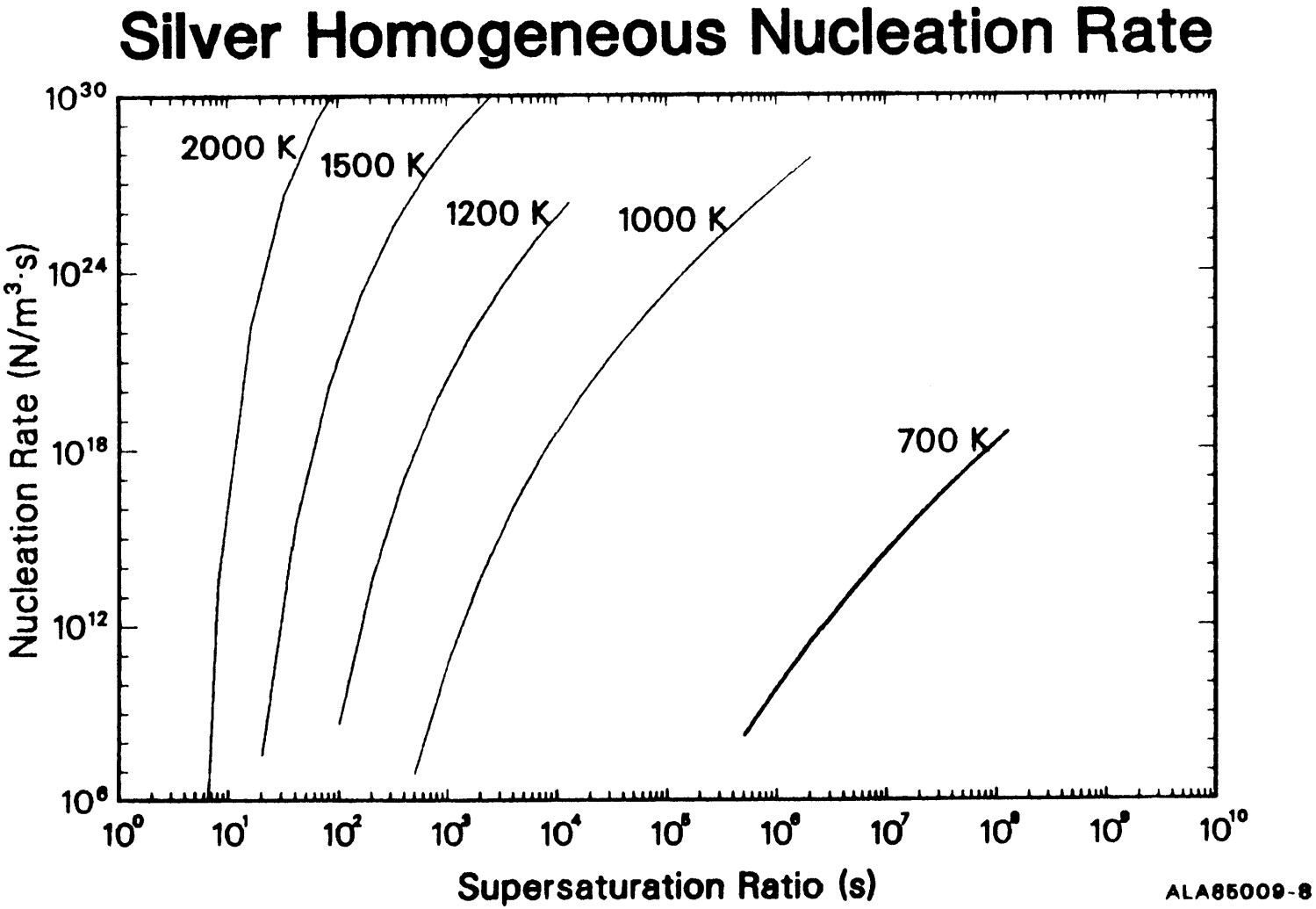
Silver Homogeneous Nucleation Rate
Nucleation Rate (N/m³·s)
10³⁰
10²⁴
10¹⁸
10¹²
10⁶
2000 K
1500 K
1200 K
1000 K
700 K
10⁰
10¹
10²
10³
10⁴
10⁵
10⁶
10⁷
10⁸
10⁹
10¹⁰
Supersaturation Ratio (s)
ALA85009-8

Figure 6.2

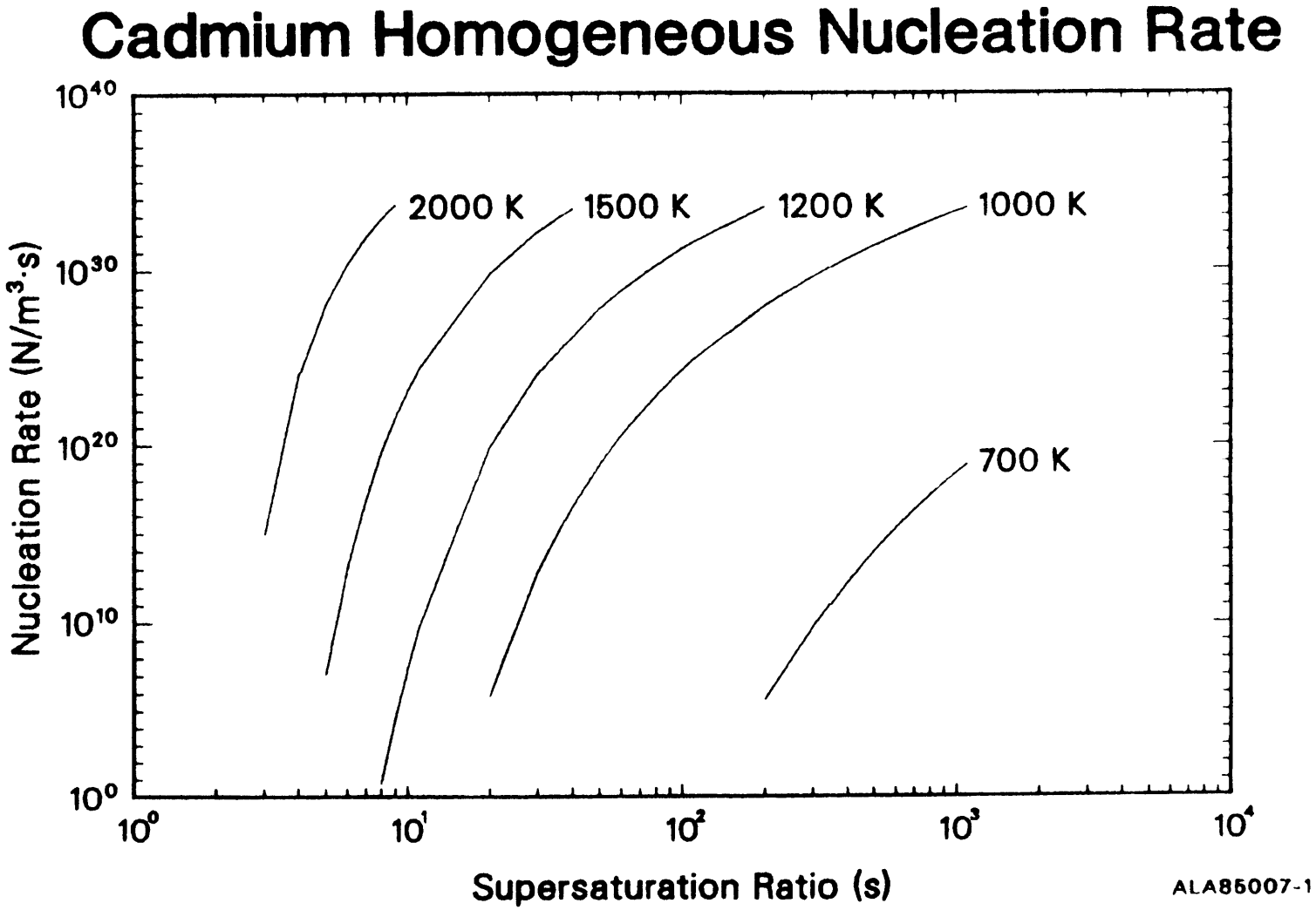
Cadmium Homogeneous Nucleation Rate
Nucleation Rate (N/m³·s)
10⁴⁰
10³⁰
10²⁰
10¹⁰
10⁰
2000 K
1500 K
1200 K
1000 K
700 K
10⁰
10¹
10²
10³
10⁴
Supersaturation Ratio (s)
ALA85007-1

Figure 6.3

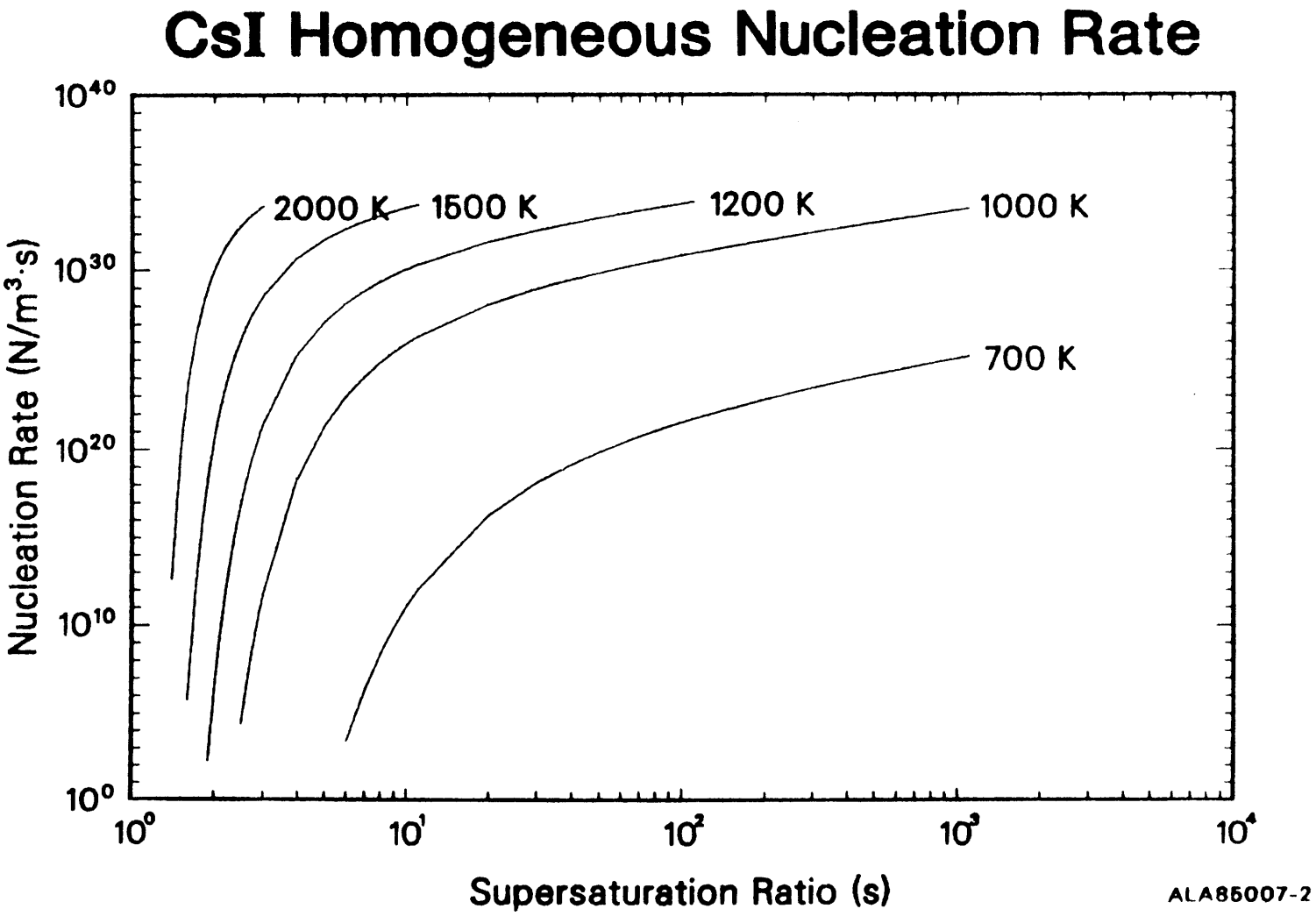
CsI Homogeneous Nucleation Rate
Nucleation Rate (N/m³·s)
10⁴⁰
10³⁰
10²⁰
10¹⁰
10⁰
2000 K
1500 K
1200 K
1000 K
700 K
10⁰
10¹
10²
10³
10⁴
Supersaturation Ratio (s)
ALA85007-2

are shown in Figures 6.4 through 6.6. The calculations assumed that (1) $\varepsilon = \infty$ and, (2) the ion density, N_a, was 10^{21} ions/cc based on a radiation level of 10^7 R/hr in the core.

As seen in the figures, the high concentrations of ions used in the calculation produce nucleation rates which are similar in magnitude to those predicted by homogeneous nucleation. However, the supersaturation at which ion-induced nucleation begins is lower than that required for homogeneous nucleation. This result can be better understood by examining the effect ions have on the system free energy. The reduction in the supersaturation is due to the presence of the electrical term in the free energy balance. At high temperatures (~2000 K), the free energy associated with the electrical potential is small compared to the condensation term (kTlnS) and the effect is less important. At lower temperatures, however, the electrical term is the dominant driving force. The electrical potential helps to reduce the height of the free energy barrier and thus lowers the supersaturation required for nucleation to occur. Moreover, this effect is most noticeable for Ag and Cd at lower temperatures, where they are less volatile and the thermal energy of the system is small. As the temperature increases, the

Figure 6.4

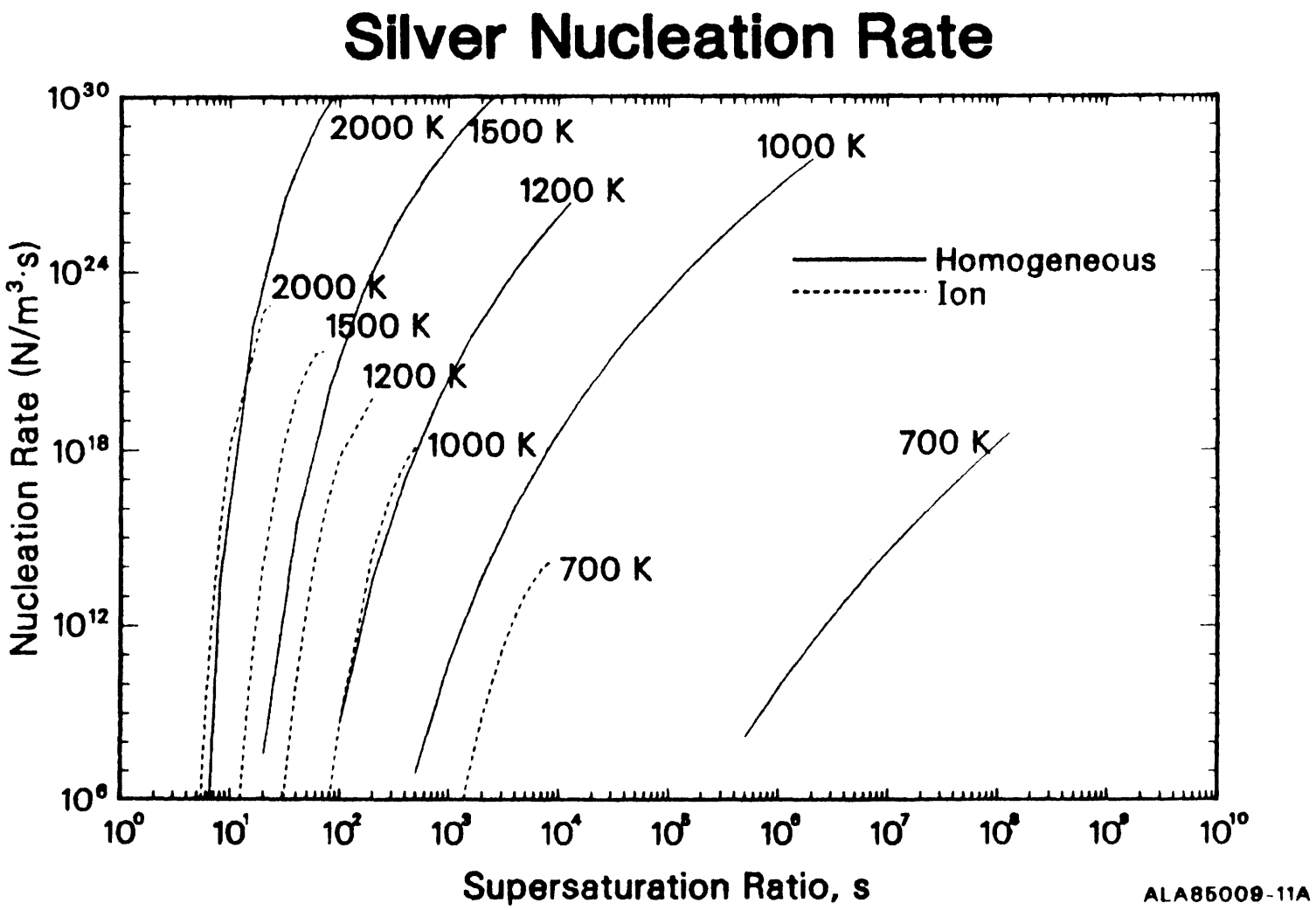
Silver Nucleation Rate
Nucleation Rate (N/m³·s)
Supersaturation Ratio, s
2000 K
1500 K
1200 K
1000 K
700 K
Homogeneous
Ion
ALA85009-11A

Figure 6.5

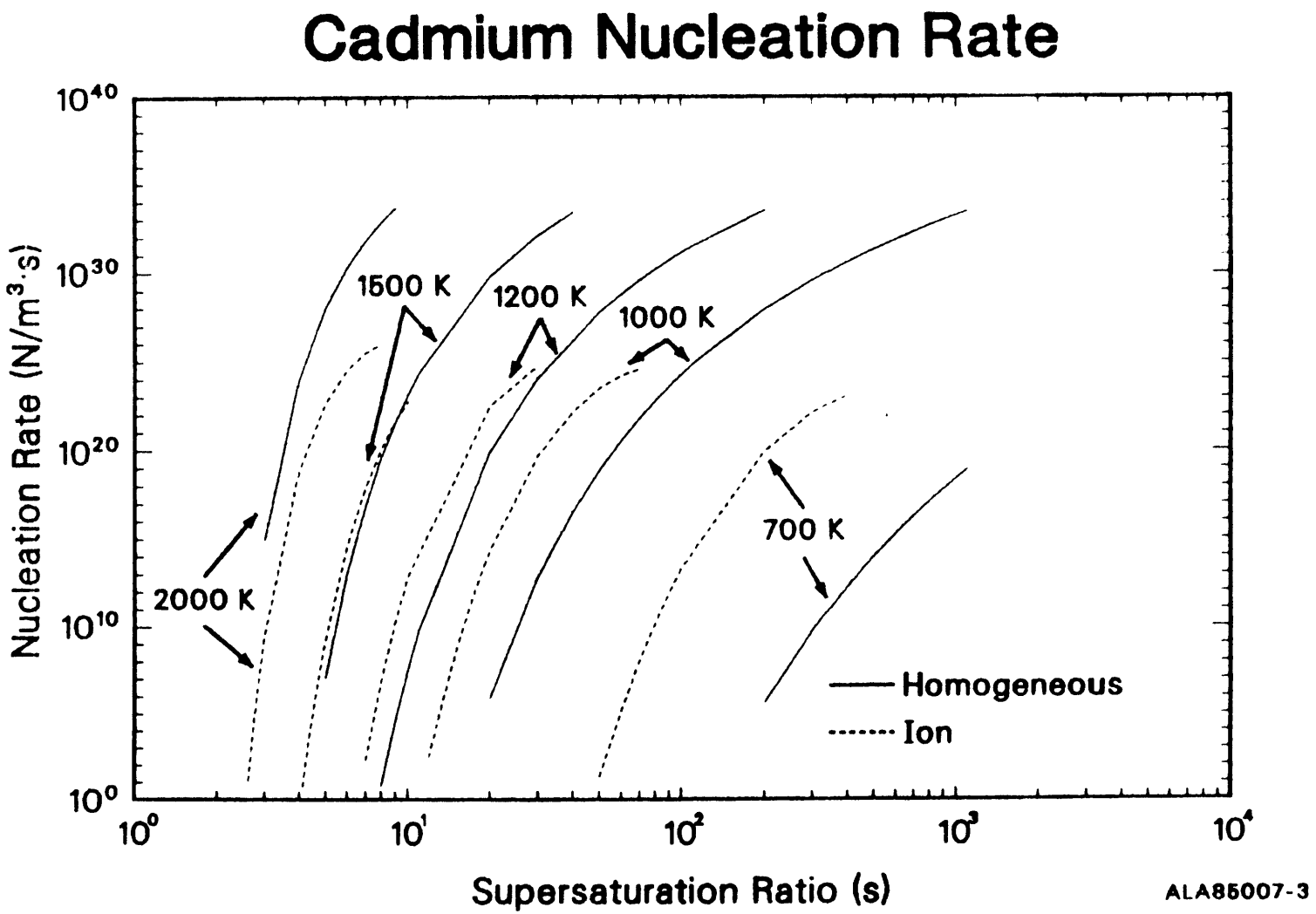
Cadmium Nucleation Rate
Nucleation Rate (N/m³·s)
10⁴⁰
10³⁰
10²⁰
10¹⁰
10⁰
10⁰
10¹
10²
10³
10⁴
Supersaturation Ratio (s)
2000 K
1500 K
1200 K
1000 K
700 K
Homogeneous
Ion
ALA85007-3

Figure 6.6

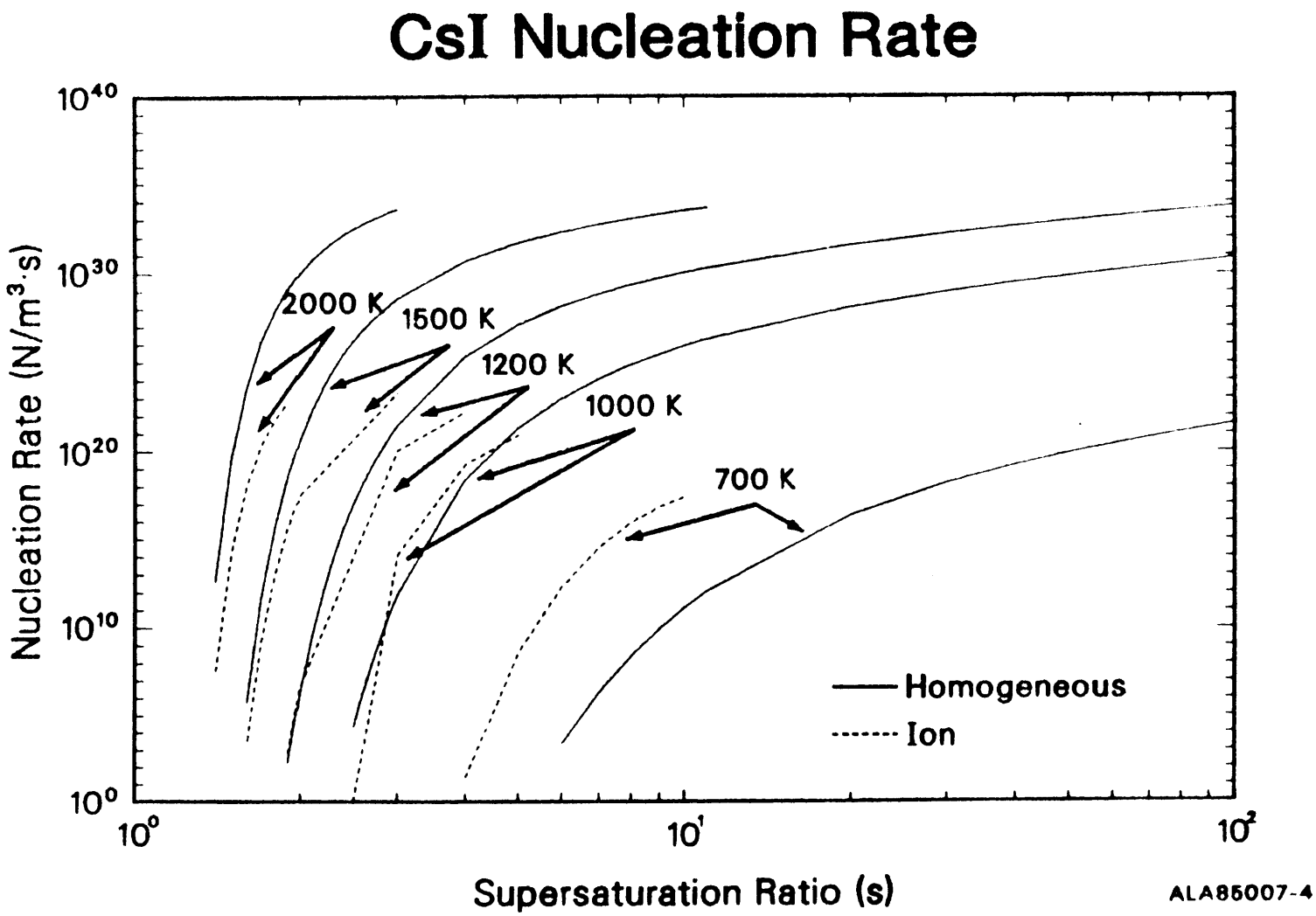
CsI Nucleation Rate
Nucleation Rate (N/m³·s)
10⁴⁰
10³⁰
10²⁰
10¹⁰
10⁰
2000 K
1500 K
1200 K
1000 K
700 K
Homogeneous
Ion
10⁰
10¹
10²
Supersaturation Ratio (s)
ALA85007-4

effect is diminished since the condensation term dominates.

6.4 Heterogeneous Nucleation Results and Discussion

Since heterogeneous nucleation or condensation onto a preexisting aerosol is a complex function of many variables, a few assumptions were made to simplify the calculations. The computations were performed using a 50/50 molar mixture of hydrogen and steam at 6.9 MPa (1000 psi) as the carrier gas. The wind effect, W, in Equation (5.47) was neglected. Cadmium was used as the condensing specie in all calculations and diffusion coefficients were calculated from Chapman-Eskong theory (see Section 3.3). The preexisting aerosol was considered to be monodisperse; the number concentration was determined by assuming that the total aerosol surface area was 1 cm^2 for all particle sizes. Hence,

$$N(d_p) = \frac{10^{-4} m^2}{\pi d_p^2} \qquad (6.1)$$

Predictions of the heterogeneous nucleation rate using the kinetic theory (Equation 5.41), diffusion (Equation 5.42) and Fuchs (Equation 5.47) models were

compared over a large range of particle size. The results of the comparison are shown in Figure 6.7 for cadmium at 1500 K and a supersaturation of 7. For very large particles, much greater than the mean free path ($\sim 10^{-8}$ m), Fuchs' model approaches the diffusion theory result, since the correction factor (Equation 5.43) approaches unity. At small particle sizes, as expected, the diffusion model is inappropriate. It is included however, to illustrate the following point. The diffusion model is currently used to determine the rate of vapor condensation onto aerosols in TRAPMELT. Since the aerosol sizes input to TRAPMELT are generally large (~ 1.0 micron), the model is appropriate. However, were this model to be used blindly to deal with the small-sized aerosols that might be generated due to ion-induced nucleation (~ 10Å), then the results would be in error. As a result, if aerosol formation is to be modeled in an aerosol code like TRAPMELT, a new heterogeneous nucleation model is needed.

The kinetic theory model predicts very large mass transfer rates. The calculation shows a slight increase with particle size but then saturates and is size independent above 1.0 micron. These results substantiate the discussion in Section 5.5 which states that this model is inappropriate to describe heterogeneous

Figure 6.7

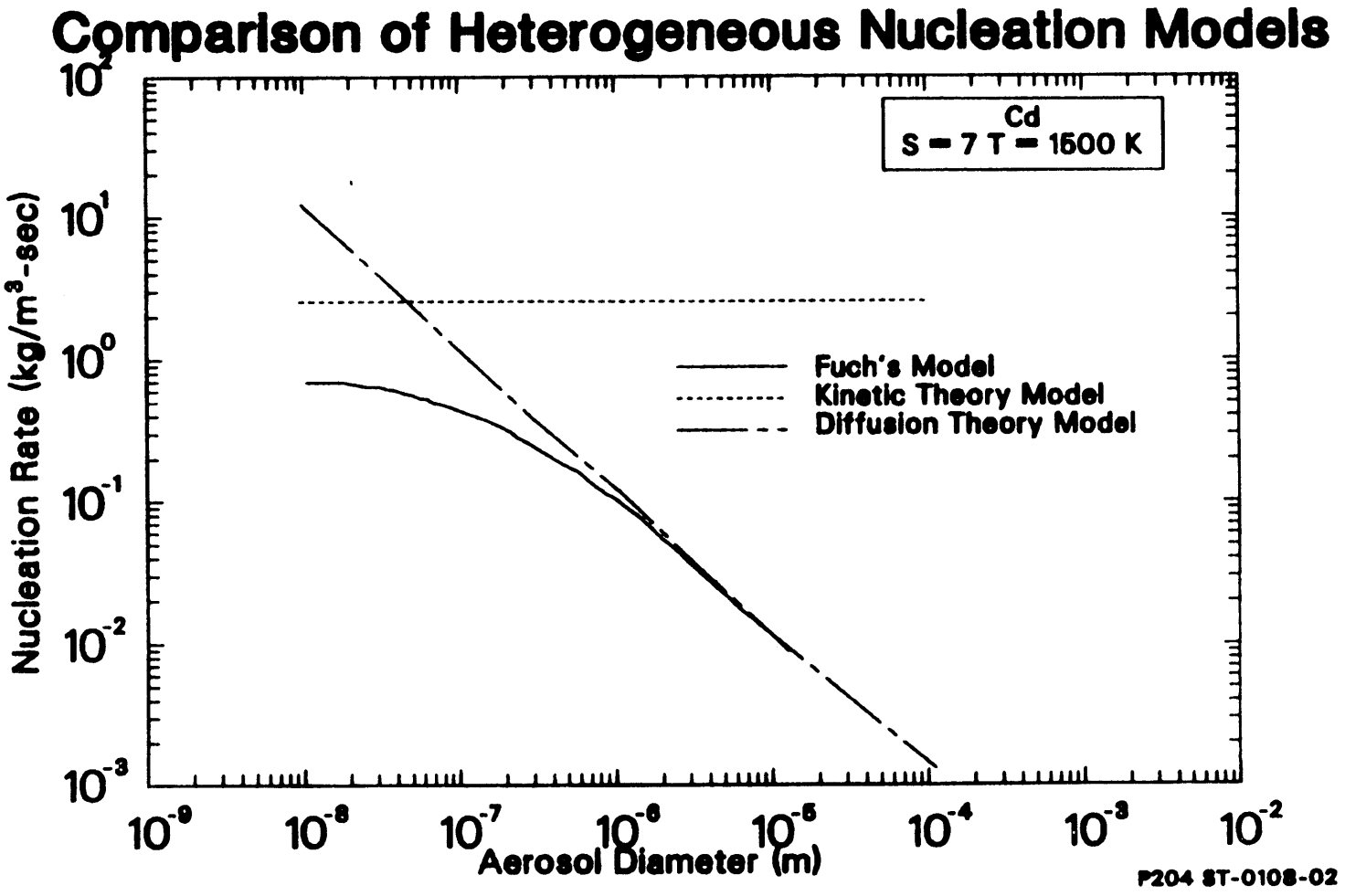
Comparison of Heterogeneous Nucleation Models
Cd
S = 7 T = 1500 K
Fuch's Model
Kinetic Theory Model
Diffusion Theory Model
Nucleation Rate (kg/m³-sec)
Aerosol Diameter (m)
P204 ST-0108-02

nucleation.

Fuchs' model predicts rates that are more reasonable for small aerosols. Since the correction factor in the Fuchs model decreases as the Knudsen number increases, the Fuchs and diffusion models diverge at small particle sizes. Based on this comparison, Fuchs' model is recommended to predict heterogeneous nucleation rates over a large range of aerosol sizes.

The Fuchs model was also used to determine the effects of supersaturation, temperature and particle size on the rate of heterogeneous nucleation for cadmium. In Figures 6.8 and 6.9, the cadmium heterogeneous nucleation rate is plotted as a function of supersaturation and temperature for both a 100 Å (10^{-10} m) and a 0.1 mm (10^{-4} m) monodisperse aerosol each having the same total aerosol surface area. The nucleation rate increases as the temperature increases in both cases because diffusion coefficients increase with temperature. The dependence of the nucleation rate on supersaturation is quite different for heterogeneous nucleation than for homogeneous or ion-induced nucleation. A critical supersaturation is not needed to initiate the process. In fact, as shown in the plots, heterogeneous nucleation exhibits a linear dependence on supersaturation. A comparison of the two figures also

Figure 6.8

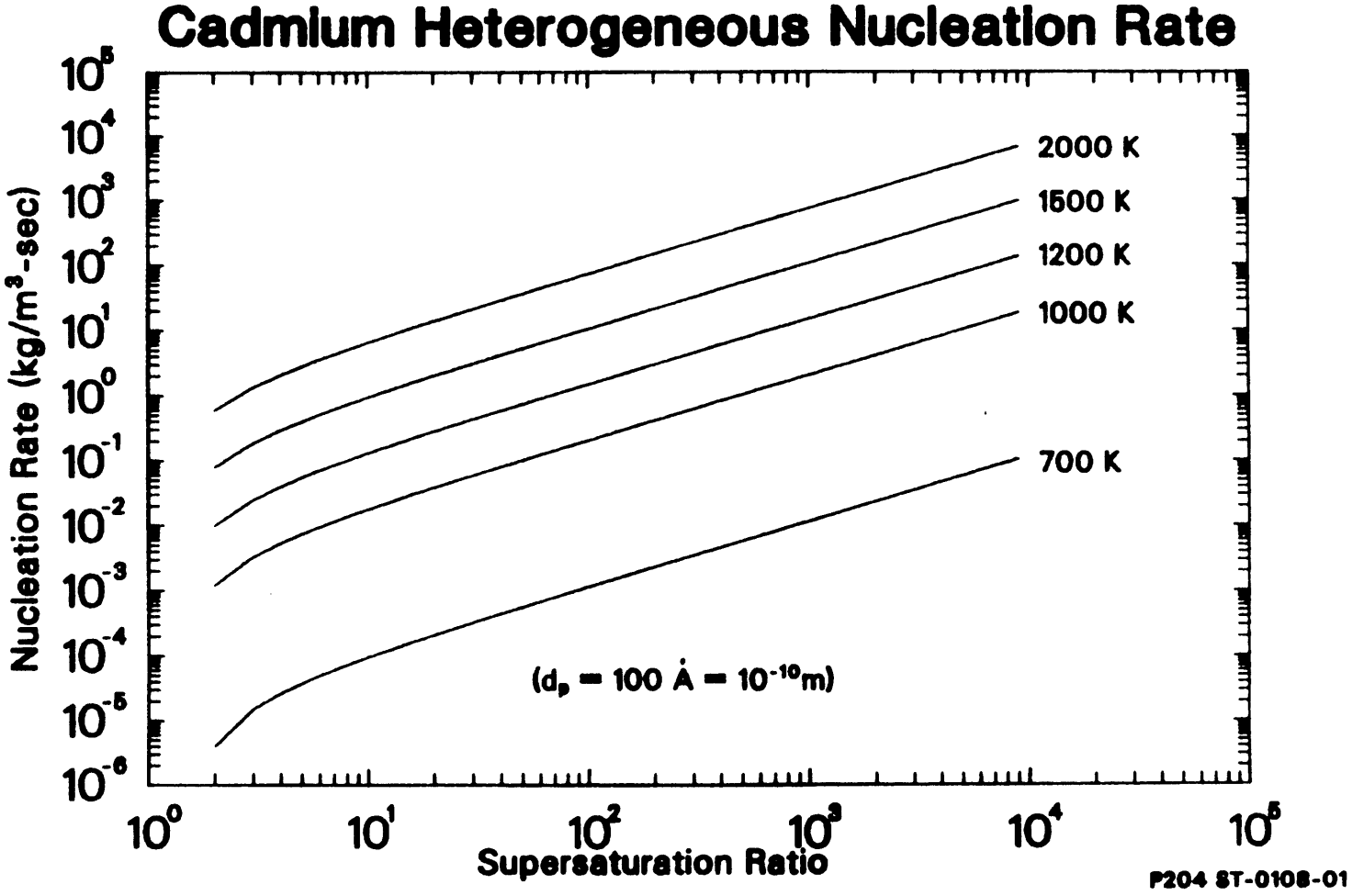
Cadmium Heterogeneous Nucleation Rate
Nucleation Rate (kg/m³-sec)
10⁵
10⁴
10³
10²
10¹
10⁰
10⁻¹
10⁻²
10⁻³
10⁻⁴
10⁻⁵
10⁻⁶
2000 K
1500 K
1200 K
1000 K
700 K
(dp = 100 Å = 10⁻¹⁰m)
10⁰
10¹
10²
10³
10⁴
10⁵
Supersaturation Ratio
P204 ST-0108-01

Figure 6.9

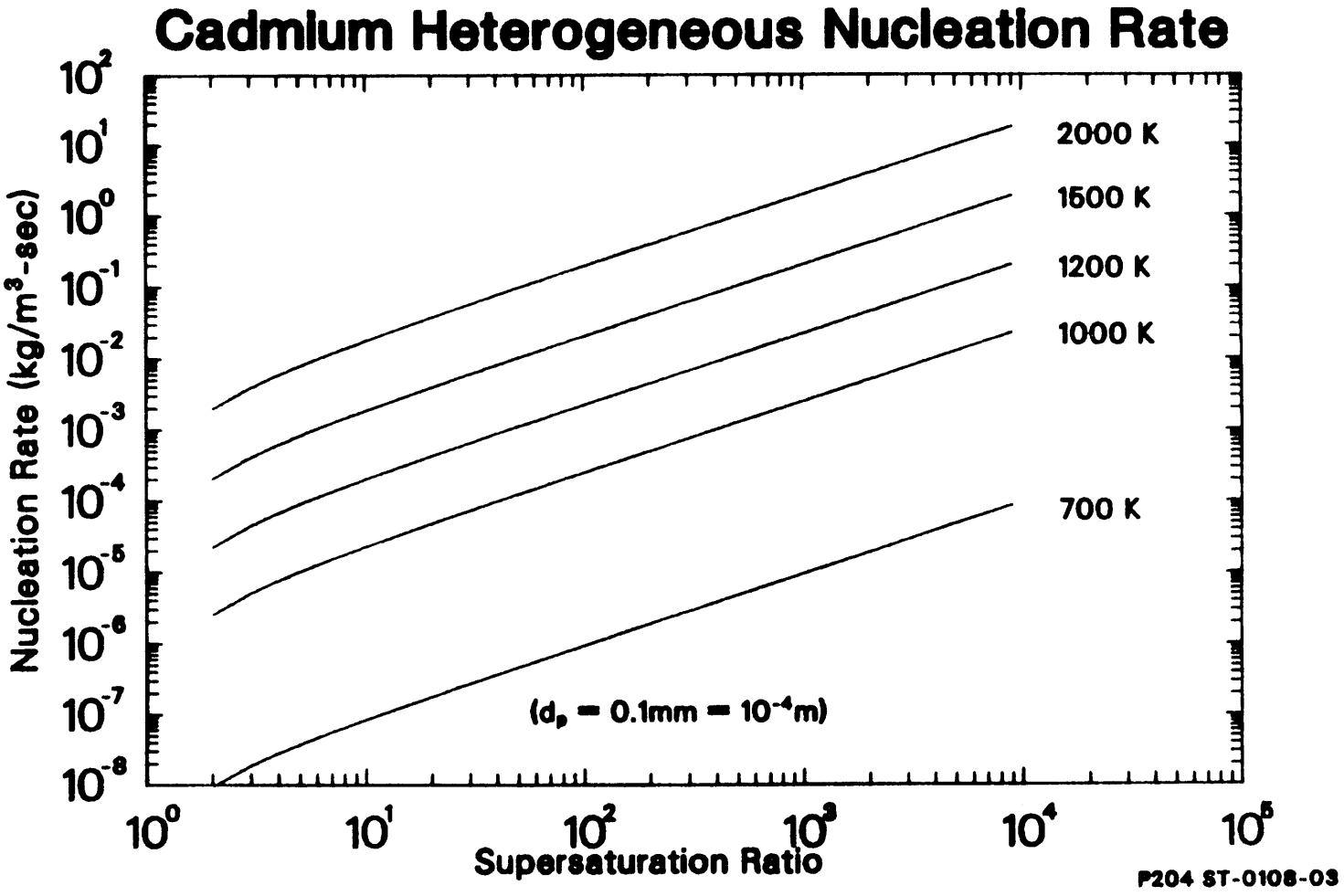
Cadmium Heterogeneous Nucleation Rate
Nucleation Rate (kg/m³-sec)
10²
10¹
10⁰
10⁻¹
10⁻²
10⁻³
10⁻⁴
10⁻⁵
10⁻⁶
10⁻⁷
10⁻⁸
2000 K
1500 K
1200 K
1000 K
700 K
(d_p = 0.1mm = 10⁻⁴m)
10⁰
10¹
10²
10³
10⁴
10⁵
Supersaturation Ratio
P204 ST-0108-03

indicates that the nucleation rate is larger for smaller particles. These results are not specific to cadmium. In general, for a constant surface area of aerosol, smaller sized aerosols are more effective than larger aerosols at condensing vapor.

6.5 Aerosol Maps

Calculating the rate of nucleation for each aerosol formation mechanism can provide some insight into the process of gas-to-particle conversion. However, an examination of these rate processes alone (homogeneous, ion-induced and heterogeneous nucleation) cannot yield information on the dynamic behavior of the vapor-aerosol system. In a severe reactor accident, vapor release will be a continuous process occurring in the presence of a preexisting aerosol. As a result, during the period of aerosol formation, homogeneous, ion-induced and heterogeneous nucleation could occur simultaneously to deplete vapor from the system. Depending on the aerosol concentration and vapor supersaturation, the preexisting aerosol may or may not provide enough surface area to be the dominant mechanism of gas-to-particle conversion. The purpose of this section is to answer the question:

Under what conditions will heterogeneous nucleation

be unable to relieve vapor supersaturation and thus cause the vapor to nucleate either homogeneously or in the presence of ions?

The answer to this question can only be found by examining all the nucleation processes simultaneously, thereby illustrating the competing pathways that exist for vapor depletion and obtaining valuable insight into the dynamic behavior of the system.

Aerosol "maps" have been developed to understand under what conditions will a vapor nucleate. The purpose of these "maps" is to determine regimes in which each nucleation mechanism occurs. The primary variables that are required to predict the dominant nucleation mechanism are

(1) release rate of vapor or vapor supersaturation,

(2) gas temperature,

(3) aerosol size and surface area, and

(4) aerosol concentration.

(If condensation onto walls were included, then both the temperature and surface area of the wall would also be needed. The effect of wall condensation is examined separately in Section 6.6. There are other variables such as ion concentration and system pressure which also affect nucleation. However, these variables are considered to be secondary and hence are not allowed to

vary in this calculation.) Since four variables are required to define the state of the system, a complete mapping of the system can only be done in four dimensional space. Given this inherent limitation, the aerosol "map" will provide a two dimensional slice of this 4-D space.

Figures 6.10 through 6.12 are nucleation maps for Ag, Cd and CsI in supersaturation-temperature space. These maps were developed by comparing the rates of homogeneous and ion-induced nucleation to the rate of heterogeneous nucleation for a given supersaturation and temperature. The calculations used a 100 Å monodisperse aerosol with a total surface area of 1 cm^2. Values of the transport properties were identical to those used previously. An algorithm termed AEROMAP was developed to determine the borders of the various nucleation regimes. A detailed discussion of this algorithm is found in Appendix E.

As can be seen from all the plots, at low supersaturations, the presence of 1 cm^2 of aerosol surface area used in the heterogeneous nucleation calculation is sufficient to provide a means of gas-to-particle conversion. As the supersaturation increases, ion-induced nucleation also becomes an important mechanism of aerosol formation. This region

Figure 6.10

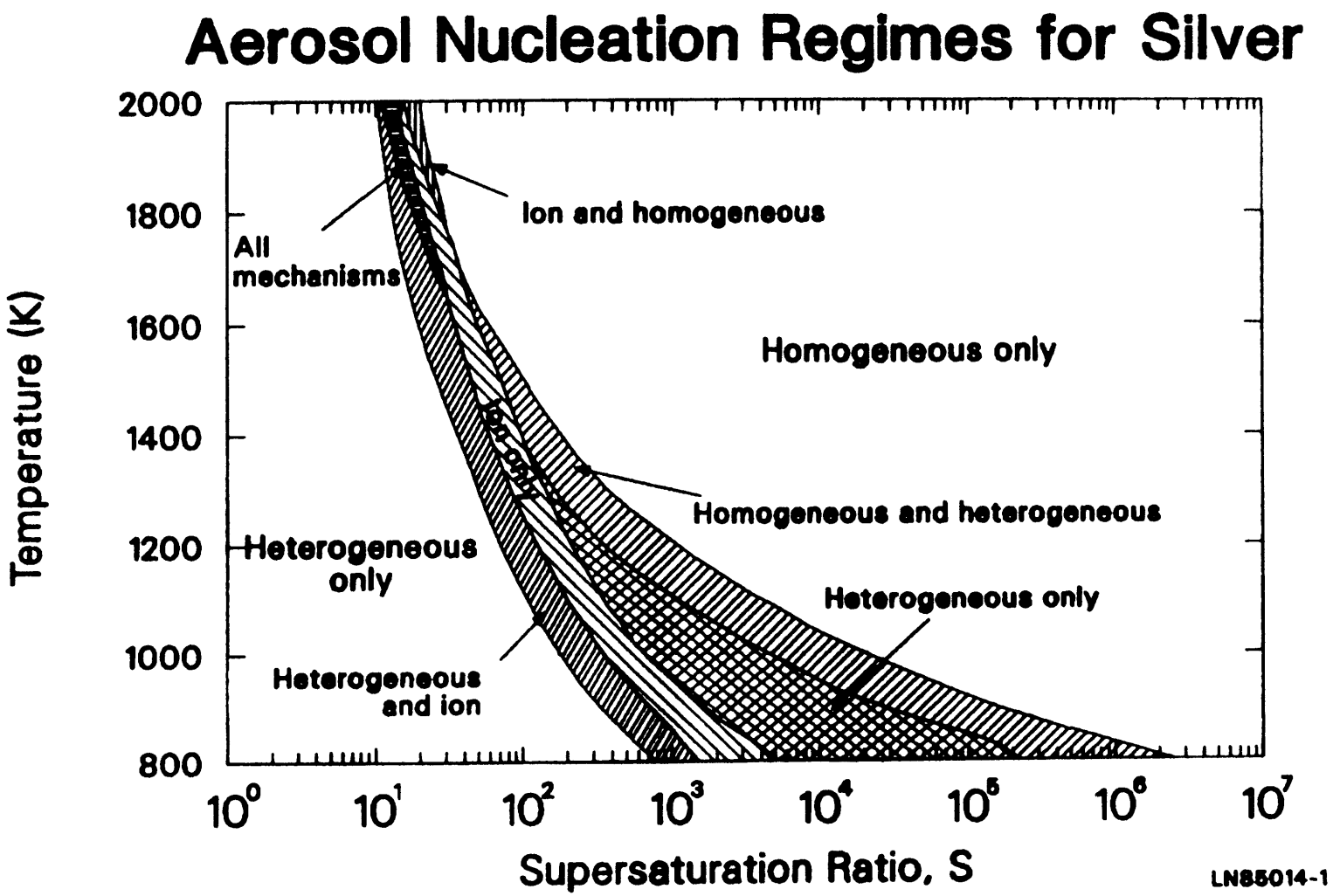
Aerosol Nucleation Regimes for Silver
Temperature (K)
2000
1800
1600
1400
1200
1000
800
All mechanisms
Ion and homogeneous
Homogeneous only
Homogeneous and heterogeneous
Heterogeneous only
Heterogeneous only
Heterogeneous and ion
10^0
10^1
10^2
10^3
10^4
10^5
10^6
10^7
Supersaturation Ratio, S
LN85014-1

Figure 6.11

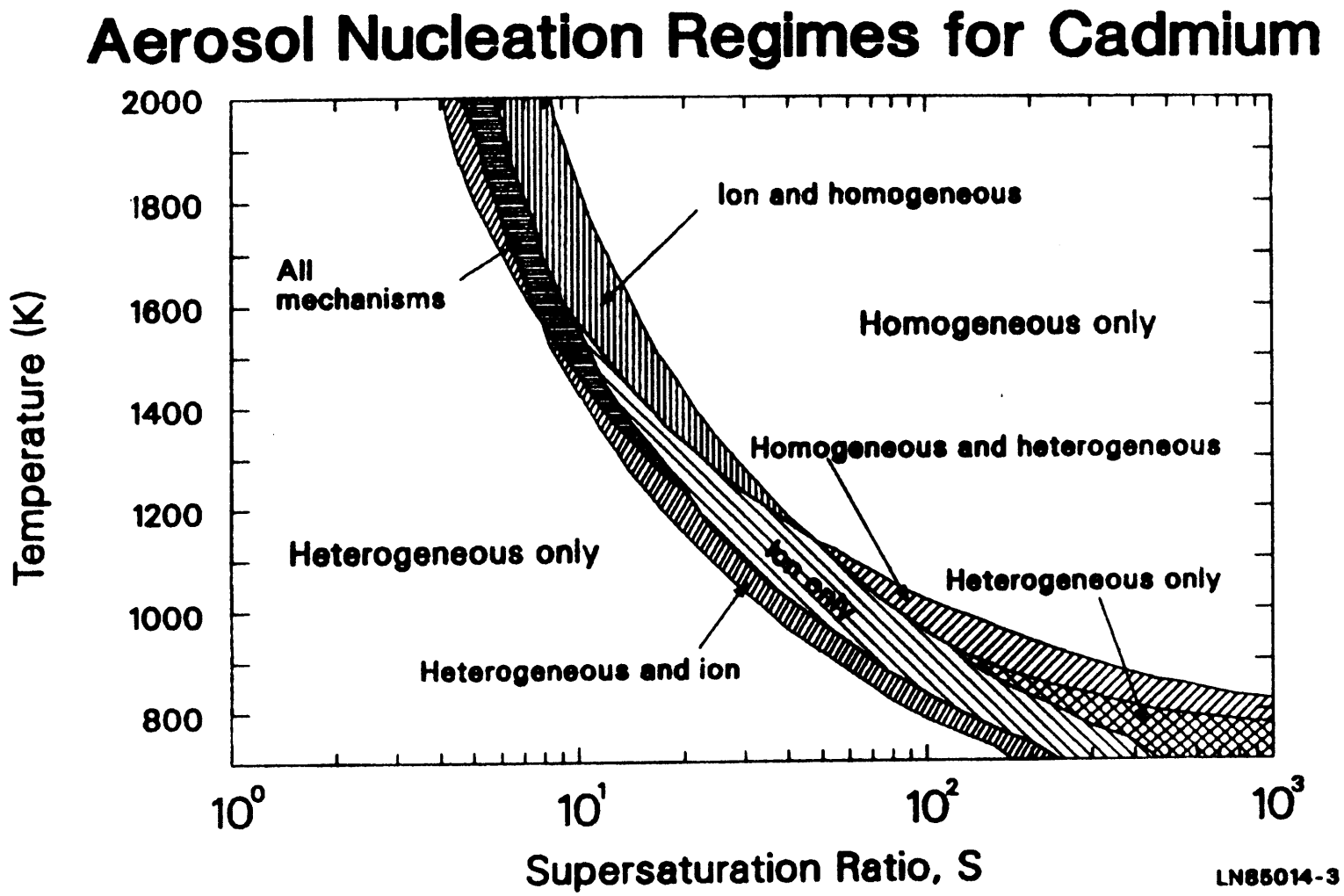
Aerosol Nucleation Regimes for Cadmium
Temperature (K)
2000
1800
1600
1400
1200
1000
800
All mechanisms
Ion and homogeneous
Homogeneous only
Homogeneous and heterogeneous
Heterogeneous only
Ion only
Heterogeneous only
Heterogeneous and ion
10^0
10^1
10^2
10^3
Supersaturation Ratio, S
LN85014-3

Figure 6.12

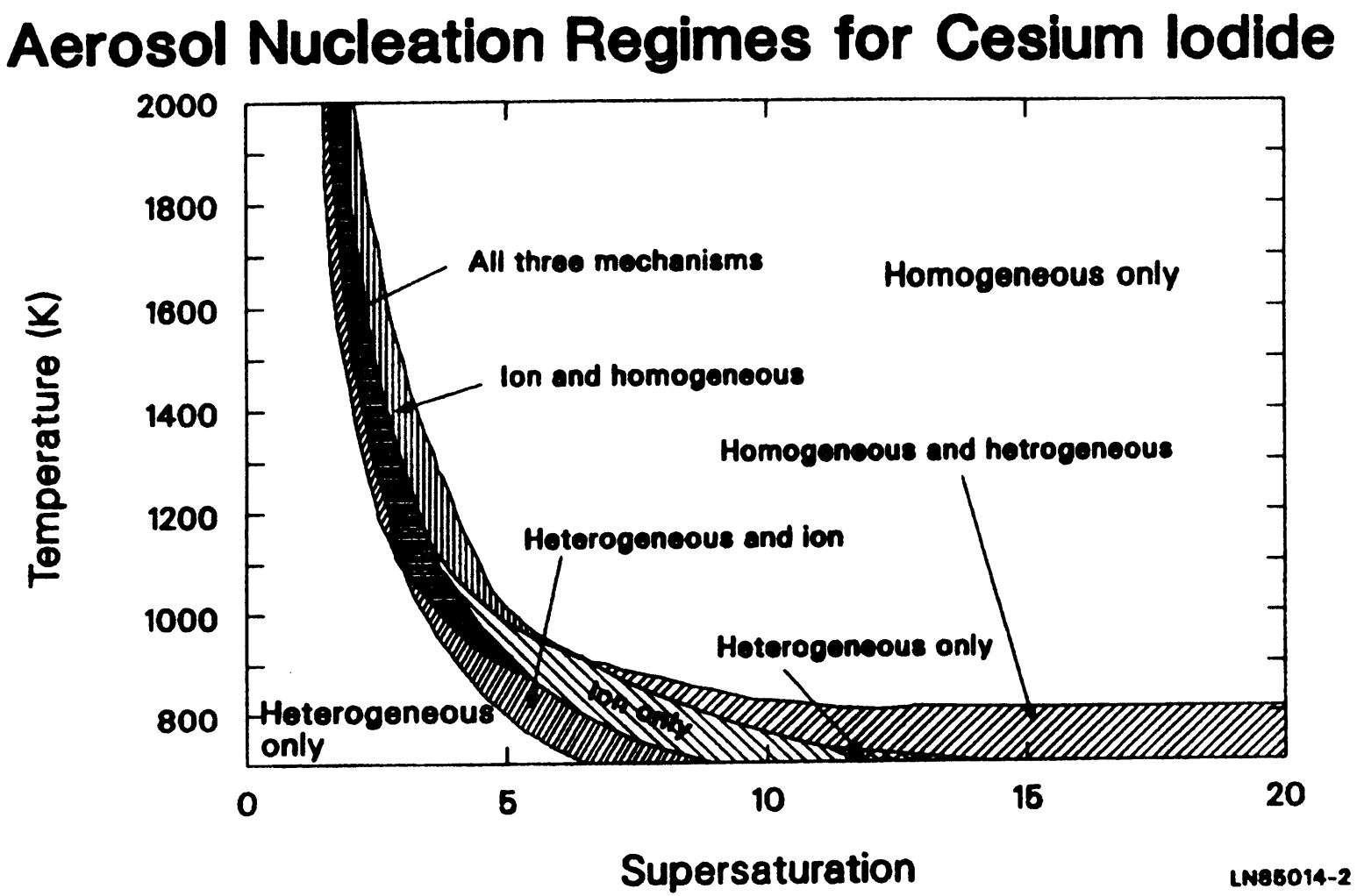
Aerosol Nucleation Regimes for Cesium Iodide
Temperature (K)
2000
1800
1600
1400
1200
1000
800
All three mechanisms
Homogeneous only
Ion and homogeneous
Homogeneous and hetrogeneous
Heterogeneous and ion
Heterogeneous only
Heterogeneous only
0
5
10
15
20
Supersaturation
LN85014-2

is labeled as the "heterogeneous and ion" regime in the figures. At moderate supersaturations and high temperatures, all three mechanisms contribute significantly as a means of removing vapor from the system. Although some of the vapor is undergoing heterogeneous nucleation, the aerosol surface area is insufficient to reduce the vapor supersaturation significantly. At lower temperatures, an "ion only" regime is present in which ion-induced nucleation will be the predominant nucleation process. In this regime, heterogeneous nucleation cannnot condense enough vapor to relieve the vapor supersaturation and yet the supersaturation is below that required for homogeneous nucleation. As shown in all the figures, this "ion only" regime occurs over a limited range of supersaturation. This is because of the free energy of the vapor in the ion environment. As in homogeneous nucleation, below a certain supersaturation, S_{crit}, the large free energy barrier prevents nucleation from occurring. However, in the presence of ions, above a certain supersaturation, S_{max}, there is no free energy barrier for the vapor to overcome and the formulation is not valid (in reality this means that it is physically impossible to attain such a supersaturation in the presence of ions). As a result, the "ion only" regime is limited by S_{max} and a

"heterogeneous only" regime appears at low temperatures. In this regime, the supersaturation is still not enough for homogeneous nucleation to occur. The "homogeneous and heterogeneous" regime occurs at slightly higher supersaturations. At very high supersaturations, homogeneous nucleation is the predominant mechanism of gas-to-particle conversion. Although the maps for each specie have a similar form, they differ in the supersaturation scale. This difference is attributed to differences in the surface tension and vapor pressure of Ag, Cd and CsI which greatly influence the nucleation behavior of these species.

6.6 The Effect of Wall Condensation

When a vapor enters a volume containing an aerosol, if the supersaturation is below that required for homogeneous or ion-induced nucleation, the vapor can condense on walls and/or condense on the preexisting aerosol. These two mechanisms compete as pathways for vapor depletion. These rates of condensation are functions of the surface-to-volume ratio of the system and the aerosols, the wall and bulk gas temperatures and the mass transfer coefficients at the wall and at the surface of the aerosol. This section will determine for

a given set of conditions which mechanism will be the dominant pathway for relieving vapor supersaturation.

The rate of condensation onto a surface is given by

$$J_{Wall} = h_D \frac{A_w}{V} (C_s^b - C_s^w) \qquad (6.2)$$

where

J_{wall} = rate of condensation (kg/m^3-sec),

h_D = mass transfer coefficient (m/s),

A_w/V = surface to volume ratio (m^{-1}),

C_s^b = concentration of specie in bulk gas (kg/m^3),and

C_s^w = equilibrium wall concentration (kg/m^3).

The mass transfer coefficient is determined using

$$h_D = \begin{cases} 3.56 \frac{D}{d} & \text{laminar flow} \qquad (6.3a) \\ 0.023 \frac{D}{d} Rey^{0.83} Sc^{0.33} & \text{turbulent flow} \qquad (6.3b) \end{cases}$$

where

Sc = Schmidt number,

Rey = Reynolds number,

D = diffusion coefficient (m^2/s), and

d = equivalent diamter of volume (m).

Using the ideal gas law, the concentration of the vapor can be rewritten as

$$C_s^b = \frac{SP_v(T_b)MW}{RT_B} \quad \text{and} \quad C_s^w = \frac{P_v(T_w)MW}{RT_w}$$

where

S = supersaturation ratio,

$p_v(T_v)$ = vapor pressure of specie at temperature T (Pa),

R = gas constant (Pa-m^3/kgmole K),

T_b = bulk gas temperature (K),

T_w = wall temperature (K), and

MW = molecular weight (kg/kgmole).

Thus Equation (6.2) becomes

$$J_{Wall} = h_D \frac{A_w}{V} \frac{p_v(T_b)M\bar{W}}{RT_b} \left(S - \frac{T_b p_v(T_w)}{T_w p_v(T_b)} \right) \qquad (6.4)$$

The rate of heterogeneous nucleation was given in Section 5.4 as

$$J_{HET} = \frac{2\pi d_p Dp_v(T_b)}{RT_b} MW(S - K)N(d_p)FW \qquad (5.47)$$

where

d_p = diameter of aerosol particle (m),

K = Kelvin effect (increase in vapor pressure due to curvature of aerosol surface),

$N(d_p)$ = aerosol number density (particle/m^3),

F = Fuchs correction factor, and

W = wind effect of aerosols.

The Fuchs correction factor accounts for condensation onto particles smaller than the mean free path of the system and is given by

$$F = \frac{1 + Kn}{1 + 1.71Kn + 1.33Kn^2} \qquad (5.43)$$

where Kn is the Knudsen number. The wind effect of aerosols W is given by

$$W = 1 + 0.276 Rep^{\frac{1}{2}} Sc^{0.33} \qquad (5.46)$$

where Rep is the Reynolds number based on particle diameter.

The supersaturation at which these two mechanism are equal can be determined by equating Equations (6.4) and (5.47). Thus,

$$h_D \frac{A_w}{V}(S - \zeta) = 2\pi d_p DN(d_p) FW (S - K) \qquad (6.5)$$

where

ζ = wall depression factor = $\left(\frac{T_b p_v(T_W)}{T_W p_v(T_D)}\right)$ and,

K = Kelvin effect = $\exp\left(\frac{4\sigma V_m}{d_p kT}\right)$.

Rearranging (6.5) yields

$$S - \zeta = \alpha(S - K) \qquad (6.6)$$

where

α = rate coefficient ratio = $\frac{2\pi d_p DN(d_p) FW}{h_D (A_w/V)}$.

Thus solving for S gives

$$S_{crit} = \frac{\zeta - \alpha K}{1 - \alpha} \qquad (6.7)$$

Equation (6.7) yields the supersaturation, S_{crit}, at which heterogeneous nucleation and wall condensation are equal. Although the actual rate equations are based on several independent variables, Equation (6.7) suggests that the problem can be reduced to one in which the important dimensionless variables are S, ζ, and K. Equation (6.7) is plotted in (S, α) space in Figure 6.13.

The value of the rate coefficient, α, determines the form of Equation (6.7) and is the most important variable for understanding the competition between the two pathways that remove vapor from the system. Plotting Equation (6.7) for α <1 yields the convex branch of the hyperbola whereas, the concave branch results if α > 1. Also plotted in the figure are the lines S = ζ, S = K, and α = 1. If S < K then Equation (5.47) predicts that evaporation (not condensation) from aerosols will occur. For large aerosol particles K is equal to 1.0; as the particle size decreases K increases. If S < ζ, then

Figure 6.13

A Comparison of Wall Condensation and Heterogeneous Nucleation in (S,α) Space

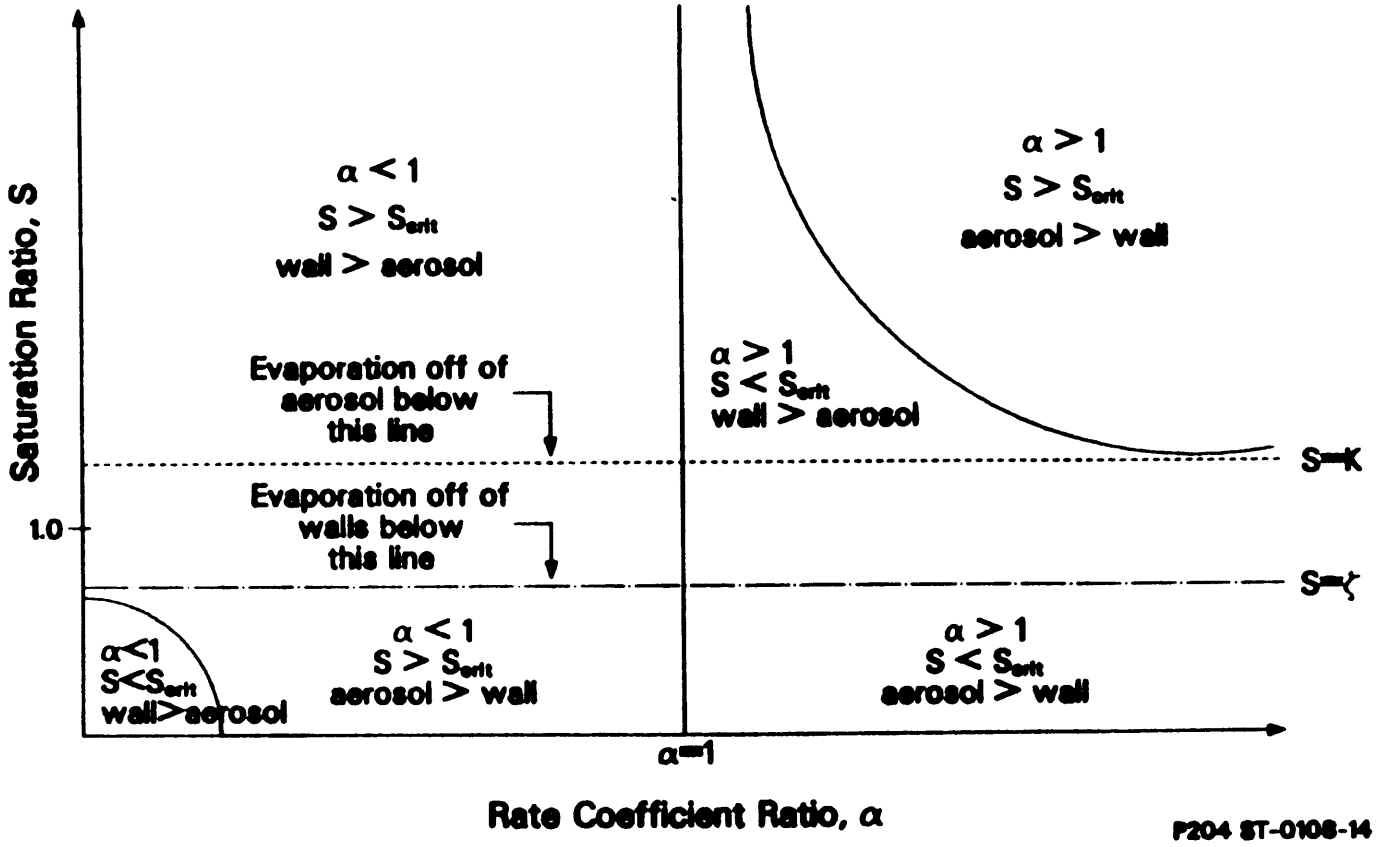

Equation (6.5) predicts that vapor will evaporate off walls. The value of K is 1.0 if the wall and gas temperatures are equal and decreases as the wall gets colder than the gas.

Consider the case of a supersaturated vapor ($S > 1.0$) If $\alpha < 1$, then the rate coefficent for wall condensation exceeds the rate coefficient for heterogeneous nucleation. Thus, under condensing conditions, wall condensation will always be the dominant mechanism for vapor depletion. If $\alpha > 1$, then the rate coefficient for condensation onto aerosols exceeds that for wall condensation. However, as seen in the figure, the condition that $\alpha > 1$ is necessary (but not sufficient) for the rate of heterogeneous nucleation to be greater than the wall condensation rate. In addition to the condition $\alpha > 1$, for aerosol condensation to remove more vapor from the volume than wall condensation the supersaturation must be greater than the critical value, S_{crit}, given by the concave hyperbola in the figure. If $\alpha > 1$ but $S < S_{crit}$, then wall condensation will exceed condensation onto aerosols. The figure also illustrates what will happen in the case of a subsaturated vapor ($S < 1$). In this case, evaporation will occur.

Figure 6.13 provides a general understanding of how

the two mechanisms, wall condensation and heterogeneous nucleation, compete for vapor in a volume. However, the exact value of α will be needed to determine which mechanism might dominate in a severe accident. The rate coefficient ratio, α, is defined as

$$\alpha = \frac{2\pi d_p DN(d_p) FW}{h_D (A_w/V)} \qquad (6.8)$$

In general, α is a function of many variables such as the aerosol number density, aerosol size, flowrate, geometry, wall and bulk temperatures. Since estimating the range of values that α could assume in the course of a severe accident is a priori difficult, a simpler approach has been adopted here. Based on the previous discussion, it is important to know if α is greater or less than unity. The purpose of this calculation is to determine under what types of conditions will $\alpha > 1$. To simplify the analysis, three assumptions were made:

(1) the volume was a circular straight piece of pipe;

(2) the aerosol was considered to be monodisperse; and

(3) the surface-to-volume ratio of the aerosol matched that of the pipe.

Assumption 3 is somewhat arbitrary since the aerosol density can vary independently of the pipe geometry. However, the assumption was made a priori to give equal weighting to wall condensation and heterogeneous nucleation. Note for comparison that the surface-to-volume ratio of a 1 m diameter pipe is similar to that of a 1 μ m monodisperse aerosol having a number density of 10^6 particles/cc. For a circular pipe of diameter d_r, the surface-to-volume ratio is given by

$$\frac{A_w}{V} = \frac{4}{d_r} \tag{6.9}$$

and hence the aerosol number density is

$$N = \frac{4}{\pi d_p^2 d_r} \tag{6.10}$$

With these assumptions, α becomes a function of only five variables, i.e.,

$$\alpha = \alpha(d_p, d_r, Rey, Sc, Kn) \qquad (6.11)$$

where

d_p = aerosol diameter (m),

d_r = pipe diameter (m),

Rey = Reynolds number based on pipe diameter,

Sc = Schmidt number, and

Kn = Knudsen number.

Explicit forms of Equation (6.11) are needed to determine what values the five variables would have to assume to require $\alpha > 1$. In laminar flow (Rey < 2200), the mass transfer coefficient is given by Equation (6.3a). Thus, substituting Equations (6.3a), (6.9) and (6.10) into Equation (6.8) yields

$$\alpha = \frac{1}{1.78} \frac{d_r}{d_p} F(Kn)\, W(Rep, Sc) \qquad (6.12)$$

where

F = Fuch's correction factor (only a function of Knudsen number), and

W = wind effect of aerosols (a function of Rep and Sc).

The functional form of W in Equation (6.12) was converted from Rep (Reynolds number based on particle diameter) to Rey (Reynolds number based on pipe diameter) using

$$Rey = Rep \cdot \eta \tag{6.13}$$

where $\eta = d_r/d_p$. Thus, Equation (6.12) states that α is really only a function of four dimensionless groups, η ,Rey,Sc and Kn. Hence, substituting Equation (6.13) into Equation (6.12) gives

$$\alpha = \eta \frac{F(Kn)\ W\ (Rey,Sc,\eta)}{1.78} \tag{6.14}$$

For $\alpha > 1$, then

$$\eta > \frac{1.78}{F(Kn)\ W\ (Rey,Sc,\eta)} \tag{6.15}$$

Therefore given a value of Rey, Sc and Kn a range of

diameter ratios, η , can be calculated which make the inequality true. The diameter ratio, η , at which $\alpha = 1$, is given implicitly by

$$\eta = \frac{1.78(1+1.71Kn+1.33Kn^2)}{(1+Kn)(1+0.276Rey^{\frac{1}{2}}Sc^{0.33}\eta^{-\frac{1}{2}})} \qquad (6.16)$$

For turbulent flow, the situation is more complex because the mass transfer coefficient has a dependence on Rey and Sc as given by Equation (6.3b). For turbulent flow, the same procedure yields,

$$\eta > 1.15x10^{-2} \left[\frac{Rey^{0.83}Sc^{0.33}}{F(Kn)\ W\ (Rey,Sc,\eta)}\right] \qquad (6.17)$$

and the diameter ratio at which $\alpha = 1$, is given implicitly by

$$\eta = \frac{1.15x10^{-2}(Rey^{0.83}Sc^{0.33})(1+1.71Kn+1.33Kn^2)}{(1+Kn)(1+0.276Rey^{\frac{1}{2}}Sc^{0.33}\eta^{-\frac{1}{2}})} \qquad (6.18)$$

Equations (6.16) and (6.18) are solved to determine

the minimum diameter ratio, η, for which the condition $\alpha > 1$ is satisfied. The results, shown in Figure 6.14, need to be compared to diameter ratios in real reactors and source term tests. Pipe diameters could vary from 1 cm in source term experiments to 1 m, the approximate size of a PWR primary system pipe. Aerosol particles considered in this analysis range from 100 A to 0.1 mm. As a result, diameter ratios under these conditions could range from 10^2 to 10^6. Comparison with the figure shows that the ratios encountered in practice are well above the minimum diameter ratio η. Therefore, if the surface-to-volume ratio of the aerosol is equal to that of the pipe, then the necessary condition $\alpha > 1$ is satisfied. Moreover, since the critical diameter ratio is much less than that expected in real reactors and source term experiments, α would be very large (> 100).

The preceding discussion suggests that in a severe accident $\alpha >> 1$. Thus, calculations have been performed using Equation (6.7) to determine representative values of S_{crit} as a function of α. Cadmium was used as the condensing vapor in all cases; three different sets of wall and bulk temperatures and two particle sizes were used to determine the values of ζ and K needed in Equation (6.7). Table 6.1 lists

Figure 6.14

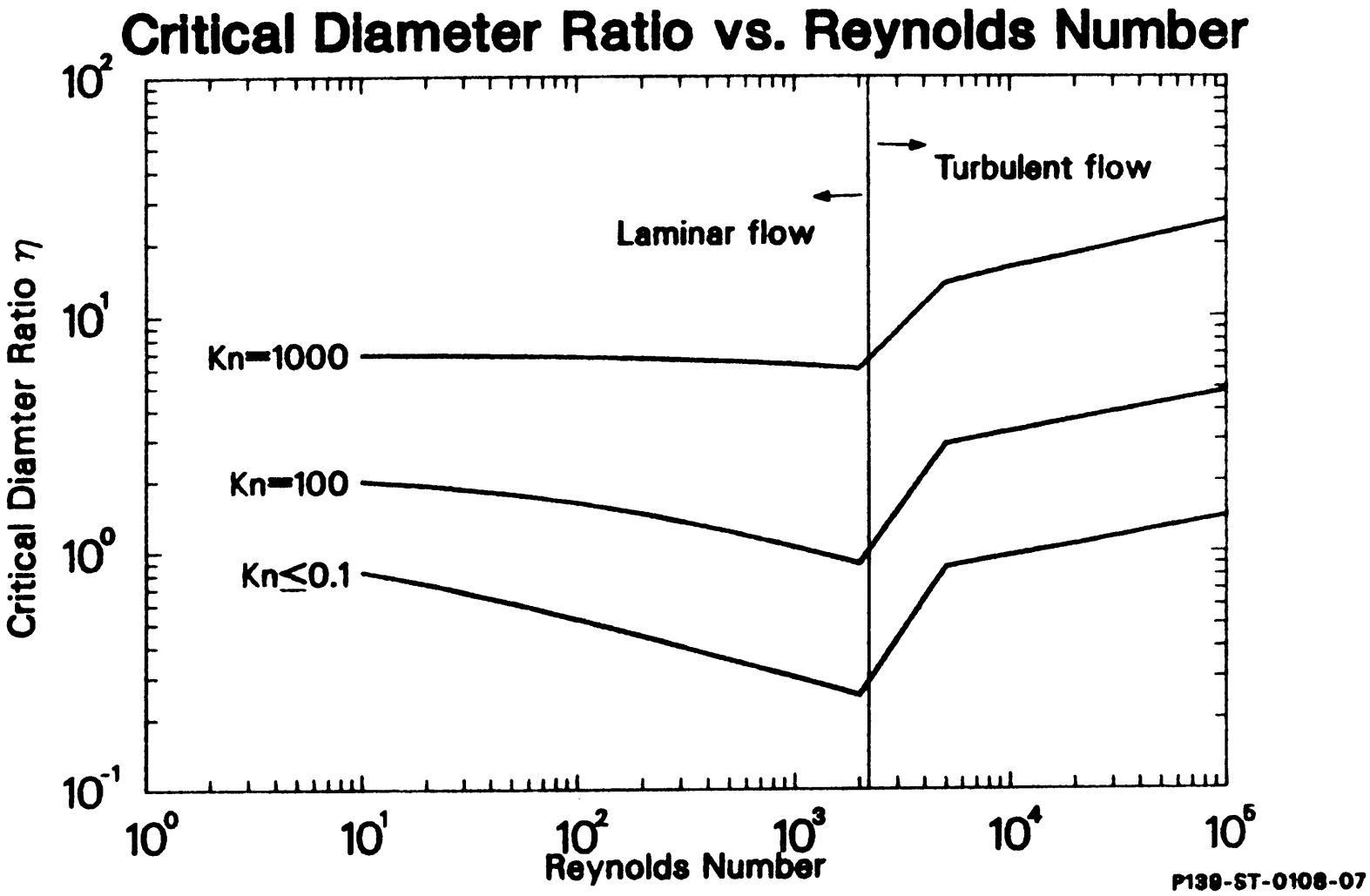
Critical Diameter Ratio vs. Reynolds Number
Critical Diamter Ratio η
Reynolds Number
Turbulent flow
Laminar flow
Kn=1000
Kn=100
Kn≤0.1
10^2
10^1
10^0
10^-1
10^0
10^1
10^2
10^3
10^4
10^5
P139-ST-0108-07

TABLE 6.1
TEST CASES IN THE
WALL CONDENSATION VS. HETEROGENEOUS NUCLEATION STUDY

Case No.	T_{bulk} (K)	T_{wall} (K)	d_p
1a	700	600	100 Å
1b	700	600	1 μm
2a	1500	1400	100 Å
2b	1500	1400	1 μm
3a	2000	1900	100 Å
3b	2000	1900	1 μm

the values of these parameters in the six cases that were considered.

The results, plotted in Figures 6.15, 6.16 and 6.17, all show the same general behavior. At high values of α, the value of S_{crit} is small and approaches K as $\alpha \rightarrow \infty$. Therefore, given that $\alpha > 1$, only slight supersaturation of the cadmium vapor is needed (i.e. S > 1.5) for heterogeneous nucleation to be more effective at removing vapor than wall condensation. Only at values of α slightly greater than unity, where the rate coefficients are similar, does S_{crit} increase thus requiring the vapor supersaturation to be significant (S ~ 2-10) for heterogeneous nucleation to exceed wall condensation.

Wall condensation and condensation onto aerosols compete as potential pathways for relieving vapor supersaturation. By examining these two rate processes, both necessary and sufficient conditions under which the heterogeneous nucleation pathway would dominate over wall condensation were derived. Examination of a range of physical situations that could exist in a severe accident indicates that the necessary and sufficient conditions would be met in most cases of interest. As a result, the relief of vapor supersaturation would be predominantly via heterogeneous nucleation rather than

Figure 6.15

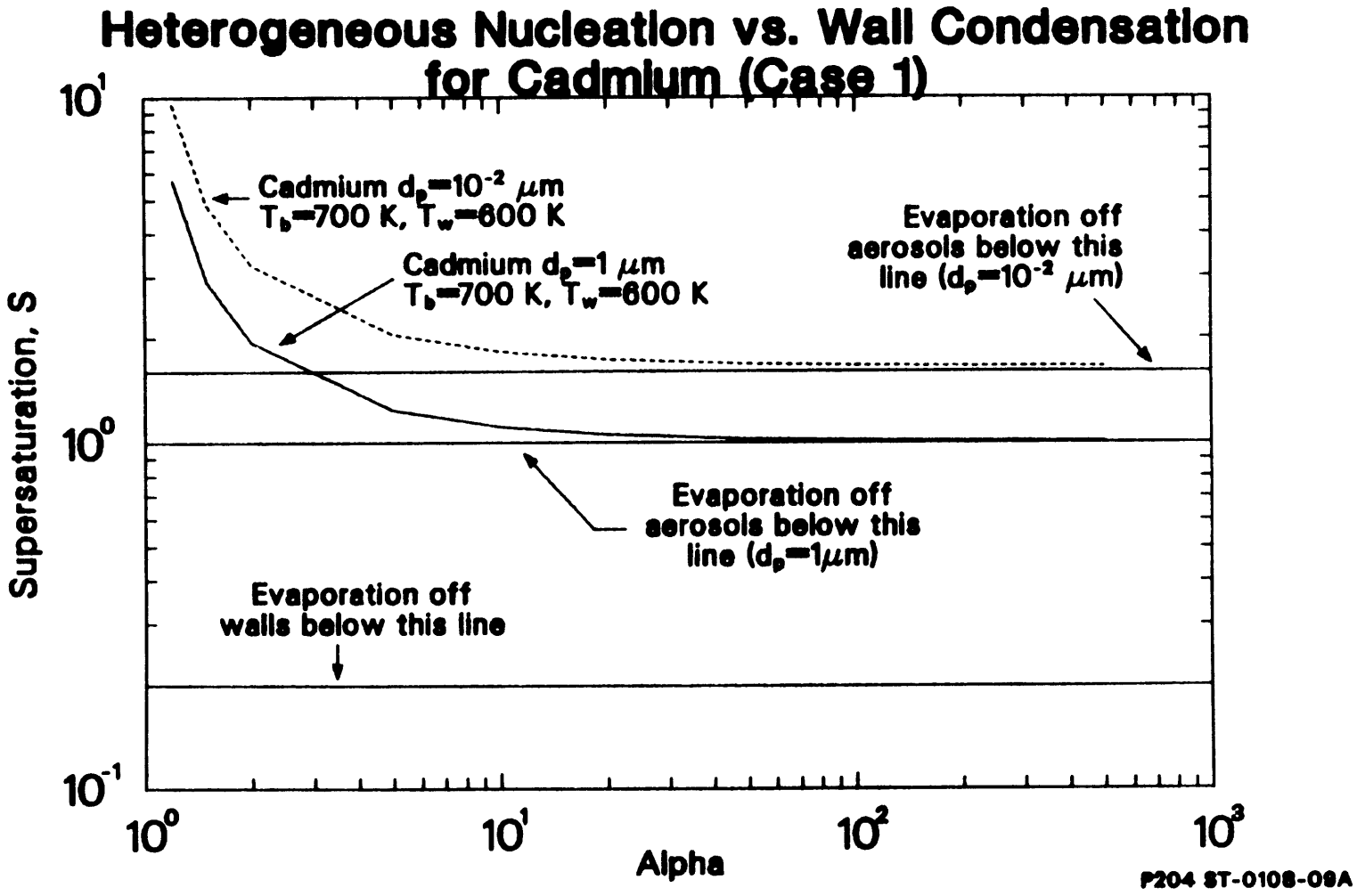
Heterogeneous Nucleation vs. Wall Condensation for Cadmium (Case 1)
Supersaturation, S
Alpha
Cadmium d_p=10^{-2} μm
T_b=700 K, T_w=600 K
Cadmium d_p=1 μm
T_b=700 K, T_w=600 K
Evaporation off aerosols below this line (d_p=10^{-2} μm)
Evaporation off aerosols below this line (d_p=1μm)
Evaporation off walls below this line
P204 ST-0108-09A

Figure 6.16

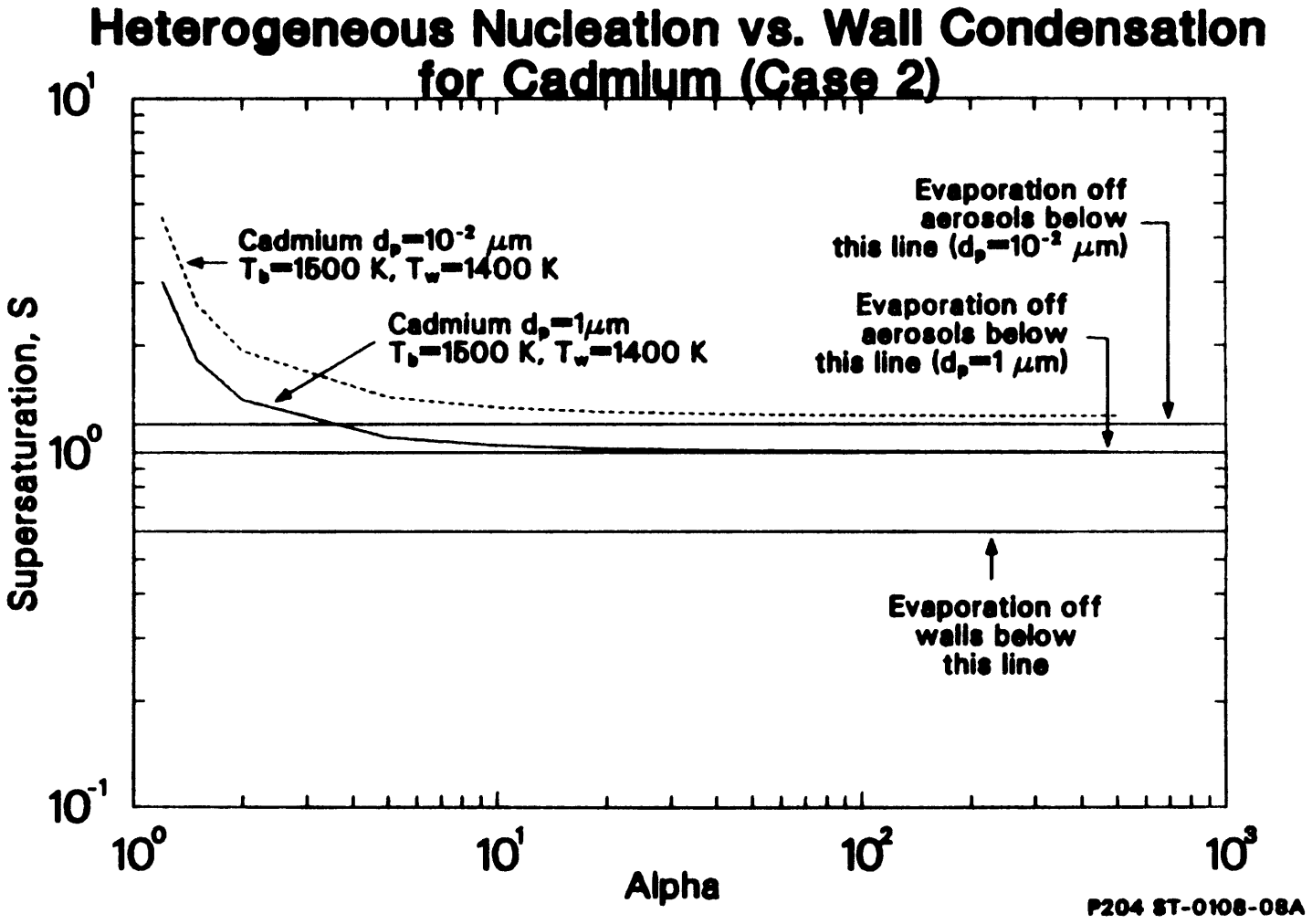
Heterogeneous Nucleation vs. Wall Condensation for Cadmium (Case 2)
Supersaturation, S
Alpha
Cadmium $d_p=10^{-2}$ μm $T_b=1500$ K, $T_w=1400$ K
Cadmium $d_p=1$μm $T_b=1500$ K, $T_w=1400$ K
Evaporation off aerosols below this line ($d_p=10^{-2}$ μm)
Evaporation off aerosols below this line ($d_p=1$ μm)
Evaporation off walls below this line
P204 ST-0108-08A

Figure 6.17

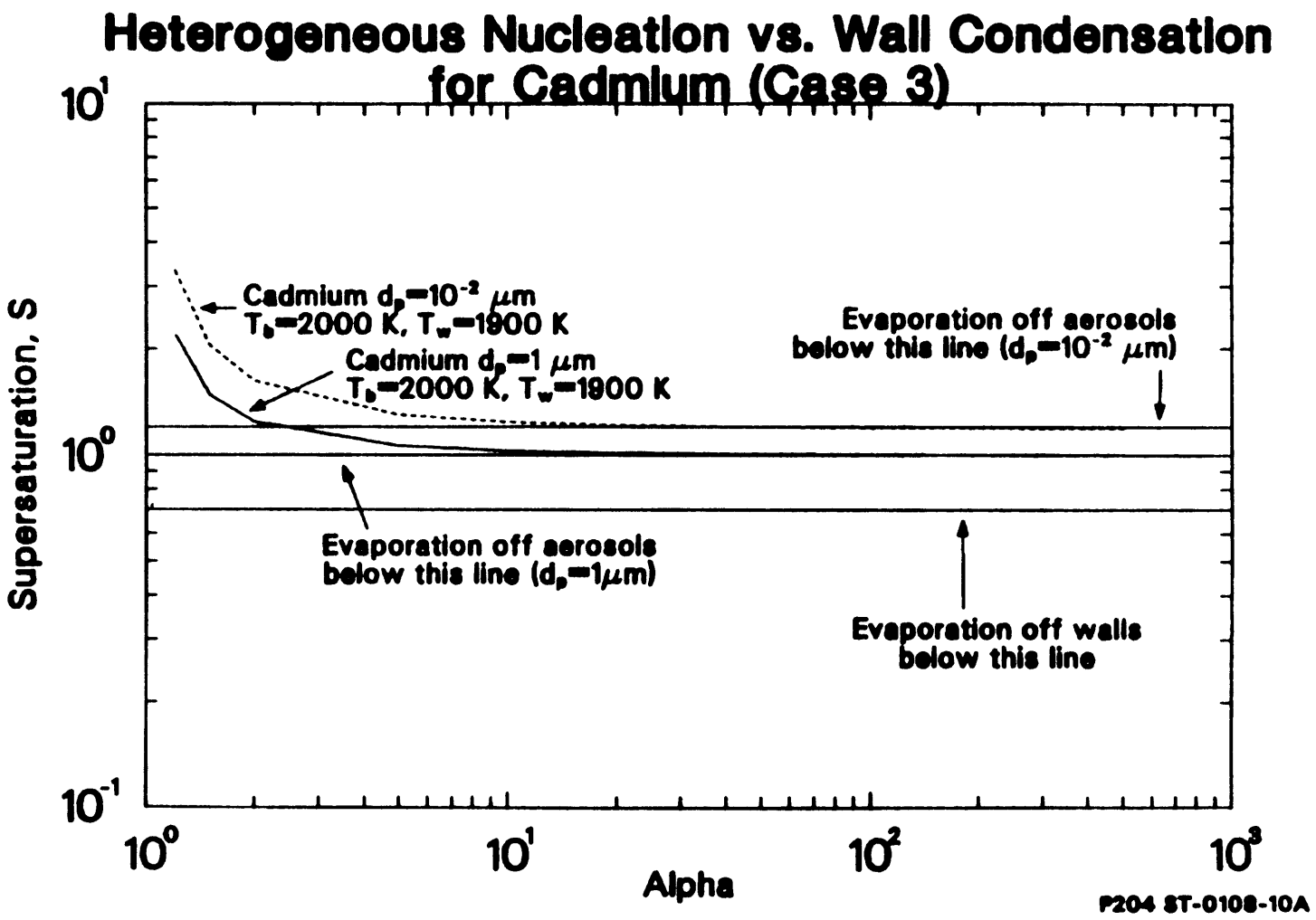
Heterogeneous Nucleation vs. Wall Condensation for Cadmium (Case 3)
Supersaturation, S
Alpha
Cadmium d_p=10^{-2} μm
T_b=2000 K, T_w=1900 K
Cadmium d_p=1 μm
T_b=2000 K, T_w=1900 K
Evaporation off aerosols below this line (d_p=10^{-2} μm)
Evaporation off aerosols below this line (d_p=1μm)
Evaporation off walls below this line
P204 ST-0108-10A

wall condensation.

6.7 Conclusions

Examining the nucleation behavior of Ag, Cd and CsI has resulted in a better understanding of gas-to-particle conversion in severe reactor accidents. Based on this analysis, several conclusions can be drawn:

(1) Metal vapors like Ag and Cd are much more difficult to nucleate than a salt like CsI because of their large surface tensions.
(2) Predicting the first specie to nucleate requires a knowledge of the timing and magnitude of the release of each vapor. Although such an analysis has not been performed, based on the high volatility of Cd and the low surface tension of CsI it appears that either CsI or Cd will be the first specie to nucleate and hence serve as an aerosol seed for heterogeneous nucleation of the other vapors.
(3) Because ion-induced nucleation lowers the supersaturation required to produce aerosols, it is probably the initial aerosol formation mechanism in a severe reactor accident. However, if enough aerosol surface area is generated, heterogeneous nucleation will be the dominant mechanism of gas-to-particle conversion.
(4) Prior to reaching saturation, in a severe reactor accident, wall condensation is not as effective as heterogeneous nucleation in reducing vapor supersaturation. However, once saturation is reached, condensation onto walls can continue causing the vapor to subsaturate. In this subsaturated environment, the aerosols would evaporate.

In addition, the aerosol maps have provided insight into the competition that exists among the various

nucleation processes during aersol formation. As a result, in a severe reactor accident the early stages of aerosol formation can now be understood. The high supersaturations required for homogeneous nucleation preclude it from being a dominant mode of aerosol generation. Instead, hot vapors released from the core would supersaturate and condense to form aerosols via ion-induced nucleation. The period of pure ion-induced nucleation is expected to be quite short ($\sim 10^{-6}$ s). Once some aerosol is introduced into the system, ion-induced nucleation and heterogeneous nucleation will operate as simultaneous pathways for gas-to-particle conversion. Obtaining details of the vapor and aerosol behavior during this time period would require a time-dependent analysis where the increase in aerosol surface area and the decrease in supersaturation could be calculated. Although such an analysis has not been done, the results of the aerosol maps suggest that such a nucleation regime does exist. The high nucleation rates predicted for Ag, Cd and CsI indicate that aerosol surface area would be generated quite rapidly. Once enough surface area has been created, the remainder of the aerosol formation period will be dominated by heterogeneous nucleation. The aerosol particle size distribution at the end of this period of

aerosol formation will be determined in the next section.

7. EQUILIBRIUM AEROSOL PARTICLE SIZE DISTRIBUTION FOLLOWING NUCLEATION

7.1 Introduction

The high vapor supersaturation that is produced by rapid cooling of hot vapor creates a large driving force to return the vapor to an equilibrium or saturated state. During the system's return to equilibrium, vapor supersaturation is relieved by the formation of aerosols. As shown in Section 6, three distinct stages characterize this period of aerosol generation or return to equilibrium. In the first stage, the high vapor supersaturation results in aerosols being formed by ion-induced nucleation. This stage is generally quite limited in duration. Once some aerosol surface area has been generated, the second stage begins. Ion-induced and heterogeneous nucleation operate as competing pathways for reducing vapor supersaturation. As the aerosol surface area grows and the vapor supersaturation decreases, ion-induced nucleation ceases and the system moves into the third and longest stage of the aerosol formation period. In this stage, heterogeneous nucleation operates as the dominant mechanism of gas-to-particle conversion until equilbrium is reached.

In a severe reactor accident, this period of aerosol formation is quite rapid. The vapor supersaturation decreases to 1.0 and equilibrium is reestablisted in well under one second. Modeling the vapor and aerosol behavior during this rapid period of aersol formation in large aerosol transport codes is unreasonable because of the small time steps that would be required to predict the system behavior. Hence, by using an analytic solution to the aerosol transport equation, this section will determine the particle size distribution once equilbrium is reestablished at the end of the period of aerosol generation.

Section 7.2 reviews analytic solutions to the aerosol transport equation under a variety of conditions. Modeling assumptions used to determine the particle size distribution immediately following nucleation are discussed in Section 7.3. In Section 7.4, the solution to the aerosol transport equation and selected results are presented. Conclusions are drawn in Section 7.5.

7.2 Solutions to the Aerosol Transport Equation

Before discussing solutions to the aerosol transport equation, it is important to understand the concept of the continuous aerosol size distribution n(v,r,t). If

dN is the number of particles per unit volume of fluid at a given time and a given position in space in the particle volume range v to v+dv, then

$$dN = n(v,r,t)dv \tag{7.1}$$

This expression defines the particle size distribution function.

The general aerosol transport equation is given by [7.1]

$$\frac{\partial n}{\partial t} + \nabla\cdot n\vec{V} + \frac{\partial I}{\partial v} = \nabla\cdot D\nabla n + \tfrac{1}{2}\int_0^v \beta(\tilde{v},v-\tilde{v})\,n(v)\,n(\tilde{v}-v)\,d\tilde{v} \tag{7.2}$$

$$- \int_0^\infty \beta(v-\tilde{v})\,n(v)\,n(\tilde{v})\,d\tilde{v} - \nabla\cdot\vec{c}n$$

where

n = aerosol size distribution,

v = volume of aerosol particle,

I = particle current or number of particles per unit time per unit volume of gas passing the point v,

D = diffusion coefficient of aerosol,

β = agglomeration coefficient,

$\vec{c}$ = deposition velocity, and

$\vec{V}$ = fluid velocity.

On the left hand side of the equation, the first term is the time derivative of the distribution, the second term represents the rate at which aerosols are

convected out of the volume and the formation and growth of the aerosol in volume space is denoted by dI/dv. This last term will be discussed further in Section 7.4. On the right hand side of the equation, the first term describes the net diffusion of aerosols out of the volume. The next two terms represent the coagulation of aerosols in the volume. Removal of aerosols in the volume is denoted by the last term on the right hand side of Equation (7.2).

Many researchers have solved Equation (7.2) for a variety of different conditions. Friedlander [7.1] presents analytic solutions to the aerosol transport equation for

(1) steady state turbulent stack plumes,

(2) coagulation and stirred settling in a well mixed closed volume,

(3) coagulation and deposition by convective diffusion in a pipe, and

(4) a continuous stirred tank reactor.

Hidy [7.2], Hidy and Lilly [7.3], and Friedlander and Wang [7.4] solved the aerosol transport equation for pure Brownian coagulation. Hidy solved the equations numerically, whereas Friedlander found analytic solutions to the upper and lower ends of the size spectrum. By using the similarity transformation

$$\psi = \frac{V(t)\eta}{N_\infty^2(t)} \qquad \text{and} \quad \eta = \frac{vN_\infty(t)}{V(t)}$$

where

n = particle size distribution,

v = volume,

$N_\infty(t)$ = total number concentration of aerosol particles in system = $\int ndv$, and

$V(t)$ = volume concentration of aerosol in the system = $\int nvdv$,

they were able to transform a reduced form of Equation (7.2) into a nonlinear integro-differential equation for ψ as a function only of η . Under certain conditions, solutions to this equation approach a self-preserving form because they are independent of the initial conditions of the problem. Hidy found the time to reach self-preserving conditions to be $\sim 9\ \mu/kTN_\infty(0)$. A plot of the self-preserving distribution is shown in Figure 7.1. For the case of pure coagulation, the volume concentration is constant. Thus, the aerosol size distribution can be determined as a function of time by using the self-preserving distribution, the analytic solution to $N_\infty(t)$ and the volume concentration of aerosol V(t=0).

Pich, Friedlander and Lai [7.5] used the same similarity transformation to find a solution for

Figure 7.1

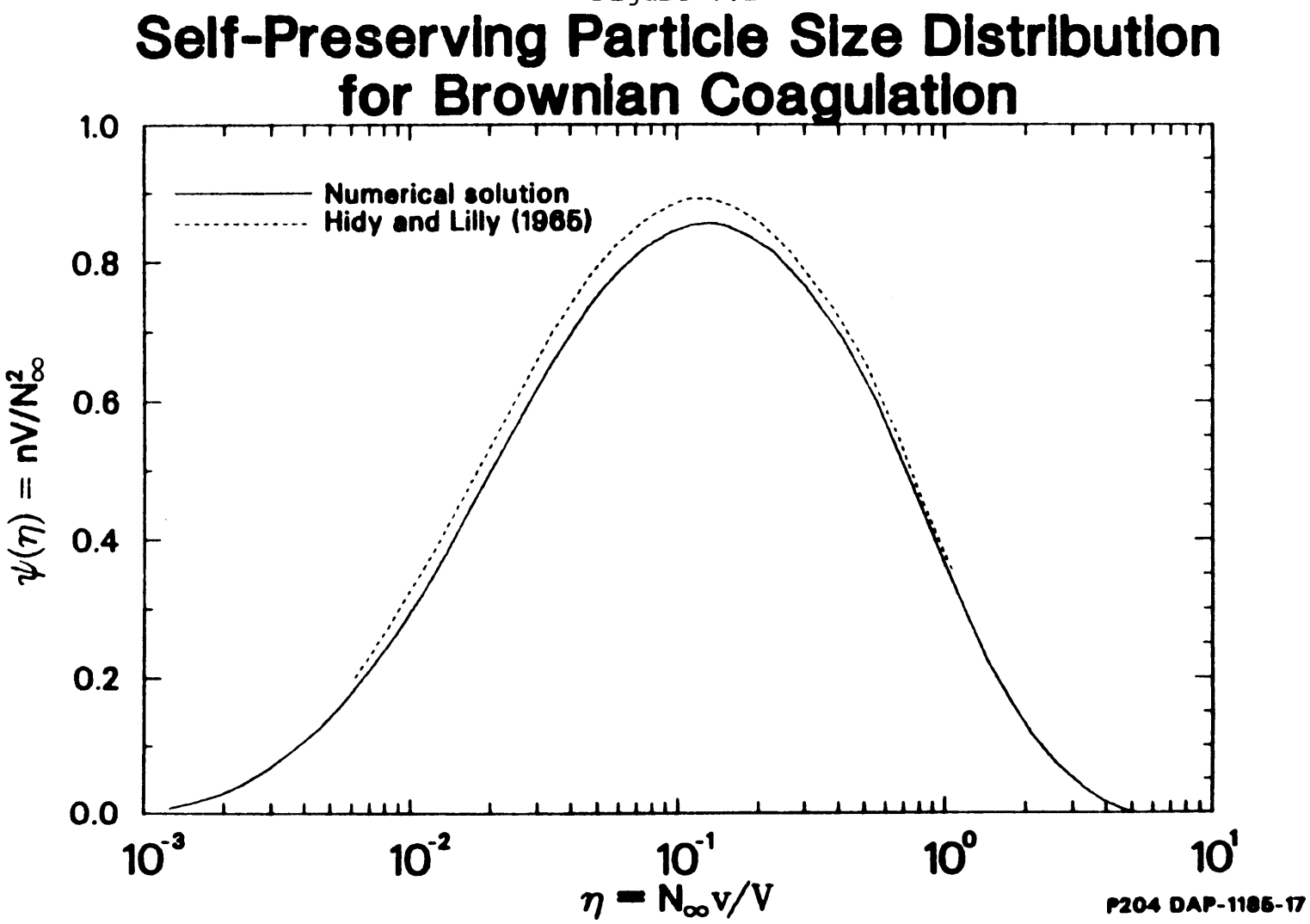
Self-Preserving Particle Size Distribution
for Brownian Coagulation
Numerical solution
Hidy and Lilly (1965)
1.0
0.8
0.6
0.4
0.2
0.0
$\psi(\eta) = nV/N_\infty^2$
10^{-3}
10^{-2}
10^{-1}
10^{0}
10^{1}
$\eta = N_\infty v/V$
P204 DAP-1185-17

simultaneous Brownian coagulation and vapor condensation onto aerosols. They found that a self preserving distribution would develop if a dimensionless group given by

$$C = \frac{3\mu}{4kT} \left(\frac{2}{V^{2/3} N_{\infty}^{1/3}} \right) B (S - 1) \qquad (7.3)$$

where

μ = gas viscosity (kg/m-s),

k = Boltzman's constant (J/K),

T = temperature (K),

V = volume concentration of aerosol in the system

N_{∞} (t)= total number concentration of aerosol,

B = constant in the growth rate equation, and

S = supersaturation,

was constant. The dimensionless group is a measure of the relative rates of condensation and coagulation. Because the theory is limited to values of $C < 1$, the rate of condensation must be less than or equal to the rate of coagulation. When condensation and coagulation occur simultaneously, both the total number concentration of particles N_{∞} and the volume

concentration V change with time. Thus, the supersaturation must change with time in a particular way in order for C to remain constant. When these conditions are satisfied, the analytic solutions for $V(t)$ and $N_\infty(t)$, and the self-preserving distribution in Figure 7.1, can be used to determine the time dependent behavior of the aerosol size distribution can be determined. If a self-preserving form is reached, then the total surface area is uniquely related to the total number concentration N_∞ and the volume concentration V; for the case of C = 1.09 the total aerosol surface area is constant and is equal to

$$A = 4.6\, N_\infty^{1/3}\, V^{2/3} \qquad (7.4)$$

Warren and Seinfeld [7.6] have examined nucleation and growth of aerosols from a continuously reinforced vapor. Dimensionless parameters were derived to characterize the behavior of the system. A simple monodisperse aerosol model was developed to simulate aerosol evolution from a continuous vapor source. Their results suggest that the total number and size of particles in the system depend on the source rate, vapor

pressure and surface tension. The vast majority of gas-to-particle conversion was found to occur by heterogeneous nucleation onto the existing aerosol rather than the creation of new particles by homogeneous nucleation.

7.3 Modeling Assumptions

If supersaturations are high, ion-induced nucleation will cause a large number of small aerosol particles to be produced. The aerosol maps presented in Section 6.5 suggest that the period of ion-induced nucleation will be quite short. Once the aerosol surface to volume ratio reaches 10^{-4} m^{-1}(= 1 cm^2 per m^3 of volume) heterogeneous nucleation will be the dominant mechanism of gas-to-particle conversion until equilibrium is reached. As a result, it is assumed in what follows that the intitial nucleation produces N_0 particles in the system where the number of particles produced depends on the supersaturation ratio of the vapor, the temperature and the volume of the system. The aerosols that are produced should be nearly monodisperse since only slight perturbations in the thermal hydraulic conditions are expected to occur during this short time period. These N_0 particles then enter the third stage of the aerosol formation period.

Coagulation and vapor condensation are the only two processes that can significantly alter the aerosol size distribution until equilibrium is attained. The analytic solution for simultaneous condensation and coagulation presented in Section 7.2 is not generally applicable because it is restricted to cases where the condensation rate is small relative to the rate of coagulation. As a result, a more general solution is required. This section will calculate time constants for both coagulation and condensation to determine the importance of each mechanism in the evolution of the aerosol particle size distribution immediately following nucleation. These results will then be used in Section 7.4 to establish the appropriate form of the aerosol transport equation to be solved for the problem at hand.

Examination of the time constant for agglomeration and condensation can yield information on the behavior of the aerosol size distribution during the period of aerosol formation. For a nearly monodisperse aerosol the change in the total aerosol number concentration due to coagulation is given by [7.1]

$$\frac{N_\infty(t)}{N_\infty(0)} = \frac{1}{1 + \frac{KN_\infty(0)}{2} t} \tag{7.5}$$

where

K = coagulation coefficient = $8kT/3\mu$.

Aerosol coagulation is considered to be an important mechanism when the change in the overall number concentration exceeds 5%. Thus, for $N_\infty(t)/N_\infty(0) = 0.95$, a time constant for coagulation calculated from Equation (7.5) is

$$\tau_{COAG} = \frac{0.105}{KN_\infty(0)} = \frac{0.0395}{kTN_\infty(0)} \qquad (7.6)$$

A time constant for aerosol growth can be determined by integrating the expression for the rate of heterogeneous nucleation. The rate of condensation onto an aerosol particle was found in Section 5.5 to be

$$\frac{dm_a}{dt} = \frac{2\pi d_p Dp_v(T)}{RT} MW(S-K)N(d_p)F(d_p)Vol \qquad (5.47)$$

where

m_a = mass on aerosol (kg),

d_p = diameter of aerosol particle (m),

D = diffusion coefficient of vapor (m^2/s),

$p_v(T_v)$ = vapor pressure of specie (Pa),

R = gas constant (Pa-m^3/kgmole-K)

T = temperature (K),

MW = molecular weight (kg/kgmole),

S = supersaturation ratio,

K = Kelvin effect,

$N(d_p)$ = number concentration of particles of size d_p,

F = Fuch's correction factor (see Section 5.5), and

Vol = volume of system (m^3).

The Fuchs correction factor is given by

$$F = \frac{1 + 2\lambda/d_p}{1 + 1.71\left(\frac{2\lambda}{d_p}\right) + 1.33\left(\frac{4\lambda^2}{d_p^2}\right)} \tag{7.7}$$

where λ is the mean free path of the gas. For a monodisperse aerosol, Equation (5.47) can be converted to a growth rate using

$$\frac{dm_a}{dt} = \frac{\pi d_p^2}{2} \rho N \frac{d}{dt}(d_p) Vol \tag{7.8}$$

where ρ is the density of the condensate (kg/m^3). Thus, the rate of growth of an aerosol particle is given by

$$\frac{dd_p}{dt} = \frac{4}{d_p} \left(\frac{Dp_v(T_v)MW}{RT}\right) \frac{F(d_p)}{\rho} (S - K) \qquad (7.9)$$

$$= \frac{\alpha_1 (S - K) F(d_p)}{d_p}$$

where

$$\alpha_1 = 4 \left(\frac{Dp_v(T_v)MW}{\rho RT}\right)$$

As vapor condenses onto the aerosol particle, the supersaturation will decrease. A simple mass balance yields the supersaturation as a function of the aerosol diameter,

$$S = S_0 - \frac{\pi}{6} \frac{\rho N(d_p)}{m^{eq}} Vol(d_p^3 - d_{p_0}^3) \qquad (7.10)$$

where

d_{p0} = initial particle size (m),

m^{eq} = equilibrium vapor mass (kg).

Hence,

$$\frac{dd_p}{dt} = \frac{\alpha_1 F(d_p)}{d_p} \left[S - \frac{\pi\rho N(d_p) Vol}{6m^{eq}}(d_p^3 - d_{p_0}^3) - K\right] \qquad (7.11)$$

Assuming K = 1, Equation (7.11) can be integrated to determine the time for a monodisperse aerosol of initial size d_{p0} to grow to size d_p.

Equation (7.11) is integrated in two parts. Equation (7.10) is first used to determine the particle diameter at which the supersaturation changes by 10%, d_s. If the final diameter of interest is less than d_s then Equation (7.9) is integrated using a constant supersaturation. Hence, for $d_p < d_s$

$$\Delta t_1 = \frac{1}{\alpha_1 (S_0 - 1)} \int_{d_{p_0}}^{d_p} \frac{x}{F(x)}\, dx$$

$$= \frac{1}{\alpha_1 (S_0 - 1)} \int_{d_{p_0}}^{d_p} \frac{x^2 + 3.42\lambda x + 5.32\lambda^2}{x + 2\lambda}\, dx \qquad (7.12)$$

Integrating yields

$$\left\{ \frac{1}{\alpha_1 (S_0 - 1)} \left[\frac{x^2}{2} - 1.42\lambda x - 6\lambda^2\right] + \frac{1}{\alpha_1 (S_0 - 1)} (2.4\lambda^2) \ln[\alpha_1 (S_0 - 1)(x + 2\lambda)] \right\}_{d_{p_0}}^{d_p} \qquad (7.13)$$

If the diameter of interest is greater than d_s, then Equation (7.13) is used to calculate the time to grow to d_s , Δt_s, and the remaining time to grow to d_p is calculated by integrating Equation (7.11) assuming that F = 1. This is a valid assumption since F approaches 1 as d_p gets large. Thus if $d_p > d_s$, then

$$\Delta t = \Delta t_s + \int_{d_s}^{d_p} \frac{x\,dx}{\alpha_1 [(S_0 + \frac{\pi \rho N Vol}{6m^{eq}} d_{p_0}^3 - 1) - \frac{\pi \rho N Vol}{6m^{eq}} x^3]} \qquad (7.14a)$$

or in simpler terms

$$\Delta t = \Delta t_s + \int_{d_s}^{d_p} \frac{x\,dx}{A - Bx^3} \qquad (7.14b)$$

where

$$A = \alpha_1 (S_0 + \frac{\pi \rho N Vol}{6m^{eq}} d_{p_0}^3 - 1)$$

$$B = \alpha_1 (\frac{\pi \rho N}{6m^{eq}} Vol)$$

Integrating Equation (7.14a) yields

$$\Delta t = \Delta t_s + \frac{1}{B}\left[\frac{1}{6\delta}\ln\left(\frac{(x-\delta)^2}{x^2+\delta x+\delta^2}\right) - \frac{\sqrt{3}}{3\delta}\tan^{-1}\left[\frac{2x+\delta}{8\sqrt{3}}\right]\right]_{d_s}^{d_p} \quad (7.15)$$

where $\delta = (A/B)^{(1/3)}$. Equations (7.13) and (7.15) can now be used as an estimate for the time constant for the growth of a monodisperse aerosol.

The time constant for coagulation and the time to grow to various particle diameters are plotted as a function of the total number of aerosol particles in Figure 7.2. Since the actual time constants for coagulation and growth are functions of many variables, this plot represents a base case calculation. Table 7.1 presents both the values used in the base case calculation and the range that these variables could assume in a severe reactor accident. Also plotted in the figure is the time to reach equilbrium (i.e., the time at which the supersaturation is equal to 1.0). The range of growth times indicated by the shaded area surrounding the base growth time is intended to reflect the potential variation in the base case values used in the calculation.

The plot suggests that the time to grow to 1 micron is very rapid, independent of the number of particles in the system. Condensation relieves the vapor

Figure 7.2

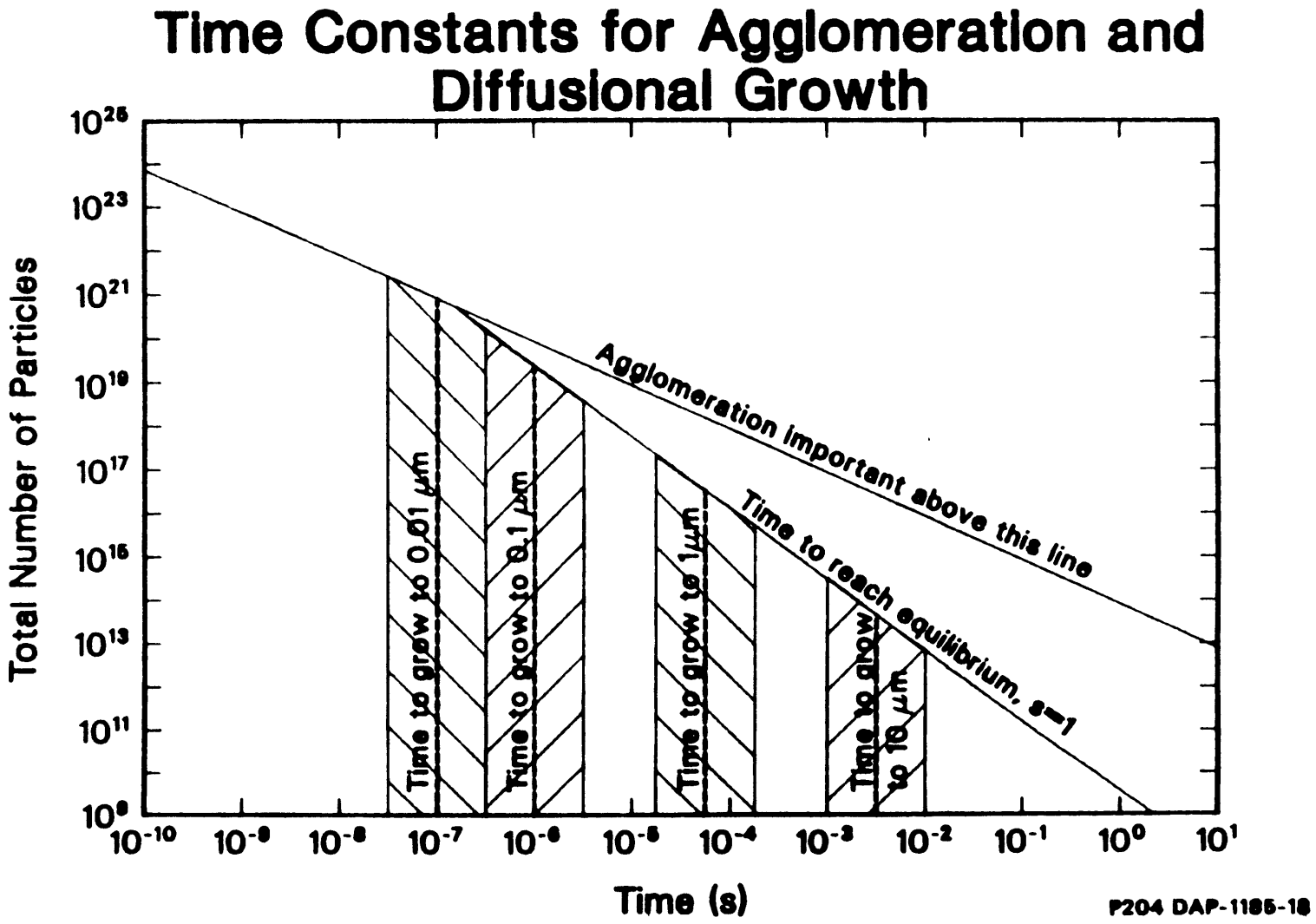
Time Constants for Agglomeration and Diffusional Growth
Total Number of Particles
10^{25}
10^{23}
10^{21}
10^{19}
10^{17}
10^{15}
10^{13}
10^{11}
10^{9}
10^{-10}
10^{-9}
10^{-8}
10^{-7}
10^{-6}
10^{-5}
10^{-4}
10^{-3}
10^{-2}
10^{-1}
10^{0}
10^{1}
Time (s)
Agglomeration important above this line
Time to reach equilibrium, s=1
Time to grow to 0.01 μm
Time to grow to 0.1 μm
Time to grow to 1 μm
Time to grow to 10 μm
P204 DAP-1185-18

TABLE 7.1
PARAMETER VALUES USED IN THE
TIME CONSTANT CALCULATION

Variable	Base Case Value	Range
Temperature	1000 K	500 - 2500
Fluid Viscosity	5.0e-05 kg/m-s [a]	1.0e-04 - 1.0e-05
Vapor Pressure	1.0e+05 Pa	1.0e+03 - 5.0e+05
Molecular Weight	100 kg/kgmole	100 - 200
Volume	1.0 m^3	1.0e-02 - 1.0
Liquid Density	1.0e+05 kg/m^3	5.0e+03 - 1.0e+05
Diffusion Coefficient	1.0e-06 m^2/s	1.0e-06 - 1.0e-05
Initial Particle Size	1.0e-09 m	1.0e-10 - 1.0e-05
Initial Supersaturation	25	1 - 50

a. means 5.0×10^{-5} kg/m-s.

supersaturation and hence causes the system to return to equilibrium very rapidly. Except for large particle concentrations ($N > 10^{20}/m^3$), the behavior of the aerosol as the system approaches equilibrium is dominated by vapor condensation and growth. Agglomeration is not important on this time scale. An analytic solution to the aerosol transport equation under these conditions is presented in the next section.

7.4 Aerosol Particle Size Distribution and Examples

Condensational growth is the only aerosol process of importance immediately following nucleation. Hence, the aerosol transport equation is reduced to

$$\frac{\partial n}{\partial t} + \frac{\partial I}{\partial v} = 0 \tag{7.16}$$

where I is the particle current or the number of particles per unit time per unit volume of gas passing through volume v. The particle current is given by [7.1]

$$I = n \frac{dv}{dt} \tag{7.17}$$

where dv/dt is the appropriate growth rate expression for aerosol growth. For particles much larger than the mean free path of the gas, the aerosol growth rate (Equation 7.9) can be transformed into

$$\frac{dV}{dt} = 3^{1/3}(4\pi)^{2/3}\frac{p_v(T_v)D}{\rho RT_v}MW\,(S(t)-1)V^{1/3} \qquad (7.18a)$$

$$= G(t)V^{1/3} \qquad (7.18b)$$

Thus, Equation (7.16) becomes

$$\frac{\partial n}{\partial t} + G(t)\frac{\partial (nv^{1/3})}{\partial v} = 0 \qquad (7.19)$$

Equation (7.19) describes the evolution of the aerosol size distribution due to diffusional growth.

Since G(t) is a function of the vapor supersaturation, S(t), Equation (7.19) and the corresponding mass balance for the vapor should be solved simultaneously. Coupling the vapor depletion to the growth of the aerosol would provide a complete description of the vapor/aerosol system. However, in reviewing previous solutions for n(v,t), Tsang and Brock [7.7] state that no analytical solution to Equation (7.19) has been found for the case of a changing supersaturation ratio. Moreover, they note the numerical difficulty in solving this first-order hyperbolic equation because of the large variation in both the magnitude and sign of the condensation coefficient. Hence, they developed a new numerical method capable of solving the aerosol transport equation for the general case of both evaporation and condensation. Comparisons between their method and other numerical methods available in the literature were made. They conclude that an asymptotic regime similar to that for coagulation develops for condensational aerosol growth.

Brock [7.8] has studied the solution to Equation (7.16) for a variety of different aerosol growth laws. If the supersaturation is constant, he suggests that for diffusional growth, the particle size distribution is of the form

$$n(v) \sim v^{-1/3} \exp(-C_1 v^{2/3}) \qquad (7.20)$$

The purpose of this section is to determine the particle size distribution following nucleation. Because no complete analytic solution exists that incorporates both the growth of the aerosol and the depletion of the vapor, a few approximations need to be made. Examination of the aerosol growth times in Figure 7.2 suggests that the vapor supersaturation changes very rapidly, indicating that the system reaches equilibrium very quickly. As a result, in the derivation that follows, the vapor is assumed to reach equilibrium instantaneously (i.e. S = 1). Moreover, uncoupling the depletion of the vapor from the growth of the aerosol allows Equation (7.19) to be solved analytically for the particle size distribution at equilibrium, $n_e(v)$. Two integral boundary conditions are required to obtain a solution. They are:

(1) The total number of particles in the system produced by nucleation is constant until the system reaches to equilibrium, i.e.,

$$N_0 = \int_0^\infty n_e dv \tag{7.21}$$

(2) the volume concentration of aerosols at equilibrium is given by

$$V_e = \int_0^\infty n_e v dv \tag{7.22}$$

The volume concentration of aerosol at equilibrium can also be written in terms of the vapor supersaturation. A simple mass balance yields

$$V_e = V_0 + \frac{p_v(T)MW}{\rho RT} (Vol)(S_0-1) \tag{7.23}$$

where

V_0 = initial volume concentration produced at nucleation

S_0 = initial supersaturation,

$p_v(T)$ = vapor pressure of specie (Pa),

MW = molecular weight (kgmole/kg),

ρ = density of liquid (kg/m^3),

R = gas constant ($Pa\text{-}m^3/kgmole\ K$),

T = temperature (K),

Vol = volume (m^3), and

S = supersaturation ratio.

The first boundary condition (Equation 7.21) restricts the time dependent behavior of the solution. For the total aerosol number concentration to be invariant with time, the time dependence of the particle size distribution must disappear when the distribution is integrated over all aerosol sizes. This constraint suggests that a solution similar in form to Brock's might be appropriate. Hence,

$$n(v,t) = \frac{C_0}{A(t)} v^{1/3} \exp\left(-\frac{v^{2/3}}{A(t)}\right) \qquad (7.24)$$

Substitution of Equation (7.24) into Equation (7.21) yields

$$N_\infty = \int_0^\infty n\,dv = \frac{C_0}{A(t)} \int_0^\infty v^{-1/3} \exp\left(-\frac{v^{2/3}}{A(t)}\right) dv \qquad (7.25)$$

Since the value of the integral is 1.5 A(t), the time dependence disappears and

$$C_0 = \frac{2}{3} N_0 \tag{7.26}$$

The value of A(t) at equilibrium, A_e, can be determined by subjecting the particle size distribution to the volume constraint given by Equation (7.22). Hence,

$$V_e = \int_0^\infty n_e v dv = \frac{C_0}{A(t)} \int_0^\infty v^{2/3} \exp\left(- \frac{v^{2/3}}{A(t)}\right) dv \tag{7.27}$$

Evaluation of the integral gives

$$V_e = \frac{9}{8} C_0 A_e^{2/3} \sqrt{\pi} \tag{7.28}$$

Combining Equations (7.26) and (7.28) yields

$$A_e = \left(\frac{4V_e}{3N_0\sqrt{\pi}} \right)^{2/3} \tag{7.29}$$

Thus, the equilibrium aersol particle size distribution immediately following nucleation is given by

$$n_e(v) = \frac{2}{3} N_0 \left(\frac{3N_0\sqrt{\pi}}{4V_e}\right) v^{-1/3} \exp\left\{ -\left(\frac{3N_0\sqrt{\pi}}{4V_e} v\right)^{2/3} \right\} \tag{7.30}$$

The cumulative distribution function at equilibrium, $N_e(v)$ is given by

$$N_e(v) = \int_0^v n_e(v)\,dv = \frac{2}{3} N_0 \left(\frac{3\sqrt{\pi}\,N_0}{4V_e}\right)^{2/3} \int_0^v v^{-1/3} \exp\left(-\left(\frac{3\sqrt{\pi}\,N_0}{4V_e} v\right)^{2/3} \right) dv \tag{7.31}$$

$$= N_0 \left[1 - \exp\left(-\left[\frac{3\sqrt{\pi}}{4Ve} v\right]^{2/3}\right) \right] \tag{7.32}$$

The occurrence of N_0/V_e in the solution suggests that the similarity transformation presented earlier is applicable here. Thus, Equation (7.30), in terms of the similarity variables, becomes

$$\psi_e = \frac{2}{3}\left(\frac{3\sqrt{\pi}}{4}\right)^{2/3} \eta^{-1/3} \exp\left[-\left(\frac{3\sqrt{\pi}}{4}\eta\right)^{2/3}\right] \qquad (7.33)$$

Thus, this solution is also self-preserving. Equation (7.33) is plotted in Figure 7.3.

A series of calculations have been performed to determine the behavior of the equilibrium particle size distribution. The fraction of the total number of particles in a given volume range, dN/N_0 was calculated using Equation (7.32). The analysis assumed an initial volume concentration of 10^{-13}. Values of the transport properties needed to calculate the equilibrium aerosol volume concentration, V_e, in Equation (7.23) were taken from Table 7.1. Calculations were performed using initial particle concentrations of 10^{12}, 10^{15}, and 10^{18}. The particle size distributions at equilibrium for these three cases are shown in Figures 7.4, 7.5 and 7.6. Initially, as a result of nucleation all the particles have a volume of $10^{-25}m^3$. However, at equilibrium a complete distribution develops as a result of vapor condensation and aerosol growth. As the total number of particles in the system increases, the average particle volume at equilibrium, $\bar{v} = V_e/N_0$ decreases. If more particles

Figure 7.3

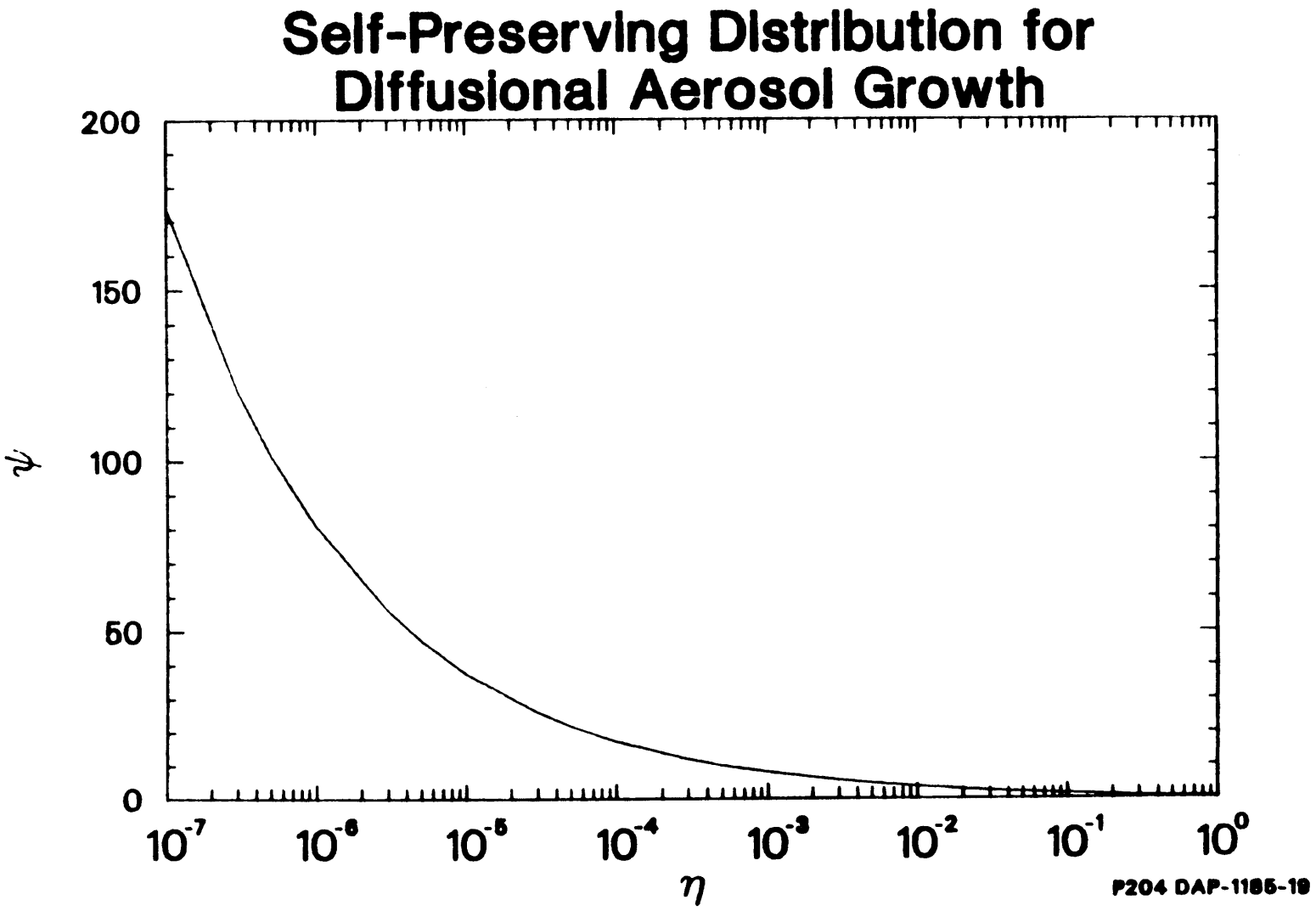
Self-Preserving Distribution for Diffusional Aerosol Growth
200
150
100
50
0
ψ
10^{-7}
10^{-6}
10^{-5}
10^{-4}
10^{-3}
10^{-2}
10^{-1}
10^{0}
η
P204 DAP-1185-19

Figure 7.4

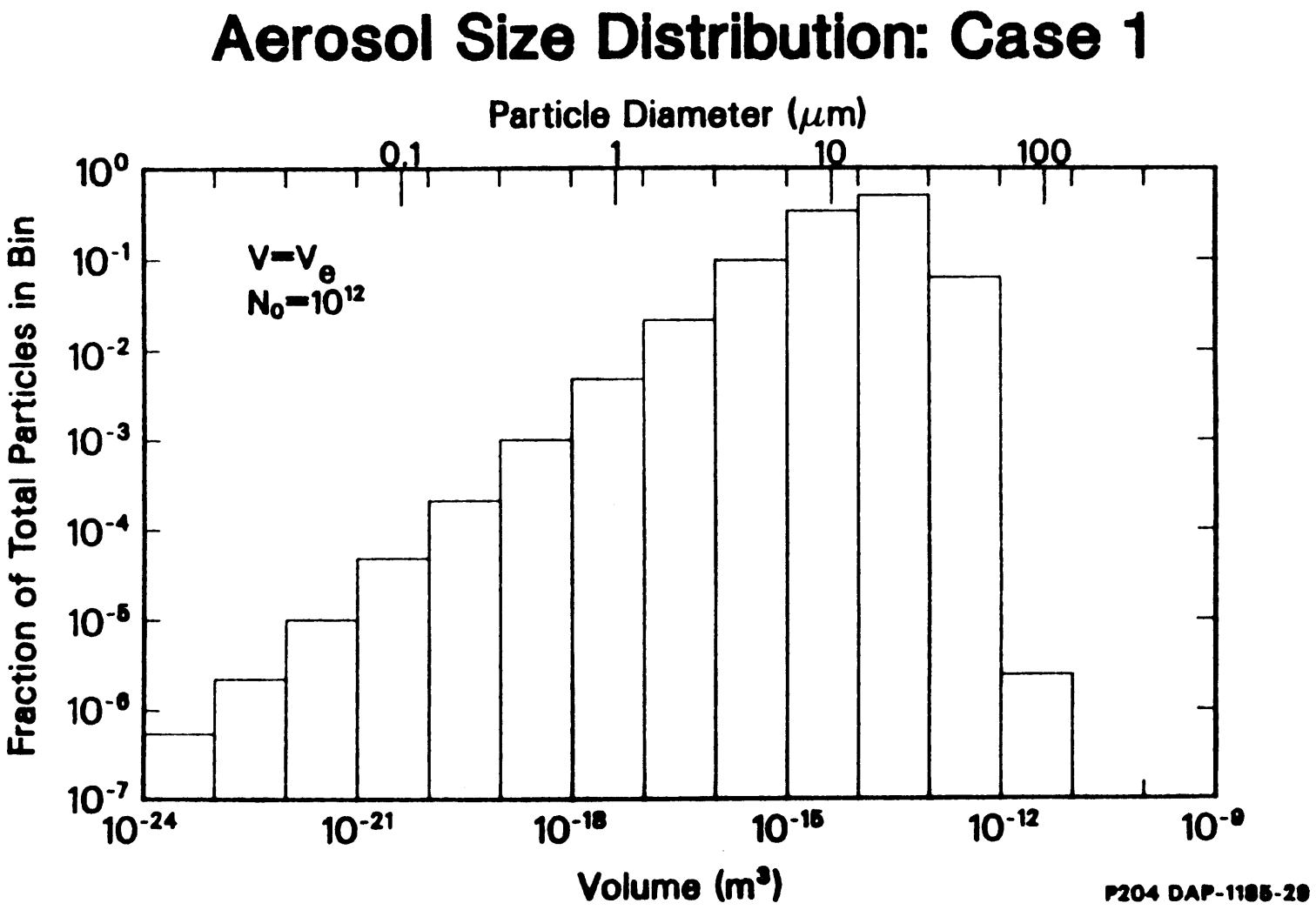
Aerosol Size Distribution: Case 1
Particle Diameter (μm)
0.1
1
10
100
V=Ve
No=10^12
Fraction of Total Particles in Bin
10^0
10^-1
10^-2
10^-3
10^-4
10^-5
10^-6
10^-7
10^-24
10^-21
10^-18
10^-15
10^-12
10^-9
Volume (m^3)
P204 DAP-1185-28

Figure 7.5

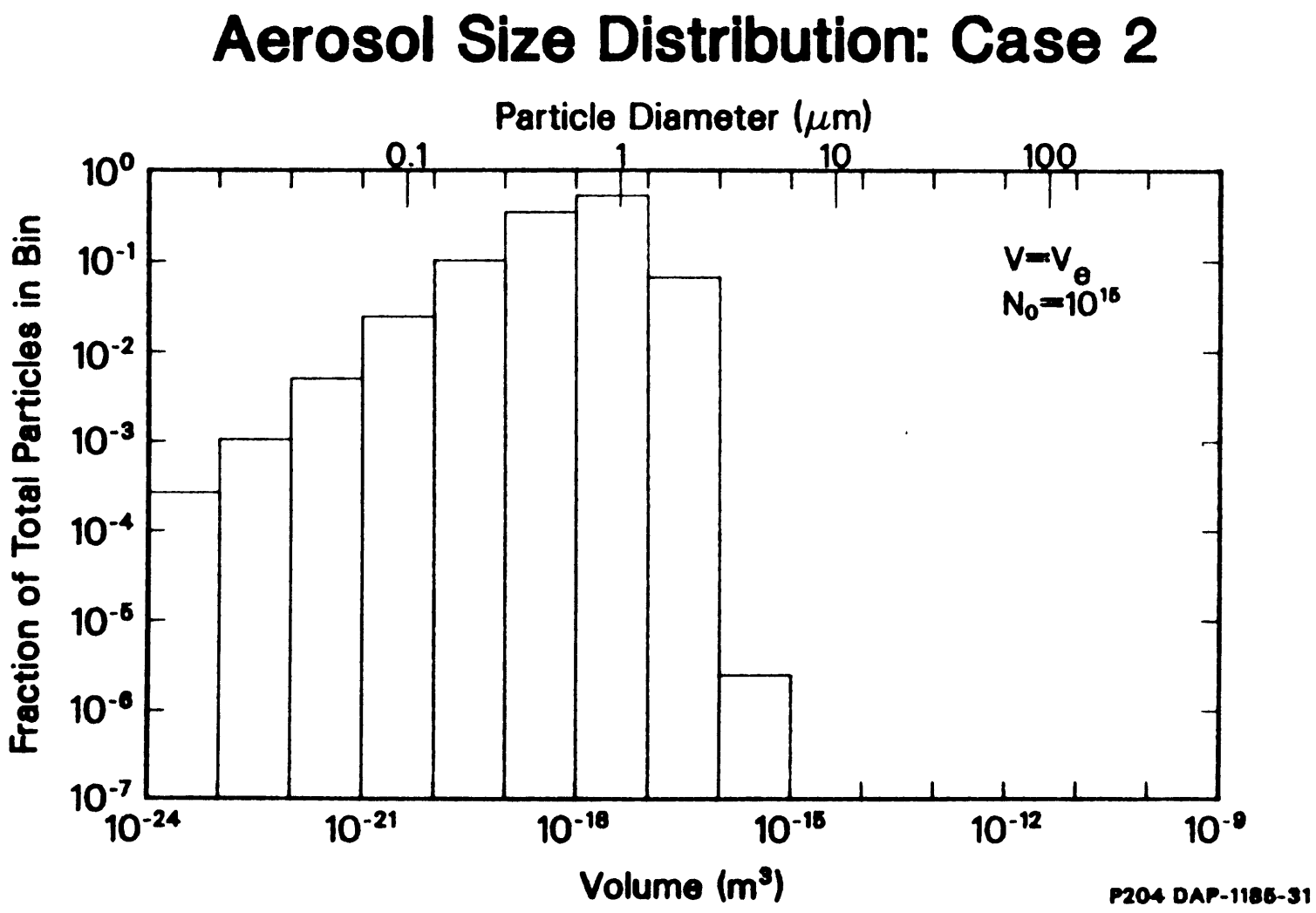
Aerosol Size Distribution: Case 2
Particle Diameter (μm)
0.1
1
10
100
Fraction of Total Particles in Bin
10^0
10^-1
10^-2
10^-3
10^-4
10^-5
10^-6
10^-7
V=V_e
N_0=10^15
10^-24
10^-21
10^-18
10^-15
10^-12
10^-9
Volume (m^3)
P204 DAP-1185-31

Figure 7.6

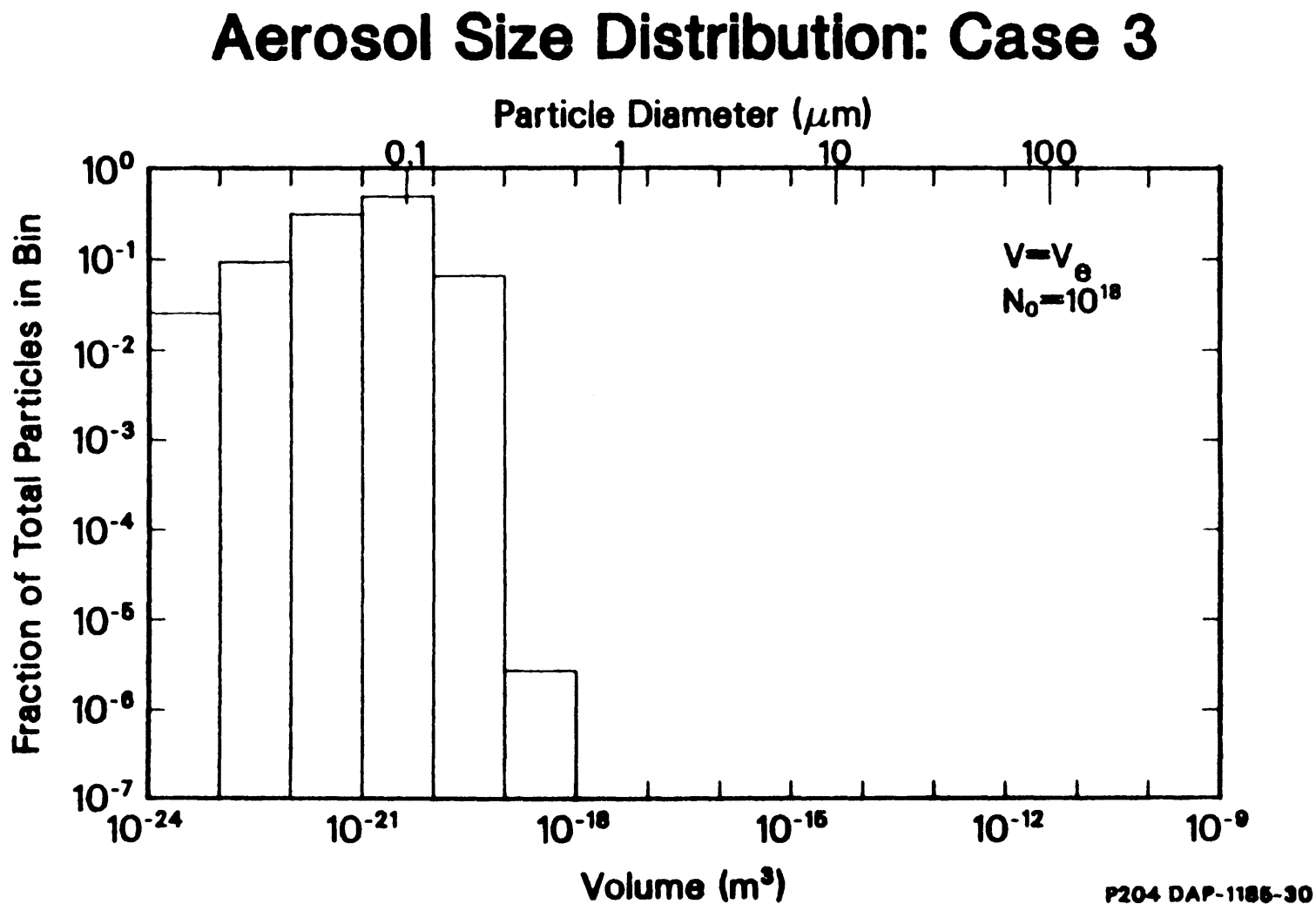
Aerosol Size Distribution: Case 3
Particle Diameter (μm)
0.1
1
10
100
10^{0}
10^{-1}
10^{-2}
10^{-3}
10^{-4}
10^{-5}
10^{-6}
10^{-7}
Fraction of Total Particles in Bin
V=V$_e$
N$_0$=10^{18}
10^{-24}
10^{-21}
10^{-18}
10^{-15}
10^{-12}
10^{-9}
Volume (m^3)
P204 DAP-1186-30

are available for vapor condensation, then each particle would grow less causing the distribution to peak towards the smaller end of the size spectrum.

7.5 Conclusions

The purpose of this analysis was to determine the equilibrium particle size distribution at the end of the period of aerosol generation. Integration of the aerosol growth rate equation indicates that equilibrium is reestablished quickly following the start of nucleation. Under a reasonable set of assumptions, an analytic solution for the aerosol size distribution was obtained that depends only on the total number of particles and the volume concentration of aerosol at equilibrium. Moreover, by incorporating these results into a fission product transport code like TRAPMELT, aerosol formation in severe reactor accidents can be modeled without adding substantial computational cost. In most aerosol transport codes available today, the user must determine a priori the magnitude, timing and location of aerosol production in the accident. In addition, the initial aerosol size distribution must be specified on input. Such a calculation can be quite difficult and subject to high uncertainty. However, by including nucleation into the code, the user

(1) obtains a better physical understanding of the system,
(2) allows the code to determine the timing, magnitude and location of aerosol production, and
(3) permits the code to generate the equilibrium particle size distribution immediately following nucleation.

7.6 REFERENCES

7.1 Friedlander, S.K., Smoke Dust and Haze: Fundamentals of Aerosol Behavior, John Wiley and Sons, New York, 1977.

7.2 Hidy, G.M., "On the Theory of the Coagulation of Noninteracting Particles in Brownian Motion", J. Colloid Sci., 20, 1965, pp. 123-144.

7.3 Hidy, G.M. and Lilly, D.K., "Solutions to the Equations forthe Kinetics of Coagulation,,"J. Colloid Sci., 20, 1965,pp. 867-874.

7.4 Friedlander, S.K. and Wang, C.S., "The Self-PreservingDistribtuion for Coagulation by Brownian Motion," J. Coll.Int. Sci., 22, 1966, pp. 126-132.

7.5 Pich, J., Friedlander, S.K., and Lai, F.S., "The Self Preserving Particle Size Distribution for Coagulation by Brownian Motion -III. Smoluchowski Coagulation and Simultaneous Maxwellian Condensation," J. of Aero. Sci., 1, 1970, pp.115-126.

7.6 Warren, D.R. and Seinfeld, J.H. "Nucleation and Growth of Aerosol from a Continuously Reinforced Vapor," Aero. Sci.and Tech., 3, 1984, pp. 135-153.

7.7 Tsang, T.H. and Brock, J.R., "Simulation of Condensation Aerosol Growth by Condensation and Evaporation," Aero. Sci.and Tech., 2, 1983, pp. 311-320.

7.8 Brock, J.R., "On Size Distributions of Atmospheric Aerosols", Atmos. Environ., 5, 1971, pp.833-841.

8. Ag-In-Cd CONTROL ROD AND AEROSOL BEHAVIOR IN PBF TEST SFD 1-4

8.1 Introduction

A series of experiments have been conducted in the Power Burst Facility (PBF) at the Department of Energy's Idaho National Engineering Laboratory to study the consequences of severe reactor accidents. The objectives of the PBF Severe Fuel Damage (SFD) test program were to obtain data about fuel behavior, fission product release, deposition and transport, and hydrogen generation during degraded core accidents.

The fourth in-pile experiment in the SFD program, PBF Test SFD 1-4, was conducted on February 7, 1985. In addition to the overall test objectives described above, a specific objective of this experiment was to investigate the behavior of Ag-In-Cd control rods during high temperature severe fuel damage events. Detailed examination of the results from this experiment has begun and will continue for the next two years. Although an extensive amount of information has been obtained from on-line instrumentation in the experiment, post-test processing of the fission product and aerosol data collected during the test is just beginning. This

information is required before a complete picture of the fission product and aerosol behavior in the experiment can be formulated. In addition, since this data is currently unavailable, a comparison with predictions from the VAPOR code and aerosol generation models presented earlier cannot be made. As a result, the following discussion is primarily based on interpretation of the preliminary results from on-line instrumentation found in the Severe Fuel Damage Test 1-4 Quick Look Report [8.1].

Proper interpretation of the control rod and aerosol behavior in a complex in-pile experiment like the SFD 1-4 test requires knowledge of the experimental setup, test procedure and some general results from the test. This information is the subject of the next two sections. Section 8.2 provides a description of the experimental configuration and test procedure. In Section 8.3, general results from PBF Test SFD 1-4 are presented. The control rod and aerosol behavior in the SFD 1-4 experiment is discussed in Section 8.4. Conclusions are drawn in Section 8.5.

8.2 System Design, Instrumentation and Test Procedure

8.2.1 Experimental Design

The PBF reactor is an annular UO_2 driver core, 1.3 m in diameter and 0.91 m in height, that encloses a vertical flux trap. The reactor is designed to test the behavior of nuclear fuels under a variety of off-normal conditions. An in-pile tube fits into the flux trap region and acts as a physical barrier between the test fuel and the driver core. Fuel bundles are inserted into the in-pile tube where they can undergo transients such as reactivity insertion events, power cooling mismatch experiments, loss of coolant accidents and severe fuel damage accidents.

A schematic of the test train and sampling system used in PBF Test SFD 1-4 is shown in Figure 8.1. The SFD 1-4 fuel bundle consists of a 32 rod array filled with 28 fuel rods and four zircaloy guide tubes each containing a stainless-steel-clad Ag-In-Cd control rod (Figure 8.2). Twenty-six of the fuel rods were previously irradiated to an average burnup of 35,000 MWD/MT. The remaining two fuel rod positions are occupied by two highly instrumented fresh fuel rods. Each rod has three axial cladding thermocouples, one fuel centerline thermocouple and a pressure switch

Figure 8.1

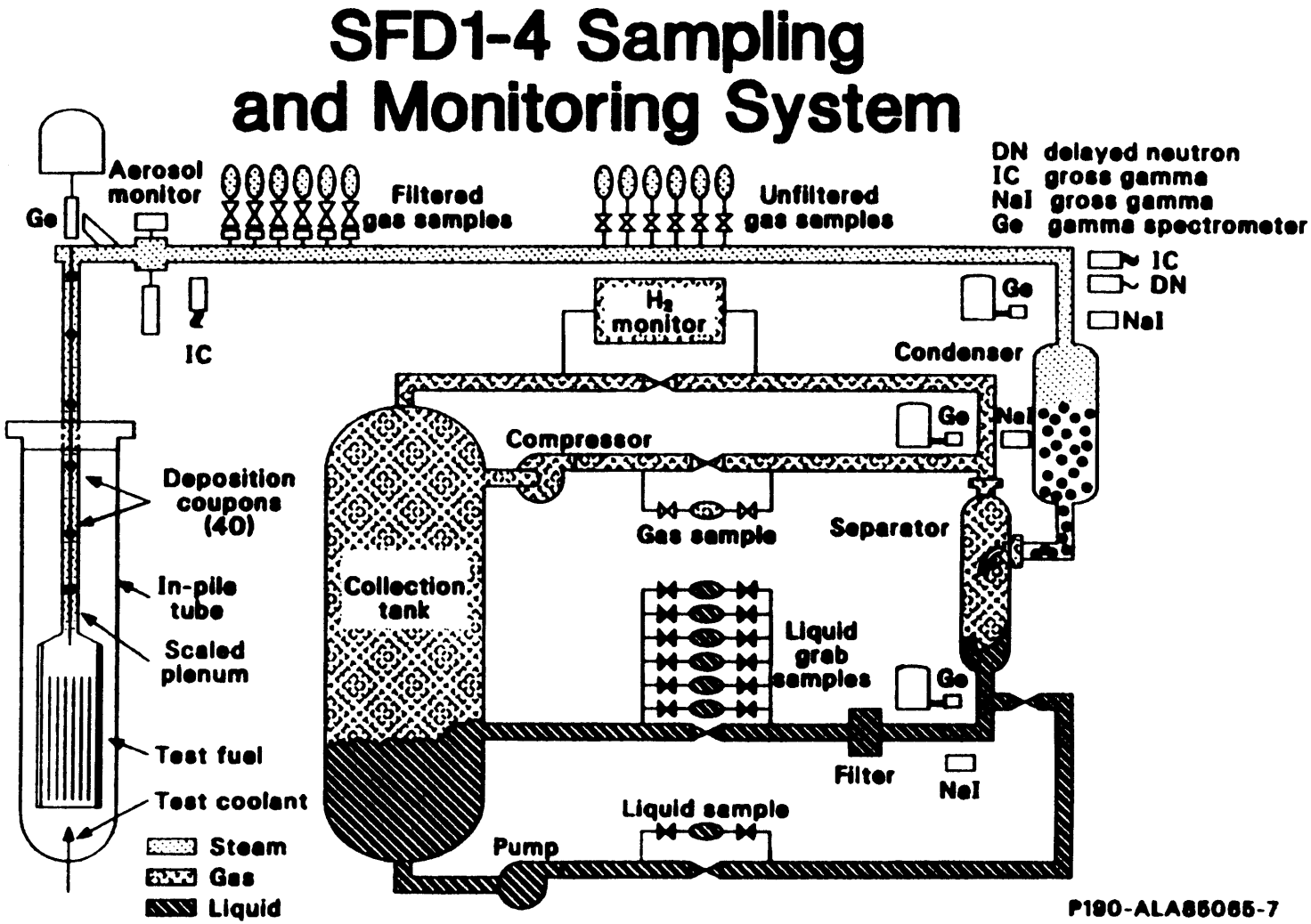
SFD1-4 Sampling and Monitoring System
DN delayed neutron
IC gross gamma
NaI gross gamma
Ge gamma spectrometer
Aerosol monitor
Ge
Filtered gas samples
Unfiltered gas samples
IC
DN
NaI
H_2 monitor
Ge
Condenser
Ge
NaI
Compressor
Deposition coupons (40)
Gas sample
Separator
In-pile tube
Collection tank
Liquid grab samples
Scaled plenum
Ge
Test fuel
Filter
NaI
Test coolant
Liquid sample
Steam
Pump
Gas
Liquid
P190-ALA85065-7

Figure 8.2

Cross-sectional View of SFD 1-4 Test Train

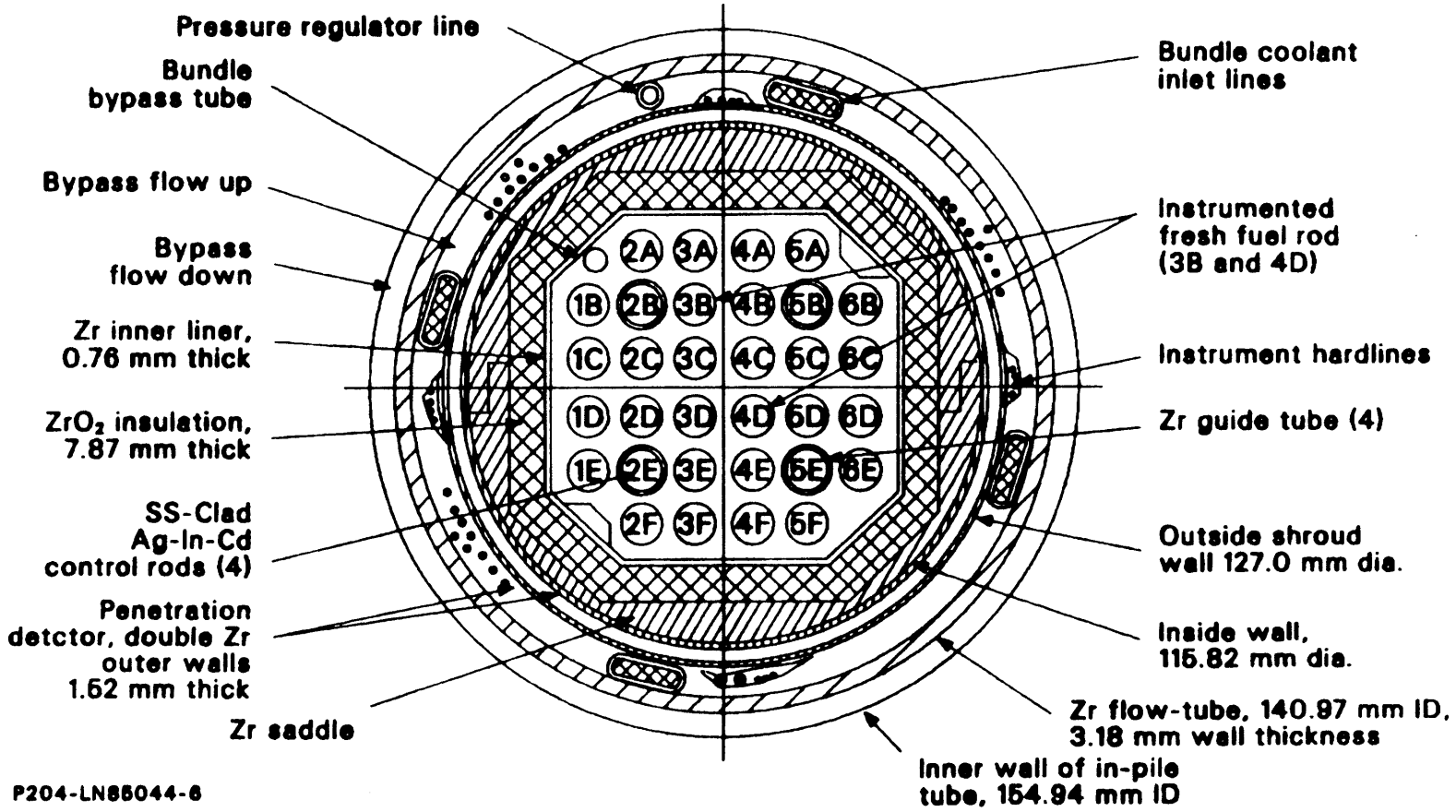

designed to indicate cladding failure. One of the four control rods is also instrumented with four thermocouples identical to those used in the fuel rods and a pressure transducer. Inconel spacer grids are used to position the fuel rods and guide tubes onto a square-pitch spacing pattern typical of a 17 x 17 PWR array. A zircaloy-lined ZrO_2 shroud surrounds the fuel bundle and acts as a physical boundary between the fuel and the in-pile tube.

A series of fission chambers are axially and azimuthally distributed around the outside of the test train. These monitors are designed to track the water level in the experiment because they are sensitive to changes in the neutron flux that occur when water changes from a two phase mixture to superheated steam. In addition, since the chambers are sensitive to thermal neutrons, they can be used to indicate the movement of both control rod absorber material and to a lesser extent fuel in the bundle during the experiment.

The simulated upper plenum above the fuel region consists of a deposition rod mounted inside a circular steam tube. Forty removable deposition coupons are mounted along the rod to characterize fission product and aerosol depostion in the experiment. Thermocouples are located at three axial positions to measure steam

and coupon surface temperatures. Three banks of heaters are installed in the steam tube wall to ensure a proper thermal environment and to prevent steam condensation in the line.

Inlet cooling in the experiment is directed into the bottom of the fuel bundle from the lower plenum. During the test, fission heat and zircaloy oxidation cause the water to vaporize and hydrogen to be generated. This steam/hydrogen mixture exits the top of the fuel region and enters the simulated upper plenum. Fission products and aerosols released from the fuel region are transported by the effluent flow into the simulated upper plenum where some deposition occurs. Upon exiting the upper plenum region, the flow is directed into the fission product and hydrogen monitoring system.

The fission product and hydrogen monitoring system (FPHMS) is a specially designed system to measure fission products, aerosols and hydrogen generated in the experiment. A schematic is shown in Figure 8.1. The FPHMS consists of a long 0.25-inch pipe which directs the effluent flow past a series of on-line instruments and grab samples into a large collection tank. The effluent line is heat traced and insulated up to the condenser to maintain steam temperatures above saturation (644 K) all along the line.

Upon exiting the upper plenum, the effluent flow passes the first of four gamma spectrometers. All four gamma spectrometers use a shielded intrinsic germanium detector and a variable aperture collimator between the sample line and the detector to allow for remote adjustment of the gamma flux incident on the detector crystal during the experiment. Immediately downstream of the first gamma spectrometer, the effluent line passes in front of an on-line aerosol monitor. The aerosol monitor measures the turbidity in the sample effluent line by projecting a light beam normal to the flow and recording the resultant beam attenuation as aerosols pass through the light path. The effluent turbidity measured in the line can be correlated to the aerosol concentration in the experiment.

After exiting the aerosol monitor, the sample line passes an ion chamber and a series of six filtered and six unfiltered steam samples. These steam samples are designed to operate remotely at different times to obtain data on fission product and aerosol behavior in the effluent line during the experiment. These samples, along with the deposition coupons in the simulated upper plenum, undergo a variety of post-test analyses to determine their elemental and chemical composition.

The sample line is then routed past an ion chamber,

a delayed neutron monitor and the second gamma spectrometer before entering the condenser. Upon leaving the condenser, the flow enters the separator. The condensed liquid effluent exits the bottom of the separator where it is diluted with additional water and passes a NaI detector and the liquid line gamma spectrometer. The liquid is then routed through a bank of in-line filters and flow-through liquid samples before entering the collection tank. The gaseous effluent exits the top of the separator due to a continuous nitrogen purge. This gas is directed past a NaI detector, the gas line gamma spectrometer and into the hydrogen analyzer. The exit line leaving the H_2 monitor is then routed to the collection tank.

8.2.2 Test Procedure

The test procedure used to conduct the SFD 1-4 experiment is quite lengthy. A brief summary of the transient and high temperature phases of the experiment follows.

The transient phase of the experiment commenced with a bundle boildown. Prior to boildown, the bundle inlet conditions were adjusted to 532 K and 6.9 MPa, a coolant mass flow rate of 0.6 g/s into the fuel bundle was established and the heaters in the upper plenum were

turned on. The bundle power was then ramped to ~ 5kW to boil off the coolant and reduce the water level. During boildown, an argon sweep gas was introduced from the bottom of the fuel bundle to help stabilize pressure caused by oscillating condensation in the effluent line. At the end of this core uncovery phase, an equilibrium two-phase steam interface was established 0.24 m above the bottom of the fuel, the bundle power was at 2.6 kW, the outlet steam temperature was 750 K and cladding temperatures were 775 K.

The high temperature phase of the transient was then initiated. By ramping bundle power at a rate of 0.3 kW/min, fuel rod temperatures increased from 800 to 1200 K at a rate of 0.36 K/s. When the average bundle temperature reached 1200 K, the bundle power ramp rate was increased to 1.3 kW/min to obtain a cladding temperature rise rate of 1.4 K/s until a temperature of 1600 K was attained. The onset of rapid oxidation began when the bundle average temperature reached 1650 K. At this point in the experiment, the bundle power was increased to 30 kW and held there for 220 seconds. Following the 220 second peak power hold, the bundle power was decreased, the argon sweep gas flow rate was increased, the inlet water flow was turned off, and the reactor was scrammed. Cooldown of the bundle was

achieved using the argon sweep gas for 50 minutes followed by a one hour nitrogen purge.

Following scram, a variety of post-test activities occurred. These included isolating the FPHMS, removing the deposition rod and steam samples, flushing the bundle and effluent line and recirculating the gas and liquid contents of the collection tank past their respective spectrometers.

8.3 General Test Results

This section will present an overview of the thermal, hydraulic and mechanical behavior of the test bundle as well as the fission product behavior that occured in the PBF SFD 1-4 experiment. Details of the control rod and aerosol behavior are discussed in Section 8.4. Zero time on all plots corresponds to the beginning of the high temperature transient.

During bundle heatup, the bundle power in the experiment was adjusted to achieve the desired temperature ramp rates described in Section 8.2. The fuel centerline and cladding temperature responses of Rod 3B, shown in Figure 8.3, are typical of the behavior of all the fuel rods in the bundle. The bundle temperature increased at an average rate of ~0.36 K/s up to 1200 K and at ~1.4 K/s from 1200 to 1600 K. The

Figure 8.3

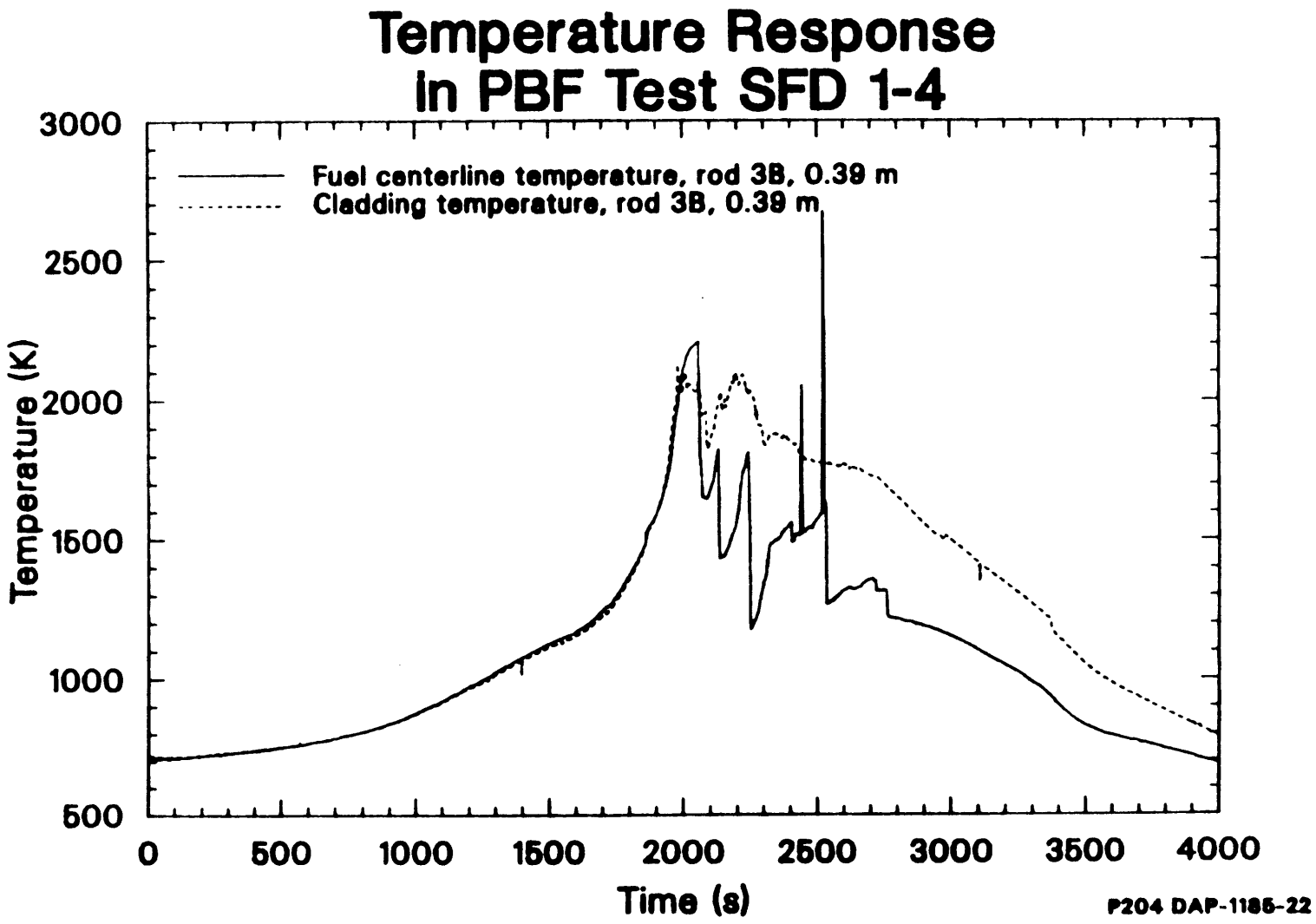
Temperature Response
in PBF Test SFD 1-4
Fuel centerline temperature, rod 3B, 0.39 m
Cladding temperature, rod 3B, 0.39 m
Temperature (K)
3000
2500
2000
1500
1000
500
0
500
1000
1500
2000
2500
3000
3500
4000
Time (s)
P204 DAP-1186-22

onset of rapid oxidation was interpreted as the 50 to 90 K step increase in temperature that occurred at approximately 1890 seconds into the transient. Beyond 1900 seconds, rapid oxidation caused temperatures to climb to values in excess of 2400 K.

The liquid flow into the bundle was provided by a positive displacement injection pump designed to deliver 0.6 g/s. In addition, during boildown, argon sweep gas was injected in the bottom of the bundle to stablize the bundle pressure. This sweep gas was used for the remainder of the experiment as a means of maintaining flow from the bundle to the FPHMS. The introduction of argon into the bundle could lead to behavior different from that expected in a severe reactor accident. The entrainment of water vapor by the argon sweep gas would probably enhance oxidation in the experiment. In addition, the presence of argon would alter the vaporization of core materials. Since argon has a larger molecular weight than hydrogen or steam, the diffusivity of a vapor in argon is less than in a hydrogen/steam mixture. Fortunately, this behavior can be accounted for in any post-test transport analysis. Finally, the use of an argon sweep gas throughout the experiment provides a continuous flow path from the bottom of the bundle to the FPHMS. As a result, the

final post-test configuration of the PBF SFD 1-4 test bundle might not represent the configuration of an LWR core expected after a severe reactor accident.

Thermocouple measurements in the simulated upper plenum suggest that steam tube wall and coupon temperatures were above saturation throughout the high temperature portion of the experiment. Three inner wall thermocouples located in the lower, middle and upper regions of the plenum indicate that the temperature of the steam tube remained uniform at values of 720, 770 and 700 K respectively. Coupon temperatures showed similar yet slightly less uniform behavior. At the peak of the transient, the bulk temperature of the steam exiting the fuel region exceeded 1700 K. However, the bulk temperature of the steam exiting the plenum remained uniform at ~650 K throughout the test indicating that significant cooling had occurred during plenum transit.

In the SFD 1-4 test, significant hydrogen was generated as a result of oxidation of zircaloy associated with cladding, guide tubes and the shroud inner liner. Results from the on-line H_2 monitor indicate that 185 $\pm$ 30 g of hydrogen was produced. This value corresponds to oxidation of 68% of the available zircaloy in the test bundle. The entrainment of water

vapor in the argon sweep gas probably aided oxidation in the experiment.

The fission product and hydrogen monitoring system (FPHMS) gathered extensive information about fission product behavior in the SFD 1-4 test. All results presented here relating to fission product behavior are plotted versus measurement time. Because of effluent transport, a delay exists between the time an event occurs in the bundle (i.e., fuel rod rupture) and the time at which the corresponding gap release is measured by the FPHMS. Transit times to various components of the FPHMS need to be considered when attempting to correlate the fission product behavior inferred from these measurements to measurements made in the fuel bundle.

Six filtered steam samples, six unfiltered steam samples and six liquid samples were taken over a wide range of temperatures (1200-2400 K), radiation levels (10^{-3}-10 R/hr) and aerosol conditions that were experienced during the experiment. Detailed post-test elemental and chemical analyses are currently being performed on these samples to aid in understanding the fission product and aerosol behavior in the experiment. Preliminary results of the six filtered steam samples are presented in the next section.

Signals from the six gross radiation monitors in the FPHMS provided general information about the timing of certain events in the bundle. The response of the ion chamber upstream of the aerosol monitor is shown in Figure 8.4. The transit time from the bundle to this ion chamber was less than one minute. At 1720 seconds into the transient, a spike was observed in the ion chamber. Similar spikes occurred in two other gross radiation monitors. This spike corresponded to the rupture of several fuel rods. The resultant gap release lasted for approximately three minutes indicating that the fuel rods ruptured at different times during this period rather than simultaneously. Little additional fission product release was observed until approximately 1900-2000 seconds when bundle temperatures were approaching 2000 K. The rapid rise in the ion chamber signal from 10^{-2} to 10 R/hr was the result of fission products being released on fuel heatup. The ion chamber signal remained elevated following the peak of the transient because of plateout of reactive fission products on the inner wall of the steam line in front of the detector.

The four on-line gamma-ray spectrometers accumulated numerous gamma ray spectra during the SFD 1-4 test. Preliminary analysis of these spectra have identified

Figure 8.4

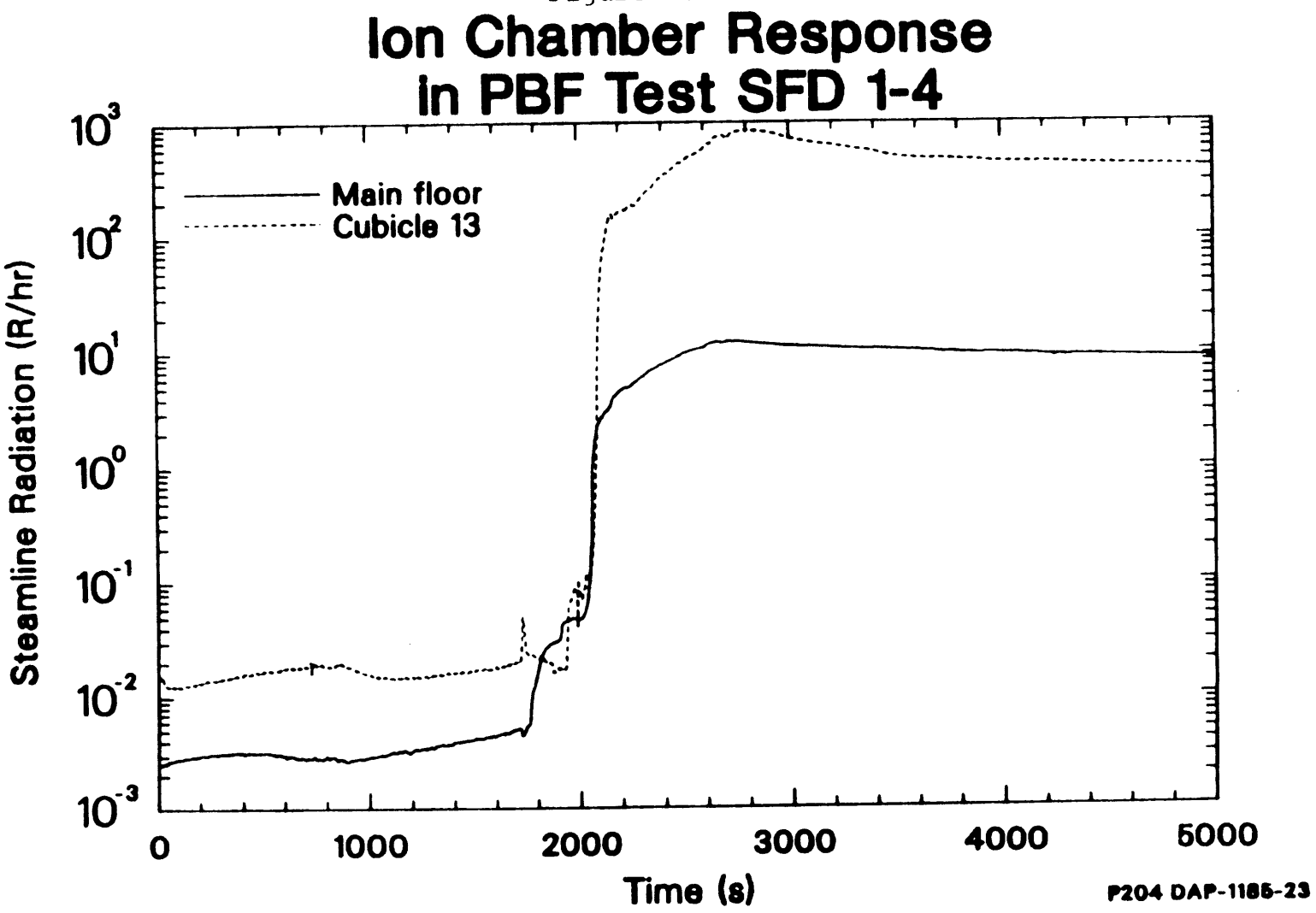
Ion Chamber Response
in PBF Test SFD 1-4
Main floor
Cubicle 13
Steamline Radiation (R/hr)
10^3
10^2
10^1
10^0
10^{-1}
10^{-2}
10^{-3}
0
1000
2000
3000
4000
5000
Time (s)
P204 DAP-1185-23

isotopes that were present in the effluent line during the experiment. A plot of the isotopic concentrations of Xe^{135}, I^{131}, Te^{132} and Cs^{137} is shown in Figure 8.5. These specific isotopes were selected because they are representative of the xenon, iodine, tellurium and cesium behavior in the test. Based on a calculated delay time of about one minute to the spectrometer, the strong increase in the concentrations of these four isotopes between 1800 and 2000 seconds coincided with the period of rapid oxidation and fuel heatup to temperatures in excess of 2400 K. The rapid rise in concentration occurred first for Xe^{135} and was followed by slightly delayed increases in the I^{131} and Cs^{137} concentrations. This delay is believed to be a result of wall condensation while fission product concentrations exceeded saturation followed by reevaporation of fission product vapors when release from the bundle diminished. Beyond 3000 seconds, the Xe concentration began to decrease corresponding to cooldown of the bundle and termination of the experiment whereas the I, Cs and Te concentrations remained very close to their peak values. As with the gross gamma measurements, these sustained elevated concentrations are a result of plateout in the effluent line viewed by the spectrometer.

Figure 8.5

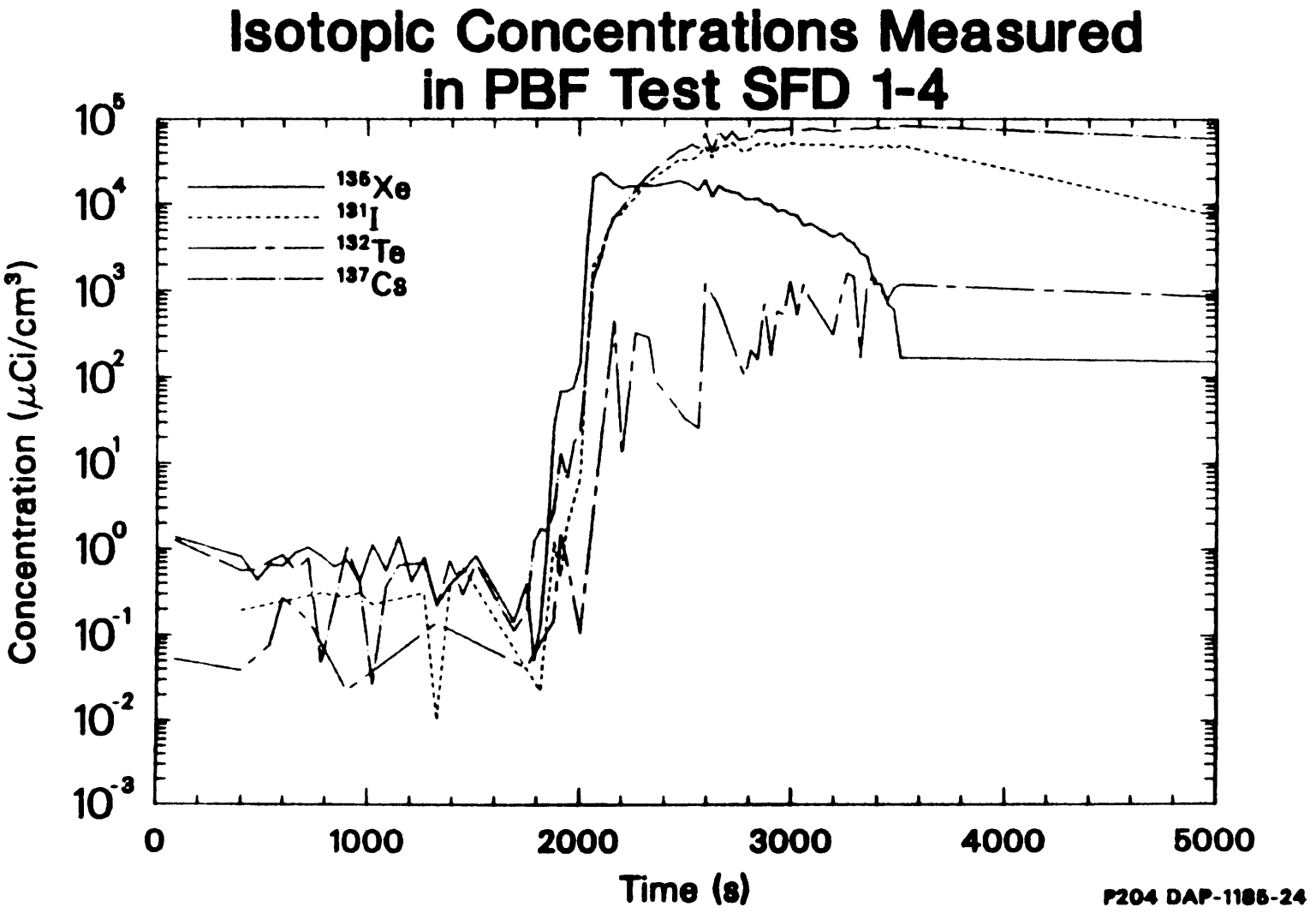
Isotopic Concentrations Measured
in PBF Test SFD 1-4
Concentration (μCi/cm³)
Time (s)
135Xe
131I
132Te
137Cs
10⁵
10⁴
10³
10²
10¹
10⁰
10⁻¹
10⁻²
10⁻³
0
1000
2000
3000
4000
5000
F204 DAP-1185-24

The concentration profiles from the gamma spectrometer immediately upstream of the condenser exhibited similar behavior to those in Figure 8.5. The delay between the rise in concentration of xenon and the volatile fission products is more pronounced and the peak isotopic concentrations of I, Cs and Te are somewhat less because of additional deposition that occurred in the FPHMS sample line during transport. Noble gas isotopes were the predominant fission products measured by the gas line spectrometer. Negligible quantities of Cs, I and Te were found in the gas line. Instead, these species were detected in the liquid line during the experiment.

Total isotopic release fractions for the SFD 1-4 experiment are shown in Table 8.1. Measurements were made both before and after the bundle flush by circulating the gas and liquid contents of the collection tank past the respective spectrometers. As noted in the table, in some cases isotopic concentrations were obtained from off-line analysis of collection tank grab samples. After the transient and prior to flushing, very little iodine, cesium, tellurium and lanthanum were detected. However, flushing the bundle caused significant increases in the concentration of all nuclides in the collection tank except for the

Table 8.1

Preliminary release fractions

Isotope	Release Fraction[a]			
	After Transient	After Steam Line Flush	After First Bundle Flush	After Second Bundle Flush
^{85}Kr	0.51±0.10	b	b	b
^{133}Xe	0.30±0.05	b	b	b
^{129m}Te	—[c]	—[c]	0.04±0.03	—[c]
^{132}Te	0.0074±0.0014	—[c]	—[c]	—[c]
^{131}I	00098±0.0020[d]	—[c]	0.24±0.14	0.07±0.81
^{133}I	0.052±0.010	—[c]	—[c]	—[c]
^{135}I	0.052±0.010	—[c]	—[c]	—[c]
^{134}Cs	0.0075±0.0015[d]	0.0246±0.0025	0.065±0.007	0.39±0.08[d]
^{137}Cs	0.009±0.001[d]	0.0288±0.0032	0.076±0.008	0.46±0.10[d]

a. Release fractions were computed by dividing the total collection tank activity at the time of measurement by the estimated bundle inventory of the isotope at the same time. Unless otherwise noted reported values are derived from the on-line measurements and are subject to biases due to deposition.

b. The gas space of the collection tank was not reanalyzed after the flushing operations.

c. Not detected.

d. From preliminary off-line analyses of a collection tank liquid grab sample.

noble gases.

Significant fission product deposition occurred during transit from the bundle to the collection tank in the SFD 1-4 test. The deposition rod in the simulated upper plenum was removed 60 days after the experiment and brought to a hot cell for preliminary examination. Visible discoloration and particulate deposits were found on the rod. In addition, heavy accumulations of solid deposits were found on upper horizontal surfaces of the coupons. Gamma scanning of the rod indicated that the overwhelming majority of the activity on the rod was associated with Cs^{134} and Cs^{137}. Other fission products (i.e. iodine) were either so short-lived that they had decayed away prior to rod removal or had such a low specific activity that they could not be detected in the presence of the cesium. The deposition coupons from the rod have been removed and are undergoing a variety of post-test elemental and chemical analyses to determine other fission product and control rod material present on the deposition rod.

Gamma spectroscopy was also performed on the portion of the effluent line on the main floor of the PBF. The measurements were made prior to bundle flushing and thus reflect some of the fission product deposition that occurred in the experiment. Isotopes of Ru, Ag, Sb, Te,

I, Cs, Ba, La, Ce and Eu were detected in widely varying concentrations along the effluent line.

8.4 Control Rod and Aerosol Behavior

This section will discuss the control rod and aerosol behavior in the PBF SFD 1-4 experiment. The response of the four Ag-In-Cd control rods in the test are discussed in Section 8.4.1. Preliminary results of the on-line aerosol monitor and steam samples are used in Section 8.4.2 to help interpret the aerosol behavior in the experiment. When appropriate, the results from previous sections are used to suggest plausible scenarios that might explain events that occurred in the experiment.

8.4.1 Control Rod Response

One of the four control rods in the SFD 1-4 test bundle was instrumented with thermocouples and an internal pressure sensor. This instrumented control rod failed 1712 seconds into the high temperature transient at a temperature of 1175 K. Five events occurred in the bundle to substantiate this claim:

(1) As shown in Figure 8.6, the control rod internal pressure dropped from 14 MPa to the bundle pressure of 6.9 MPa within 0.1 seconds.
(2) A 0.4 MPa pressure spike was created in the bundle by the rapid production of steam

Figure 8.6

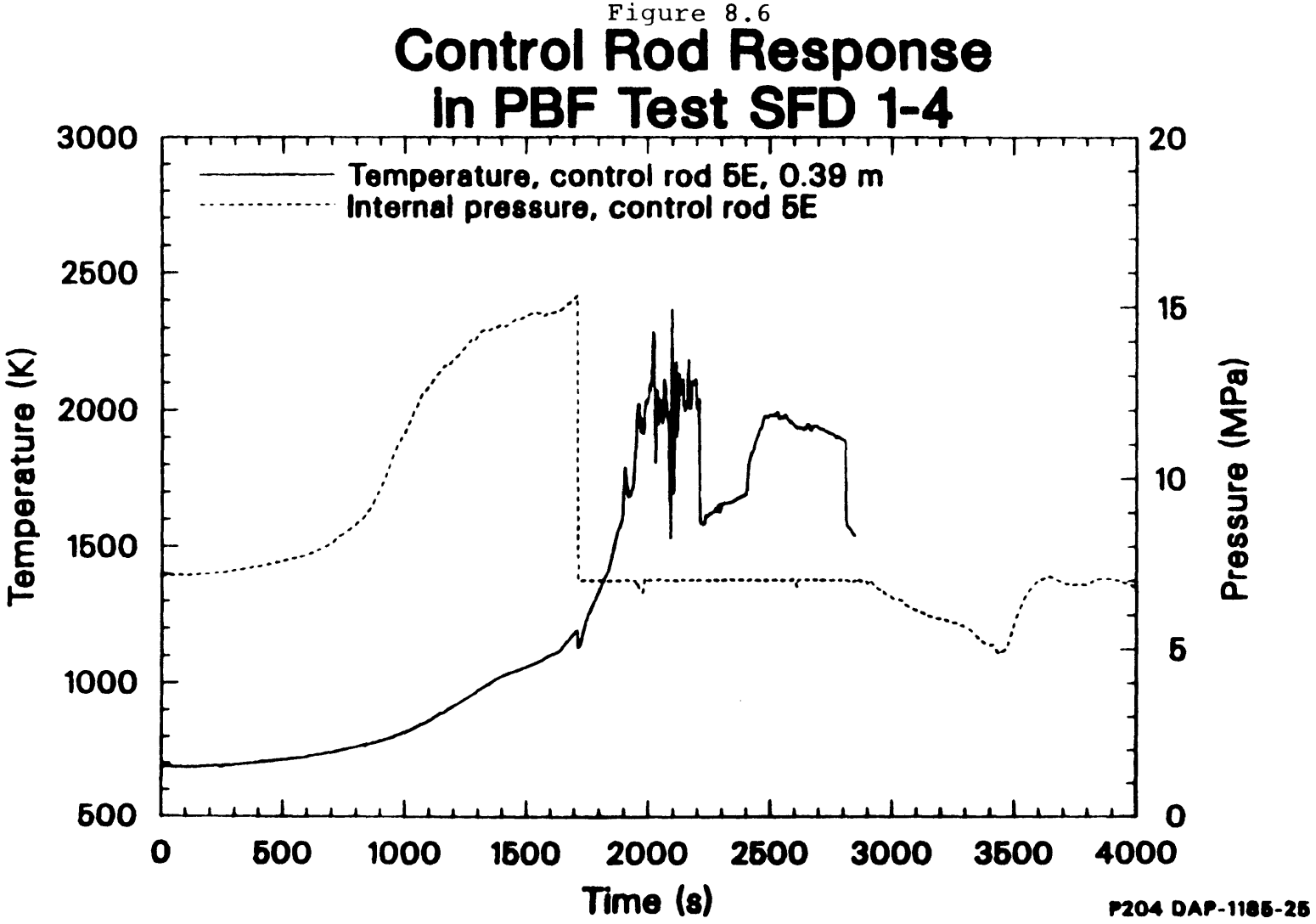
Control Rod Response
In PBF Test SFD 1-4
Temperature, control rod 5E, 0.39 m
Internal pressure, control rod 5E
Temperature (K)
Pressure (MPa)
Time (s)
3000
2500
2000
1500
1000
500
20
15
10
5
0
0
500
1000
1500
2000
2500
3000
3500
4000
P204 DAP-1185-25

when the molten absorber material entered the pool of water in the lower plenum. A thermocouple in the lower plenum indicated a corresponding temperature spike.

(3) A sudden increase in steam flow was registered by the gas flowmeter upstream of the condenser in the effluent line.

(4) All the fission chambers below the 0.51-m elevation showed sudden changes. The fission chambers at 0.35 and 0.51 m showed a temporary decrease for about 0.5 seconds and then recovered, indicating that control rod absorber material had passed that elevation in the bundle. The four fission chambers below the 0.35-m elevation all showed rapid decreases in their output, indicating the relocation of control rod material to these elevations in the bundle.

(5) Aerosols were detected 40 seconds later by the aerosol monitor in the FPHMS.

Failure of this control rod because of excessive internal pressure when its temperature reached 1175 K is not typical of control rod behavior expected in severe accidents. Thermodynamic calculations, performed in Section 2, indicate that the internal pressure is expected to be well below the system pressure in the experiment at 1175 K. Thus, the overpressurization failure of the control rod at this temperature was not due to vaporization of the alloy. Instead, the control rod is believed to have had a small leak and to have been waterlogged before the high temperature portion of the transient.

The failure of the remaining three control rods was not as noticeable as that of the instrumented rod. No

noticeable perturbations occurred in either the bundle pressure or the steam flow. However, sudden changes in the output of the fission chamber located below the bottom of the fuel (see Figure 8.7) indicate that the three uninstrumented rods failed between 1925 and 1975 seconds. About 60 seconds later, an increase in the aerosol concentration was detected at the aerosol monitor. The estimated maximum temperature of the control rods at the time of failure was about 1700 K.

From these observations, the scenario postulated in Section 2 for control rod behavior in the SFD 1-4 test appears plausible. The three uninstrumented rod did not burst. Instead, the stainless steel sheath lost its integrity at or near its melting point (1700 - 1750 K), causing the control rod alloy to contact the zircaloy guide tube. The Ag and In then reacted with the zircaloy, causing it to breach. The alloy material then flowed out of the breach, down the guide tube, and into the lower plenum of the test train.

8.4.2 Interpretation of Aerosol Measurements

The aerosol monitor, installed downstream of the first gamma spectrometer in the FPHMS, was designed to measure the attenuation of a light beam across the flow stream as aerosols pass through its path. The

Figure 8.7

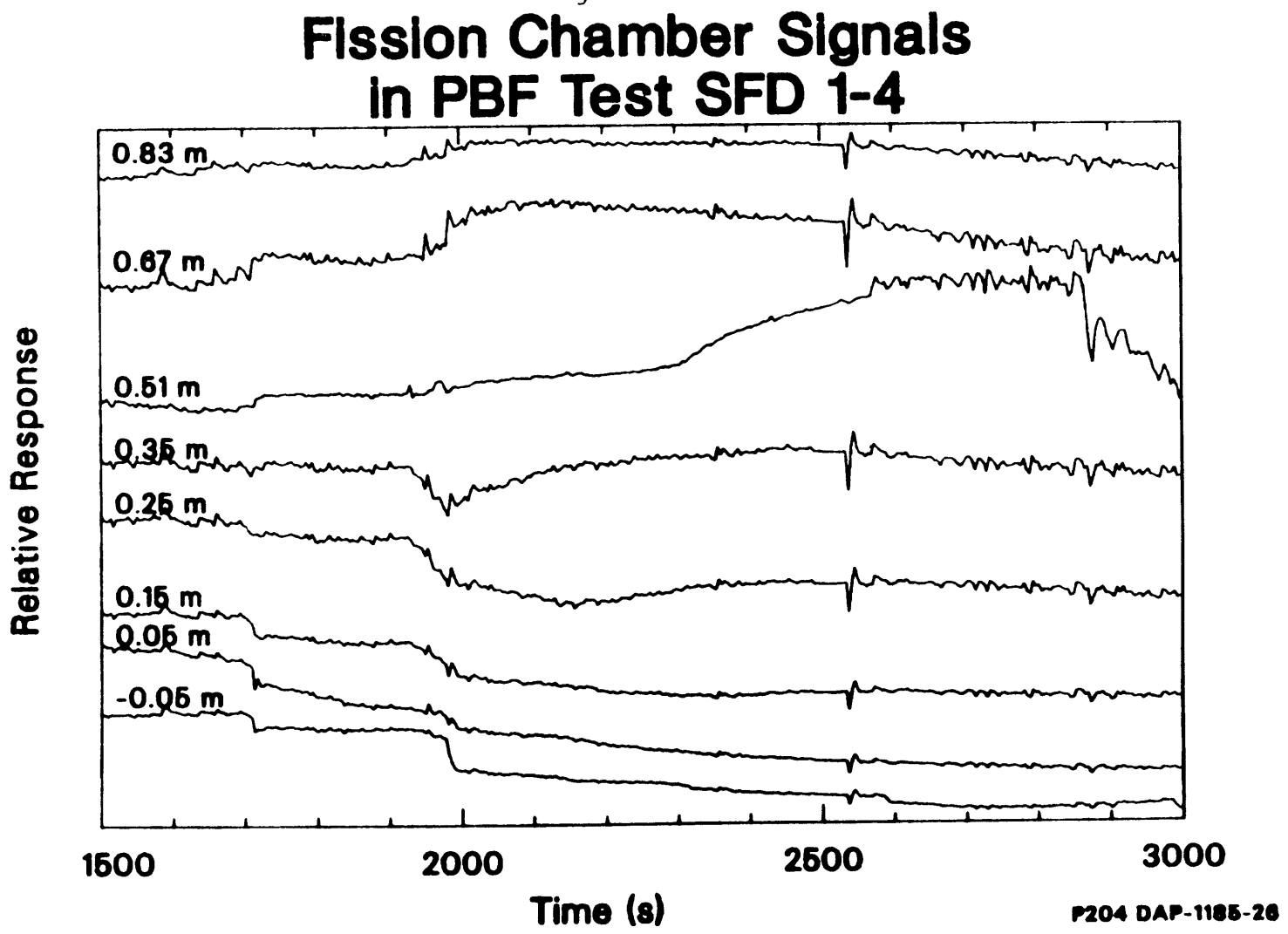
Fission Chamber Signals
in PBF Test SFD 1-4
0.83 m
0.67 m
0.51 m
0.35 m
0.25 m
0.15 m
0.05 m
-0.05 m
Relative Response
1500
2000
2500
3000
Time (s)
P204 DAP-1185-26

attenuated light beam signal is then converted to an aerosol particle density using a calibration. Details of the results of the calibration are found in Appendix F. Two different light path channels were used in an attempt to provide measurements over a range of approximately 5×10^5 to 2×10^8 particles/cc assuming a lognormal aerosol distribution with a mass mean particle diameter of 0.5 microns. Plots of the two aerosol signals obtained during the test are shown in Figures 8.8 and 8.9. The scale on the y axis is percent transmission; higher aerosol densities correspond to lower transmission percentages. The predicted aerosol number concentrations based on the aerosol transmission signals and the calibration for a 0.5 micron lognormal distribution are presented in Figures 8.10 and 8.11.

Both signals show the same qualitative behavior throughout the experiment. The 4-cm path length detector is more sensitive than the 1 cm-path length instrument, but the 4-cm instrument saturates at lower concentrations. Both systems first responded at 1742 seconds, 30 seconds after the first control rod failed. The 1-cm path signal and the 4-cm path signal correspond to aerosol number densities of approximately 2×10^7 particles/cc. The high internal pressure at the time of rod failure suggests that the molten alloy may have been

Figure 8.8

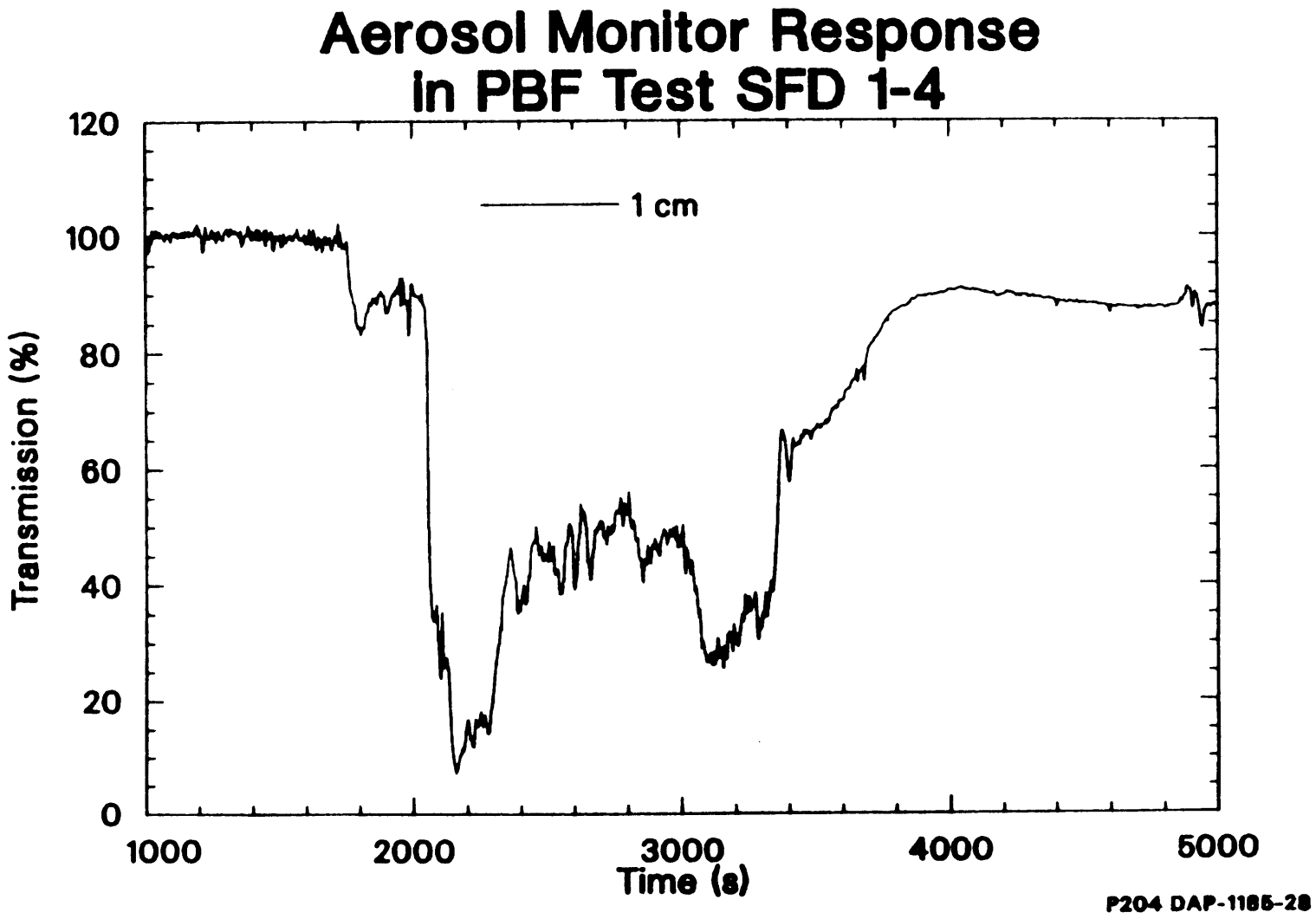
Aerosol Monitor Response
in PBF Test SFD 1-4
1 cm
Transmission (%)
120
100
80
60
40
20
0
1000
2000
3000
4000
5000
Time (s)
P204 DAP-1185-28

Figure 8.9

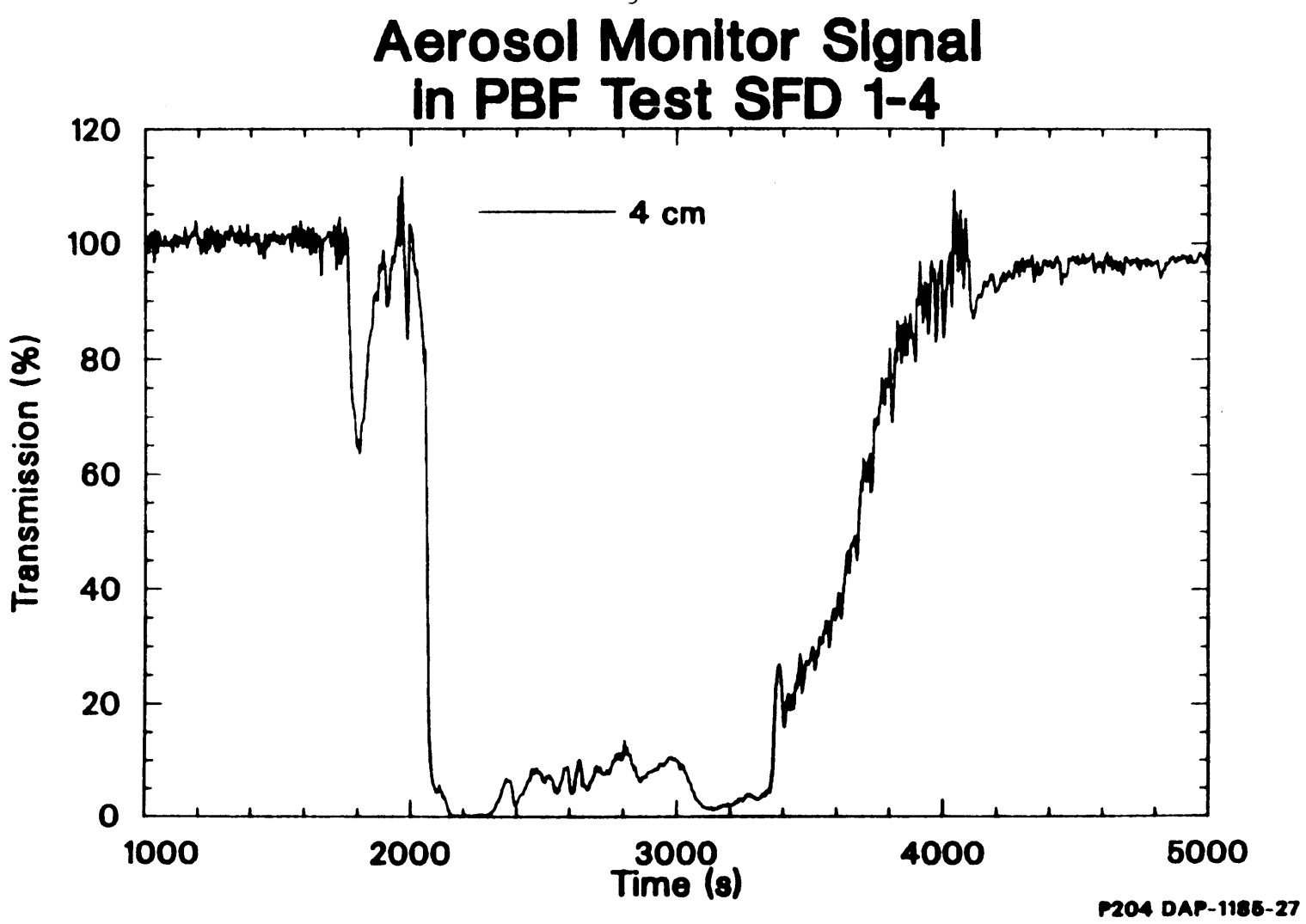
Aerosol Monitor Signal
in PBF Test SFD 1-4
4 cm
Transmission (%)
120
100
80
60
40
20
0
1000
2000
3000
4000
5000
Time (s)
P204 DAP-1185-27

Figure 8.10

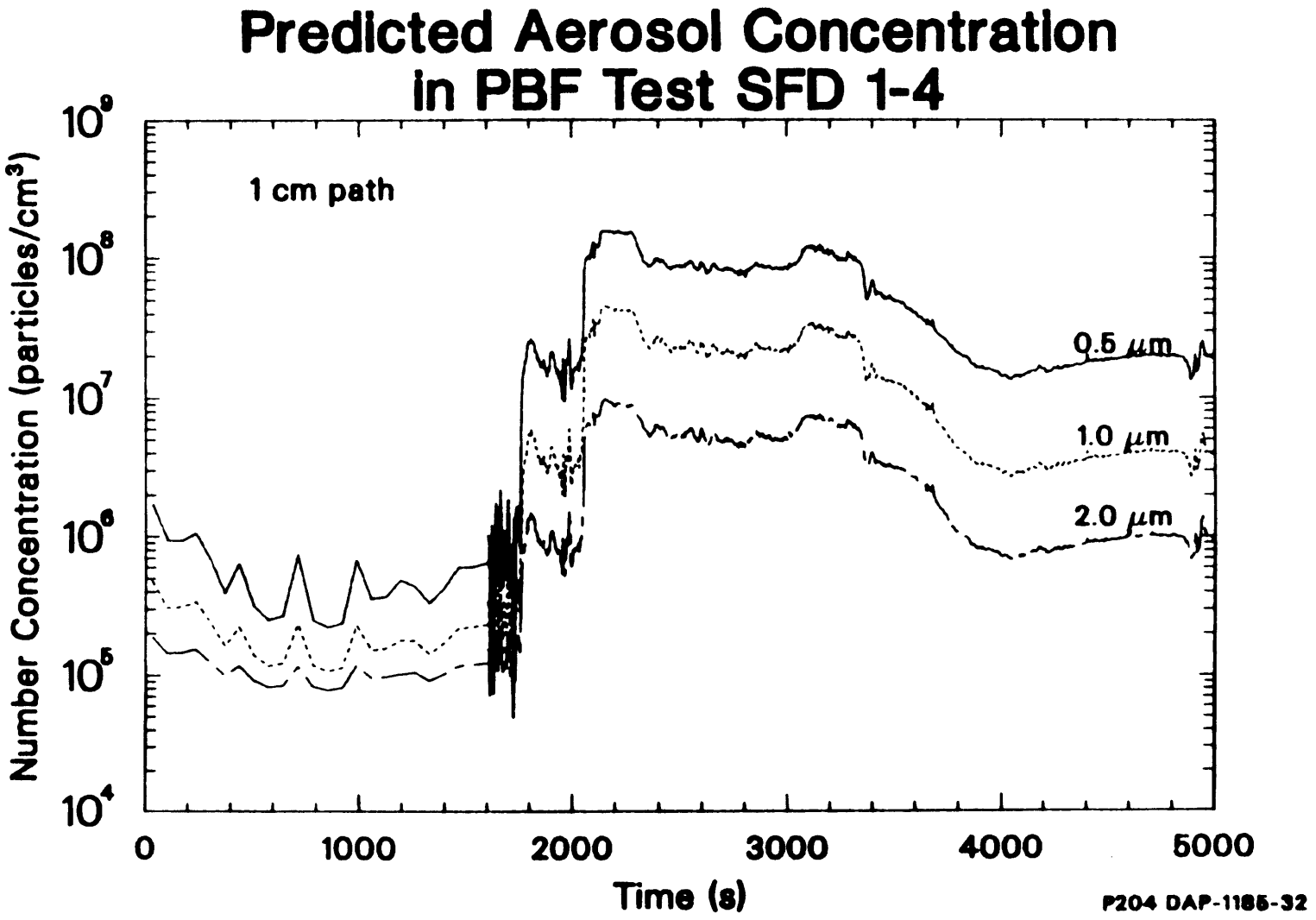
Predicted Aerosol Concentration
in PBF Test SFD 1-4
1 cm path
0.5 μm
1.0 μm
2.0 μm
Number Concentration (particles/cm³)
10⁹
10⁸
10⁷
10⁶
10⁵
10⁴
0
1000
2000
3000
4000
5000
Time (s)
P204 DAP-1185-32

Figure 8.11

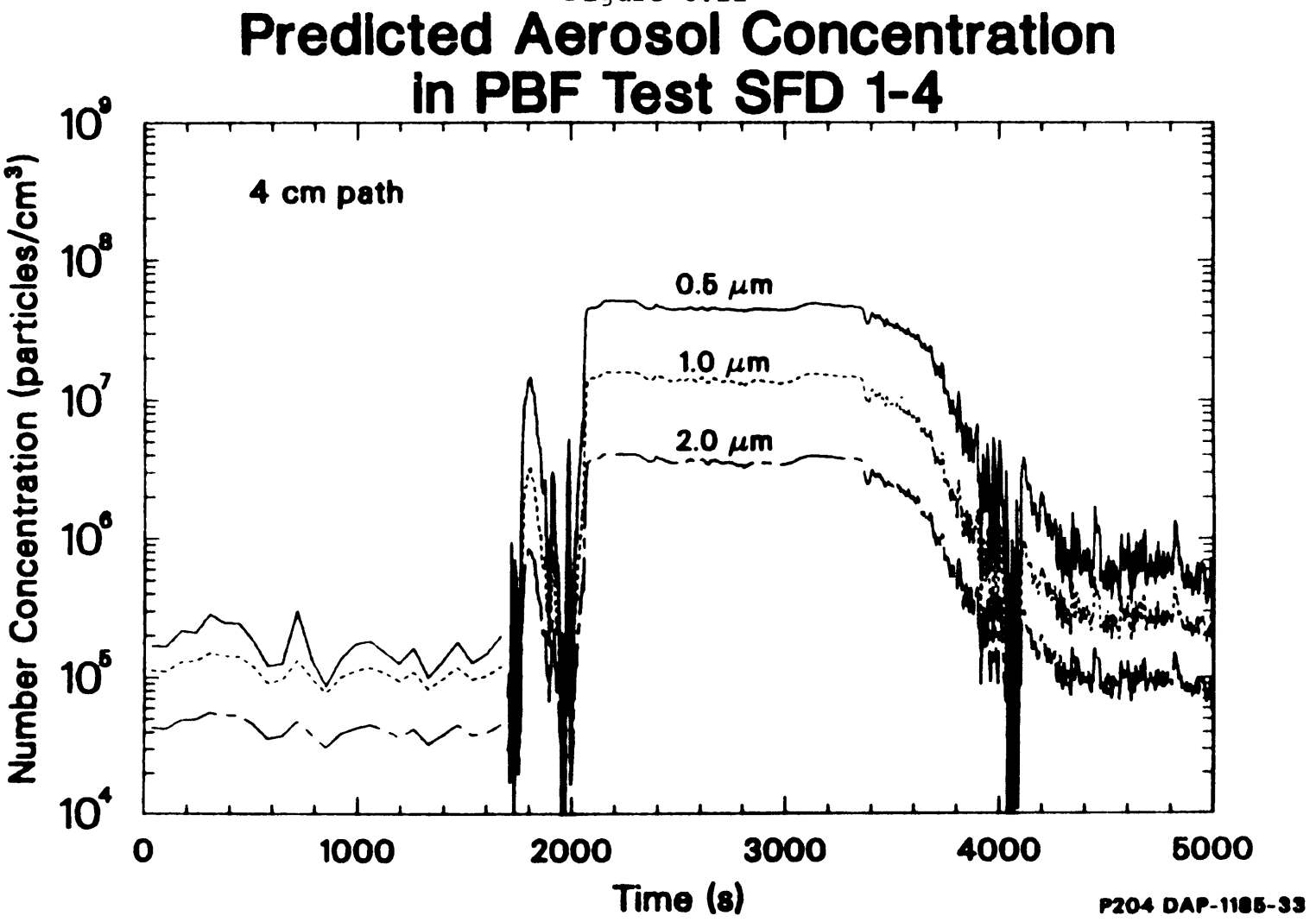
Predicted Aerosol Concentration
in PBF Test SFD 1-4
4 cm path
0.5 μm
1.0 μm
2.0 μm
Number Concentration (particles/cm³)
10⁹
10⁸
10⁷
10⁶
10⁵
10⁴
0
1000
2000
3000
4000
5000
Time (s)
P204 DAP-1185-33

ejected from the control rod breach. The small burst of aerosols measured by both channels is thought to be due to the vaporization of the Ag, In and Cd from the molten alloy and the subsequent formation of aerosols. Since the vapor pressure of Ag and In are quite low at 1150 K, the failure temperature of the first control rod, the aerosol is most likely dominated by cadmium.

Both signals show a very large drop in transmission starting at 2050 seconds. The 4-cm test cell saturates 100 seconds later while the 1-cm test cell reaches a minimum at 7% transmission. These results suggest that aerosol densities in excess of 5×10^7 particles/cc were detected by the 4-cm path length detector and that based on the 1-cm test cell, the particle concentration may have been as large as 2×10^8 particles/cc.

This large initial burst of aerosol activity that begins at 2050 seconds can be correlated to events occurring in the bundle. Between 1925 and 1975 seconds, the three remaining control rods failed. Assuming a reasonable delay time of 60 to 120 seconds between the center of the bundle and the aerosol monitor, the large drop in transmission can be attributed to the failure of the remaining control rods. The 1-cm test cell indicates that this burst of aerosol activity lasts roughly 250 seconds. This sustained aerosol signal when

corrected for delay time coincides with the onset of high temperatures in the bundle.

At this point in the experiment, many phenomena are occurring simultaneously, all of which could cause aerosols to be formed. Based on the physics of aerosol formation, the three predominant aerosol sources in the experiment are:

(1) vaporization of control rod material,

(2) the nucleation of volatile fission products like CsI, and

(3) the vaporization of Sn from the hot zircaloy cladding.

Estimation of the timing and duration of each aerosol source is difficult. Fission chamber responses indicate that the downward relocation of the control rod alloy to cooler portions of the bundle was very rapid. However, the control rod aerosol source could last longer than this initial relocation period due to vaporization of alloy material on the surface of the guide tube and on grid spaces and/or the release and vaporization of control material beneath the break location in the rod. Thus, it is reasonable to assume that the control rod aerosol source could have lasted a few hundred seconds.

Between 2000 and 2380 seconds, temperatures in the

bundle were increasing rapidly to values in excess of 2400 K. During this portion of the experiment, significant fission product release occurred as is evidenced by the substantial increases in iodine and cesium detected in the effluent line beginning at 2000 seconds. Experiments at Sandia [8.2] suggest that Sn release from hot zircaloy is an additional aerosol source.

Thus, the sustained aerosol signal that begins at 2050 seconds and lasts for 250 seconds is probably a superposition of the three aerosol sources discussed above. As seen in Table 8.2, results from a preliminary radioisotopic analysis of the filtered steam samples taken during the experiment support this scenario. The first two steam samples, taken during this first aerosol burst, indicate the presence of Ag^{110m}, In^{114m}, I^{131}, Cs^{134}, Cs^{136}, and Cs^{137}. Most of the Sn and Cd present in the experiment was nonradioactive. Any of the radioactive Cd or Sn isotopes that might be present were below the detectability level of the gamma spectroscopy system. Additional elemental analysis currently underway should help to determine the magnitude, timing and duration of each of these aerosol sources.

At 2300 seconds, the signals from the two aerosol

Table 8.2

Radioisotopic analysis of steam sample filters (μCi/filter)

Isotope	Sample Number 1	2	3	4	5	6	6 After Vacuum	Ratio[a]
^{110m}Ag	5.0 E+00	1.3 E+00	1.8 E+00	—	5.4 E+00	1.5 E+01	7.2 E+00	2.1
^{114m}In	2.2 E+01	2.6 E+01	3.5 E+01	—	2.2 E+01	7.5 E+01	3.4 E+01	2.2
^{129m}Te	2.4 E+01	4.9 E+01	7.1 E+01	—	1.1 E+02	3.4 E+02	2.1 E+02	1.6
^{131}I	3.0 E+01	1.9 E+02	1.8 E+02	7.6 E+01	1.2 E+02	2.7 E+02	9.3 E+01	2.9
^{134}Cs	1.8 E+02	7.9 E+02	2.9 E+02	3.6 E+02	2.5 E+02	4.1 E+02	2.0 E+02	2.0
^{136}Cs	5.0 E+00	1.7 E+01	7.2 E+00	7.7 E+00	7.1 E+00	9.3 E+00	5.6 E+00	1.7
^{137}Cs	8.3 E+02	3.7 E+03	1.3 E+03	1.5 E+03	1.2 E+03	1.9 E+03	9.4 E+02	2.0

a. Ratio of sample 6 activity before and after exposure to the vacuum.

monitor channels began to show decreases in the aerosol concentration. The 1-cm channel registered a decline from a peak of 2×10^8 particles/cc to 10^8 particles/cc. Although the 4-cm test cell saturated at the peak, it indicates that the drop in aerosol concentration also levels off at 4×10^7 particle/cc. This decrease coincides with the start of the 220-second hold at peak power and continues for about 700 seconds. The exact reason for this decrease is not known for certain at this time. However, several explanations appear plausible: (1) The decrease in aerosol signal may be due to the termination of the control rod aerosol source. The additional alloy below the failure location in the rod may have chemically interacted with the guide tube and flowed down to cooler portions of the bundle where it cooled and ceased to be an aerosol source; (2) the rate of zircaloy oxidation in the bundle began to decrease probably due to a reduction in the available steam. A lower oxidation rate would have lowered temperatures in the bundle and hence may have caused a decrease in the aerosol production rate; and (3) molten zircaloy may have flowed away from its original location to lower portions of the bundle, where it cooled thus trapping the Sn. Any or all of these phenomena could explain the reduction in aerosol concentration. Results

from the third and fourth filter steam samples taken during this decrease in aerosol concentration indicate that no Ag or In aerosol or vapor were present in the effluent line. The samples were dominated by cesium and iodine.

At 2900 seconds, both aerosol channels registered a second increase in aerosol concentration. The 1-cm cell registered an increase to 1.5×10^8 particles/cc while the 4-cm cell almost saturated. The reason for this increase in aerosol density which started slightly after the end of the power hold and lasted for 350 seconds is a source of speculation. Two potential explanations are presented. First, the increase in aerosol concentration could be attributed to cooldown of the system. Readings from all the steam and cladding thermocouples indicated that temperatures in the system were decreasing. In addition, the flowmeter on the condenser inlet showed a slight reduction in flow rate. The reduction in flow rate could have caused an increase in the concentration of vapors in the core. This increase in mass of condensible vapors in the core, coupled with decreasing temperatures in the bundle would cause the vapors to supersaturate and nucleate to form small, easily transported aerosols.

A second possible explanation for the increase in

the aerosol signal is the reactivation of a prior aerosol source. If significant relocation of molten material was occurring during cooldown, then this hot material could have contacted control rod material that was frozen in the lower bundle/plenum region. The energy carried by this relocated material could have been enough to heat the alloy, thus causing additional vaporization of the Ag, In and Cd to occur. Based on results from the last two filtered steam samples, this second explanation appears more plausible. Analysis of filtered steam samples 5 and 6, taken at this time in the experiment, indicate that large quantities of Ag and In were present in the effluent line. In addition, a heavy material deposit was found on filter 6. Energy dispersive spectroscopy was performed on a sample of this material. The results indicate that the sample was predominantly cadmium.

8.5 Preliminary Conclusions from PBF Test SFD 1-4

Test SFD 1-4 provided the first in-pile high temperature testing of Ag-In-Cd control rods at high pressure. Voluminous data was collected about fuel, fission product and aerosol behavior under severe accident conditions. Although additional work needs to be done to interpret fully the results of the SFD 1-4

experiment, some preliminary conclusions concerning control rod and aerosol behavior can be made:

(1) All data from the experiment are consistent with the following description of control rod behavior in PBF Test SFD 1-4. As predicted in Section 2, the three non-instrumented control rods failed at a temperature of 1700 K, very close to the melting point of the stainless steel. Upon failure, the absorber material flowed out of the breach, down the outside of the control rod guide tube and into the lower plenum of the test train where it refroze. During this downward relocation, vapors released from the molten control rod material condensed to form an aerosol that was transported out of the bundle and into the effluent line. The single instrumented control rod failed earlier, apparently as a result of prior waterlogging.

(2) Aerosol production began with the first control rod rupture and increased greatly during rapid heatup. High aerosol number concentrations (~ 10^8 particles/cc) were generated and sustained during the high temperature transient.

(3) Aerosol generation in the SFD 1-4 test could be correlated to events that occurred in the bundle. Vaporization of molten control rod material, nucleation of volatile fission products released during the experiment, and the heating of zircaloy clad were all phenomena that occurred in the test that could lead to the observed aerosol behavior. Evidence from on-line monitors and preliminary analysis of filtered steam samples indicate that aerosols contained both control rod material and fission products.

Post-test analyses are currently underway to help interpret the existing measurements more completely and to acquire additional data that can be used to understand the control rod and aerosol behavior in the SFD 1-4 test.

8.7 REFERENCES

8.1 Miller, R.W. et. al., Severe Fuel Damage Test 1-4 Quick Look Report, July 1985.

8.2 Ostensen, R.W., "DF-2 Experiment", Severe Fuel Damage Program Review Meeting, April 16-20, 1985, Idaho Falls, ID.

9. SUMMARY AND CONCLUSIONS

The purpose of this work has been to investigate Ag-In-Cd control rod behavior and aerosol formation in severe reactor accidents. These processes are two of several complex physical and chemical phenomena for which accurate descriptions are required to estimate the radiological source term from a severe reactor accident. Conclusions from this work and recommendations for future study are now presented.

9.1 Ag-In-Cd Control Rod Behavior

The behavior of Ag-In-Cd control rods during severe reactor accidents is a function of system pressure and the control rod design. At low system pressure and when no zircaloy is present, the control rod fails between 1623 and 1723 K when the stainless steel clad loses its integrity as it approaches melting. For low system pressures (< 200 psi) and designs that use zircaloy guide tubes, failure occurs at 1473 K because of thermal expansion, physical contact and chemical interaction between the stainless steel clad and the zircaloy guide tube. However, as shown in PBF Test SFD 1-4, Ag-In-Cd control rods at high system pressure fail at 1700 K as a

result of stainless steel melting and subsequent chemical attack on the zircaloy guide tube by molten Ag, In and stainless steel.

At low ambient pressures, the molten material is forcibly ejected from the control rod because of the high cadmium vapor pressure. At high system pressures, overpressurization of the rod does not occur. Instead, upon failure, the alloy is expected to flow down the outside of the guide tube to cooler portions of the reactor core.

A code named VAPOR has been developed to model the downward relocation and simultaneous vaporization of the control rod alloy after failure. A sensitivity study has been performed to highlight the key variables and assumptions that influence the release of Ag, In and Cd in severe reactor accidents. In addition, the VAPOR code has been used to predict the Ag, In and Cd vapor release in PBF Test SFD 1-4. The results of these studies indicate that

(1) Vaporization is pressure-dependent. Since diffusion coefficients vary inversely with system pressure, vapor release is greater at low pressure than at high pressure;
(2) The release of Cd vapor is very sensitive to the ideal solution model used to describe the vapor pressure behavior of Cd over the alloy; and
(3) The release of Ag, In and Cd is predicted to be quite low. Downward relocation of the alloy to cooler portions of the core is predicted to be so rapid that the residence

time for the alloy in the system is quite short. As a result the integrated release is small.

The framework used to develop the VAPOR code has some limitations. The effects of grid spacers on alloy flow are neglected. The grid spacer could hold up the flowing control rod material and act as an additional surface from which vaporization can occur. Because the current formulation does not use an explicit energy balance, the relocation and vaporization behavior of the control rod alloy is currently uncoupled from other thermal-hydraulic phenomena that occur in a severe reactor accident. As a result, a phenomenon such as refreezing of the alloy as it travels down the rod is not modeled. In addition, potential interactions between molten core material and control rod alloy that can alter the refreezing behavior of the alloy have not been considered. The behavior of the control rod alloy after substantial core degradation has occurred is not very well known. Although the VAPOR code models the rapid relocation of the alloy to lower portions of the core, it assumes that after leaving the fuel region the alloy refreezes and ceases to be an aerosol source. This was not the behavior observed in the PBF SFD 1-4 experiment. Near the end of the high temperature transient, additional Ag, In and Cd vapors were

released, which were thought to be the result of hot molten zircaloy or UO_2 contacting and vaporizing refrozen control rod material in the lower plenum. These potential interactions could affect the timing and magnitude of Ag, In and Cd vapor release in severe reactor accidents. Despite these limitations, the VAPOR code is a simple yet mechanistic attempt to describe Ag, In and Cd vapor release in a severe reactor accident. It provides an suitable framework upon which some of the changes described above can be implemented.

The conclusions presented here have an impact on reactor accident source term estimates. Specifically, the timing and magnitude of Ag, In and Cd vapor release from the core will depend on the nature of the accident sequence. In low pressure accident sequences like AB and V, the control rods would fail early in the transient at 1473 K. The rods would burst as a result of the high cadmium vapor pressure. The release of alloy vapors would be somewhat greater because of forcible ejection of the control rod alloy and the increased vaporization at low pressures. However, at this point in the accident, any control rod aerosols that are formed would have minimal impact on fission product transport because little fission product release would be expected at this low temperature. In high

pressure sequences like TMLB' and S_2D, the rods would fail much later - at 1700 K near the melting point of the stainless steel. Because of the rapid relocation of the alloy into the lower plenum, the quantity of Ag, In and Cd released on heatup would be small. However, control rod failure at high system pressures would occur during the rapid oxidation phase of a severe accident. At that point in the transient, temperatures would be rising quite fast and substantial fission product release would be occurring. Hence, any control rod aerosols that are formed would alter the transport of fission products through the primary system and into containment.

9.2 Aerosol Formation

A review of potential aerosol formation mechanisms in a severe reactor accident has been performed. Specifically, this work has investigated models for homogeneous nucleation, ion-induced nucleation, heteromolecular nucleation and heterogeneous nucleation. With the exception of heteromolecular nucleation, these models have been applied to Ag, Cd and CsI in an attempt to illustrate the nucleation behavior of these three potential aerosol sources in the heatup phase of a severe accident and also to investigate the

competition among these nucleation mechanisms for scavenging vapor. Finally, the aerosol transport equation has been solved analytically to determine the equilibrium aerosol particle size distribution following nucleation. The results of this study indicate:

(1) The high vapor supersaturations that are required for homogeneous nucleation to occur preclude it from being a primary aerosol formation mechanism. Because ion-induced nucleation lowers the supersaturation required to produced aerosols, it would probably be the initial aerosol formation mechanism in a severe reactor accident. The period of ion-induced nucleation would be very limited because once enough aerosol surface area is generated, heterogeneous nucleation would become the dominant mechanism of gas-to-particle conversion.
(2) Detailed information about the chemical interactions of a multicomponent system of vapors is required to predict the rate of heteromolecular nucleation. Since such information is not available for the vapors produced in a severe reactor accident, this model could not be applied here.
(3) Metal vapors like Ag and Cd are much more difficult to nucleate than a salt like CsI because of their large surface tensions. Because of the high volatility of Cd and the low surface tension of CsI, it appears that either CsI or Cd would be the first specie to nucleate in a severe accident and hence serve as an aerosol seed for heterogeneous nucleation of other vapors. A prediction of the timing and magnitude of the release of Cd and CsI would be required to determine the first specie to nucleate.
(4) The condensation and growth of aerosols following nucleation is very rapid. Integration of aerosol growth laws indicate that equilibrium is usually reached in under one second. An analytic solution to the aerosol transport equation indicates that the equilibrium aerosol particle size

distribution following nucleation depends only on the total number of particles in the system and the volume fraction of aerosols at equilibrium.

Based on these results, aerosol formation is thought to occur in three stages during a severe reactor accident. Hot vapors are released from the core primarily as a result of heating of core materials and the release of fission products. Rapid cooling in the upper plenum causes these vapors to supersaturate. In the first stage of aerosol formation, ion-induced nucleation begins to relieve the supersaturation by forming a large quantity of small aerosols. This stage is generally quite limited in duration. In the second phase, both ion-induced and heterogeneous nucleation operate simultaneously as competing pathways for gas-to-particle conversion. However, once sufficient aerosol surface area is generated, the third stage begins. Ion-induced nucleation ceases and heterogeneous nucleation becomes the dominant mechanism for relieving vapor supersaturation. Diffusional growth of the aerosol continues until equilibrium is established (i.e., $S = 1$). The entire process is expected to occur in well under one second.

The fact that a severe reactor accident is postulated to last for a few hours has led several

investigators to question the feasibility of modeling this rapid return to equilibrium during the period of aerosol formation. Using mechanistic nucleation models to calculate the rapid nucleation and growth of aerosols as well as the decrease in vapor supersaturation would provide valuable information about the process of aerosol formation. However, such a calculation would be very costly because of the small time steps needed to obtain an accurate solution. As a result, most source term analyses usually use semi-empirical temperature-dependent correlations to determine aerosol release from the core as a function of time. Fission products and other vapors are then allowed to condense onto these aerosols if conditions permit. Both of these approaches have drawbacks. The detailed calculation is too expensive to perform for accident sequences in an LWR, yet, the semi-empirical approach does not provide a mechanistic model for aerosol formation.

The results of this work indicate that a third approach, termed the mechanistic equilibrium model, is feasible. The system's return to equilibrium is dominated by heterogeneous nucleation, i.e., diffusional growth of the aerosol caused by vapor condensation. Ion-induced nucleation merely acts as a trigger to form enough aerosol surface area for heterogeneous nucleation

to become the dominant mechanism of gas-to-particle conversion. Because aerosol formation is very rapid, this model assumes that the details of the transition from a supersaturated vapor state to equilibrium are unimportant. A saturated vapor and the equilibrium aerosol size distribution following nucleation are assumed to be produced instantaneously. The intial vapor supersaturation is used in conjunction with the mechanistic model for ion-induced nucleation to determine the total number of particles created and the volume concentration of aerosols at equilibrium.

The impact of using the mechanistic equilibrium model instead of a semi-empirical correlation to predict aerosol formation should be assessed. Such an assessment would require a comparison of the estimated radiological source terms for a few risk-dominant accident sequences using these two different models of aerosol formation. Since this exercise was considered to be outside the scope of this work, no definitive conclusions can be made. Despite this fact, some points are worth noting:

(1) The semi-empirical models may be accurate enough to describe aerosol formation in a severe reactor accident. The large radial temperature gradients that are expected to exist in a reactor core may cause aerosol formation to occur over a wide spectrum of conditions. Upon exiting the core region, the aerosols mix and the details of their

generation history are lost. As a result, a semi-empirical model may be adequate to describe aerosol formation on a core-wide basis. Such a contention, however, still needs to be proved.

(2) This work has indicated that an accurate estimate of the magnitude and timing of vapors released from the core is required to predict the rate of aerosol formation. Nucleation models are sensitive to the vapor supersaturation which depends on the rate of vapor release. In addition, since heterogeneous nucleation is the dominant mechanism of gas-to-particle conversion, this phenomena must be acccurately modeled in the aerosol formation process.

(3) The differences in these two modeling approaches might alter the details of the fission product and aerosol behavior in the core and reactor coolant system. However, as long as containment failure is predicted to occur late in the accident sequence, these differences should have an insignificant impact on the radiological source term to the environment due to aerosol depletion processes that occur in containment. In containment bypass sequences, this conclusion may not be valid.

9.3 Recommendations for Future Study

Based on this work, several avenues of future study are listed in order of the priority with which they should be pursued.

(1) The capabilities of the VAPOR code need to be assessed. Such an assessment ideally should be made by comparing VAPOR code predictions with a well-controlled out-of-pile experiment conducted at high pressure. Such an experiment has not been performed to date. However, the PBF SFD 1-4 experiment could provide some valuable data to be used for code

comparison. In order to perform a more complete comparison, the behavior of Ag, In and Cd in the experiment needs to be characterized. If possible, a complete mass balance should be conducted. The deposition coupons in the upper plenum as well as the filtered and unfiltered steam samples should be examined for their Ag, In and Cd content. In addition, an attempt should be made to determine the amount of control rod alloy that remained in the bundle. This data could then be compared to VAPOR code predictions and the results of a fission product and aerosol transport analysis performed for the PBF SFD 1-4 experiment.

(2) To overcome some of the limitations of the VAPOR code presented earlier, the following modifications are recommended. The zircaloy dissolution model could be improved to describe more accurately the degradation behavior of the control rod alloy. Complex chemical interactions occur between all of the materials in the core which could alter the refreezing and vaporization behavior of the absorber material. In addition, the VAPOR code could be incorporated into a thermal hydraulic core heatup code. This modification would allow coupling between the relocation and vaporization behavior of the alloy and the other thermal hydraulic phenomena in a severe reactor accident.

(3) The impact of aerosol nucleation in reactor accident source term estimation could be assessed. The predicted source terms for a few risk-dominant accident sequences using both the mechanistic equilibrium model and the current semi-empirical temperature-dependent correlations could be compared.

These recommmendation are offered as a way of increasing the accuracy of the models developed in this work. The results of these further studies could provide

additional understanding about Ag-In-Cd control rod behavior and aerosol formation in severe reactor accidents.

APPENDIX A

CALCULATION OF CONTROL ROD INTERNAL PRESSURE

This appendix describes the thermodynamic analysis used to determine the internal control rod pressure as a function of temperature. The assumptions used in the analysis are

(1) each constituent of the alloy obeys Raoult's law;

(2) the rod is backfilled with helium;

(3) the liquid alloy has a constant density of 8.85 g/cc; and

(4) the stainless steel clad acts as a rigid barrier because deformation is neglected.

The control rod is modeled in Figure A.1 as an isothermal volume at equilibrium. The lower portion of the rod is filled with the liquid alloy. Above the alloy is a gas space containing the helium backfill gas and Ag, In and Cd vapors. The internal pressure is determined by the quantity of vapor in the gas space. The gas volume, V_g, is given by

$$V_g = V_{tot} - V_l \qquad (A.1)$$

Figure A.1

Control Rod Volume Modeling

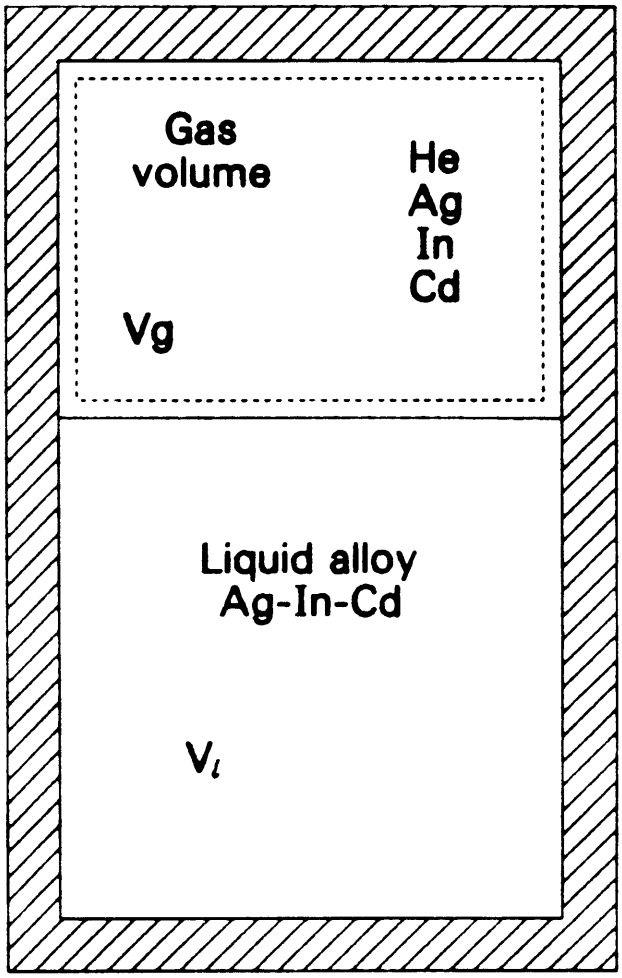

P204-LN85044-10

where

V_{tot} = total internal volume of the control rod (m^3) and

V_l = liquid volume (m^3).

The liquid volume is calculated using

$$V_\ell = \sum_i m_{i,\ell}/\rho_\ell \qquad \text{(A.2)}$$

where

$m_{i,\ell}$ = mass of specie i in liquid (kg), and

ρ_ℓ = density of alloy (kg/m^3).

The mass of each liquid specie in the alloy is given by

$$m_{i,\ell} = m_{i,0} - m_{i,v} \qquad \text{(A.3)}$$

where

$m_{i,0}$ = initial mass of specie (kg), and

$m_{i,v}$ = mass vaporized (kg).

Thus,

$$V_g = V_{tot} - \sum_i (m_{i,0} - m_{i,v})/\rho_\ell \qquad (A.4)$$

The partial pressure of each specie is given by Raoult's law, i.e.,

$$p_i = p_v(T) Y_i \qquad (A.5)$$

where

$p_v(T)$ = pure vapor pressure of specie (Pa), and

Y_i = mole fraction in liquid.

The mole fraction is defined by

$$Y_i = \frac{m_{i,\ell}/A_i}{\sum_i (m_{i,\ell}/A_i)} \qquad (A.6)$$

where A_i is the molecular weight of specie i. The partial pressure of helium is determined from the ideal gas law to be

$$p_{He} = \frac{m_{He} RT}{V_g A_{He}} \qquad (A.7)$$

Thus, the total pressure of the rod is given by

$$p_{tot} = p_{He} + \sum_i p_i \qquad (A.8)$$

The control rod vapor is assumed to behave as an ideal gas. Thus, the mass of each vapor specie is

$$m_{i,v} = \frac{p_i V_g A_i}{RT} \qquad (A.9)$$

A code called CROD has been developed to calculate the internal pressure of the control rod using these equations. The problem is coupled because of the vapor pressure behavior of the alloy. The amount of Ag, In and Cd vapor that is generated depends on the mole fraction of each specie in the liquid which in turn depends on the quantity of each constituent remaining in the alloy after vaporization. To bypass this coupling, a few assumptions were made in the solution technique shown in Figure A.2. The calculation determines the internal rod pressure at 100 degree temperature

Figure A.2

Flowchart of CROD Code

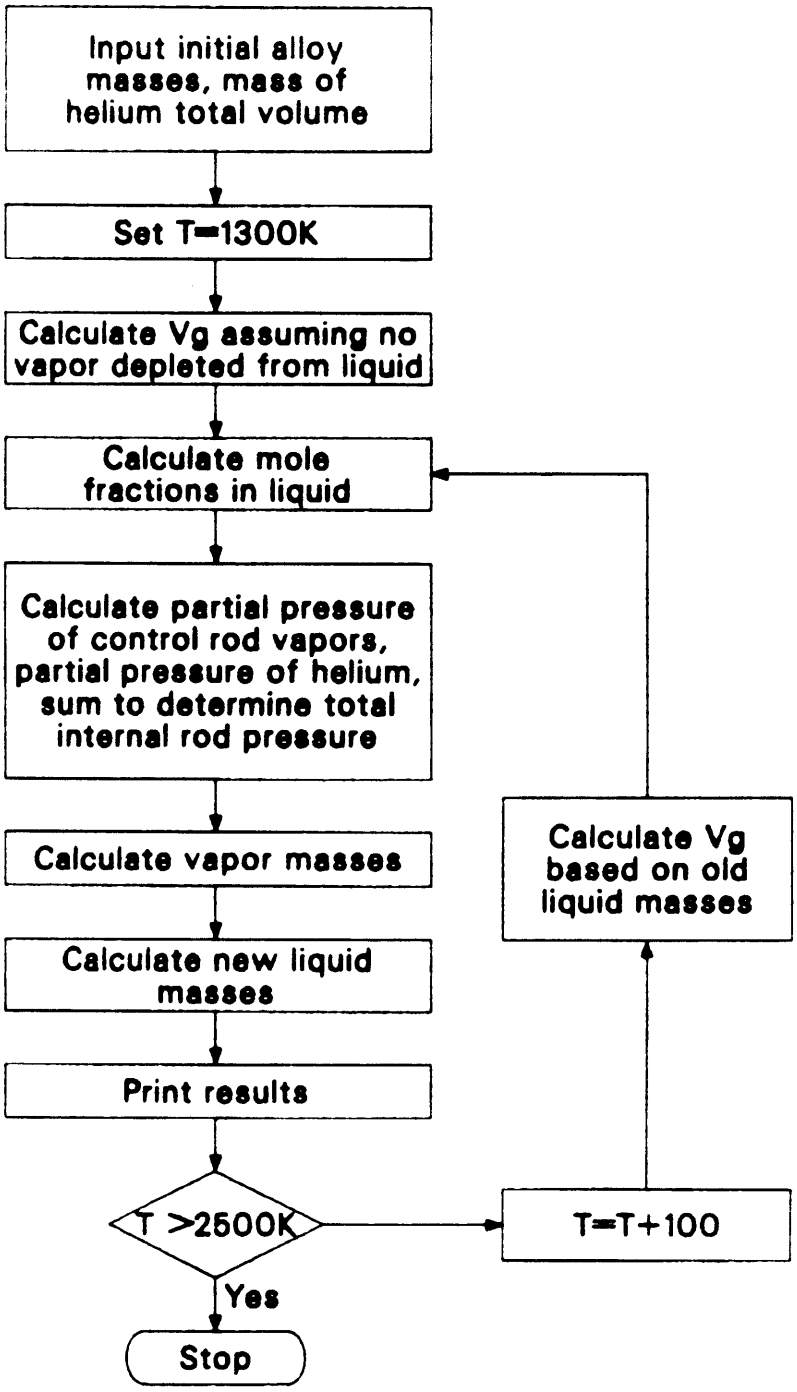

P204-LN85044-9

intervals between 1300 K and 2500 K. Input to the calculation include: the constitutive masses of the alloy, the mass of helium gas and the total system volume. At 1300 K, the gas volume is calculated using Equation (A.4) assuming that no control rod vapor is present (i.e., $m_{i,v}= 0$). This is a reasonable assumption because of the low volatility of Ag, In and Cd at 1300 K. Mole fractions in the liquid are then calculated using Equation (A.6). The partial pressure of the helium gas and each alloy constituent are calculated and summed to obtain the total internal rod pressure using Equations (A.5), (A.7) and (A.8). Vapor masses are calculated by Equation (A.9) and subtracted from the initial alloy masses (Equation A.3) to obtain new liquid masses for Ag, In and Cd. These new liquid masses are then used as a basis to calculate the mole fraction in the liquid for the next temperature value. This process continues until the temperature reaches 2500 K.

A listing of the code is attached.

```
      PROGRAM CROD(INPUT,OUTPUT,TAPE5=INPUT,TAPE6=OUTPUT)
      DIMENSION P(3),XMV(3),XML(3),Y(3),W(3),A(3),B(3)
C
C  CALCULATE THE INTERNAL PRESSURE OF THE CONTROL ROD
C
C  INPUT DATA
      DATA W/107.8,114.82,112.4/
      DATA WHE/4.0/
      DATA A/1.26E+04,1.27E+04,5.31E+03/
      DATA B/7.989,8.284,7.990/
      DATA XML/357.44,67.02,22.34/
      DATA VTOT,XMHE /62.603,3.027E-03/
      DATA PERC/0.01/
C
C       INITIALIZE TEMPERATURE
C
      T= 1200
      DO 999 NTEMP= 1,12
      KOUNT = 0
      T = T + 100
C
C       SUM CONSTITUENT ALLOY MASSES
C
 10    XMTOT = 0.0
      DO 20 J=1,3
         XMTOT= XMTOT + XML(J)
 20    CONTINUE
C
C       CALCULATE GAS VOLUME
C
      RHO = 8.85
      VG = VTOT - XMTOT/RHO
      R = 82.05
C
C
      DENOM = 0.0
      DO 30 K= 1,3
        DENOM = XML(K)/W(K) + DENOM
 30    CONTINUE
C
C       CALCULATE MOLE FRACTION IN LIQUID
C
      DO 40 L = 1,3
         Y(L)=(XML(L)/W(L))/DENOM
 40    CONTINUE
C
C       CALCULATE PARTIAL PRESSURE OF ALLOY VAPORS AND
C       USE IDEAL GAS TO DETERMINE VAPOR MASSES
C
      DO 50 M= 1,3
```

```
          P(M)= 10**(B(M)-A(M)/T)*Y(M)/760.0
          XMV(M)= P(M)*W(M)*VG/(R*T)
 50      CONTINUE
C
C        CALCULATE HELIUM GAS PRESSURE
C
        PHE= XMHE*R*T/(VG*WHE)
C
C        SUM PRESSURE COMPONENTS
C
        PTOT= 0.0
        DO 70 I = 1,3
        PTOT= PTOT + P(I)
 70      CONTINUE
        PTOT= PTOT + PHE
C
C        UPDATE LIQUID MASSES FOR NEXT TEMPERATURE PASS
C
        DO 80 I1= 1,3
          XML(I1) = XML(I1) - XMV(I1)
 80      CONTINUE
C
C        PRINT RESULTS
C
 90      WRITE(6,99)
        WRITE(6,100) T
        WRITE(6,97)
        WRITE(6,98)
        WRITE(6,101) P(1),P(2),P(3),PHE,PTOT
        WRITE(6,102)
        WRITE(6,103) XMV(1),XMV(2),XMV(3)
        WRITE(6,104)
        WRITE(6,103) XML(1),XML(2),XML(3)
        WRITE(6,105)
        WRITE(6,107) Y(1),Y(2),Y(3)
C
 99      FORMAT(2X,"THE TEMPERATURE IS")
 97      FORMAT(2X,"    AG       IN       CD       HE       TOTAL")
 98      FORMAT(2X,"PARTIAL PRESSURE(ATM)")
 100     FORMAT(2X,F8.3)
 101     FORMAT(2X,5F8.3)
 102     FORMAT(2X,"VAPOR MASSES (GM)")
 103     FORMAT(2X,3E10.3)
 104     FORMAT(2X,"LIQUID MASSES (GM)")
 105     FORMAT(2X,"MOLE FRACTION IN LIQUID")
 107     FORMAT(2X,3E10.3)
 999     CONTINUE
        STOP
        END
```

APPENDIX B

THE VAPOR CODE

Attached in Section B.1 is a listing of the VAPOR code described in Section 3. Sample input and output from the high pressure/high flow simulation discussed in Section 4 are included in Sections B.2 and B.3.

B.1 VAPOR Code Listing

```
      PROGRAM VAPOR(TAPE8,TAPE12,TAPE21,TAPE44)
C*****************************************************************
C     $$$$$  BEGINNING OF CODE DESCRIPTION $$$$$
C*****************************************************************
C THE VAPOR PROGRAM IS AN ANALYSIS
C USING MULTICOMPONENT MASS TRANSFER TO DESCRIBE THE RELEASE
C OF AG IN AND CD IN A SEVERE REACTOR ACCIDENT.
C THE CODE MODELS MASS TRANSFER FROM A LIQUID FILM TO A
C GAS STREAM IN A COUNTERCURRENT FLOW ARRANGEMENT. THE
C CODE CAN HANDLE UP TO 10 LIQUID AND 10 VAPOR NODES WITH
C FOUR SPECIES IN THE LIQUID (AG,IN,CD AND ONE OTHER SPECIE
C IF DESIRED) AND SIX SPECIES IN THE VAPOR (AG,IN,CD,H2,H2O
C PLUS ONE OTHER SPECIE).  THE PROGRAM SOLVES CONSERVATION OF
C OF MASS EQUATIN FOR EACH SPECIE IN EACH NODE USING A STIFF
C DIFFERENTIAL EQUATION SOLVER FROM THE MINERVA LIBRARY. IN
C ADDITION THE CODE MODELS THE FLOW OF THE LIQUID CONTROL ROD
C ALLOY DOWN THE ROD, DESCRIBING THE THICKNESS AND THE VELOCITY
C OF THE FILM AT EACH NODE.
C
C THE MAJOR THERMAL HYDRAULIC INPUT ARE THE TIME DEPENDENT WALL
C AND BULK TEMPERATURES, THE HYDROGEN AND STEAM FLOWRATES
C AND THE SYSTEM PRESSURE AT EACH NODE.  TWO OUTPUT FILES ARE
C GENERATED. ONE HAS DETAILED INFORMATION ON THE STATE OF
C OF ALL THE SPECIES AND THE THERMAL HYDRAULIC RESULTS AT EACH
C NODE.  IT IS NOT IN  CWAF FORMAT.  THE OTHER OUTPUT
C FILE GIVES THE RELEASE RATES AS A FUNCTION OF TIME. IT IS TYP7
C THUS CAN BE USED IN MAGNUM FOR PLOTTING.
C
C A DETAILED DESCRIPTION OF THE VARIABLES USED IN THE PROGRAM ARE
C BELOW BY COMMON BLOCK AND THE SUBROUTINE IN WHICH THEY APPEAR.
C THE USER IS CAUTIONED THAT THIS LIST MIGHT NOT BE COMPLETE
C
C*****************************************************************
C  VARIABLE             DESCRIPTION                 SUBROUTINES
C*****************************************************************
C       COMMON BLOCK /TH/ THERMAL HYDRAULIC COMMON BLOCK
C*****************************************************************
C   TROD(10)     ROD OR WALL TEMPERATURE(K)      ASSIGN,DIFFC
C   TCOOL(10)    BULK COOLANT TEMPERATURE(K)     ASSIGN,MIXPROP,VALCAL
C                                                FLOW,BULK
C   WH2(10)      MASS FLOW OF H2 (G/S)           ASSIGN,VALCAL,FLOW
C                                                MOMEN
C   WH2O(10)     MASS FLOW OF H2O(G/S)           ASSIGN,VALCAL,FLOW
C                                                MOMEN
C   SH2(10)      HYDROGEN ADDITION RATE          ASSIGN,XMDOT
C                DUE TO OXIDATION (G/S)
C   SH2O(10)     STEAM REMOVAL RATE              ASSIGN,XMDOT
C                DUE TO OXIDATION (G/S)
C   RHOMIX(10)   DENSITY OF HYDROGEN/STEAM       CORR,MOMEN
C                MIXTURE(KG/M**3)                MIXPROP
C   VISC(10)     VISCOSITY OF HYDROGEN/STEAM
C                MIXTURE (KG/M-S)                MIXPROP,CORR
C   REY(10)      REYNOLDS NUMBER OF FLOW         CORR
C   IFLAG        FLAG USED TO SELECT A MASS
C                TRANSFER CORRELATION
C                =1 USE TUBE CORRELATION
C                =2 USE FLAT PLATE CORRELATION
C                (NOT RECOMMENDED TO USE 2 FOR THIS PROBLEM)
C                * OTHER ERROR MESSAGE           ASSIGN,CORR
```

```
690 C    PTOT(10)     SYSTEM PRESSURE(ATM)            BULK,MOLECALC
700 C    FWG(10)      WALL FRICTION FACTOR DUE TO     CORR,MOMEN
710 C                 GAS FLOW
720 ****************************************************************
730 C     COMMON /IN/   INPUT VARIABLE COMMON BLOCK(TIME DEPENDENT B.C.)
740 ****************************************************************
750 C    X(50)        TIME (SEC)                      DISKRD,ASSIGN,READ1
760 C    T1(50,10)    ROD TEMPERATURE (K)             DISKRD,ASSIGN,READ1
770 C    T2(50,10)    COOLANT TEMPERATURE (K)         DISKRD,ASSIGN,READ1
780 C    W1(50,10)    MASS FLOWRATE OF H2 (G/S)       DISKRD,ASSIGN,READ1
790 C    W2(50,10)    MASS FLOWRATE OF H2O (G/S)      DISKRD,ASSIGN,READ1
800 C    H2RXD(50,10)HYDROGEN ADDITION RATE           DISKRD,ASSIGN,READ1
810 C                 DUE TO OXIDATION (G/S)
820 C    H2ORXD(50,10) STEAM REMOVAL RATE             DISKRD,ASSIGN,READ1
830 C                 DUE TO OXIDATION (G/S)
840 C    PRES(10)     SYSTEM PRESSURE (ATM)           READ1,VALCAL
850 ****************************************************************
860 C        COMMON /A/ TIME STEP CONTROL COMMON BLOCK
870 ****************************************************************
880 C    T            INITIAL TIME (SEC)              VAPOR (MAIN),TSTEP
890 C    K            COUNTER                         ASSIGN,VAPOR(MAIN)
900 C    TMAX         MAXIMUM TIME IN PROBLEM (SEC)   DATA1,VAPOR(MAIN)
910 C    TFLAG        TIME FLAG USED TO DETERMINE IF
920 C                 OUTPUT IS WANTED AT EVERY INPUT
930 C                 INTERVAL OR MORE OFTEN THAN THAT  TSTEP,DATA1
940 C    FRACT        FRACTION OF A SECOND DESIRED FOR
950 C                 OUTPUT (I.E,IF FRACT=1.0 THEN
960 C                 OUTPUT EVERY SECOND)            TSTEP,DATA1
970 C    NDATA        NUMBER OF INPUT DATA TO
980 C                 BE READ (< 50)                  DISKRD,DATA1
990 C    DT           TIME STEP (SEC)                 DATA1,TSTEP,VAPOR
1000 ****************************************************************
1010 C        COMMON /GEOM/ GEOMETRY INPUT COMMON BLOCK
1020 ****************************************************************
1030 C    CLEN(10)     CHARACTERISTIC LENGTH (M)        DATA1,CORR
1040 C    AFLOW(10)    FLOW AREA (M*2)                  DATA1,CORR
1050 C    SA(10)       SURFACE AREA OF LIQUID (M*2)     DATA1,FLUX
1060 C    VOL(10)      VOLUME OF NODE (M*3)             BULK,VALCAL,DATA1
1070 C    DELZ(10)     AXIAL LENGTH OF LIQUID NODE(M)   VALCAL,FLOW,MOMEN
1080 C    DROD         CONTROL ROD GUIDE TUBE OUTER
1090 C                 DIAMTER (M)                      VALCAL,BULK,MOMEN
1100 ****************************************************************
1110 C        COMMON /CRIT/  CRITICAL CONSTANTS COMMON BLOCK
1120 ****************************************************************
1130 C    TC(6)        CRITICAL TEMPERATURE (K)         DIFFC,DATA1
1140 C                 (1=AG   2= IN  3= CD)
1150 C    VC(6)        CRITICAL VOLUME (GMMOLE/CM*3)    DIFFC,DATA1
1160 C    WT(6)        ATOMIC WEIGHT                    DIFFC,BULK,XMDOT,
1170 C                                                  DATA1
1180 C    A(6)         THERMODYNAMIC CONSTANT           PARPRES,DATA1
1190 C    B(6)         THERMODYNAMIC CONSTANT           PARPRES,DATA1
1200 C    TCM(10)      PSEUDO CRITICAL TEMPERATURE
1210 C                 OF H2/H2O MIXTURE (K)             DIFFC
1220 C    VCM(10)      PSEUDO CRITICAL VOLUME OF
1230 C                 H2/H2O MIXTURE (GMMOLE/CM*3)      DIFFC
1240 C    WTM(10)      PSEUDO CRITICAL MOLECULAR
1250 C                 WEIGHT OF H2/H2O MIXTURE          DIFFC
1260 ****************************************************************
1270 C     COMMON /VAPOR/  PHYSICAL STATES OF ALL SPECIES IN THE VAPOR
1280 ****************************************************************
```

```
C   CWALL(6,10) WALL CONCENTRATION (GMMOLE/CM*3) INIT,FLUX,BULK
C   CBULK(6,10) BULK CONCENTRATION (GMMOLE/CM*3) INIT,BULK,FLUX
C   PWALL(6,10) PARTIAL PRESSURE AT WALL (ATM)   INIT,BULK
C   PBULK(6,10) PARTIAL PRESSURE IN BULK (ATM)   INIT,BULK
C   XWALL(6,10) MOLE FRACTION AT WALL            INIT,BULK
C   XBULK(6,10) MOLE FRACTION IN BULK            INIT,BULK,DIFFC,
C                                                FLOW
C   DIFF(6,10)  DIFFUSION COEFFICIENT (M*2/S)    DIFFC,CORR
C   HD(6,10)    MASS TRANSFER COEFFICIENT (M/S)  CORR,FLUX
C   SC(6,10)    SCHMIDT NUMBER                   CORR
C   WVJUNC(6,10)FLOW OF VAPOR SPECIES AT
C               JUNCTION (G/S)                   INIT,FLOW,XMDOT
C   FLVOUT(6)   FLOW OUT OF LAST VAPOR
C               NODE (RELEASE RATE) (G/S)        FLOW,XMDOR,OUTPUT1
C   DFLUX(6,10) DIFFUSIVE FLUX (MOLES/M*2-S)     FLUX
C   XN(6,10)    MOLAR FLOW FROM WALL
C               TO BULK (MOLES/S)                INIT,FLUX,XMDOT
C ***************************************************************
C      COMMON /LIQUID/ LIQUID FILM PARAMETERS COMMON BLOCK
C ***************************************************************
C  WLJUNC(4,10)  FLOW OF LIQUID SPECIES          INIT,FLOW,XMDOT
C                AT JUNCTION (G/S)
C  DELTA(10)     FILM THICKNESS OF NODE (M)      INIT,BULK,MOMEN
C  VEL(10)       VELOCITY OF FILM AT NODE (M/S)  INIT,FLOW,MOMEN
C  Y(4,10)       MOLE FRACTION OF EACH SPECIE    INIT,BULK
C                IN LIQUID
C  VISCL(10)     VISCOSITY OF LIQUID (KG/M-S)    LIQPROP,MOMEN
C  RHOL(10)      DENSITY OF LIQUID ALLOY (KG/M*3)VALCAL,FLOW,BULK
C                                                LIQPROP,MOMEN
C  RSOURCE(4)    SOURCE RATE OF ALLOY EXITING    FLOW,XMDOT
C                THE GUIDE TUBE
C ***************************************************************
C      COMMON /FAIL/ PARAMETER FOR ROD FAILURE MODEL
C ***************************************************************
C  DIROD         INNER DIAMTER OF CONTROL ROD    DATA1,VALCAL,
C                GUIDE TUBE                      RODFAIL
C  AFAIL         AREA OF FAILURE IN GUIDE        DATA1,FLOW,MOMEN,
C                TUBE (M*2)                      RODFAIL
C  HO            INITIAL HEIGHT OF ALLOY ABOVE   DATA1,RODFAIL
C                THE BREAK (M)
C  VO            VELOCITY AT BREAK (M/S)         FLOW,MOMEN,RODFAIL
C  HEIGHT        HEIGHT OF ALLOY ABOVE BREAK (M) RODFAIL
C  WTFRAC(4)     WEIGHT FRACTION OF EACH         DATA1,FLOW,RODFAIL
C                CONSTITUENT IN ALLOY
C ***************************************************************
C    COMMON /CNTRL/ CONTROL COMMON BLOCK
C ***************************************************************
C   NSPV   NUMBER OF SPECIES IN VAPOR            DATA1 (PLUS OTHERS)
C   NSPL   NUMBER OF SPECIES IN LIQUID FILM      DATA1 (PLUS OTHERS)
C   NCV    NUMBER OF CONTROL VOLUMES             DATA1 (PLUS OTHERS)
C   SW(10) SWITCH (THIS VARIABLE DOES NOTHING IN THE CODE AT PRESENT)
C ***************************************************************
C              OTHER MAJOR VARIABLES
C ***************************************************************
C   VMASS(6,10)  MASS OF SPECIES IN VAPOR NODE   INIT VALCAL,XMDOT
C                (1=AG  2=IN  3=CD;4=H2;5=H2O,6=??)DSGEDR,BULK
C
C   RMASS(4,10)  MASS OF SPECIES IN LIQUID NODE  INIT,VALCAL,FLOW,
C                (1=AG,2=IN,3=CD,4=??)           BULK,XMDOR,DSGEDR
C ***************************************************************
```

```
1890 C    DESCRIPTION OF THE SUBROUTINES IN VAPOR
1900 ************************************************************
1910 C   NAME                DESCRIPTION
1920 ************************************************************
1930 C   DATA1          READS IN AND ECHOS BACK DATA FOR CODE USE
1940 C   INIT           INITIALIZES SOME ARRAYS TO ZERO
1950 C   ASSIGN         ASSIGNS THERMAL HYDRAULIC INPUT VARIABLES TO
1960 C                  VARIABLES USED IN THE CODE
1970 C   VALCAL         CALCULATES PARTIAL PRESSURE,MOLE FRACTION AND
1980 C                   INITIAL MASSES OF STEAM AND HYDROGEN IN EACH NODE
1990 C   DIFFC          CALCULATES THE DIFFUSION COEFFICIENT OF EACH
2000 C                  SPECIE IN THE FLOW
2010 C   MIXPROP        CALCULATES MIXTURE PROPERTIES (DENSITY,VISCOSITY)
2020 C                  H2/H2O MIXTURE
2030 C   CORR           CALCULATES THE MASS TRANSFER COEFFICIENTS FOR AG,
2040 C                  IN AND CD AND FRICTION FACTORS IN THE GAS
2050 C   FLUX           CALCULATES THE DIFFUSIVE FLUX FOR EACH SPECIES
2060 C                  FROM THE LIQUID TO THE VAPOR
2070 C   FLOW           CALCULATES FLOWS AT LIQUID AND VAPOR NODES
2080 C   READ1          SET UP TO READ IN ALL THERMAL/HYDRAULIC DATA
2090 C                  IN CWAF FORMAT
2100 C   LIQPROP        CALCULATES VISCOSITY AND DENSITY OF LIQUID ALLOY
2110 C   VSOLVE         SOLVES FOR THE VELOCITY OF THE FILM AT EACH NODE
2120 C                  USING A MOMENTUM BALANCE (ANALYTIC SOLUTION IF
2130 C                  FILM IS LAMINAR; NEWTON'S METHOD IF FILM IS
2140 C                  TURBULENT
2150 C   MOMEN         SETS UP COEFFICIENTS OF MOMENTUM EQUATION TO
2160 C                  BE USED IN VSOLVE
2170 C   RODFAIL       CALCULATES THE VELOCITY OF ALLOY AT FAILURE
2180 C                  IN THE GUIDE TUBE
2190 C   TSTEP          CALCULATES TIME STEP AND ADVANCES TIME COUNTER TO
2200 C                  NEXT VALUE
2210 C   XMDOT          CALCULATES THE RIGHT HAND SIDE OF THE DIFFERENTIA
2220 C                  EQUATIONS FOR ALL SPECIES AT ALL NODES
2230 C   BULK           CALCULATES BULK AND WALL PRESSURE,CONCENTRATION
2240 C                  AND MOLE FRACTIONS AT EACH NODE VOLUME
2250 C                  AS WELL AS CALCULATING THE MOLE
2260 C                  FRACTION IN THE LIQUID AND THE THICKNESS OF THE
2270 C                  LIQUID FILM AT EACH NODE
2280 C   OUTPUT         OUTPUT DUMP OF MAJOR VARIABLES (NON CWAF)
2290 C   OUTPUT1        OUTPUTS RELEASE RATES (FLOW OUT OF NODE) IN G/S
2300 C                  (IN TYP7 FORMAT)
2310 C   JAC            DUMMY SUBROUTINE
2320 C   DISKRD         READS FROM A CWAF FILES
2330 C   DSGEDR         STIFF DIFFERENTIAL EQUATION SOLVER
2340 C   LIQMOVE        MOVE ALLOY OUT OF A NODE AND INTO THE NEXT
2350 C                  NODE IF TROD >  STAINLESS STEEL MELTING
2360 C                   ALLOY-ZIRCALLOY EUTECTIC INTERACTION)
2370 ************************************************************
2380 C
2390 C
2400 C
2410 C              $$$$$  END OF CODE DESCRIPTION  $$$$$
2420 C
2430 ************************************************************
2440          EXTERNAL XMDOT,JAC
2450          REAL RPARM(10),RTOL,ATOL,WK(10900),VMASS(6,10),RMASS(4,10)
2460          REAL XMASS(100)
2470          EQUIVALENCE (VMASS,XMASS(1)),(RMASS,XMASS(61))
2480 C NOTE EQUIVALENCE FIRST 60 ELEMENTS OF XMASS TO VMASS AND THE
```

```
2490 C LAST 40 ELEMENTS OF XMASS TO RMASS (THIS IS NEEDED FOR THE
2500 C DIFFERENTIAL EQUATION SOLVER)
2510          INTEGER IPARM(12),IWK(100),JOB(5),INFO
2520          COMMON /TH/ TROD(10),TCOOL(10),WH2(10),WH2O(10),SH2(10),
2530       +    SH2O(10),RHOMIX(10),VISC(10),REY(10),IFLAG,PTOT(10),FWG(10)
2540          COMMON /IN/ X(50),T1(50,10),T2(50,10),W1(50,10),
2550       +    W2(50,10),H2RXD(50,10),H2ORXD(50,10),PRES(10)
2560          COMMON /A/ K,TMAX,NDATA,DT,TFLAG,FRACT
2570          COMMON /CNTRL/ NSPV,NSPL,NCV,SW(10)
2580          COMMON /GEOM/ CLEN(10),AFLOW(10),SA(10),VOL(10),
2590       +                DELZ(10),DROD
2600          COMMON /CRIT/ TC(6),VC(6),WT(6),A(6),B(6),
2610       +                TCM(10),VCM(10),WTM(10)
2620          COMMON /VAPOR/ CWALL(6,10),CBULK(6,10),PWALL(6,10),
2630       +  PBULK(6,10),XWALL(6,10),XBULK(6,10),DIFF(6,10),
2640       +  HD(6,10),SC(6,10),WVJUNC(6,10),DFLUX(6,10),FLVOUT(6),
2650       +  XN(6,10)
2660          COMMON /LIQUID/ WLJUNC(4,10),DELTA(10),VEL(10),Y(4,10),
2670       +                  VISCL(10),RHOL(10),RSOURCE(4)
2680          COMMON /FAIL/ DIROD,AFAIL,HO,VO,HEIGHT,WTFRAC(4)
2690 C  ***************************************************************
2700 C  *************   MAIN PROGRAM ************************************
2710 C
2720 C    INPUT DATA FOR STIFF EQUATION SOLVER ****************
2730          DATA RTOL,ATOL/1E-07,1E-04/
2740          RPARM(1)= 100.0
2750          RPARM(2)= 0.0
2760          RPARM(3)= 0.0
2770          RPARM(4)= 0.0
2780          RPARM(5)= 0.0
2790          IPARM(1)= 6
2800          IPARM(2)= 10900
2810          IPARM(3)= 100
2820          IPARM(4)= 0
2830          IPARM(5)= 0
2840          IPARM(6)= 0
2850          DATA JOB/3,1,2,2,1/
2860          DATA ND/100/
2870 C    END OF INPUT DATA FOR STIFF EQUATION SOLVER ***********
2880          K=1
2890          DT=0.0
2900          CALL INIT (VMASS,RMASS)
2910          CALL DATA1
2920          CALL READ 1
2930          T=X(K)
2940          CALL ASSIGN(NCV,T)
2950          CALL LIQPROP
2960          CALL VALCAL (VMASS,RMASS)
2970   77     DO 88 NV=1,NCV
2980            IF (SW(NV) .EQ. 0.0) GO TO 88
2990            CALL DIFFC(NV)
3000            CALL MIXPROP(NV)
3010            CALL CORR(NV)
3020   88     CONTINUE
3030          IF (T .EQ. X(1)) THEN
3040            TIME=T-X(1)
3050            CALL RODFAIL(TIME)
3060            CALL MOMEN
3070            CALL OUTPUT (VMASS,RMASS,T)
3080          ENDIF
```

```
3090          CALL TSTEP(T,TEND)
3100          CALL LIQPROP
3110          CALL DSGEDR(XMDOT,ND,T,XMASS,TEND,JAC,RTOL,ATOL,
3120         +    RPARM,IPARM,WK,IWK,JOB,INFO)
3130          IF (T .LT. TMAX) CALL ASSIGN(NCV,T)
3140          CALL OUTPUT(VMASS,RMASS,T)
3150          CALL OUTPUT1(FLVOUT,NSPV,T)
3160          TSSMELT=1750
3170          DO 44 JJ=1,NCV
3180             IF ((TROD(JJ) .GT. TSSMELT) .AND.(SW(JJ) .EQ. 1))THEN
3190               CALL LIQMOVE(RMASS,JJ)
3200 C           ****RESTART DIFFERENTIAL EQUATION SOLVER ****
3210               JOB(2)= 1
3220             ENDIF
3230   44     CONTINUE
3240          DO 80 NT=1,10
3250           DO 60 KL=1,NSPL
3260            IF(RMASS(KL,NT).LT. 0.0) THEN
3270              RMASS(KL,NT) = 0.0
3280 C          **** RESTART DIFFERENTIAL EQUATION SOLVER *****
3290              JOB(2) = 1
3300            ENDIF
3310   60       CONTINUE
3320           DO 70 JL=1,NSPV
3330            IF(VMASS(JL,NT) .LT. 0.0) THEN
3340              VMASS(JL,NT) = 0.0
3350 C          **** RESTART DIFFERENTIAL EQUATION SOLVER *****
3360              JOB(2)= 1
3370            ENDIF
3380   70       CONTINUE
3390   80     CONTINUE
3400          KSUM = 0
3410          DO 33 KK=1,NCV
3420             IF (SW(KK) .EQ. 0) KSUM = KSUM + 1
3430   33     CONTINUE
3440          IF (KSUM .GE. NCV) GO TO 111
3450          LSUM = 0
3460          DO 52 JT = 1,NCV
3470             IF((DELTA(JT).LT.1.0E-05).OR.(VEL(JT).LT.5.0E-04))
3480         +          LSUM = LSUM + 1
3490   52     CONTINUE
3500          IF (LSUM .GE. NCV) GO TO 111
3510          IF (T.GE. TMAX) GO TO 111
3520          GO TO 77
3530   111    STOP
3540          END
3550 C
3560 C
3570 C
3580 C    ************************************************************
3590 C    ********  MAIN SUBROUTINES ********************************
3600 C
3610          SUBROUTINE DATA1
3620          COMMON /CRIT/ TC(6),VC(6),WT(6),A(6),B(6),
3630         +              TCM(10),VCM(10),WTM(10)
3640          COMMON /CNTRL/ NSPV,NSPL,NCV,SW(10)
3650          COMMON /A/ K,TMAX,NDATA,DT,TFLAG,FRACT
3660          COMMON /GEOM/ CLEN(10),AFLOW(10),SA(10),VOL(10),
3670         +              DELZ(10),DROD
3680          COMMON /FAIL/ DIROD,AFAIL,HO,VO,HEIGHT,WTFRAC(4)
```

```
3690 C THIS SUBROUTINE READS IN  DATA FOR CODE USE
3700          READ(12,85) NSPV,NSPL,NCV
3710          DO 99 I=1,NSPV
3720             IF ((I .EQ. 4) .OR. (I .EQ. 5)) THEN
3730               READ (12,101) TC(I),VC(I),WT(I)
3740             ELSE
3750               READ (12,100) TC(I),VC(I),A(I),B(I),WT(I),WTFRAC(I)
3760             ENDIF
3770   99     CONTINUE
3780          DO 15 L=1,NCV
3790              READ(12,300) AFLOW(L),CLEN(L),SA(L),VOL(L),DELZ(L)
3800   15     CONTINUE
3810          READ (12,600) DROD,DIROD,AFAIL,HO
3820          READ(12,500) TMAX,NDATA,TFLAG,FRACT
3830          WRITE(8,90)
3840          WRITE (8,95)
3850          WRITE (8,96) NSPV,NSPL,NCV
3860          WRITE(8,150)
3870          DO 10 K1= 1,NSPV
3880             IF ((K1 .EQ. 4) .OR. (K1 .EQ. 5))THEN
3890                WRITE(8,101) TC(K1),VC(K1),WT(K1)
3900             ELSE
3910                WRITE(8,100) TC(K1),VC(K1),A(K1),B(K1),WT(K1),WTFRAC(K1)
3920             ENDIF
3930   10     CONTINUE
3940          WRITE(8,275)
3950          DO 20 L1= 1,NCV
3960             WRITE(8,300) AFLOW(L1),CLEN(L1),SA(L1),VOL(L1),DELZ(L1)
3970   20     CONTINUE
3980          WRITE (8,600)DROD,DIROD,AFAIL,HO
3990          WRITE(8,405)
4000          WRITE(8,500) TMAX,NDATA,TFLAG,FRACT
4010 C
4020   85     FORMAT(2X,3I5)
4030   90     FORMAT(2X,"ECHO INPUT DATA")
4040   95     FORMAT (2X,"VAPOR SPECIES, LIQUID SPECIES,CONTROL VOLUMES")
4050   96     FORMAT(3(3X,I5,2X))
4060   100    FORMAT(F8.2,F8.2,E10.3,3(F8.3))
4070   101    FORMAT(3F8.2)
4080   150    FORMAT(2X,"CRITCAL CONSTANT PARAMETERS")
4090   200    FORMAT(3F7.2)
4100   250    FORMAT(F7.2,F7.2,F7.2)
4110   275    FORMAT(2X,"GEOMETRICAL PARAMETERS")
4120   300    FORMAT(5E10.3)
4130   405    FORMAT(2X,"TIME PARAMETERS")
4140   500    FORMAT(F8.3,I5,2F8.3)
4150   600    FORMAT(2X,4(E10.3))
4160          RETURN
4170          END
4180 C
4190 C
4200 C
4210 C
4220          SUBROUTINE INIT (VMASS,RMASS)
4230          REAL VMASS(6,10),RMASS(4,10)
4240          COMMON /VAPOR/ CWALL(6,10),CBULK(6,10),PWALL(6,10),
4250       +  PBULK(6,10),XWALL(6,10),XBULK(6,10),DIFF(6,10),
4260       +  HD(6,10),SC(6,10),WVJUNC(6,10),DFLUX(6,10),FLVOUT(6),
4270       +  XN(6,10)
4280          COMMON /LIQUID/ WLJUNC(4,10),DELTA(10),VEL(10),Y(4,10),
```

```
     +                        VISCL(10),RHOL(10),RSOURCE(4)
      COMMON /CNTRL/ NSPV,NSPL,NCV,SW(10)
C THIS SUBROUTINE INITIALIZES SOME ARRAYS TO ZERO
      DO 20 MC= 1,10
          DO 18 NY= 1,6
              CWALL(NY,MC)=0.0
              CBULK(NY,MC)=0.0
              PWALL(NY,MC)=0.0
              PBULK(NY,MC)=0.0
              XWALL(NY,MC)=0.0
              XBULK(NY,MC)=0.0
              VMASS(NY,MC)=0.0
              XN(NY,MC)=0.0
              WVJUNC(NY,MC)=0.0
 18       CONTINUE
          DO 19 NZ=1,4
              WLJUNC(NZ,MC)=0.0
              Y(NZ,MC)=0.0
              RMASS(NZ,MC)=0.0
 19       CONTINUE
          VEL(MC)=0.0
          DELTA(MC)=0.0
          SW(MC) = 1.0
 20   CONTINUE
      RETURN
      END
C
      SUBROUTINE ASSIGN(JEND,T)
C     THIS SUBROUTINE ASSIGN T/H BOUNDARY CONDITION FROM THE TIME
C     DEPENDENT T/H INPUT USING LINEAR INTERPOLATION
      INTEGER JEND
      REAL T
      COMMON /TH/ TROD(10),TCOOL(10),WH2(10),WH2O(10),SH2(10),
     +   SH2O(10),RHOMIX(10),VISC(10),REY(10),IFLAG,PTOT(10),FWG(10)
      COMMON /IN/ X(50),T1(50,10),T2(50,10),W1(50,10),
     +   W2(50,10),H2RXD(50,10),H2ORXD(50,10),PRES(10)
      COMMON /A/ K,TMAX,NDATA,DT,TFLAG,FRACT
      ALPHA=(T-X(K))/(X(K+1)-X(K))
      DO 10 J = 1,JEND
        TROD(J)=T1(K,J) + ALPHA*(T1(K+1,J)-T1(K,J))
        TCOOL(J)=T2(K,J) + ALPHA*(T2(K+1,J)-T2(K,J))
        WH2O(J)=W1(K,J) + ALPHA*(W1(K+1,J)-W1(K,J))
        WH2(J)=W2(K,J) + ALPHA*(W2(K+1,J) - W2(K,J))
        SH2O(J)=H2ORXD(K,J)+ALPHA*(H2ORXD(K+1,J)-H2ORXD(K,J))
        SH2(J)=H2RXD(K,J)+ALPHA*(H2ORXD(K+1,J)-H2RXD(K,J))
 10   CONTINUE
      IFLAG=1
      RETURN
      END
C
C
C
C
C
C
      SUBROUTINE VALCAL (VMASS,RMASS)
      REAL VMASS(6,10), RMASS(4,10)
      COMMON /LIQUID/ WLJUNC(4,10),DELTA(10),VEL(10),Y(4,10),
     +                VISCL(10),RHOL(10),RSOURCE(4)
      COMMON /FAIL/ DIROD,AFAIL,HO,VO,HEIGHT,WTFRAC(4)
```

```
4890          COMMON /VAPOR/ CWALL(6,10),CBULK(6,10),PWALL(6,10),
4900         +  PBULK(6,10),XWALL(6,10),XBULK(6,10),DIFF(6,10),
4910         +  HD(6,10),SC(6,10),WVJUNC(6,10),DFLUX(6,10),FLVOUT(6),
4920         +  XN(6,10)
4930          COMMON /CNTRL/ NSPV,NSPL,NCV,SW(10)
4940          COMMON /TH/ TROD(10),TCOOL(10),WH2(10),WH2O(10),SH2(10),
4950         +    SH2O(10),RHOMIX(10),VISC(10),REY(10),IFLAG,PTOT(10),FWG(10)
4960          COMMON /GEOM/ CLEN(10),AFLOW(10),SA(10),VOL(10),
4970         +                DELZ(10),DROD
4980          COMMON /CRIT/ TC(6),VC(6),WT(6),A(6),B(6),
4990         +                TCM(10),VCM(10),WTM(10)
5000          COMMON /IN/ X(50),T1(50,10),T2(50,10),W1(50,10),

5010         +    W2(50,10),H2RXD(50,10),H2ORXD(50,10),PRES(10)
5020 C
5030 C THIS SUBROUTINE CALCULATES THE MOLE FRACTION AND PARTIAL PRESSURE
5040 C STEAM AND HYDROGEN IN THE INITIALLY
5050 C
5060          R= 82.05
5070          DO 10 N=1,NCV
5080            DENOM= (WH2(N)/WT(4)) + (WH2O(N)/WT(5))
5090            XBULK(4,N)=(WH2(N)/WT(4))/DENOM
5100            XBULK(5,N)=(WH2O(N)/WT(5))/DENOM
5110            PTOT(N)=PRES(N)
5120            PBULK(4,N) = XBULK(4,N)*PTOT(N)
5130            PBULK(5,N) = XBULK(5,N)*PTOT(N)
5140            VOL(N)=VOL(N)*(1.0E+06)
5150            VMASS(4,N)=(PBULK(4,N)*VOL(N)/(R*TCOOL(N)))*WT(4)
5160            VMASS(5,N)=(PBULK(5,N)*VOL(N)/(R*TCOOL(N)))*WT(5)
5170   10     CONTINUE
5180 C INITIALLY PUT 1/3% OF THE MASS IN THE ROD IN EACH NODE
5190 C AND CALCUALTE THE CORRESPONDING THICKNESS OF THE LIQUID FILM
5200          PI = 3.14159
5210          ZMTOT= PI*(DIROD**2.0)*HO*RHOL(1)*1000/(4*300)
5220          DO 15 J=1,NCV
5230             DO 20 L=1,NSPL
5240                RMASS(L,J)=ZMTOT*WTFRAC(L)
5250   20        CONTINUE
5260             DELTA(J)=ZMTOT/(4*PI*DROD*DELZ(J)*RHOL(J)*1000)
5270   15     CONTINUE
5280          RETURN
5290          END
5300 C
5310 C
5320 C
5330 C
5340 C
5350 C
5360 C
5370 C
5380          SUBROUTINE DIFFC(J1)
5390          INTEGER J1
5400          COMMON /TH/ TROD(10),TCOOL(10),WH2(10),WH2O(10),SH2(10),
5410         +    SH2O(10),RHOMIX(10),VISC(10),REY(10),IFLAG,PTOT(10),FWG(10)
5420          COMMON /CNTRL/ NSPV,NSPL,NCV,SW(10)
5430          COMMON /CRIT/ TC(6),VC(6),WT(6),A(6),B(6),
5440         +                TCM(10),VCM(10),WTM(10)
5450          COMMON /VAPOR/ CWALL(6,10),CBULK(6,10),PWALL(6,10),
5460         +  PBULK(6,10),XWALL(6,10),XBULK(6,10),DIFF(6,10),
5470         +  HD(6,10),SC(6,10),WVJUNC(6,10),DFLUX(6,10),FLVOUT(6),
```

```
5480      +  XN(6,10)
5490 C THIS SUBROUTINE CALCULATES PSEUDO CRITICAL PROPERTIES OF THE
5500 C H2/H2O MIXTURE AND BINARY DIFFUSION COEFFICIENTS
5510          TCM(J1) = TC(4)*XBULK(4,J1) + TC(5)*XBULK(5,J1)
5520          VCM(J1) = VC(4)*XBULK(4,J1) + VC(5)*XBULK(5,J1)
5530          WTM(J1) = WT(4)*XBULK(4,J1) + WT(5)*XBULK(5,J1)
5540          DO 25 N= 1,3
5550            SIGMA1 = (5/6.)*(VCM(J1))**(1/3.0)
5560            SIGMA2 = (5/6.)*(VC(N))**(1/3.0)
5570            SIGMA = 0.5*(SIGMA1 + SIGMA2)
5580            EPK1 = 0.75*TCM(J1)
5590            EPK2 = 0.75*TC(N)
5600            A1= 1.06036
5610            B1= 0.15610
5620            C= 0.193
5630            D= 0.47635
5640            E= 1.03587
5650            F=1.52996
5660            G= 1.76474
5670            H= 3.89411
5680            CONST= 1.85E-03
5690            EPK = SQRT(EPK1*EPK2)
5700            TSTAR=TROD(J1)/EPK
5710            OMEGA = A1/(TSTAR)**B1 + C*EXP(-D*TSTAR) +
5720      +     E*EXP(-F*TSTAR) + G*EXP(-H*TSTAR)
5730            XMMOL= SQRT((WTM(J1) + WT(N))/(WTM(J1)*WT(N)))
5740            DENOM = PTOT(J1)*((SIGMA)**2.)*OMEGA
5750            DIFF(N,J1)= CONST*((TROD(J1)**(1.5))*XMMOL)/DENOM
5760            DIFF(N,J1)=DIFF(N,J1)*(1E-04)
5770   25     CONTINUE
5780          RETURN
5790          END
5800 C
5810 C
5820 C
5830 C
5840          SUBROUTINE MIXPROP(LX)
5850          INTEGER LX
5860          COMMON /TH/ TROD(10),TCOOL(10),WH2(10),WH2O(10),SH2(10),
5870      +     SH2O(10),RHOMIX(10),VISC(10),REY(10),IFLAG,PTOT(10),FWG(10)
5880          COMMON /CNTRL/ NSPV,NSPL,NCV,SW(10)
5890          COMMON /CRIT/ TC(6),VC(6),WT(6),A(6),B(6),
5900      +                 TCM(10),VCM(10),WTM(10)
5910          COMMON /VAPOR/ CWALL(6,10),CBULK(6,10),PWALL(6,10),
5920      +   PBULK(6,10),XWALL(6,10),XBULK(6,10),DIFF(6,10),
5930      +   HD(6,10),SC(6,10),WVJUNC(6,10),DFLUX(6,10),FLVOUT(6),
5940      +   XN(6,10)
5950 C THIS SUBROUTINE CALCULATES MIXTURE PROPERTIES (RHO,VISC)
5960 C WHICH ARE NEEDED IN FLUID CALCULATIONS
5970          R= 8.314E+03
5980          RHOH2O=(PBULK(5,LX))*(1.013E+05)/(R*TCOOL(LX))
5990          RHOH2= (PBULK(4,LX))*(1.013E+05)/(R*TCOOL(LX))
6000          RHOMIX(LX)= WT(4)*RHOH2 + RHOH2O*WT(5)
6010 C
6020          VISH2O= (0.407*TCOOL(LX) - 30.)*(1E-07)
6030          A2= 1.16145
6040          B2= 0.14874
6050          C= 0.52487
6060          D= 0.77320
6070          E= 2.16178
```

```
6080          F= 2.43787
6090          SIGMA= 2.827
6100          EPK= 59.7
6110          TSTAR=TCOOL(LX)/EPK
6120          OMEGA= A2/(TSTAR**B2) +C*EXP(-D*TSTAR) + E*EXP(-F*TSTAR)
6130          VISH2 = (2.6693E-05)*(SQRT(2.016*TCOOL(LX)))
6140          VISH2=VISH2/((SIGMA**2.)*OMEGA)
6150 C
6160          A21=1+(WT(4)/WT(5))**(0.5)
6170          B21= 1 +SQRT(VISH2/VISH20)*((WT(5)/WT(4))**(0.25))
6180          PHI21= 0.354*(B21**2)/A21
6190 C
6200          A12= 1 +(WT(5)/WT(4))**(0.5)
6210          B12= 1 +SQRT(VISH20/VISH2)*((WT(4)/WT(5))**(0.25))
6220          PHI12= 0.354*(B12**2.)/A12
6230          VISC(LX)= (VISH20*XBULK(5,LX))/(XBULK(5,LX)+XBULK(4,LX)
6240       +  *PHI21)+(VISH2*XBULK(4,LX))/(XBULK(4,LX)+
6250       +   XBULK(5,LX)*PHI12)
6260          RETURN
6270          END
6280 C
6290 C
6300 C
6310 C
6320 C
6330 C
6340 C
6350 C
6360          SUBROUTINE CORR(K)
6370          INTEGER K
6380          COMMON /TH/ TROD(10),TCOOL(10),WH2(10),WH20(10),SH2(10),
6390       +    SH20(10),RHOMIX(10),VISC(10),REY(10),IFLAG,PTOT(10),FWG(10)
6400          COMMON /CNTRL/ NSPV,NSPL,NCV,SW(10)
6410          COMMON /GEOM/ CLEN(10),AFLOW(10),SA(10),VOL(10),
6420       +                DELZ(10),DROD
6430          COMMON /VAPOR/ CWALL(6,10),CBULK(6,10),PWALL(6,10),
6440       +  PBULK(6,10),XWALL(6,10),XBULK(6,10),DIFF(6,10),
6450       +  HD(6,10),SC(6,10),WVJUNC(6,10),DFLUX(6,10),FLVOUT(6),
6460       +  XN(6,10)
6470 C THIS SUBROUTINE CALCULATES THE MASS TRANSFER COEFFICIENTS FOR
6480 C AG,IN AND CD. ITCULATES FRICTIN FACTORS DUE TO THE GAS FLOW
6490          WTOT= WH2(K) + WH20(K)
6500          GFLUX = WTOT/(AFLOW(K)*1000.0)
6510          REY(K)= GFLUX*CLEN(K)/VISC(K)
6520          IF (REY(K) .LT. 2000) THEN
6530             FWG(K)= 16/REY(K)
6540          ELSE
6550             FWG(K)= 0.046/(REY(K)**0.2)
6560          ENDIF
6570          DO 75 L=1,NSPL
6580              SC(L,K)= VISC(K)/(RHOMIX(K)*DIFF(L,K))
6590  75      CONTINUE
6600          IF (IFLAG .LE. 0) GO TO 30
6610          IF (IFLAG .EQ. 1) GO TO 10
6620          IF (IFLAG .EQ. 2) GO TO 20
6630          IF (IFLAG .GE. 3) GO TO 30
6640 C
6650 C  FLOW IN TUBES
6660  10      DO 15 KA=1,NSPL
6670              IF(REY(K) .GT. 2000) THEN
```

```
6680                HD(KA,K)= 0.023*DIFF(KA,K)*(REY(K)**0.83)*
6690       +           (SC(KA,K)**0.44)/CLEN(K)
6700               ELSE
6710                 HD(KA,K)= 3.656*DIFF(KA,K)/CLEN(K)
6720               ENDIF
6730   15        CONTINUE
6740             GO TO 40
6750 C FLOW OVERFLAT PLATE
6760 C
6770   20        DO 24 KB= 1,NSPL
6780               IF (REY(K) .LT. 10000) THEN
6790                 HD(KB,K)= 0.664*DIFF(KB,K)*(REY(K)**0.5)*
6800       +          (SC(KB,K)**(0.3333))/CLEN(K)
6810               ELSE
6820                 HD(KB,K)= 0.037*DIFF(KB,K)*(REY(K)**0.8)*
6830       +          (SC(KB,K)**(0.3333))/CLEN(K)
6840               ENDIF
6850   24        CONTINUE
6860
6870             GO TO 40
6880   30        WRITE(8,33)
6890   33        FORMAT (2X,"NO CORRELATION SELECTED")
6900             STOP
6910   40        RETURN
6920             END
6930 C
6940 C
6950 C
6960 C
6970             SUBROUTINE FLUX (VMASS,RMASS)
6980             REAL VMASS(6,10),RMASS(4,10)
6990 C THIS SUBROUTINE CALCULATES THE VAPOR FLUX OF EACH SPECIES
7000             COMMON /TH/ TROD(10),TCOOL(10),WH2(10),WH2O(10),SH2(10),
7010       +       SH2O(10),RHOMIX(10),VISC(10),REY(10),IFLAG,PTOT(10),FWG(10)
7020             COMMON /CNTRL/ NSPV,NSPL,NCV,SW(10)
7030             COMMON /VAPOR/ CWALL(6,10),CBULK(6,10),PWALL(6,10),
7040       +     PBULK(6,10),XWALL(6,10),XBULK(6,10),DIFF(6,10),
7050       +     HD(6,10),SC(6,10),WVJUNC(6,10),DFLUX(6,10),FLVOUT(6),
7060       +     XN(6,10)
7070             COMMON /GEOM/ CLEN(10),AFLOW(10),SA(10),VOL(10),
7080       +                   DELZ(10),DROD
7090             INTEGER IBOIL
7100 C
7110             DO 20 IS=1,NCV
7120              DO 95 M=1,3
7130                 DFLUX(M,IS)= HD(M,IS)*(CWALL(M,IS) - CBULK(M,IS))
7140                 DFLUX(M,IS)=DFLUX(M,IS)*(1.0E+06)
7150                 TEST = CWALL(M,IS)- CBULK(M,IS)
7160                 IF (TEST .LT. 0.0) DFLUX(M,IS)=0.0
7170                 IF(DFLUX(M,IS) .LT. 0.0) DFLUX(M,IS)= 0.0
7180   95         CONTINUE
7190   20        CONTINUE
7200             IBOIL = 0
7210             DO 10 J4 = 1,NCV
7220              DO 30 IN=1,NSPL
7230                 IF (PWALL(IN,J4) .GT. PTOT(J4)) THEN
7240                   IBOIL= 1
7250 C                 *** DO NOT USE MULTICOMPONENT MASS TRANSFER
7260 C                     SINCE BOILING IS OCCURING. AS AN APPROXIMATION
7270 C                     USE UNCOUPLED CONVECTIVE MASS TRANSFER
```

```
7280              ENDIF
7290   30       CONTINUE
7300            IF (IBOIL .EQ. 0) THEN
7310               SUM=0.0
7320               DO 40 I=1,3
7330                 SUM = SUM +XWALL(I,J4)
7340   40          CONTINUE
7350               DO 70 I2=1,3
7360                 SUM2 = 0.0
7370                 SUM3 = 0.0
7380                 DO 50 J = 1,3
7390                   IF (J .EQ. I2) GO TO 50
7400                   SUM2=SUM2 + DFLUX(J,J4)
7410                   SUM3= SUM3 +XWALL(J,J4)
7420   50              CONTINUE
7430                 XN(I2,J4)=(DFLUX(I2,J4)*(1-SUM3) + XWALL(I2,J4)*SUM2)*
7440       +           SA(J4)/(1 - SUM)
7450                 IF (XN(I2,J4) .LT. 0.0) XN(I2,J4) = 0.0
7460   70          CONTINUE
7470            ELSE
7480               DO 60 L=1,NSPL
7490                 XN(L,J4) = DFLUX(L,J4)*SA(J4)
7500   60          CONTINUE
7510            ENDIF
7520    10     CONTINUE
7530           RETURN
7540           END
7550 C
7560 C
7570 C
7580 C
7590 C
7600 C
7610 C
7620 C
7630           SUBROUTINE FLOW(VMASS,RMASS)
7640           REAL VMASS(6,10),RMASS(4,10)
7650           COMMON /TH/ TROD(10),TCOOL(10),WH2(10),WH2O(10),SH2(10),
7660       +     SH2O(10),RHOMIX(10),VISC(10),REY(10),IFLAG,PTOT(10),FWG(10)
7670           COMMON /IN/ X(50),T1(50,10),T2(50,10),W1(50,10),
7680       +     W2(50,10),H2RXD(50,10),H2ORXD(50,10),PRES(10)
7690           COMMON /A/ K,TMAX,NDATA,DT,TFLAG,FRACT
7700           COMMON /CNTRL/ NSPV,NSPL,NCV,SW(10)
7710           COMMON /LIQUID/ WLJUNC(4,10),DELTA(10),VEL(10),Y(4,10),
7720       +                    VISCL(10),RHOL(10),RSOURCE(4)
7730           COMMON /GEOM/ CLEN(10),AFLOW(10),SA(10),VOL(10),
7740       +                 DELZ(10),DROD
7750           COMMON /VAPOR/ CWALL(6,10),CBULK(6,10),PWALL(6,10),
7760       +   PBULK(6,10),XWALL(6,10),XBULK(6,10),DIFF(6,10),
7770       +   HD(6,10),SC(6,10),WVJUNC(6,10),DFLUX(6,10),FLVOUT(6),
7780       +   XN(6,10)
7790           COMMON /FAIL/ DIROD,AFAIL,HO,VO,HEIGHT,WTFRAC(4)
7800           COMMON /CRIT/ TC(6),VC(6),WT(6),A(6),B(6),
7810       +                 TCM(10),VCM(10),WTM(10)
7820 C CALCULATE THE VAPOR FLOWS AT THE JUNCTIONS
7830           WVJUNC(4,NCV)=WH2(NCV)
7840           WVJUNC(5,NCV)= WH2O(NCV)
7850           DO 99 L=1,3
7860    99         WVJUNC(L,NCV)= 0.0
7870           DO 10 N= 1,NCV
```

```
7880            NVOL = NCV + 1 - N
7890            R=82.05
7900            TOTIN=0.0
7910     •      FLINT=0.0
7920            XNTOT=0.0
7930            TEXPN= 0.0
7940            IF (DT .EQ. 0.0) THEN
7950               DTDT=0.0
7960            ELSE
7970               IF (TFLAG .NE. 1.0) THEN
7980                 DTDT=(TCOOL(NVOL) - T2(K-1,NVOL))/DT
7990               ELSE
8000                 DTDT=(TCOOL(NVOL) - T2(K,NVOL))/DT
8010               ENDIF
8020            ENDIF
8030            TEXPN= DTDT*PTOT(NVOL)*VOL(NVOL)/(R*(TCOOL(NVOL)**2.0))
8040            DO 35 M=1,NSPV
8050               IF ((M .EQ. 4) .OR. (M .EQ. 5)) GO TO 40
8060               XNTOT= XNTOT+ XN(M,NVOL)
8070  40           FLINT= FLINT + WVJUNC(M,NVOL)/WT(M)
8080  35        CONTINUE
8090            TOTIN = FLINT + XNTOT
8100            DO 50 M1=1,NSPV
8110               IF (NVOL .NE. 1) THEN
8120                 IF (M1 .EQ. 4) THEN
8130                    WVJUNC(4,NVOL-1)=WH2(NVOL-1)
8140                 ELSE IF (M1 .EQ. 5) THEN
8150                    WVJUNC(5,NVOL-1)=WH2O(NVOL-1)
8160                 ELSE
8170                    WVJUNC(M1,NVOL-1)=XBULK(M1,NVOL)*(TOTIN+TEXPN)*WT(M1)
8180                    IF (WVJUNC(M1,NVOL-1).LT. 0.0) WVJUNC(M1,NVOL-1)=0.0
8190                 ENDIF
8200               ELSE
8210                 IF (M1 .EQ. 4) THEN
8220                    FLVOUT(M1)=WH2(NVOL)
8230                 ELSE IF (M1 .EQ. 5) THEN
8240                    FLVOUT(M1)=WH2O(NVOL)
8250                 ELSE
8260                    FLVOUT(M1)= XBULK(M1,NVOL)*(TOTIN + TEXPN)*WT(M1)
8270                    IF (FLVOUT(M1) .LT. 0.0) FLVOUT(M1)=0.0
8280                 ENDIF
8290               ENDIF
8300  50        CONTINUE
8310  10     CONTINUE
8320 C CALCULATE LIQUID FLOWS AT JUNCTIONS
8330         DO 70 I=1,NCV
8340           DO 80 J=1,NSPL
8350               WLJUNC(J,I)=VEL(I)*RMASS(J,I)/DELZ(I)
8360               IF (WLJUNC(J,I) .LT. 0.0) WLJUNC(J,I)=0.0
8370  80       CONTINUE
8380  70     CONTINUE
8390 C CALCULATE THE FLOW OF EACH SPECIES OUT OF THE ROD
8400           DO 66 I=1,NSPL
8410               RSOURCE(I)=RHOL(1)*AFAIL*VO*WTFRAC(I)*1000
8420  66       CONTINUE
8430         RETURN
8440         END
8450 C
8460         SUBROUTINE XMDOT(RHS,INT,XMASS,TIME)
8470         DIMENSION XMASS(INT),RHS(INT)
```

```
8480          COMMON /VAPOR/ CWALL(6,10),CBULK(6,10),PWALL(6,10),
8490       +  PBULK(6,10),XWALL(6,10),XBULK(6,10),DIFF(6,10),
8500       +  HD(6,10),SC(6,10),WVJUNC(6,10),DFLUX(6,10),FLVOUT(6),
8510       +  XN(6,10)
8520          COMMON /CNTRL/ NSPV,NSPL,NCV,SW(10)
8530          COMMON /IN/ X(50),T1(50,10),T2(50,10),W1(50,10),
8540       +    W2(50,10),H2RXD(50,10),H2ORXD(50,10),PRES(10)
8550          COMMON /CRIT/ TC(6),VC(6),WT(6),A(6),B(6),
8560       +                TCM(10),VCM(10),WTM(10)
8570          COMMON /TH/ TROD(10),TCOOL(10),WH2(10),WH2O(10),SH2(10),
8580       +    SH2O(10),RHOMIX(10),VISC(10),REY(10),IFLAG,PTOT(10),FWG(10)
8590          COMMON /LIQUID/ WLJUNC(4,10),DELTA(10),VEL(10),Y(4,10),
8600       +                  VISCL(10),RHOL(10),RSOURCE(4)
8610          COMMON /FAIL/ DIROD,AFAIL,HO,VO,HEIGHT,WTFRAC(4)
8620  C THIS SUBROUTINE SETS UP THE RIGHT HAND OF THE DIFFERENTIAL
8630  C EQUATION FOR USE BY THE STIFF DIFFERENTIAL EQUATION SOLVER
8640          CALL BULK (XMASS(1),XMASS(61))
8650          CALL FLUX(XMASS(1),XMASS(61))
8660          TSTART=TIME- X(1)
8670          CALL RODFAIL(TSTART)
8680          CALL MOMEN
8690          CALL FLOW(XMASS(1),XMASS(61))
8700          K=0
8710          DO 10 J=1,10
8720            DO 20 I=1,6
8730              K=K+1
8740              IF ((I .GT. NSPV) .OR. (J .GT. NCV)) THEN
8750                RHS(K)=0.0
8760                GO TO 20
8770              ENDIF
8780              IF (J .NE. 1) THEN
8790                IF (I .EQ. 4) THEN
8800                  RHS(K)=SH2(J) + WVJUNC(I,J) - WVJUNC(I,J-1)
8810                ELSE IF (I .EQ.  5) THEN
8820                  RHS(K)=SH2O(J) + WVJUNC(I,J) - WVJUNC(I,J-1)
8830                ELSE
8840                  RHS(K)=XN(I,J)*WT(I) + WVJUNC(I,J) - WVJUNC(I,J-1)
8850                ENDIF
8860              ELSE
8870                IF (I .EQ. 4) THEN
8880                  RHS(K)=SH2(J) + WVJUNC(I,J)-FLVOUT(I)
8890                ELSE IF (I .EQ.  5) THEN
8900                  RHS(K)= SH2O(J) + WVJUNC(I,J) - FLVOUT(I)
8910                ELSE
8920                  RHS(K)=XN(I,J)*WT(I) + WVJUNC(I,J) - FLVOUT(I)
8930                ENDIF
8940              ENDIF
8950  20        CONTINUE
8960  10      CONTINUE
8970          K=60
8980          DO 30 J=1,10
8990            DO 40 I=1,4
9000              K=K+1
9010              IF ((I .GT. NSPL) .OR. (J .GT. NCV)) THEN
9020                RHS(K)=0.0
9030                GO TO 40
9040              ENDIF
9050              IF (J .NE. 1) THEN
9060                RHS(K)= WLJUNC(I,J-1) - WLJUNC(I,J) - XN(I,J)*WT(I)
9070              ELSE
```

```
9080                RHS(K)= RSOURCE(I) - WLJUNC(I,J) - XN(I,J)*WT(I)
9090              ENDIF
9100   40       CONTINUE
9110   30     CONTINUE
9120          RETURN
9130          END
9140  C
9150  C
9160  C
9170  C
9180          SUBROUTINE BULK (VMASS,RMASS)
9190          REAL VMASS(6,10),RMASS(4,10)
9200          COMMON /TH/ TROD(10),TCOOL(10),WH2(10),WH2O(10),SH2(10),
9210       +    SH2O(10),RHOMIX(10),VISC(10),REY(10),IFLAG,PTOT(10),FWG(10)
9220          COMMON /CNTRL/ NSPV,NSPL,NCV,SW(10)
9230          COMMON /GEOM/ CLEN(10),AFLOW(10),SA(10),VOL(10),
9240       +                DELZ(10),DROD
9250          COMMON /CRIT/ TC(6),VC(6),WT(6),A(6),B(6),
9260       +                TCM(10),VCM(10),WTM(10)
9270          COMMON /VAPOR/ CWALL(6,10),CBULK(6,10),PWALL(6,10),
9280       +  PBULK(6,10),XWALL(6,10),XBULK(6,10),DIFF(6,10),
9290       +  HD(6,10),SC(6,10),WVJUNC(6,10),DFLUX(6,10),FLVOUT(6),
9300       +  XN(6,10)
9310          COMMON /LIQUID/ WLJUNC(4,10),DELTA(10),VEL(10),Y(4,10),
9320       +                  VISCL(10),RHOL(10),RSOURCE(4)
9330  C THIS SUBROUTINE CALCULATES THE WALL AND BULK PRESSURES,CONCENTRATIONS
9340  C AND MOLE FRACTIONS AS WELL AS THE MOLE FRACTION OF EACH SPECIE IN
9350  C THE LIQUID FILM AND LIQUID FILM THICKNESS AT EACH NODE
9360          R=82.05
9370          DO 50 K=1,NCV
9380            PTOT(K)=0.0
9390            DO 10 J= 1,NSPV
9400              PBULK(J,K)=VMASS(J,K)*R*TCOOL(K)/(WT(J)*VOL(K))
9410              CBULK(J,K)=PBULK(J,K)/(R*TCOOL(K))
9420              PTOT(K)=PTOT(K) + PBULK(J,K)
9430   10       CONTINUE
9440            DO 20 N=1,NSPV
9450              IF (PTOT(K) .EQ. 0.0) THEN
9460                XBULK(N,K)=0.0
9470              ELSE
9480                XBULK(N,K)=PBULK(N,K)/PTOT(K)
9490              ENDIF
9500   20       CONTINUE
9510   50     CONTINUE
9520          DO 99 L=1,NCV
9530              SUMROD=0.0
9540              RMTOT= 0.0
9550              DO 100 NX=1,NSPL
9560                  SUMROD= SUMROD + RMASS(NX,L)/WT(NX)
9570                  RMTOT= RMASS(NX,L) + RMTOT
9580   100        CONTINUE
9590              DO 105 MX=1,NSPL
9600                  IF (SUMROD .EQ. 0.0) THEN
9610                     Y(MX,L)=0.0
9620                  ELSE
9630                     Y(MX,L)=RMASS(MX,L)/(WT(MX)*SUMROD)
9640                  ENDIF
9650   105        CONTINUE
9660              DELTA(L)= RMTOT/(3.14159*DROD*DELZ(L)*RHOL(L)*1000)
9670   99     CONTINUE
```

```
 9680           DO 29 I=1,NCV
 9690              DO 15 M = 1,NSPL
 9700               PWALL(M,I)=10.0**(B(M) - A(M)/TROD(I))
 9710               PWALL(M,I)=PWALL(M,I)*Y(M,I)/760.0
 9720               CWALL(M,I)= PWALL(M,I)/(R*TROD(I))
 9730               XWALL(M,I)= PWALL(M,I)/PTOT(I)
 9740   15         CONTINUE
 9750   29      CONTINUE
 9760           RETURN
 9770           END
 9780 C
 9790 C
 9800           SUBROUTINE JAC(PD,LDPD,N,XMASS,T)
 9810           INTEGER LDPD,N
 9820           REAL PD(LDPD,N), XMASS(N),T
 9830           RETURN
 9840           END
 9850 C
 9860 C
 9870           SUBROUTINE DISKRD(X,Y,NPNTS,NREC,NTAPE)
 9880 C THIS SUBROUTINE READS FROM A CWAF FILE
 9890           DIMENSION X(NPNTS),Y(NPNTS),ICTRL(11),CTRL(11),
 9900       +    INFO(5),IUNIT(1)
 9910           EQUIVALENCE(CTRL,ICTRL)
 9920           DATA IUNIT/L"TAPE21"/
 9930           DATA ICTRL/11*0/
 9940           DO 10 I=1, NPNTS
 9950                X(I)=0.0
 9960                Y(I)=0.0
 9970   10      CONTINUE
 9980           ICTRL(1)=0
 9990           ICTRL(2)=0
10000           ICTRL(3)=0

10010           ICTRL(4)=IUNIT(NTAPE - 20)
10020           ICTRL(10)=NREC
10030           KNT=0
10040           ISTAT=0
10050           N2=NPNTS
10060           N5=5
10070           CALL TIMRD(ICTRL,X,Y,N2,INFO,N5,KNT,ISTAT)
10080           RETURN
10090           END
10100 C
10110 C
10120 C
10130 C
10140           SUBROUTINE OUTPUT1(Q,N,TO)
10150 C THIS SUBROUTINE PRINTS OUT A VARIABLE IN TYP7 FORMAT
10160           INTEGER N
10170           REAL Q(N),TO
10180           WRITE(44,10) TO,(Q(K), K=1,N)
10190   10      FORMAT(2X,6(E12.5))
10200           RETURN
10210           END
10220 C
10230 C
10240           SUBROUTINE READ1
10250 C THIS SUBROUTINE IS A SET UP TO READ EACH CHANNEL OF T/H DATA
10260 C USING DISKRD
```

```
10270           COMMON /CNTRL/ NSPV,NSPL,NCV,SW(10)
10280           COMMON /IN/ X(50),T1(50,10),T2(50,10),W1(50,10),
10290       +     W2(50,10),H2RXD(50,10),H2ORXD(50,10),PRES(10)
10300           COMMON /A/ K,TMAX,NDATA,DT,TFLAG,FRACT
10310           DIMENSION YBUFF(50),XX(50)
10320           INTEGER NREC,NTAPE
10330           NREC=1
10340           NTAPE=21
10350           DO 10 K1=1,NCV
10360               CALL DISKRD(X,YBUFF,NDATA,NREC,NTAPE)
10370               NREC = NREC+1
10380               DO 15 K2= 1,NDATA
10390                   T1(K2,K1)=YBUFF(K2)
10400                   YBUFF(K2)=0.0
10410   15          CONTINUE
10420   10      CONTINUE
10430           DO 20 K3= 1,NCV
10440               CALL DISKRD(X,YBUFF,NDATA,NREC,NTAPE)
10450               NREC = NREC + 1
10460               DO 25 K4= 1, NDATA
10470                   T2(K4,K3)= YBUFF(K4)
10480                   YBUFF(K4)=0.0
10490   25          CONTINUE
10500   20      CONTINUE
10510           DO 30 K5=1,NCV
10520               CALL DISKRD(X,YBUFF,NDATA,NREC,NTAPE)
10530               NREC= NREC + 1
10540               DO 35 K6 = 1,NDATA
10550                   W1(K6,K5)=YBUFF(K6)
10560                   YBUFF(K6)=0.0
10570   35          CONTINUE
10580   30      CONTINUE
10590           DO 40 K7=1,NCV
10600               CALL DISKRD(X,YBUFF,NDATA,NREC,NTAPE)
10610               NREC= NREC + 1
10620               DO 45 K8= 1,NDATA
10630                    W2(K8,K7)=YBUFF(K8)
10640                    YBUFF(K8)=0.0
10650   45          CONTINUE
10660   40      CONTINUE
10670           DO 50 K9=1,NCV
10680               CALL DISKRD(X,YBUFF,NDATA,NREC,NTAPE)
10690               NREC= NREC + 1
10700               DO 55 L1=1,NDATA
10710                    H2ORXD(L1,K9)=YBUFF(K9)
10720                    YBUFF(K9)=0.0
10730   55          CONTINUE
10740   50      CONTINUE
10750           DO 60 L2=1,NCV
10760               CALL DISKRD(X,YBUFF,NDATA,NREC,NTAPE)
10770               NREC=NREC+1
10780               DO 65 L3=1,NDATA
10790                   H2RXD(L3,L2)=YBUFF(L2)
10800                   YBUFF(L2)=0.0
10810   65          CONTINUE
10820   60      CONTINUE
10830           CALL DISKRD(XX,YBUFF,NCV,NREC,NTAPE)
10840           DO 70 L4=1,NCV
10850               PRES(L4)=YBUFF(L4)
10860               YBUFF(L4)=0.0
```

```
10870  70     CONTINUE
10880         RETURN
10890         END
10900         SUBROUTINE LIQMOVE(RMASS,J)
10910         INTEGER J
10920         REAL RMASS(4,10),RODINV(4,10)
10930         COMMON /GEOM/ CLEN(10),AFLOW(10),SA(10),VOL(10),
10940     +                 DELZ(10),DROD
10950         COMMON /CNTRL/ NSPV,NSPL,NCV,SW(10)
10960         COMMON /FAIL/ DIROD,AFAIL,HO,VO,HEIGHT,WTFRAC(4)
10970         COMMON /LIQUID/ WLJUNC(4,10),DELTA(10),VEL(10),Y(4,10),
10980     +                   VISCL(10),RHOL(10),RSOURCE(4)
10990 C THIS SUBROUTINE IS A "QUICK FIX" USED TO TRY TO MODEL THE
11000 C POTENTIAL EUTECTIC FORMATION BETWEEN THE ALLOY AND ZIRCALLOY
11010 C IF THE TEMPERATURE OF THE NODE IS ABOVE STAINLESS STEEL
11020 C MELTING THEN ALL OF THE CONTROL ROD MASS IN THAT NODE (BOTH
11030 C THAT ON THE INSIDE AND THAT ON THE OUTSIDE OF THE ROD) IS
11040 C MOVED TO THE NEXT NODE. THE INTEGRATION BY THE DIFFERENTIAL
11050 C EQUATION SOLVER IS RESTARTED AND A SWITCH IS SET. WHEN ALL
11060 C NODES ARE ABOVE STAINLESS STEEL MELTING THE CODE IS STOPPED.
11070         DO 10 K=1,NSPL
11080           RODINV(K,J)= 3.14159*(DIROD**2.0)*RHOL(J)*DELZ(J)
11090           RODINV(K,J)=RODINV(K,J)*1000*WTFRAC(K)/4.0
11100           IF (J .NE. NCV) THEN
11110              RMASS(K,J+1) = RMASS(K,J+1)+RMASS(K,J) + RODINV(K,J)
11120              RMASS(K,J)=0.0
11130           ELSE
11140              RMASS(K,J)=0.0
11150           ENDIF
11160  10     CONTINUE
11170         SW(J)= 0.0
11180         RETURN
11190         END
11200 C
11210 C
11220 C
11230         SUBROUTINE LIQPROP
11240         COMMON /CNTRL/ NSPV,NSPL,NCV,SW(10)
11250         COMMON /TH/ TROD(10),TCOOL(10),WH2(10),WH2O(10),SH2(10),
11260     +    SH2O(10),RHOMIX(10),VISC(10),REY(10),IFLAG,PTOT(10),FWG(10)
11270         COMMON /LIQUID/ WLJUNC(4,10),DELTA(10),VEL(10),Y(4,10),
11280     +                   VISCL(10),RHOL(10),RSOURCE(4)
11290 C CALCULATE THE VISCOSITY AND DENSITY OF THE LIQUID ALLOY
11300 C VALUE OF THE VISCOSITY IS OF AG AT 1470K
11310         DO 5 N= 1,NCV
11320           VISCL(N)=2.98E-03
11330           IF (TROD(N) .LT. 1270) THEN
11340               RHOL(N)= 10120. - TROD(N)
11350           ELSE
11360               RHOL(N) = 8.85E+03
11370           ENDIF
11380   5     CONTINUE
11390         RETURN
11400         END
11410 C
11420 C
11430         SUBROUTINE VSOLVE(IFLAG,N,C1,C2,C3,C4,C,ROOT,GUESS,LFLOW)
11440 C THIS SUBROUTINE SOLVES FOR THE FILM VELOCITY AT EACH NODE
11450         REAL C1,C2,C3,C4,C,ROOT,GUESS
11460         REAL ROOT1,ROOT2
```

```
11470          INTEGER IFLAG,N,KOUNT,LFLOW
11480 C DETERMINE IF THE FLOW IS LAMINATOR OR TURBULENT BASED ON IFLAG
11490 C TO DETERMINE THE FORM OF THE MOMENTUM BALANCE
11500 C SOLUTIONS ARE CHECKED TO SEE IF THE VELOCITIES ARE IN THE RIGHT
11510 C REGIMES ROUGHLY BASED ON A CHECK WITH A TRANSITION REYNOLDS
11520 C NUMBER WHICH IS 1.33 TIMES THE ACTUAL TRANSITION REYNOLDS NUMBER
11530 C FOR LAMINAR FLOW AND IS 0.75 TIMES THE ACTUAL TRANSITION REYNOLDS
11540 C NUMBER IN TURBULENT FLOW.
11550          TOL=1.0E-05
11560          IF (IFLAG .EQ. 1) THEN
11570              ARG = (C2**2.0) - 4*C1*C3
11580              IF (ARG .LT. 0.0) GO TO 99
11590              ROOT1= -(C2/(2*C1)) + SQRT(ARG)/(2*C1)
11600              ROOT2= -(C2/(2*C1)) - SQRT(ARG)/(2*C1)
11610              IF ((ROOT1 .LT. 0.0) .AND. (ROOT2 .LT. 0.0)) THEN
11620                 GO TO 99
11630              ELSE IF ((ROOT1 .LT. 0) .AND. (ROOT2 .GE. 0.0)) THEN
11640                 IF (ROOT2 .GT. 1.33*C) THEN
11650                    IF (LFLOW  .EQ. 999) THEN
11660                      GO TO 99
11670                    ELSE
11680                      LFLOW=-999
11690                      GO TO 105
11700                    ENDIF
11710                 ELSE
11720                    ROOT= ROOT2
11730                    LFLOW=0
11740                 ENDIF
11750              ELSE IF((ROOT1 .GE. 0.0) .AND. (ROOT2 .LT. 0.0)) THEN
11760                 IF (ROOT1 .GT. 1.33*C) THEN
11770                    IF (LFLOW  .EQ. 999) THEN
11780                      GO TO 99
11790                    ELSE
11800                      LFLOW=-999
11810                      GO TO 105
11820                    ENDIF
11830                 ELSE
11840                    ROOT = ROOT1
11850                    LFLOW=0
11860                 ENDIF
11870              ELSE
11880                 IF ((ROOT1 .GT. 1.33*C) .AND. (ROOT2 .GT. 1.33*C)) THEN
11890                    IF (LFLOW  .EQ. 999) THEN
11900                      GO TO 99
11910                    ELSE
11920                      LFLOW=-999
11930                      GO TO 105
11940  *                 ENDIF
11950                 ELSE IF (ROOT2 .GT. 1.33*C) THEN
11960                    ROOT= ROOT1
11970                    LFLOW=0
11980                 ELSE
11990                    ROOT= ROOT2
12000                    LFLOW=0
12010                 ENDIF
12020              ENDIF
12030          ELSE
12040              KOUNT = 0
12050   15         TEMP= GUESS
12060              Z = C1*(GUESS**2.0) + C2*(GUESS**1.8) + C3*GUESS + C4
```

```
12070              ZPRIME= 2*C1*GUESS + 1.8*C2*(GUESS**0.8) + C3
12080              GUESS= GUESS -(Z/ZPRIME)
12090              TEST = (GUESS - TEMP)/TEMP
12100              IF (KOUNT .GE. 50) GO TO 99
12110              KOUNT = KOUNT + 1
12120              IF (ABS(TEST) .GT. TOL) GO TO 15
12130              IF (GUESS .LT. 0.75*C) THEN
12140                IF (LFLOW .EQ. -999) THEN
12150                  GO TO 99
12160                ELSE
12170                  LFLOW=999
12180                  GO TO 105
12190                ENDIF
12200              ENDIF
12210              ROOT= GUESS
12220              LFLOW=0
12230           ENDIF
12240           GO TO 105
12250   99      WRITE (8,100) N
12260   100     FORMAT (2X, "NO SOLUTION IN EITHER REGIME AT NODE",I5)
12270           WRITE (8,101) IFLAG,LFLOW,C1,C2,C3,C4,ROOT,GUESS,C
12280   101     FORMAT(2X,2I3,7E10.3)
12290           STOP
12300   105     RETURN
12310           END
12320           SUBROUTINE MOMEN
12330           COMMON /LIQUID/ WLJUNC(4,10),DELTA(10),VEL(10),Y(4,10),
12340        +                  VISCL(10),RHOL(10),RSOURCE(4)
12350           COMMON /TH/ TROD(10),TCOOL(10),WH2(10),WH2O(10),SH2(10),
12360        +   SH2O(10),RHOMIX(10),VISC(10),REY(10),IFLAG,PTOT(10),FWG(10)
12370           COMMON /FAIL/ DIROD,AFAIL,HO,VO,HEIGHT,WTFRAC(4)
12380           COMMON /CNTRL/ NSPV,NSPL,NCV,SW(10)
12390           COMMON /GEOM/ CLEN(10),AFLOW(10),SA(10),VOL(10),
12400        +                DELZ(10),DROD
12410           REAL X
12420           INTEGER IFLOW,LCHK
12430           G= 9.8
12440 C SET UP COEFFICIENTS OF MOMENTUM EQUATION
12450           DO 25 N= 1,NCV
12460                IF (DELTA(N) .LE. 1.0E-07) THEN
12470                   VEL(N)=0.0
12480                   GO TO 25
12490                ENDIF
12500 C              DETERMINE IF FLOW IS LAMINAR OR TURBULENT
12510 C              BASED ON THE VELOCITY AT PREVIOUS  TIME STEP
12520 C              THE TRANSITION OCCURS AT RE=1800 WHERE
12530 C              RE = 4*VEL*DELTA*RHOL/VISCL
12540 C              HOWEVER INORDER TO MAKE THE TRANSITION FROM LAMINAR
12550 C              SMOOTHER A RE=1502 WAS SELECTED.  THE SOLUTION TO THE
12560 C              MOMENTUM BALANCE IS THE SAME FOR LAMINAR AND TURBULENT
12570 C              FLOW AT THIS POINT SINCE THE FRICTION FACTORS MATCH.
12580                IFLOW = 0.0
12590                CUTOFF = (375.4931)*VISCL(N)/(RHOL(N)*DELTA(N))
12600                UG= (WH2(N) + WH2O(N))/(RHOMIX(N)*AFLOW(N))
12610                UG=UG/1000.
12620 C
12630                IF (VEL(N) .GE. CUTOFF) THEN
12640                   IFLOW= 2
12650                ELSE
12660                   IFLOW= 1
```

```
12670                ENDIF
12680                LCHK=0
12690 C
12700   17           IF (IFLOW .EQ. 1) THEN
12710 C                 LAMINAR FLOW
12720 C
12730 C                 INTERFACIAL SHEAR TERM
12740 C
12750                   ALPHA= -0.5*FWG(N)*RHOMIX(N)*DELZ(N)
12760                   ALPHA=ALPHA*(1 + 300*DELTA(N)/CLEN(N))
12770                   ALPHA=ALPHA*(DROD + 2*DELTA(N))
12780 C
12790 C                 WALL  SHEAR TERM
12800 C
12810                   BETA = -2*VISCL(N)*DROD*DELZ(N)/DELTA(N)
12820 C
12830 C                 ACCELERATION AND GRAVITY TERMS
12840 C
12850                   GAMMA= -DROD*RHOL(N)*DELTA(N)
12860                   IF (N .EQ. 1) THEN
12870                      DEL= DROD*RHOL(N)*DELTA(N)*G*DELZ(N)
12880       +                   + RHOL(N)*AFAIL*(VO**2.0)/3.14159
12890                   ELSE
12900                      DEL= DROD*RHOL(N)*DELTA(N)*G*DELZ(N)
12910       +                        + DROD*RHOL(N-1)*DELTA(N-1)*(VEL(N-1)**2)
12920                   ENDIF
12930 C REARRANGE TERMS FOR VELOCITY SOLVER
12940                   A = ALPHA + GAMMA
12950                   B = BETA - 2*UG*ALPHA
12960                   C = ALPHA*(UG**2.0) + DEL
12970                   D = 0.0
12980                   GUESS = 0.0
12990                ELSE
13000 C
13010 C TURBULENT FLOW CASE
13020 C
13030 C                 INTERFACIAL SHEAR TERM
13040                   ALPHA= -0.5*FWG(N)*(1 + 300*DELTA(N)/CLEN(N))*RHOMIX(N)
13050                   ALPHA=ALPHA*(DROD + 2*DELTA(N))*DELZ(N)
13060 C
13070 C                 WALL SHEAR TERM
13080                   BETA= - 0.01743*DELZ(N)*((VISCL(N)/DELTA(N))**0.2)
13090                   BETA= BETA*(RHOL(N)**0.8)*DROD
13100 C
13110 C                 ACCELERATION AND GRAVITY TERMS
13120 C
13130                   GAMMA= -DROD*RHOL(N)*DELTA(N)
13140                   IF (N .EQ. 1) THEN
13150                      DEL= DROD*RHOL(N)*DELTA(N)*G*DELZ(N)
13160       +                   + RHOL(N)*AFAIL*(VO**2.0)/3.14159
13170                   ELSE
13180                      DEL= DROD*RHOL(N-1)*DELTA(N-1)*(VEL(N-1)**2)
13190       +                        + DROD*RHOL(N)*DELTA(N)*G*DELZ(N)
13200                   ENDIF
13210 C REARRANGE FOR VELOCITY SOLVER
13220                      A = ALPHA + GAMMA
13230                      B = BETA
13240                      C = -2*UG*ALPHA
13250                      D = ALPHA*(UG**2.0) + DEL
13260 C
```

```
C SET UP INITIAL GUESS FOR NEWTON'S METHOD
C BASED ON A BALANCE BETWEEN GRAVITY AND WALL FRICTION (TURBULENT FLOW)
                    GUESS = 9.48*(DELTA(N)**0.667)*(G**0.556)
     +                          *((RHOL(N)/VISCL(N))**0.111)
              ENDIF
C
                 CALL VSOLVE(IFLOW,N,A,B,C,D,CUTOFF,X,GUESS,LCHK)
                 IF (LCHK .EQ. 0) THEN
                   GO TO 22
                 ELSE IF(LCHK .EQ. -999) THEN
                   IFLOW=2
                   GO TO 17
                 ELSE
                   IFLOW=1
                   GO TO 17
                 ENDIF
 22              VEL(N) = X
 25      CONTINUE
         RETURN
         END
C
C
         SUBROUTINE RODFAIL(TIME)
         COMMON /FAIL/ DIROD,AFAIL,HO,VO,HEIGHT,WTFRAC(4)
         REAL TIME
C THIS SUBROUTINE CALCULATE THE VELOCITY OF THE ALLOY AT THE
C POINT OF FAILURE IN THE GUIDE TUBE.  IT IS BASED ON A QUASI-
C STEADY BERNOULLI ANALYSIS INCORPORATING AN UNSTEADY MASS
C BALANCE WHICH RESULT IN THE GRAVITY HEAD CHANGING WITH TIME.
         PI=3.14159
         G=9.8
         AROD=PI*(DIROD**2.0)/4.0
         ALPHA=AFAIL/AROD
         IF (ALPHA .GT. 0.4712) THEN
            FORM = ALPHA**2.0
         ELSE
            FORM=0.42*(1-ALPHA)
         ENDIF
         GAMMA=SQRT(2*G*(ALPHA**2.0)/(1+FORM-(ALPHA**2.0)))
         TDRAIN=2*SQRT(HO)/GAMMA
         IF (TIME .LE. TDRAIN) THEN
            HEIGHT=(SQRT(HO)-0.5*GAMMA*TIME)**2.0
            VO=SQRT(2*G*HEIGHT/(1+FORM-(ALPHA**2.0)))
         ELSE
            HEIGHT= 0.0
            VO=0.0
         ENDIF
         RETURN
         END
C
C
         SUBROUTINE OUTPUT(VMASS,RMASS,T)
         REAL VMASS(6,10),RMASS(4,10),T
         COMMON /CNTRL/ NSPV,NSPL,NCV,SW(10)
         COMMON /A/ K,TMAX,NDATA,DT,TFLAG,FRACT
         COMMON /VAPOR/ CWALL(6,10),CBULK(6,10),PWALL(6,10),
     +   PBULK(6,10),XWALL(6,10),XBULK(6,10),DIFF(6,10),
     +   HD(6,10),SC(6,10),WVJUNC(6,10),DFLUX(6,10),FLVOUT(6),
     +   XN(6,10)
         COMMON /TH/ TROD(10),TCOOL(10),WH2(10),WH2O(10),SH2(10),
```

```
13870      +    SH2O(10),RHOMIX(10),VISC(10),REY(10),IFLAG,PTOT(10),FWG(10)
13880           COMMON /LIQUID/ WLJUNC(4,10),DELTA(10),VEL(10),Y(4,10),
13890      +                    VISCL(10),RHOL(10),RSOURCE(4)
13900           COMMON /FAIL/ DIROD,AFAIL,HO,VO,HEIGHT,WTFRAC(4)
13910           WRITE(8,90)
13920           WRITE(8,95)
13930           WRITE(8,94) T
13940           WRITE(8,96)
13950           WRITE(8,97) VO,HEIGHT
13960           WRITE(8,98)
13970           WRITE(8,99) (I,RSOURCE(I),I=1,NSPL)
13980           WRITE(8,95)
13990           WRITE(8,101)
14000           DO 5 J=1,NCV
14010             WRITE(8,102)J
14020             WRITE(8,100)
14030             WRITE(8, 103) TROD(J),TCOOL(J),PTOT(J),DELTA(J),VEL(J)
14040             WRITE(8,104)
14050             WRITE(8,105)
14060             DO 10 K1=1,NSPV
14070               IF (J .EQ. 1) THEN
14080                 WRITE(8,106) K1,PBULK(K1,J),XN(K1,J),VMASS(K1,J),
14090      +                       WVJUNC(K1,J),FLVOUT(K1)
14100               ELSE
14110                 WRITE(8,107) K1,PBULK(K1,J),XN(K1,J),VMASS(K1,J)
14120      +                                  ,WVJUNC(K1,J)
14130               ENDIF
14140  10         CONTINUE
14150             WRITE(8,95)
14160             WRITE(8,108)
14170             WRITE(8,109)
14180             DO 15 L=1,NSPL
14190               WRITE(8,110) L,PWALL(L,J),RMASS(L,J),WLJUNC(L,J)
14200  15         CONTINUE
14210  5        CONTINUE
14220  90       FORMAT(2X,"***** OUTPUT RESULTS *****")
14230  95       FORMAT(2X)
14240  94       FORMAT(2X,"TIME=",2X,F8.3,2X,"SEC")
14250  96       FORMAT(2X,"***** ROD FAILURE DATA *****")
14260  97       FORMAT(2X,"VELOCITY AT EXIT (M/S)",1X,F8.3,1X,"HEIGHT (M)="
14270      +          ,1X,F8.3)
14280  98       FORMAT(2X,"SPECIES NO.",3X,"SOURCE RATE (G/S)")
14290  99       FORMAT(3X,I5,11X,F8.3)
14300  101      FORMAT(2X,"***** THERMAL HYDRAULIC RESULTS *****")
14310  102      FORMAT(2X,"VOLUME OR JUNCTION NUMBER = ",I5)
14320  103      FORMAT(2X,3(F8.3,2X),2(E10.3,2X))
14330  100      FORMAT(2X,"TROD(K)",3X,"TCOOL(K)",3X,"PTOT(ATM)",3X,
14340      +            "DELTA(M)",3X,"VELOCITY OF ALLOY (M/S)")
14350  104      FORMAT(2X,"***** VAPOR RESULTS *****")
14360  105      FORMAT(2X,"SPECIES NO.",2X,"PBULK(ATM)",2X,"XN(MOLES/S)",
14370      +       2X,"VAPOR(G)",3X,"WVJUNC(G/S)",2X,"FLVOUT(G/S)")
14380  106      FORMAT(3X,I4,7X,5(E10.3,2X))
14390  107      FORMAT(6X,I4,4(E10.3,2X))
14400  108      FORMAT(2X,"***** LIQUID RESULTS *****")
14410  109      FORMAT(2X,"SPECIES NO",4X,"PWALL(ATM)",2X,"LIQUID(G)",
14420      +         2X,"WLJUNC(G/S)")
14500  110      FORMAT(4X,I4,6X,3(E10.3,2X))
14510           RETURN
14520           END
14530 C
```

```
14540           SUBROUTINE TSTEP(TIME,TEND)
14550           COMMON /A/ K,TMAX,NDATA,DT,TFLAG,FRACT
14560           COMMON /IN/ X(50),T1(50,10),T2(50,10),W1(50,10),
14570       +     W2(50,10),H2RXD(50,10),H2ORXD(50,10),PRES(10)
14580           REAL TIME,TEND
14590           INTEGER KSTOP,KNEW
14600 C   THIS SUBROUTINE DTERMINES THE TIME STEP FOR THE DIFFERENTIAL
14601 C   EQUATION SOLVER. IF TFLAG = -1 THEN INTEGRATE TO THE NEXT
14602 C   NEAREST INPUT TIME X(K). IF TFLAG > 0.0 THEN USE THE VALUE
14603 C   OF FRACT TO DETERMINE THE TIME STEP. FOR TFLAG > 0, THE TIME
14604 C   STEP IS EQUAL TO FRACT IF TIME + FRACT < THE NEXT INPUT TIME
14605 C   (FOR THIS CASE TFLAG=1.0) IF TIME + FRACT > THE NEXT
14606 C   INPUT TIME THEN THE TIME STEP IS SET EQUAL TO X(K)-TIME
14607 C   (TFLAG = 0.0 FOR THIS CASE).
14610           IF (TIME .LT. X(K+1)) THEN
14620             IF ( K .EQ. 1) THEN
14630                DT = 0.0
14640                GO TO 19
14650             ENDIF
14660             IF (TIME .EQ. X(K)) THEN
14670               DT = TIME - X(K-1)
14680             ELSE
14690               DT = TIME - X(K)
14700             ENDIF
14710   19        IF (TFLAG .EQ. -1) THEN
14720               K = K+1
14730               TEND= X(K)
14740               GO TO 10
14750             ENDIF
14760             TAU = 1.0*FRACT
14770             IF ((TIME + TAU) .GT. X(K+1)) THEN
14780               TFLAG= 0.0
14790               K = K+1
14800               TEND = X(K)
14810             ELSE
14820               TEND = TIME + TAU
14830               TFLAG = 1.0
14840             ENDIF
14850           ELSE
14860            KNEW = 50
14870            KSTOP= K
14880            DO 11 L=50,KSTOP,-1
14890              IF (TIME .LT. X(L)) KNEW = L
14900   11       CONTINUE
14910            K= KNEW
14920            TEND = X(K)
14930            DT= TIME - X(K-1)
14940           ENDIF
14950   10      RETURN
14960           END
>  end of vapor code listing
```

B.2 VAPOR Input

This input file contains material properties for Ag, In and Cd and geometrical input needed for VAPOR. Thermal hydraulic input for VAPOR is contained in a non-ASCII file and hence cannot be printed. The reader is recommended to look at Tables 4.2 and 4.3 for a description of the thermal hydraulic conditions.

```
      5     3     3
4767.0     339.0   1.26E+04    7.989   107.8     0.85
4377.0     347.5   1.27E+04    8.284   114.82    0.15
1903.0     217.6   5.31E+03    7.990   112.4     0.05
  33.3     65.0        2.0
 647.38    56.7       18.0
 8.46E-04   1.13E-02   3.83E-03    8.46E-05    1.0E-01
 8.46E-04   1.13E-02   3.83E-03    8.46E-05    1.0E-01
 8.46E-04   1.13E-02   3.83E-03    8.46E-05    1.0E-01
  1.224E-02 1.143E-02    1.0E-05    5.0E-01
   20.      20       0.0       0.5
```

B.3 VAPOR Output

Two output files from VAPOR are attached. The first output file provides detailed time dependent information from the various models in VAPOR on the downward relocation and vaporization behavior of the Ag-In-Cd alloy. The second output file contains the release rates of Ag, In and Cd as functions of time and is used for preparing plots.

```
 ECHO INPUT DATA
 VAPOR SPECIES, LIQUID SPECIES,CONTROL VOLUMES
      5          3          3
 CRITCAL CONSTANT PARAMETERS
4767.00   339.00   .126E+05    7.989  107.800     .850
4377.00   347.50   .127E+05    8.284  114.820     .150
1903.00   217.60   .531E+04    7.990  112.400     .050
  33.30    65.00     2.00
 647.38    56.70    18.00
 GEOMETRICAL PARAMETERS
 .846E-03   .113E-01   .383E-02   .846E-04   .100E+00
 .846E-03   .113E-01   .383E-02   .846E-04   .100E+00
 .846E-03   .113E-01   .383E-02   .846E-04   .100E+00
   .122E-01   .114E-01   .100E-04   .500E+00
 TIME PARAMETERS
 20.000    20
 ***** OUTPUT RESULTS *****

 TIME=      1.000  SEC
 ***** ROD FAILURE DATA *****
 VELOCITY AT EXIT (M/S)     2.675 HEIGHT (M)=      .500
 SPECIES NO.    SOURCE RATE (G/S)
           1          -I

           2          -I
           3          -I

 ***** THERMAL HYDRAULIC RESULTS *****
 VOLUME OR JUNCTION NUMBER =      1
 TROD(K)    TCOOL(K)  PTOT(ATM) DELTA(M)  VELOCITY OF ALLOY (M/S)
 1800.000  1810.000    68.030     .111E-04     .309E+00
 ***** VAPOR RESULTS *****
 SPECIES NO.   PBULK(ATM)  XN(MOLES/S) VAPOR(G)   WVJUNC(G/S) FLVOUT(G/S)
             1  .000E+00     .000E+00     .000E+00     .000E+00          -I
             2  .000E+00     .000E+00     .000E+00     .000E+00          -I
             3  .000E+00     .000E+00     .000E+00     .000E+00          -I
             4  .340E+02     .000E+00     .388E-01     .000E+00          -I
             5  .340E+02     .000E+00     .349E+00     .000E+00          -I

 ***** LIQUID RESULTS *****
 SPECIES NO  PWALL(ATM)  LIQUID(G)  WLJUNC(G/S)
             1  .000E+00     .129E+01     .000E+00
             2  .000E+00     .227E+00     .000E+00
             3  .000E+00     .757E-01     .000E+00
 VOLUME OR JUNCTION NUMBER =      2
 TROD(K)    TCOOL(K)  PTOT(ATM) DELTA(M)  VELOCITY OF ALLOY (M/S)
 1780.000  1790.000    68.030     .111E-04     .179E-02

 ***** VAPOR RESULTS *****
 SPECIES NO.   PBULK(ATM)  XN(MOLES/S) VAPOR(G)   WVJUNC(G/S) FLVOUT(G/S)
         1  .000E+00     .000E+00     .000E+00     .000E+00
         2  .000E+00     .000E+00     .000E+00     .000E+00
         3  .000E+00     .000E+00     .000E+00     .000E+00
         4  .340E+02     .000E+00     .392E-01     .000E+00
         5  .340E+02     .000E+00     .353E+00     .000E+00

 ***** LIQUID RESULTS *****
 SPECIES NO  PWALL(ATM)  LIQUID(G)  WLJUNC(G/S)
             1  .000E+00     .129E+01     .000E+00
```

```
          2   .000E+00     .227E+00     .000E+00
          3   .000E+00     .757E-01     .000E+00
VOLUME OR JUNCTION NUMBER =      3
TROD(K)    TCOOL(K)   PTOT(ATM) DELTA(M)   VELOCITY OF ALLOY (M/S)
1760.000   1770.000     68.030     .111E-04     .161E-02
***** VAPOR RESULTS *****
SPECIES NO.   PBULK(ATM)   XN(MOLES/S) VAPOR(G)    WVJUNC(G/S) FLVOUT(G/S)
       1   .000E+00     .000E+00     .000E+00     .000E+00
       2   .000E+00     .000E+00     .000E+00     .000E+00
       3   .000E+00     .000E+00     .000E+00     .000E+00
       4   .340E+02     .000E+00     .396E-01     .000E+00
       5   .340E+02     .000E+00     .357E+00     .000E+00


***** LIQUID RESULTS *****
SPECIES NO   PWALL(ATM)   LIQUID(G)   WLJUNC(G/S)
          1   .000E+00     .129E+01     .000E+00
          2   .000E+00     .227E+00     .000E+00
          3   .000E+00     .757E-01     .000E+00
***** OUTPUT RESULTS *****

TIME=      2.034   SEC
***** ROD FAILURE DATA *****
VELOCITY AT EXIT (M/S)     1.954 HEIGHT (M)=      .267
SPECIES NO.    SOURCE RATE (G/S)
          1     146.972
          2      25.936
          3       8.645

***** THERMAL HYDRAULIC RESULTS *****
VOLUME OR JUNCTION NUMBER =      1
TROD(K)    TCOOL(K)   PTOT(ATM) DELTA(M)   VELOCITY OF ALLOY (M/S)
1805.171   1815.171     68.289     .417E-03     .129E+01
***** VAPOR RESULTS *****
SPECIES NO.   PBULK(ATM)   XN(MOLES/S) VAPOR(G)    WVJUNC(G/S) FLVOUT(G/S)
          1   .282E-03     .298E-06     .173E-04     .465E-04     .744E-04

          2   .811E-04     .858E-07     .530E-05     .142E-04     .228E-04
          3   .259E+00     .249E-03     .166E-01     .475E-01     .712E-01
          4   .340E+02     .000E+00     .388E-01     .167E+00     .167E+00
          5   .340E+02     .000E+00     .349E+00     .150E+01     .150E+01

***** LIQUID RESULTS *****
SPECIES NO   PWALL(ATM)   LIQUID(G)   WLJUNC(G/S)
          1   .105E-01     .115E+02     .148E+03
          2   .302E-02     .203E+01     .261E+02
          3   .664E+01     .674E+00     .868E+01
VOLUME OR JUNCTION NUMBER =      2
TROD(K)    TCOOL(K)   PTOT(ATM) DELTA(M)   VELOCITY OF ALLOY (M/S)
1785.171   1795.171     68.203     .481E-03     .113E+01
***** VAPOR RESULTS *****
SPECIES NO.   PBULK(ATM)   XN(MOLES/S) VAPOR(G)    WVJUNC(G/S) FLVOUT(G/S)
       1   .176E-03     .245E-06     .109E-04     .215E-04
       2   .506E-04     .706E-07     .335E-05     .658E-05
       3   .173E+00     .229E-03     .112E-01     .234E-01
       4   .340E+02     .000E+00     .392E-01     .167E+00
       5   .340E+02     .000E+00     .353E+00     .150E+01

***** LIQUID RESULTS *****
SPECIES NO   PWALL(ATM)   LIQUID(G)   WLJUNC(G/S)
```

```
           1   .876E-02     .133E+02     .150E+03
           2   .252E-02     .234E+01     .265E+02
           3   .614E+01     .775E+00     .878E+01
VOLUME OR JUNCTION NUMBER =      3
TROD(K)    TCOOL(K)  PTOT(ATM) DELTA(M)  VELOCITY OF ALLOY (M/S)
1765.171   1775.171    68.115    .507E-03     .109E+01
***** VAPOR RESULTS *****
SPECIES NO.   PBULK(ATM)  XN(MOLES/S) VAPOR(G)   WVJUNC(G/S) FLVOUT(G/S)
       1   .814E-04     .202E-06     .511E-05     .000E+00
       2   .234E-04     .580E-07     .156E-05     .000E+00
       3   .848E-01     .210E-03     .555E-02     .000E+00
       4   .340E+02     .000E+00     .396E-01     .167E+00
       5   .340E+02     .000E+00     .357E+00     .150E+01

***** LIQUID RESULTS *****
SPECIES NO  PWALL(ATM)  LIQUID(G)  WLJUNC(G/S)
           1   .728E-02     .140E+02     .153E+03
           2   .209E-02     .247E+01     .270E+02
           3   .566E+01     .815E+00     .891E+01
***** OUTPUT RESULTS *****

TIME=      3.164  SEC
***** ROD FAILURE DATA *****
VELOCITY AT EXIT (M/S)     1.166 HEIGHT (M)=      .095
SPECIES NO.    SOURCE RATE (G/S)
           1      87.698
           2      15.476
           3       5.159

***** THERMAL HYDRAULIC RESULTS *****
VOLUME OR JUNCTION NUMBER =      1
TROD(K)    TCOOL(K)  PTOT(ATM) DELTA(M)  VELOCITY OF ALLOY (M/S)
1810.821   1820.821    68.511    .351E-03     .930E+00
***** VAPOR RESULTS *****
SPECIES NO.   PBULK(ATM)  XN(MOLES/S) VAPOR(G)   WVJUNC(G/S) FLVOUT(G/S)
           1   .319E-03     .312E-06     .195E-04     .507E-04     .841E-04
           2   .918E-04     .900E-07     .598E-05     .155E-04     .258E-04
           3   .286E+00     .253E-03     .182E-01     .503E-01     .786E-01
           4   .341E+02     .000E+00     .388E-01     .167E+00     .167E+00

           5   .341E+02     .000E+00     .349E+00     .150E+01     .150E+01

***** LIQUID RESULTS *****
SPECIES NO  PWALL(ATM)  LIQUID(G)  WLJUNC(G/S)
           1   .110E-01     .968E+01     .900E+02
           2   .316E-02     .171E+01     .159E+02
           3   .676E+01     .566E+00     .526E+01
VOLUME OR JUNCTION NUMBER =      2
TROD(K)    TCOOL(K)  PTOT(ATM) DELTA(M)  VELOCITY OF ALLOY (M/S)
1790.821   1800.821    68.410    .375E-03     .900E+00
***** VAPOR RESULTS *****
SPECIES NO.   PBULK(ATM)  XN(MOLES/S) VAPOR(G)   WVJUNC(G/S) FLVOUT(G/S)
       1   .193E-03     .258E-06     .119E-04     .230E-04
       2   .554E-04     .743E-07     .364E-05     .703E-05
       3   .183E+00     .233E-03     .118E-01     .241E-01
       4   .341E+02     .000E+00     .392E-01     .167E+00
       5   .341E+02     .000E+00     .353E+00     .150E+01

***** LIQUID RESULTS *****
```

```
SPECIES NO  PWALL(ATM)  LIQUID(G)  WLJUNC(G/S)
           1  .919E-02    .103E+02    .930E+02
           2  .264E-02    .182E+01    .164E+02
           3  .624E+01    .602E+00    .542E+01

VOLUME OR JUNCTION NUMBER =     3
TROD(K)   TCOOL(K)  PTOT(ATM) DELTA(M)  VELOCITY OF ALLOY (M/S)
1770.821  1780.821    68.317    .387E-03    .903E+00
***** VAPOR RESULTS *****
SPECIES NO.  PBULK(ATM)  XN(MOLES/S) VAPOR(G)   WVJUNC(G/S) FLVOUT(G/S)
       1  .872E-04    .213E-06    .544E-05    .000E+00
       2  .251E-04    .611E-07    .166E-05    .000E+00
       3  .879E-01    .214E-03    .572E-02    .000E+00
       4  .341E+02    .000E+00    .396E-01    .167E+00
       5  .341E+02    .000E+00    .357E+00    .150E+01

***** LIQUID RESULTS *****
SPECIES NO  PWALL(ATM)  LIQUID(G)  WLJUNC(G/S)
           1  .764E-02    .107E+02    .963E+02
           2  .219E-02    .188E+01    .170E+02
           3  .575E+01    .619E+00    .559E+01
***** OUTPUT RESULTS *****

TIME=     4.135  SEC
***** ROD FAILURE DATA *****
VELOCITY AT EXIT (M/S)     .489 HEIGHT (M)=     .017
SPECIES NO.   SOURCE RATE (G/S)
           1     36.754
           2      6.486
           3      2.162

***** THERMAL HYDRAULIC RESULTS *****
VOLUME OR JUNCTION NUMBER =     1
TROD(K)   TCOOL(K)  PTOT(ATM) DELTA(M)  VELOCITY OF ALLOY (M/S)
1815.676  1825.676    68.729    .239E-03    .625E+00
***** VAPOR RESULTS *****
SPECIES NO.  PBULK(ATM)  XN(MOLES/S) VAPOR(G)   WVJUNC(G/S) FLVOUT(G/S)
           1  .336E-03    .329E-06    .206E-04    .533E-04    .884E-04
           2  .969E-04    .949E-07    .630E-05    .163E-04    .271E-04
           3  .292E+00    .257E-03    .186E-01    .510E-01    .799E-01
           4  .342E+02    .000E+00    .388E-01    .167E+00    .167E+00
           5  .342E+02    .000E+00    .349E+00    .150E+01    .150E+01

***** LIQUID RESULTS *****
SPECIES NO  PWALL(ATM)  LIQUID(G)  WLJUNC(G/S)

           1  .116E-01    .658E+01    .412E+02
           2  .333E-02    .116E+01    .726E+01
           3  .686E+01    .383E+00    .239E+01
VOLUME OR JUNCTION NUMBER =     2
TROD(K)   TCOOL(K)  PTOT(ATM) DELTA(M)  VELOCITY OF ALLOY (M/S)
1795.676  1805.676    68.628    .247E-03    .666E+00
***** VAPOR RESULTS *****
SPECIES NO.  PBULK(ATM)  XN(MOLES/S) VAPOR(G)   WVJUNC(G/S) FLVOUT(G/S)
       1  .203E-03    .272E-06    .125E-04    .241E-04
       2  .584E-04    .783E-07    .384E-05    .739E-05
       3  .186E+00    .236E-03    .120E-01    .244E-01
       4  .342E+02    .000E+00    .392E-01    .167E+00
       5  .342E+02    .000E+00    .353E+00    .150E+01
```

```
***** LIQUID RESULTS *****
SPECIES NO  PWALL(ATM)  LIQUID(G)  WLJUNC(G/S)
           1  .967E-02    .682E+01    .454E+02
           2  .278E-02    .120E+01    .801E+01
           3  .632E+01    .393E+00    .262E+01
VOLUME OR JUNCTION NUMBER =     3
TROD(K)   TCOOL(K)  PTOT(ATM) DELTA(M)  VELOCITY OF ALLOY (M/S)
1775.676  1785.676    68.535    .259E-03    .691E+00
***** VAPOR RESULTS *****

SPECIES NO.  PBULK(ATM)  XN(MOLES/S) VAPOR(G)   WVJUNC(G/S) FLVOUT(G/S)
       1  .919E-04    .224E-06    .575E-05    .000E+00
       2  .264E-04    .645E-07    .176E-05    .000E+00
       3  .892E-01    .217E-03    .581E-02    .000E+00
       4  .342E+02    .000E+00    .396E-01    .167E+00
       5  .342E+02    .000E+00    .357E+00    .150E+01

***** LIQUID RESULTS *****
SPECIES NO  PWALL(ATM)  LIQUID(G)  WLJUNC(G/S)
           1  .806E-02    .715E+01    .494E+02
           2  .231E-02    .126E+01    .872E+01
           3  .581E+01    .410E+00    .284E+01
***** OUTPUT RESULTS *****

TIME=     5.002  SEC
***** ROD FAILURE DATA *****
VELOCITY AT EXIT (M/S)     .000 HEIGHT (M)=     .000
SPECIES NO.   SOURCE RATE (G/S)
          1       .000
          2       .000
          3       .000

***** THERMAL HYDRAULIC RESULTS *****

VOLUME OR JUNCTION NUMBER =     1
TROD(K)   TCOOL(K)  PTOT(ATM) DELTA(M)  VELOCITY OF ALLOY (M/S)
1820.012  1830.012    68.910    .929E-04    .121E+00
***** VAPOR RESULTS *****
SPECIES NO.  PBULK(ATM)  XN(MOLES/S) VAPOR(G)   WVJUNC(G/S) FLVOUT(G/S)
           1  .352E-03    .342E-06    .214E-04    .557E-04    .923E-04
           2  .101E-03    .986E-07    .658E-05    .171E-04    .283E-04
           3  .290E+00    .245E-03    .184E-01    .504E-01    .793E-01
           4  .343E+02    .000E+00    .388E-01    .167E+00    .167E+00
           5  .343E+02    .000E+00    .349E+00    .150E+01    .150E+01

***** LIQUID RESULTS *****
SPECIES NO  PWALL(ATM)  LIQUID(G)  WLJUNC(G/S)
           1  .121E-01    .257E+01    .312E+01
           2  .348E-02    .453E+00    .551E+00
           3  .659E+01    .141E+00    .171E+00
VOLUME OR JUNCTION NUMBER =     2
TROD(K)   TCOOL(K)  PTOT(ATM) DELTA(M)  VELOCITY OF ALLOY (M/S)
1800.012  1810.012    68.811    .118E-03    .196E+00
***** VAPOR RESULTS *****
SPECIES NO.  PBULK(ATM)  XN(MOLES/S) VAPOR(G)   WVJUNC(G/S) FLVOUT(G/S)
       1  .213E-03    .283E-06    .131E-04    .252E-04
       2  .612E-04    .816E-07    .401E-05    .773E-05

       3  .185E+00    .227E-03    .118E-01    .240E-01
       4  .343E+02    .000E+00    .392E-01    .167E+00
```

```
       5  .343E+02     .000E+00     .353E+00     .150E+01

***** LIQUID RESULTS *****
SPECIES NO  PWALL(ATM)  LIQUID(G)  WLJUNC(G/S)
           1  .101E-01     .327E+01     .641E+01
           2  .291E-02     .577E+00     .113E+01
           3  .611E+01     .179E+00     .350E+00
VOLUME OR JUNCTION NUMBER =      3
TROD(K)   TCOOL(K)  PTOT(ATM) DELTA(M)  VELOCITY OF ALLOY (M/S)
1780.012  1790.012    68.721     .135E-03     .255E+00
***** VAPOR RESULTS *****
SPECIES NO.  PBULK(ATM)  XN(MOLES/S) VAPOR(G)   WVJUNC(G/S) FLVOUT(G/S)
       1  .963E-04     .234E-06     .600E-05     .000E+00
       2  .277E-04     .673E-07     .184E-05     .000E+00
       3  .879E-01     .210E-03     .571E-02     .000E+00
       4  .343E+02     .000E+00     .396E-01     .167E+00
       5  .343E+02     .000E+00     .357E+00     .150E+01

***** LIQUID RESULTS *****
SPECIES NO  PWALL(ATM)  LIQUID(G)  WLJUNC(G/S)
           1  .845E-02     .373E+01     .951E+01

           2  .242E-02     .658E+00     .168E+01
           3  .565E+01     .204E+00     .519E+00
***** OUTPUT RESULTS *****

TIME=     6.114  SEC
***** ROD FAILURE DATA *****
VELOCITY AT EXIT (M/S)      .000 HEIGHT (M)=      .000
SPECIES NO.    SOURCE RATE (G/S)
           1         .000
           2         .000
           3         .000

***** THERMAL HYDRAULIC RESULTS *****
VOLUME OR JUNCTION NUMBER =      1
TROD(K)   TCOOL(K)  PTOT(ATM) DELTA(M)  VELOCITY OF ALLOY (M/S)
1825.568  1835.568    69.026     .479E-04     .321E-01
***** VAPOR RESULTS *****
SPECIES NO.  PBULK(ATM)  XN(MOLES/S) VAPOR(G)   WVJUNC(G/S) FLVOUT(G/S)
           1  .363E-03     .347E-06     .221E-04     .574E-04     .949E-04
           2  .105E-03     .100E-06     .677E-05     .176E-04     .291E-04
           3  .244E+00     .175E-03     .154E-01     .428E-01     .664E-01
           4  .344E+02     .000E+00     .388E-01     .167E+00     .167E+00
           5  .344E+02     .000E+00     .349E+00     .150E+01     .150E+01


***** LIQUID RESULTS *****
SPECIES NO  PWALL(ATM)  LIQUID(G)  WLJUNC(G/S)
           1  .127E-01     .134E+01     .431E+00
           2  .366E-02     .237E+00     .761E-01
           3  .488E+01     .528E-01     .170E-01
VOLUME OR JUNCTION NUMBER =      2
TROD(K)   TCOOL(K)  PTOT(ATM) DELTA(M)  VELOCITY OF ALLOY (M/S)
1805.568  1815.568    68.948     .633E-04     .565E-01
***** VAPOR RESULTS *****
SPECIES NO.  PBULK(ATM)  XN(MOLES/S) VAPOR(G)   WVJUNC(G/S) FLVOUT(G/S)
       1  .220E-03     .290E-06     .135E-04     .260E-04
       2  .632E-04     .834E-07     .413E-05     .797E-05
       3  .157E+00     .178E-03     .101E-01     .205E-01
```

```
       4  .344E+02     .000E+00     .392E-01     .167E+00
       5  .344E+02     .000E+00     .353E+00     .150E+01

***** LIQUID RESULTS *****
SPECIES NO  PWALL(ATM)  LIQUID(G)  WLJUNC(G/S)
           1  .106E-01     .177E+01     .998E+00
           2  .306E-02     .312E+00     .176E+00
           3  .489E+01     .754E-01     .426E-01
VOLUME OR JUNCTION NUMBER =      3

TROD(K)   TCOOL(K)  PTOT(ATM) DELTA(M)  VELOCITY OF ALLOY (M/S)
1785.568  1795.568    68.875    .750E-04     .796E-01
***** VAPOR RESULTS *****
SPECIES NO.  PBULK(ATM)  XN(MOLES/S) VAPOR(G)   WVJUNC(G/S) FLVOUT(G/S)
       1  .995E-04     .241E-06     .618E-05     .000E+00
       2  .286E-04     .692E-07     .189E-05     .000E+00
       3  .753E-01     .173E-03     .488E-02     .000E+00
       4  .344E+02     .000E+00     .396E-01     .167E+00
       5  .344E+02     .000E+00     .357E+00     .150E+01

***** LIQUID RESULTS *****
SPECIES NO  PWALL(ATM)  LIQUID(G)  WLJUNC(G/S)
           1  .886E-02     .209E+01     .166E+01
           2  .254E-02     .369E+00     .294E+00
           3  .474E+01     .934E-01     .744E-01
***** OUTPUT RESULTS *****

TIME=     7.094  SEC
***** ROD FAILURE DATA *****
VELOCITY AT EXIT (M/S)      .000 HEIGHT (M)=      .000
SPECIES NO.    SOURCE RATE (G/S)
           1         .000
           2         .000

           3         .000

***** THERMAL HYDRAULIC RESULTS *****
VOLUME OR JUNCTION NUMBER =      1
TROD(K)   TCOOL(K)  PTOT(ATM) DELTA(M)  VELOCITY OF ALLOY (M/S)
1830.468  1840.468    69.177    .372E-04     .192E-01
***** VAPOR RESULTS *****
SPECIES NO.  PBULK(ATM)  XN(MOLES/S) VAPOR(G)   WVJUNC(G/S) FLVOUT(G/S)
           1  .377E-03     .356E-06     .227E-04     .598E-04     .982E-04
           2  .109E-03     .103E-06     .698E-05     .183E-04     .301E-04
           3  .185E+00     .115E-03     .117E-01     .334E-01     .503E-01
           4  .345E+02     .000E+00     .388E-01     .167E+00     .167E+00
           5  .345E+02     .000E+00     .349E+00     .150E+01     .150E+01

***** LIQUID RESULTS *****
SPECIES NO  PWALL(ATM)  LIQUID(G)  WLJUNC(G/S)
           1  .135E-01     .105E+01     .203E+00
           2  .389E-02     .186E+00     .358E-01
           3  .330E+01     .272E-01     .523E-02
VOLUME OR JUNCTION NUMBER =      2
TROD(K)   TCOOL(K)  PTOT(ATM) DELTA(M)  VELOCITY OF ALLOY (M/S)
1810.468  1820.468    69.125    .492E-04     .339E-01
***** VAPOR RESULTS *****

SPECIES NO.  PBULK(ATM)  XN(MOLES/S) VAPOR(G)   WVJUNC(G/S) FLVOUT(G/S)
       1  .229E-03     .299E-06     .139E-04     .274E-04
```

```
       2   .661E-04     .863E-07     .427E-05     .841E-05
       3   .123E+00     .130E-03     .783E-02     .164E-01
       4   .345E+02     .000E+00     .392E-01     .167E+00
       5   .345E+02     .000E+00     .353E+00     .150E+01

***** LIQUID RESULTS *****
SPECIES NO  PWALL(ATM)  LIQUID(G)  WLJUNC(G/S)
           1  .113E-01     .139E+01     .471E+00
           2  .324E-02     .245E+00     .831E-01
           3  .365E+01     .429E-01     .146E-01
VOLUME OR JUNCTION NUMBER =      3
TROD(K)   TCOOL(K)  PTOT(ATM) DELTA(M)  VELOCITY OF ALLOY (M/S)
1790.468  1800.468    69.073    .584E-04     .480E-01
***** VAPOR RESULTS *****
SPECIES NO.  PBULK(ATM)  XN(MOLES/S) VAPOR(G)   WVJUNC(G/S) FLVOUT(G/S)
       1  .105E-03     .250E-06     .641E-05     .000E+00
       2  .303E-04     .720E-07     .196E-05     .000E+00
       3  .605E-01     .135E-03     .387E-02     .000E+00
       4  .345E+02     .000E+00     .396E-01     .167E+00
       5  .345E+02     .000E+00     .357E+00     .150E+01


***** LIQUID RESULTS *****
SPECIES NO  PWALL(ATM)  LIQUID(G)  WLJUNC(G/S)
           1  .940E-02     .164E+01     .789E+00
           2  .270E-02     .290E+00     .139E+00
           3  .376E+01     .564E-01     .271E-01
***** OUTPUT RESULTS *****

TIME=     8.218  SEC
***** ROD FAILURE DATA *****
VELOCITY AT EXIT (M/S)     .000 HEIGHT (M)=      .000
SPECIES NO.   SOURCE RATE (G/S)
           1        .000
           2        .000
           3        .000

***** THERMAL HYDRAULIC RESULTS *****
VOLUME OR JUNCTION NUMBER =      1
TROD(K)   TCOOL(K)  PTOT(ATM) DELTA(M)  VELOCITY OF ALLOY (M/S)
1836.090  1846.090    69.298    .309E-04     .131E-01
***** VAPOR RESULTS *****
SPECIES NO.  PBULK(ATM)  XN(MOLES/S) VAPOR(G)   WVJUNC(G/S) FLVOUT(G/S)
           1  .386E-03     .365E-06     .234E-04     .611E-04     .100E-03
           2  .111E-03     .105E-06     .718E-05     .187E-04     .308E-04

           3  .122E+00     .634E-04     .772E-02     .229E-01     .332E-01
           4  .346E+02     .000E+00     .388E-01     .167E+00     .167E+00
           5  .346E+02     .000E+00     .349E+00     .150E+01     .150E+01

***** LIQUID RESULTS *****
SPECIES NO  PWALL(ATM)  LIQUID(G)  WLJUNC(G/S)
           1  .142E-01     .882E+00     .116E+00
           2  .410E-02     .156E+00     .205E-01
           3  .188E+01     .126E-01     .166E-02
VOLUME OR JUNCTION NUMBER =      2
TROD(K)   TCOOL(K)  PTOT(ATM) DELTA(M)  VELOCITY OF ALLOY (M/S)
1816.090  1826.090    69.273    .408E-04     .232E-01
***** VAPOR RESULTS *****
SPECIES NO.  PBULK(ATM)  XN(MOLES/S) VAPOR(G)   WVJUNC(G/S) FLVOUT(G/S)
```

```
       1  .235E-03     .308E-06     .144E-04     .280E-04
       2  .677E-04     .887E-07     .441E-05     .858E-05
       3  .844E-01     .829E-04     .538E-02     .116E-01
       4  .346E+02     .000E+00     .392E-01     .167E+00
       5  .346E+02     .000E+00     .353E+00     .150E+01

***** LIQUID RESULTS *****
SPECIES NO  PWALL(ATM)  LIQUID(G)  WLJUNC(G/S)
           1  .119E-01     .116E+01     .269E+00

           2  .342E-02     .205E+00     .475E-01
           3  .238E+01     .228E-01     .528E-02
VOLUME OR JUNCTION NUMBER =      3
TROD(K)   TCOOL(K)  PTOT(ATM) DELTA(M)  VELOCITY OF ALLOY (M/S)
1796.090  1806.090    69.244     .484E-04     .328E-01
***** VAPOR RESULTS *****
SPECIES NO.  PBULK(ATM)  XN(MOLES/S) VAPOR(G)   WVJUNC(G/S) FLVOUT(G/S)
       1  .108E-03     .258E-06     .661E-05     .000E+00
       2  .310E-04     .742E-07     .203E-05     .000E+00
       3  .427E-01     .940E-04     .274E-02     .000E+00
       4  .346E+02     .000E+00     .396E-01     .167E+00
       5  .346E+02     .000E+00     .357E+00     .150E+01

***** LIQUID RESULTS *****
SPECIES NO  PWALL(ATM)  LIQUID(G)  WLJUNC(G/S)
           1  .991E-02     .137E+01     .451E+00
           2  .285E-02     .242E+00     .795E-01
           3  .266E+01     .325E-01     .107E-01
***** OUTPUT RESULTS *****

TIME=     9.360  SEC
***** ROD FAILURE DATA *****
VELOCITY AT EXIT (M/S)      .000 HEIGHT (M)=      .000

SPECIES NO.    SOURCE RATE (G/S)
           1        .000
           2        .000
           3        .000

***** THERMAL HYDRAULIC RESULTS *****
VOLUME OR JUNCTION NUMBER =      1
TROD(K)   TCOOL(K)  PTOT(ATM) DELTA(M)  VELOCITY OF ALLOY (M/S)
1841.801  1851.801    69.463     .269E-04     .996E-02
***** VAPOR RESULTS *****
SPECIES NO.  PBULK(ATM)  XN(MOLES/S) VAPOR(G)   WVJUNC(G/S) FLVOUT(G/S)
           1  .401E-03     .378E-06     .242E-04     .629E-04     .104E-03
           2  .116E-03     .109E-06     .742E-05     .193E-04     .319E-04
           3  .756E-01     .317E-04     .472E-02     .146E-01     .204E-01
           4  .347E+02     .000E+00     .388E-01     .167E+00     .167E+00
           5  .347E+02     .000E+00     .349E+00     .150E+01     .150E+01

***** LIQUID RESULTS *****
SPECIES NO  PWALL(ATM)  LIQUID(G)  WLJUNC(G/S)
           1  .150E-01     .774E+00     .771E-01
           2  .433E-02     .137E+00     .136E-01
           3  .965E+00     .552E-02     .552E-03
VOLUME OR JUNCTION NUMBER =      2

TROD(K)   TCOOL(K)  PTOT(ATM) DELTA(M)  VELOCITY OF ALLOY (M/S)
1821.801  1831.801    69.456     .356E-04     .175E-01
```

```
***** VAPOR RESULTS *****
SPECIES NO.   PBULK(ATM)   XN(MOLES/S) VAPOR(G)    WVJUNC(G/S) FLVOUT(G/S)
       1   .243E-03     .319E-06     .149E-04     .278E-04
       2   .700E-04     .921E-07     .458E-05     .852E-05
       3   .541E-01     .490E-04     .343E-02     .742E-02
       4   .347E+02     .000E+00     .392E-01     .167E+00
       5   .347E+02     .000E+00     .353E+00     .150E+01

***** LIQUID RESULTS *****
SPECIES NO   PWALL(ATM)   LIQUID(G)   WLJUNC(G/S)
           1   .126E-01     .102E+01     .179E+00
           2   .362E-02     .180E+00     .315E-01
           3   .143E+01     .117E-01     .205E-02
VOLUME OR JUNCTION NUMBER =      3
TROD(K)    TCOOL(K)   PTOT(ATM) DELTA(M)   VELOCITY OF ALLOY (M/S)
1801.801   1811.801     69.445     .422E-04     .248E-01
***** VAPOR RESULTS *****
SPECIES NO.   PBULK(ATM)   XN(MOLES/S) VAPOR(G)    WVJUNC(G/S) FLVOUT(G/S)
       1   .107E-03     .268E-06     .691E-05     .000E+00
       2   .309E-04     .772E-07     .212E-05     .000E+00
       3   .275E-01     .613E-04     .181E-02     .000E+00

       4   .347E+02     .000E+00     .396E-01     .167E+00
       5   .347E+02     .000E+00     .357E+00     .150E+01

***** LIQUID RESULTS *****
SPECIES NO   PWALL(ATM)   LIQUID(G)   WLJUNC(G/S)
           1   .105E-01     .120E+01     .299E+00
           2   .302E-02     .212E+00     .528E-01
           3   .176E+01     .183E-01     .455E-02
***** OUTPUT RESULTS *****

TIME=     10.122  SEC
***** ROD FAILURE DATA *****
VELOCITY AT EXIT (M/S)      .000 HEIGHT (M)=      .000
SPECIES NO.    SOURCE RATE (G/S)
           1         .000
           2         .000
           3         .000

***** THERMAL HYDRAULIC RESULTS *****
VOLUME OR JUNCTION NUMBER =      1
TROD(K)    TCOOL(K)   PTOT(ATM) DELTA(M)   VELOCITY OF ALLOY (M/S)
1845.608   1855.608     69.654     .250E-04     .858E-02
***** VAPOR RESULTS *****

SPECIES NO.   PBULK(ATM)   XN(MOLES/S) VAPOR(G)    WVJUNC(G/S) FLVOUT(G/S)
           1   .427E-03     .395E-06     .250E-04     .682E-04     .110E-03
           2   .123E-03     .114E-06     .767E-05     .209E-04     .339E-04
           3   .528E-01     .189E-04     .331E-02     .106E-01     .142E-01
           4   .348E+02     .000E+00     .388E-01     .167E+00     .167E+00
           5   .348E+02     .000E+00     .349E+00     .150E+01     .150E+01

***** LIQUID RESULTS *****
SPECIES NO   PWALL(ATM)   LIQUID(G)   WLJUNC(G/S)
           1   .158E-01     .722E+00     .619E-01
           2   .456E-02     .127E+00     .109E-01
           3   .587E+00     .308E-02     .263E-03
VOLUME OR JUNCTION NUMBER =      2
TROD(K)    TCOOL(K)   PTOT(ATM) DELTA(M)   VELOCITY OF ALLOY (M/S)
```

```
1825.608  1835.608    69.658    .330E-04    .151E-01
***** VAPOR RESULTS *****
SPECIES NO.  PBULK(ATM)  XN(MOLES/S) VAPOR(G)   WVJUNC(G/S) FLVOUT(G/S)
       1  .264E-03    .333E-06    .154E-04    .324E-04
       2  .762E-04    .962E-07    .473E-05    .995E-05
       3  .393E-01    .331E-04    .246E-02    .584E-02
       4  .348E+02    .000E+00    .392E-01    .167E+00
       5  .348E+02    .000E+00    .353E+00    .150E+01


***** LIQUID RESULTS *****
SPECIES NO  PWALL(ATM)  LIQUID(G)  WLJUNC(G/S)
           1  .133E-01    .949E+00    .143E+00
           2  .382E-02    .167E+00    .253E-01
           3  .978E+00    .728E-02    .110E-02
VOLUME OR JUNCTION NUMBER =     3
TROD(K)   TCOOL(K)  PTOT(ATM) DELTA(M)  VELOCITY OF ALLOY (M/S)
1805.608  1815.608    69.658    .392E-04    .213E-01
***** VAPOR RESULTS *****
SPECIES NO.  PBULK(ATM)  XN(MOLES/S) VAPOR(G)   WVJUNC(G/S) FLVOUT(G/S)
       1  .126E-03    .280E-06    .715E-05    .000E+00
       2  .362E-04    .807E-07    .219E-05    .000E+00
       3  .217E-01    .446E-04    .133E-02    .000E+00
       4  .348E+02    .000E+00    .396E-01    .167E+00
       5  .348E+02    .000E+00    .357E+00    .150E+01

***** LIQUID RESULTS *****
SPECIES NO  PWALL(ATM)  LIQUID(G)  WLJUNC(G/S)
           1  .111E-01    .112E+01    .240E+00
           2  .319E-02    .198E+00    .423E-01
           3  .129E+01    .123E-01    .261E-02
***** OUTPUT RESULTS *****


TIME=    11.150  SEC
***** ROD FAILURE DATA *****
VELOCITY AT EXIT (M/S)      .000 HEIGHT (M)=      .000
SPECIES NO.   SOURCE RATE (G/S)
           1        .000
           2        .000
           3        .000

***** THERMAL HYDRAULIC RESULTS *****
VOLUME OR JUNCTION NUMBER =     1
TROD(K)   TCOOL(K)  PTOT(ATM) DELTA(M)  VELOCITY OF ALLOY (M/S)
1850.749  1860.749    69.777    .231E-04    .724E-02
***** VAPOR RESULTS *****
SPECIES NO.  PBULK(ATM)  XN(MOLES/S) VAPOR(G)   WVJUNC(G/S) FLVOUT(G/S)
           1  .450E-03    .406E-06    .259E-04    .712E-04    .116E-03
           2  .130E-03    .117E-06    .795E-05    .219E-04    .357E-04
           3  .325E-01    .880E-05    .196E-02    .665E-02    .874E-02
           4  .349E+02    .000E+00    .388E-01    .167E+00    .167E+00
           5  .349E+02    .000E+00    .349E+00    .150E+01    .150E+01

***** LIQUID RESULTS *****
SPECIES NO  PWALL(ATM)  LIQUID(G)  WLJUNC(G/S)
           1  .164E-01    .666E+00    .482E-01
           2  .472E-02    .117E+00    .850E-02
           3  .282E+00    .135E-02    .971E-04
VOLUME OR JUNCTION NUMBER =     2
```

```
TROD(K)   TCOOL(K)  PTOT(ATM) DELTA(M)  VELOCITY OF ALLOY (M/S)
1830.749  1840.749    69.788    .304E-04    .127E-01
***** VAPOR RESULTS *****
SPECIES NO.  PBULK(ATM)  XN(MOLES/S) VAPOR(G)   WVJUNC(G/S) FLVOUT(G/S)
       1  .276E-03    .342E-06    .160E-04    .331E-04
       2  .797E-04    .987E-07    .490E-05    .102E-04
       3  .248E-01    .185E-04    .150E-02    .364E-02
       4  .349E+02    .000E+00    .392E-01    .167E+00
       5  .349E+02    .000E+00    .353E+00    .150E+01

***** LIQUID RESULTS *****
SPECIES NO  PWALL(ATM)  LIQUID(G)  WLJUNC(G/S)
           1  .137E-01    .875E+00    .111E+00
           2  .396E-02    .154E+00    .197E-01

           3  .553E+00    .374E-02    .474E-03
VOLUME OR JUNCTION NUMBER =     3
TROD(K)   TCOOL(K)  PTOT(ATM) DELTA(M)  VELOCITY OF ALLOY (M/S)
1810.749  1820.749    69.797    .360E-04    .180E-01
***** VAPOR RESULTS *****
SPECIES NO.  PBULK(ATM)  XN(MOLES/S) VAPOR(G)   WVJUNC(G/S) FLVOUT(G/S)
       1  .128E-03    .288E-06    .738E-05    .000E+00
       2  .370E-04    .829E-07    .227E-05    .000E+00
       3  .135E-01    .277E-04    .841E-03    .000E+00
       4  .349E+02    .000E+00    .396E-01    .167E+00
       5  .349E+02    .000E+00    .357E+00    .150E+01

***** LIQUID RESULTS *****
SPECIES NO  PWALL(ATM)  LIQUID(G)  WLJUNC(G/S)
           1  .115E-01    .103E+01    .186E+00
           2  .331E-02    .183E+00    .329E-01
           3  .809E+00    .697E-02    .125E-02
***** OUTPUT RESULTS *****

TIME=    12.445  SEC
***** ROD FAILURE DATA *****
VELOCITY AT EXIT (M/S)      .000 HEIGHT (M)=      .000
SPECIES NO.   SOURCE RATE (G/S)
           1        .000
           2        .000
           3        .000

***** THERMAL HYDRAULIC RESULTS *****
VOLUME OR JUNCTION NUMBER =     1
TROD(K)   TCOOL(K)  PTOT(ATM) DELTA(M)  VELOCITY OF ALLOY (M/S)
1857.223  1867.223    69.954    .211E-04    .606E-02
***** VAPOR RESULTS *****
SPECIES NO.  PBULK(ATM)  XN(MOLES/S) VAPOR(G)   WVJUNC(G/S) FLVOUT(G/S)
           1  .472E-03    .423E-06    .269E-04    .750E-04    .121E-03
           2  .136E-03    .122E-06    .828E-05    .231E-04    .373E-04
           3  .159E-01    .328E-05    .964E-03    .331E-02    .425E-02
           4  .350E+02    .000E+00    .388E-01    .167E+00    .167E+00
           5  .350E+02    .000E+00    .349E+00    .150E+01    .150E+01

***** LIQUID RESULTS *****
SPECIES NO  PWALL(ATM)  LIQUID(G)  WLJUNC(G/S)
           1  .171E-01    .611E+00    .370E-01
           2  .494E-02    .108E+00    .653E-02
           3  .109E+00    .452E-03    .283E-04
VOLUME OR JUNCTION NUMBER =     2
```

```
TROD(K)   TCOOL(K)  PTOT(ATM) DELTA(M)  VELOCITY OF ALLOY (M/S)

1837.223  1847.223    69.971    .278E-04    .107E-01
***** VAPOR RESULTS *****
SPECIES NO.  PBULK(ATM)  XN(MOLES/S) VAPOR(G)   WVJUNC(G/S) FLVOUT(G/S)
       1  .292E-03    .356E-06    .166E-04    .357E-04
       2  .843E-04    .103E-06    .510E-05    .110E-04
       3  .123E-01    .841E-05    .761E-03    .199E-02
       4  .350E+02    .000E+00    .392E-01    .167E+00
       5  .350E+02    .000E+00    .353E+00    .150E+01

***** LIQUID RESULTS *****
SPECIES NO  PWALL(ATM)  LIQUID(G)  WLJUNC(G/S)
           1  .144E-01    .804E+00    .856E-01
           2  .415E-02    .142E+00    .151E-01
           3  .254E+00    .154E-02    .163E-03
VOLUME OR JUNCTION NUMBER =     3
TROD(K)   TCOOL(K)  PTOT(ATM) DELTA(M)  VELOCITY OF ALLOY (M/S)
1817.223  1827.223    69.988    .330E-04    .150E-01
***** VAPOR RESULTS *****
SPECIES NO.  PBULK(ATM)  XN(MOLES/S) VAPOR(G)   WVJUNC(G/S) FLVOUT(G/S)
       1  .139E-03    .300E-06    .769E-05    .000E+00
       2  .400E-04    .864E-07    .236E-05    .000E+00
       3  .743E-02    .144E-04    .444E-03    .000E+00
       4  .350E+02    .000E+00    .396E-01    .167E+00

       5  .350E+02    .000E+00    .357E+00    .150E+01

***** LIQUID RESULTS *****
SPECIES NO  PWALL(ATM)  LIQUID(G)  WLJUNC(G/S)
           1  .121E-01    .950E+00    .143E+00
           2  .347E-02    .168E+00    .252E-01
           3  .424E+00    .328E-02    .492E-03
***** OUTPUT RESULTS *****

TIME=    13.092  SEC
***** ROD FAILURE DATA *****
VELOCITY AT EXIT (M/S)     .000 HEIGHT (M)=     .000
SPECIES NO.   SOURCE RATE (G/S)
           1       .000
           2       .000
           3       .000

***** THERMAL HYDRAULIC RESULTS *****
VOLUME OR JUNCTION NUMBER =     1
TROD(K)   TCOOL(K)  PTOT(ATM) DELTA(M)  VELOCITY OF ALLOY (M/S)
1860.460  1870.460    70.192    .203E-04    .560E-02
***** VAPOR RESULTS *****
SPECIES NO.  PBULK(ATM)  XN(MOLES/S) VAPOR(G)   WVJUNC(G/S) FLVOUT(G/S)

           1  .449E-03    .448E-06    .277E-04    .693E-04    .115E-03
           2  .129E-03    .130E-06    .853E-05    .213E-04    .353E-04
           3  .103E-01    .210E-05    .665E-03    .218E-02    .275E-02
           4  .351E+02    .000E+00    .388E-01    .167E+00    .167E+00
           5  .351E+02    .000E+00    .349E+00    .150E+01    .150E+01

***** LIQUID RESULTS *****
SPECIES NO  PWALL(ATM)  LIQUID(G)  WLJUNC(G/S)
           1  .181E-01    .588E+00    .330E-01
           2  .522E-02    .104E+00    .582E-02
```

```
          3  .701E-01     .254E-03     .158E-04
VOLUME OR JUNCTION NUMBER =      2
TROD(K)    TCOOL(K)  PTOT(ATM) DELTA(M)  VELOCITY OF ALLOY (M/S)
1840.460   1850.460    70.213    .268E-04     .985E-02
***** VAPOR RESULTS *****
SPECIES NO.   PBULK(ATM)  XN(MOLES/S) VAPOR(G)   WVJUNC(G/S) FLVOUT(G/S)
       1   .271E-03     .378E-06     .171E-04     .307E-04
       2   .781E-04     .109E-06     .526E-05     .943E-05
       3   .817E-02     .575E-05     .531E-03     .126E-02
       4   .351E+02     .000E+00     .392E-01     .167E+00
       5   .351E+02     .000E+00     .353E+00     .150E+01

***** LIQUID RESULTS *****

SPECIES NO  PWALL(ATM)  LIQUID(G)  WLJUNC(G/S)
           1  .152E-01     .774E+00     .762E-01
           2  .439E-02     .137E+00     .135E-01
           3  .173E+00     .959E-03     .971E-04
VOLUME OR JUNCTION NUMBER =      3
TROD(K)    TCOOL(K)  PTOT(ATM) DELTA(M)  VELOCITY OF ALLOY (M/S)
1820.460   1830.460    70.234    .317E-04     .139E-01
***** VAPOR RESULTS *****
SPECIES NO.   PBULK(ATM)  XN(MOLES/S) VAPOR(G)   WVJUNC(G/S) FLVOUT(G/S)
       1   .120E-03     .318E-06     .796E-05     .000E+00
       2   .346E-04     .916E-07     .244E-05     .000E+00
       3   .473E-02     .105E-04     .317E-03     .000E+00
       4   .351E+02     .000E+00     .396E-01     .167E+00
       5   .351E+02     .000E+00     .357E+00     .150E+01

***** LIQUID RESULTS *****
SPECIES NO  PWALL(ATM)  LIQUID(G)  WLJUNC(G/S)
           1  .128E-01     .915E+00     .127E+00
           2  .368E-02     .161E+00     .225E-01
           3  .309E+00     .221E-02     .311E-03
***** OUTPUT RESULTS *****

TIME=     14.387  SEC

***** ROD FAILURE DATA *****
VELOCITY AT EXIT (M/S)      .000 HEIGHT (M)=      .000
SPECIES NO.    SOURCE RATE (G/S)
           1         .000
           2         .000
           3         .000

***** THERMAL HYDRAULIC RESULTS *****
VOLUME OR JUNCTION NUMBER =      1
TROD(K)    TCOOL(K)  PTOT(ATM) DELTA(M)  VELOCITY OF ALLOY (M/S)
1866.934   1876.934    70.308    .190E-04     .487E-02
***** VAPOR RESULTS *****
SPECIES NO.   PBULK(ATM)  XN(MOLES/S) VAPOR(G)   WVJUNC(G/S) FLVOUT(G/S)
           1  .494E-03     .458E-06     .293E-04     .766E-04     .126E-03
           2  .143E-03     .133E-06     .902E-05     .236E-04     .389E-04
           3  .494E-02     .684E-06     .303E-03     .103E-02     .132E-02
           4  .352E+02     .000E+00     .388E-01     .167E+00     .167E+00
           5  .352E+02     .000E+00     .349E+00     .150E+01     .150E+01

***** LIQUID RESULTS *****
SPECIES NO  PWALL(ATM)  LIQUID(G)  WLJUNC(G/S)
           1  .188E-01     .550E+00     .268E-01
```

```
           2   .536E-02     .970E-01     .472E-02

           3   .245E-01     .770E-04     .442E-05
VOLUME OR JUNCTION NUMBER =      2
TROD(K)    TCOOL(K)  PTOT(ATM) DELTA(M)  VELOCITY OF ALLOY (M/S)
1846.934   1856.934     70.332     .250E-04     .856E-02
***** VAPOR RESULTS *****
SPECIES NO.   PBULK(ATM)  XN(MOLES/S) VAPOR(G)   WVJUNC(G/S) FLVOUT(G/S)
        1   .300E-03     .386E-06     .181E-04     .346E-04
        2   .865E-04     .112E-06     .556E-05     .106E-04
        3   .385E-02     .231E-05     .246E-03     .606E-03
        4   .352E+02     .000E+00     .392E-01     .167E+00
        5   .352E+02     .000E+00     .353E+00     .150E+01

***** LIQUID RESULTS *****
SPECIES NO  PWALL(ATM)  LIQUID(G)  WLJUNC(G/S)
            1   .157E-01     .723E+00     .620E-01
            2   .452E-02     .128E+00     .109E-01
            3   .703E-01     .354E-03     .316E-04
VOLUME OR JUNCTION NUMBER =      3
TROD(K)    TCOOL(K)  PTOT(ATM) DELTA(M)  VELOCITY OF ALLOY (M/S)
1826.934   1836.934     70.356     .296E-04     .121E-01
***** VAPOR RESULTS *****
SPECIES NO.   PBULK(ATM)  XN(MOLES/S) VAPOR(G)   WVJUNC(G/S) FLVOUT(G/S)
        1   .135E-03     .325E-06     .836E-05     .000E+00

        2   .390E-04     .938E-07     .257E-05     .000E+00
        3   .227E-02     .492E-05     .152E-03     .000E+00
        4   .352E+02     .000E+00     .396E-01     .167E+00
        5   .352E+02     .000E+00     .357E+00     .150E+01

***** LIQUID RESULTS *****
SPECIES NO  PWALL(ATM)  LIQUID(G)  WLJUNC(G/S)
            1   .132E-01     .856E+00     .103E+00
            2   .379E-02     .151E+00     .182E-01
            3   .145E+00     .956E-03     .117E-03
***** OUTPUT RESULTS *****

TIME=     15.549  SEC
***** ROD FAILURE DATA *****
VELOCITY AT EXIT (M/S)      .000 HEIGHT (M)=      .000
SPECIES NO.    SOURCE RATE (G/S)
            1         .000
            2         .000
            3         .000

***** THERMAL HYDRAULIC RESULTS *****
VOLUME OR JUNCTION NUMBER =      1
TROD(K)    TCOOL(K)  PTOT(ATM) DELTA(M)  VELOCITY OF ALLOY (M/S)

1872.746   1882.746     70.549     .180E-04     .436E-02
***** VAPOR RESULTS *****
SPECIES NO.   PBULK(ATM)  XN(MOLES/S) VAPOR(G)   WVJUNC(G/S) FLVOUT(G/S)
            1   .436E-03     .487E-06     .305E-04     .653E-04     .111E-03
            2   .126E-03     .141E-06     .940E-05     .200E-04     .341E-04
            3   .245E-02     .513E-06     .138E-03     .461E-03     .650E-03
            4   .353E+02     .000E+00     .388E-01     .167E+00     .167E+00
            5   .353E+02     .000E+00     .349E+00     .150E+01     .150E+01

***** LIQUID RESULTS *****
```

```
SPECIES NO  PWALL(ATM)  LIQUID(G)  WLJUNC(G/S)
           1  .196E-01    .521E+00    .227E-01
           2  .566E-02    .919E-01    .401E-02
           3  .171E-01    .214E-04    .256E-05
VOLUME OR JUNCTION NUMBER =      2
TROD(K)   TCOOL(K)  PTOT(ATM) DELTA(M)  VELOCITY OF ALLOY (M/S)
1852.746  1862.746    70.576    .237E-04    .767E-02
***** VAPOR RESULTS *****
SPECIES NO.  PBULK(ATM)  XN(MOLES/S) VAPOR(G)   WVJUNC(G/S) FLVOUT(G/S)
       1  .256E-03    .410E-06    .188E-04    .290E-04
       2  .739E-04    .119E-06    .579E-05    .888E-05
       3  .174E-02    .126E-05    .113E-03    .312E-03
       4  .353E+02    .000E+00    .392E-01    .167E+00
       5  .353E+02    .000E+00    .353E+00    .150E+01

***** LIQUID RESULTS *****
SPECIES NO  PWALL(ATM)  LIQUID(G)  WLJUNC(G/S)
           1  .166E-01    .686E+00    .526E-01
           2  .478E-02    .121E+00    .928E-02
           3  .379E-01    .131E-03    .141E-04
VOLUME OR JUNCTION NUMBER =      3
TROD(K)   TCOOL(K)  PTOT(ATM) DELTA(M)  VELOCITY OF ALLOY (M/S)
1832.746  1842.746    70.604    .281E-04    .108E-01
***** VAPOR RESULTS *****
SPECIES NO.  PBULK(ATM)  XN(MOLES/S) VAPOR(G)   WVJUNC(G/S) FLVOUT(G/S)
       1  .114E-03    .345E-06    .871E-05    .000E+00
       2  .327E-04    .995E-07    .268E-05    .000E+00
       3  .118E-02    .268E-05    .722E-04    .000E+00

       4  .353E+02    .000E+00    .396E-01    .167E+00
       5  .353E+02    .000E+00    .357E+00    .150E+01

***** LIQUID RESULTS *****
SPECIES NO  PWALL(ATM)  LIQUID(G)  WLJUNC(G/S)
           1  .140E-01    .811E+00    .879E-01
           2  .402E-02    .143E+00    .155E-01
           3  .791E-01    .423E-03    .530E-04
***** OUTPUT RESULTS *****

TIME=    16.711  SEC
***** ROD FAILURE DATA *****
VELOCITY AT EXIT (M/S)     .000 HEIGHT (M)=      .000
SPECIES NO.   SOURCE RATE (G/S)
           1        .000
           2        .000
           3        .000

***** THERMAL HYDRAULIC RESULTS *****
VOLUME OR JUNCTION NUMBER =      1
TROD(K)   TCOOL(K)  PTOT(ATM) DELTA(M)  VELOCITY OF ALLOY (M/S)
1878.557  1888.557    70.766    .172E-04    .394E-02
***** VAPOR RESULTS *****
SPECIES NO.  PBULK(ATM)  XN(MOLES/S) VAPOR(G)   WVJUNC(G/S) FLVOUT(G/S)
           1  .540E-03    .508E-06    .319E-04    .838E-04    .137E-03
           2  .156E-03    .147E-06    .981E-05    .258E-04    .422E-04
           3  .917E-03   -.351E-11    .557E-04    .202E-03    .243E-03
           4  .354E+02    .000E+00    .388E-01    .167E+00    .167E+00
           5  .354E+02    .000E+00    .349E+00    .150E+01    .150E+01

***** LIQUID RESULTS *****
```

```
SPECIES NO  PWALL(ATM)  LIQUID(G)  WLJUNC(G/S)
           1  .206E-01    .496E+00    .196E-01
           2  .595E-02    .875E-01    .345E-02
           3 -.379E-03    .000E+00   -.480E-07
VOLUME OR JUNCTION NUMBER =     2
TROD(K)   TCOOL(K)  PTOT(ATM) DELTA(M)  VELOCITY OF ALLOY (M/S)
1858.557  1868.557    70.796    .226E-04    .694E-02
***** VAPOR RESULTS *****
SPECIES NO.  PBULK(ATM)  XN(MOLES/S) VAPOR(G)   WVJUNC(G/S) FLVOUT(G/S)
       1  .330E-03    .429E-06    .197E-04    .385E-04
       2  .953E-04    .124E-06    .606E-05    .118E-04
       3  .762E-03    .246E-06    .465E-04    .137E-03
       4  .354E+02    .000E+00    .392E-01    .167E+00

       5  .354E+02    .000E+00    .353E+00    .150E+01

***** LIQUID RESULTS *****
SPECIES NO  PWALL(ATM)  LIQUID(G)  WLJUNC(G/S)
           1  .174E-01    .653E+00    .453E-01
           2  .502E-02    .115E+00    .800E-02
           3  .786E-02    .374E-04    .248E-05
VOLUME OR JUNCTION NUMBER =     3
TROD(K)   TCOOL(K)  PTOT(ATM) DELTA(M)  VELOCITY OF ALLOY (M/S)
1838.557  1848.557    70.827    .267E-04    .981E-02
***** VAPOR RESULTS *****
SPECIES NO.  PBULK(ATM)  XN(MOLES/S) VAPOR(G)   WVJUNC(G/S) FLVOUT(G/S)
       1  .152E-03    .361E-06    .915E-05    .000E+00
       2  .438E-04    .104E-06    .281E-05    .000E+00
       3  .516E-03    .994E-06    .320E-04    .000E+00
       4  .354E+02    .000E+00    .396E-01    .167E+00
       5  .354E+02    .000E+00    .357E+00    .150E+01

***** LIQUID RESULTS *****
SPECIES NO  PWALL(ATM)  LIQUID(G)  WLJUNC(G/S)
           1  .147E-01    .773E+00    .758E-01
           2  .423E-02    .136E+00    .134E-01
           3  .294E-01    .171E-03    .166E-04

***** OUTPUT RESULTS *****

TIME=    17.874  SEC
***** ROD FAILURE DATA *****
VELOCITY AT EXIT (M/S)      .000 HEIGHT (M)=      .000
SPECIES NO.    SOURCE RATE (G/S)
           1         .000
           2         .000
           3         .000

***** THERMAL HYDRAULIC RESULTS *****
VOLUME OR JUNCTION NUMBER =     1
TROD(K)   TCOOL(K)  PTOT(ATM) DELTA(M)  VELOCITY OF ALLOY (M/S)
1888.738  1898.738    70.984    .164E-04    .361E-02
***** VAPOR RESULTS *****
SPECIES NO.  PBULK(ATM)  XN(MOLES/S) VAPOR(G)   WVJUNC(G/S) FLVOUT(G/S)
           1  .581E-03    .533E-06    .335E-04    .903E-04    .147E-03
           2  .168E-03    .154E-06    .103E-04    .278E-04    .453E-04
           3  .740E-03    .584E-06    .210E-04    .151E-03    .196E-03
           4  .355E+02    .000E+00    .388E-01    .167E+00    .167E+00
           5  .355E+02    .000E+00    .349E+00    .150E+01    .150E+01
```

```
***** LIQUID RESULTS *****

SPECIES NO  PWALL(ATM)  LIQUID(G)  WLJUNC(G/S)
           1  .216E-01    .475E+00    .171E-01
           2  .624E-02    .838E-01    .302E-02
           3  .175E-01    .000E+00    .190E-05
VOLUME OR JUNCTION NUMBER =     2
TROD(K)   TCOOL(K)  PTOT(ATM) DELTA(M)  VELOCITY OF ALLOY (M/S)
1868.738  1878.738    71.017    .216E-04    .635E-02
***** VAPOR RESULTS *****
SPECIES NO.  PBULK(ATM)  XN(MOLES/S) VAPOR(G)   WVJUNC(G/S) FLVOUT(G/S)
       1  .357E-03    .450E-06    .207E-04    .411E-04
       2  .103E-03    .130E-06    .638E-05    .126E-04
       3  .571E-03    .728E-06    .187E-04    .837E-04
       4  .355E+02    .000E+00    .392E-01    .167E+00
       5  .355E+02    .000E+00    .353E+00    .150E+01

***** LIQUID RESULTS *****
SPECIES NO  PWALL(ATM)  LIQUID(G)  WLJUNC(G/S)
           1  .183E-01    .625E+00    .397E-01
           2  .528E-02    .110E+00    .701E-02
           3  .216E-01    .946E-06    .583E-05
VOLUME OR JUNCTION NUMBER =     3
TROD(K)   TCOOL(K)  PTOT(ATM) DELTA(M)  VELOCITY OF ALLOY (M/S)
1848.738  1858.738    71.050    .256E-04    .898E-02

***** VAPOR RESULTS *****
SPECIES NO.  PBULK(ATM)  XN(MOLES/S) VAPOR(G)   WVJUNC(G/S) FLVOUT(G/S)
       1  .162E-03    .380E-06    .963E-05    .000E+00
       2  .469E-04    .110E-06    .296E-05    .000E+00
       3  .317E-03    .912E-06    .138E-04    .000E+00
       4  .355E+02    .000E+00    .396E-01    .167E+00
       5  .355E+02    .000E+00    .357E+00    .150E+01

***** LIQUID RESULTS *****
SPECIES NO  PWALL(ATM)  LIQUID(G)  WLJUNC(G/S)
           1  .154E-01    .740E+00    .664E-01
           2  .445E-02    .130E+00    .117E-01
           3  .269E-01    .575E-04    .130E-04
***** OUTPUT RESULTS *****

TIME=    19.036  SEC
***** ROD FAILURE DATA *****
VELOCITY AT EXIT (M/S)      .000 HEIGHT (M)=      .000
SPECIES NO.    SOURCE RATE (G/S)
           1         .000
           2         .000
           3         .000


***** THERMAL HYDRAULIC RESULTS *****
VOLUME OR JUNCTION NUMBER =     1
TROD(K)   TCOOL(K)  PTOT(ATM) DELTA(M)  VELOCITY OF ALLOY (M/S)
1895.181  1905.181    71.366    .158E-04    .331E-02
***** VAPOR RESULTS *****
SPECIES NO.  PBULK(ATM)  XN(MOLES/S) VAPOR(G)   WVJUNC(G/S) FLVOUT(G/S)
           1  .605E-03    .580E-06    .359E-04    .923E-04    .152E-03
           2  .175E-03    .168E-06    .111E-04    .284E-04    .469E-04
           3  .418E-03    .263E-06    .750E-05    .826E-04    .110E-03
           4  .357E+02    .000E+00    .388E-01    .167E+00    .167E+00
```

```
          5   .357E+02     .000E+00     .349E+00     .150E+01     .150E+01

***** LIQUID RESULTS *****
SPECIES NO  PWALL(ATM)  LIQUID(G)  WLJUNC(G/S)
           1   .235E-01     .456E+00     .151E-01
           2   .678E-02     .804E-01     .267E-02
           3   .792E-02     .000E+00     .733E-06
VOLUME OR JUNCTION NUMBER =      2
TROD(K)   TCOOL(K)  PTOT(ATM) DELTA(M)  VELOCITY OF ALLOY (M/S)
1875.181  1885.181    71.403     .208E-04     .584E-02
***** VAPOR RESULTS *****
SPECIES NO.  PBULK(ATM)  XN(MOLES/S) VAPOR(G)   WVJUNC(G/S) FLVOUT(G/S)
       1   .366E-03     .491E-06     .223E-04     .419E-04

       2   .106E-03     .142E-06     .686E-05     .129E-04
       3   .315E-03     .284E-06     .668E-05     .292E-04
       4   .357E+02     .000E+00     .392E-01     .167E+00
       5   .357E+02     .000E+00     .353E+00     .150E+01

***** LIQUID RESULTS *****
SPECIES NO  PWALL(ATM)  LIQUID(G)  WLJUNC(G/S)
           1   .199E-01     .600E+00     .351E-01
           2   .575E-02     .106E+00     .619E-02
           3   .851E-02     .000E+00     .196E-05
VOLUME OR JUNCTION NUMBER =      3
TROD(K)   TCOOL(K)  PTOT(ATM) DELTA(M)  VELOCITY OF ALLOY (M/S)
1855.181  1865.181    71.441     .246E-04     .826E-02
***** VAPOR RESULTS *****
SPECIES NO.  PBULK(ATM)  XN(MOLES/S) VAPOR(G)   WVJUNC(G/S) FLVOUT(G/S)
       1   .166E-03     .415E-06     .104E-04     .000E+00
       2   .481E-04     .120E-06     .320E-05     .000E+00
       3   .111E-03     .420E-06     .511E-05     .000E+00
       4   .357E+02     .000E+00     .396E-01     .167E+00
       5   .357E+02     .000E+00     .357E+00     .150E+01

***** LIQUID RESULTS *****
SPECIES NO  PWALL(ATM)  LIQUID(G)  WLJUNC(G/S)

           1   .168E-01     .710E+00     .587E-01
           2   .485E-02     .125E+00     .104E-01
           3   .123E-01     .110E-04     .510E-05
***** OUTPUT RESULTS *****

TIME=     19.036  SEC
***** ROD FAILURE DATA *****
VELOCITY AT EXIT (M/S)      .000 HEIGHT (M)=      .000
SPECIES NO.    SOURCE RATE (G/S)
           1         .000
           2         .000
           3         .000

***** THERMAL HYDRAULIC RESULTS *****
VOLUME OR JUNCTION NUMBER =      1
TROD(K)   TCOOL(K)  PTOT(ATM) DELTA(M)  VELOCITY OF ALLOY (M/S)
1895.181  1905.181    71.366     .158E-04     .331E-02
***** VAPOR RESULTS *****
SPECIES NO.  PBULK(ATM)  XN(MOLES/S) VAPOR(G)   WVJUNC(G/S) FLVOUT(G/S)
           1   .605E-03     .580E-06     .359E-04     .923E-04     .152E-03
           2   .175E-03     .168E-06     .111E-04     .284E-04     .469E-04
           3   .418E-03     .263E-06     .750E-05     .826E-04     .110E-03
```

```
          4   .357E+02     .000E+00     .388E-01     .167E+00     .167E+00

          5   .357E+02     .000E+00     .349E+00     .150E+01     .150E+01

***** LIQUID RESULTS *****
SPECIES NO  PWALL(ATM)  LIQUID(G)  WLJUNC(G/S)
           1  .235E-01     .456E+00     .151E-01
           2  .678E-02     .804E-01     .267E-02
           3  .792E-02     .000E+00     .733E-06
VOLUME OR JUNCTION NUMBER =      2
TROD(K)   TCOOL(K)  PTOT(ATM) DELTA(M)  VELOCITY OF ALLOY (M/S)
1875.181  1885.181    71.403    .208E-04     .584E-02
***** VAPOR RESULTS *****
SPECIES NO.  PBULK(ATM)  XN(MOLES/S) VAPOR(G)   WVJUNC(G/S) FLVOUT(G/S)
       1  .366E-03     .491E-06     .223E-04     .419E-04
       2  .106E-03     .142E-06     .686E-05     .129E-04
       3  .315E-03     .284E-06     .668E-05     .292E-04
       4  .357E+02     .000E+00     .392E-01     .167E+00
       5  .357E+02     .000E+00     .353E+00     .150E+01

***** LIQUID RESULTS *****
SPECIES NO  PWALL(ATM)  LIQUID(G)  WLJUNC(G/S)
           1  .199E-01     .600E+00     .351E-01
           2  .575E-02     .106E+00     .619E-02
           3  .851E-02     .000E+00     .196E-05

VOLUME OR JUNCTION NUMBER =      3
TROD(K)   TCOOL(K)  PTOT(ATM) DELTA(M)  VELOCITY OF ALLOY (M/S)
1855.181  1865.181    71.441    .246E-04     .826E-02
***** VAPOR RESULTS *****
SPECIES NO.  PBULK(ATM)  XN(MOLES/S) VAPOR(G)   WVJUNC(G/S) FLVOUT(G/S)
       1  .166E-03     .415E-06     .104E-04     .000E+00
       2  .481E-04     .120E-06     .320E-05     .000E+00
       3  .111E-03     .420E-06     .511E-05     .000E+00
       4  .357E+02     .000E+00     .396E-01     .167E+00
       5  .357E+02     .000E+00     .357E+00     .150E+01

***** LIQUID RESULTS *****
SPECIES NO  PWALL(ATM)  LIQUID(G)  WLJUNC(G/S)
           1  .168E-01     .710E+00     .587E-01
           2  .485E-02     .125E+00     .104E-01
           3  .123E-01     .110E-04     .510E-05
***** OUTPUT RESULTS *****

TIME=    20.199  SEC
***** ROD FAILURE DATA *****
VELOCITY AT EXIT (M/S)      .000 HEIGHT (M)=      .000
SPECIES NO.    SOURCE RATE (G/S)
           1        .000

           2        .000
           3        .000

***** THERMAL HYDRAULIC RESULTS *****
VOLUME OR JUNCTION NUMBER =      1
TROD(K)   TCOOL(K)  PTOT(ATM) DELTA(M)  VELOCITY OF ALLOY (M/S)
1895.181  1905.181    71.608    .152E-04     .307E-02
***** VAPOR RESULTS *****
SPECIES NO.  PBULK(ATM)  XN(MOLES/S) VAPOR(G)   WVJUNC(G/S) FLVOUT(G/S)
           1  .689E-03     .609E-06     .385E-04     .107E-03     .173E-03
```

```
           2  .200E-03     .176E-06     .118E-04     .331E-04     .534E-04
           3 -.117E-04     .704E-07     .103E-05    -.267E-04    -.306E-04
           4  .358E+02     .000E+00     .388E-01     .167E+00     .167E+00
           5  .358E+02     .000E+00     .349E+00     .150E+01     .150E+01

***** LIQUID RESULTS *****
SPECIES NO  PWALL(ATM)  LIQUID(G)  WLJUNC(G/S)
           1  .247E-01     .440E+00     .135E-01
           2  .715E-02     .775E-01     .238E-02
           3  .201E-02     .000E+00     .162E-06
VOLUME OR JUNCTION NUMBER =     2
TROD(K)   TCOOL(K)  PTOT(ATM) DELTA(M)  VELOCITY OF ALLOY (M/S)
1875.181  1885.181    71.648     .200E-04     .541E-02

***** VAPOR RESULTS *****
SPECIES NO.  PBULK(ATM)  XN(MOLES/S) VAPOR(G)   WVJUNC(G/S) FLVOUT(G/S)
       1  .428E-03     .516E-06     .238E-04     .505E-04
       2  .124E-03     .149E-06     .734E-05     .155E-04
       3 -.102E-03     .174E-06     .858E-06    -.643E-05
       4  .358E+02     .000E+00     .392E-01     .167E+00
       5  .358E+02     .000E+00     .353E+00     .150E+01

***** LIQUID RESULTS *****
SPECIES NO  PWALL(ATM)  LIQUID(G)  WLJUNC(G/S)
           1  .210E-01     .578E+00     .313E-01
           2  .607E-02     .102E+00     .552E-02
           3  .493E-02     .000E+00     .989E-06
VOLUME OR JUNCTION NUMBER =     3
TROD(K)   TCOOL(K)  PTOT(ATM) DELTA(M)  VELOCITY OF ALLOY (M/S)
1855.181  1865.181    71.689     .237E-04     .765E-02
***** VAPOR RESULTS *****
SPECIES NO.  PBULK(ATM)  XN(MOLES/S) VAPOR(G)   WVJUNC(G/S) FLVOUT(G/S)
       1  .201E-03     .436E-06     .111E-04     .000E+00
       2  .582E-04     .126E-06     .342E-05     .000E+00
       3 -.246E-04     .220E-06     .103E-05     .000E+00
       4  .358E+02     .000E+00     .396E-01     .167E+00
       5  .358E+02     .000E+00     .357E+00     .150E+01


***** LIQUID RESULTS *****
SPECIES NO  PWALL(ATM)  LIQUID(G)  WLJUNC(G/S)
           1  .178E-01     .684E+00     .524E-01
           2  .513E-02     .121E+00     .923E-02
           3  .641E-02     .000E+00     .231E-05
```

.20342E+01	.74409E-04	.22805E-04	.71227E-01	.16667E+00	.15000E+01
.31641E+01	.84077E-04	.25774E-04	.78624E-01	.16667E+00	.15000E+01
.41352E+01	.88372E-04	.27100E-04	.79924E-01	.16667E+00	.15000E+01
.50024E+01	.92301E-04	.28314E-04	.79324E-01	.16667E+00	.15000E+01
.61135E+01	.94940E-04	.29133E-04	.66384E-01	.16667E+00	.15000E+01
.70936E+01	.98188E-04	.30143E-04	.50286E-01	.16667E+00	.15000E+01
.82180E+01	.10039E-03	.30828E-04	.33160E-01	.16667E+00	.15000E+01
.93602E+01	.10384E-03	.31899E-04	.20432E-01	.16667E+00	.15000E+01
.10122E+02	.11019E-03	.33869E-04	.14225E-01	.16667E+00	.15000E+01
.11150E+02	.11596E-03	.35655E-04	.87362E-02	.16667E+00	.15000E+01
.12445E+02	.12123E-03	.37287E-04	.42540E-02	.16667E+00	.15000E+01
.13092E+02	.11490E-03	.35324E-04	.27525E-02	.16667E+00	.15000E+01
.14387E+02	.12631E-03	.38858E-04	.13168E-02	.16667E+00	.15000E+01
.15549E+02	.11100E-03	.34109E-04	.64976E-03	.16667E+00	.15000E+01
.16711E+02	.13719E-03	.42226E-04	.24990E-03	.16667E+00	.15000E+01
.17874E+02	.14705E-03	.45281E-04	.19554E-03	.16667E+00	.15000E+01
.19036E+02	.15238E-03	.46932E-04	.10984E-03	.16667E+00	.15000E+01
.19036E+02	.15238E-03	.46932E-04	.10984E-03	.16667E+00	.15000E+01
.20199E+02	.17309E-03	.53353E-04	-.30568E-05	.16667E+00	.15000E+01

APPENDIX C

COMPILATION OF MATERIALS PROPERTIES

The material properties used in the VAPOR code and in the calculations of aerosol nucleation rates are given in Table C.1. Critical temperatures and volumes used in calculating the diffusion coefficients were taken from Reference C.1. For CsI, the diffusion coefficient was calculated using [C.2]

$$D(m^2/s) = 9.8 \times 10^{-5} T^{1.75}/p \qquad (C.1)$$

where T is the temperature (K) and p is the pressure in Pascals. Surface tension data was taken from Reference C.3. Vapor pressure constants for Ag, In and Cd were fit to data given in Reference C.3; the vapor pressure correlation for CsI was provided by Reference C.4. The viscosity of the Ag-In-Cd alloy was based on data from Reference C.5. Reference C.6 provided the density of the Ag-In-Cd alloy. In most cases, point estimates reflect that little information existed on the temperature-dependent behavior of the specific material property.

TABLE C.1
MATERIALS PROPERTIES

Property	Material: Ag	In	Cd	CsI	Ag-In-Cd
T_c, Critical Temperature (K)	4764	4337	1903	a	a
V_c, Critical Volume (cm^3/gmole)	339	347.5	217.6	a	a
Molecular Weight (kg/kgmole)	107.8	114.82	112.4	260	a
Density (kg/m^3)	10000	a	10000	3140	$\rho = 10120 - T$ $T < 1270$ K $\rho = 8850$ $T > 1270$ K
Viscosity (kg/m-s)	a	a	a	a	2.98e-03 [b]
Surface Tension (N/m)	0.9	0.8	0.65	0.073	a
Vapor Pressure Constants					
A	7.989	8.284	7.99	51.7 ($T < 886$ K) 50.2 ($T > 886$ K)	a
B	1.26e+04	1.27e+05	5.31e+03	2.23e+04 ($T < 886$ K) 2.40e+04 ($T > 886$ K)	a
C	c c	c c	c c	8.11 [d] 6.95 [d]	a

a. not applicable for this material.
b. means 2.98×10^{-3}
c. vapor pressure of the form $p = 10^{(A - B/T)}$ where p is in mm Hg.
d. vapor pressure of the form $p = \exp(A - B/T - C\ln T)$ where p is in Pascals.

REFERENCES

C.1 Gates, D. and Thodos, G., "The Critical Constants of the Elements," AIChE Journal, 6, (1), March 1960, pp. 50-54.

C.2 Jordan, H., Gieseke, J.A., and Baybutt, P., "TRAPMELT User's Manual," NUREG/CR-0632, 1979.

C.3. Weast, R. (ed.),Handbook of Chemistry and Physics, CRC Press Inc., 59th edition, 1979.

C.4. Cronenburg, A.W. et. al., Fission Product Behavior During the PBF Severe Fuel Damage Scoping Test, EG&G, Idaho, June 1985.

C.5 Lyon, R. (ed.), Liquid Metals Handbook, U.S. Government Printing Office, Second Edition, June 1952.

C.6 Hagrman, D.L., Material Property Models for Severe Core Damage Analysis, EGG-CDD-5801, May 1985.

APPENDIX D

MOMENTUM EQUATION IN THE LIQUID FILM MODEL

The purpose of this appendix is to derive the simplified form of the axial momentum equation that is used to describe the velocity of the Ag-In-Cd liquid film. The quasi-steady axial momentum for a node of liquid is

$$G - \tau_i P_i \Delta z - \tau_w P_w \Delta z = (\dot{m}V)_{out} - (\dot{m}V)_{in} \qquad (D.1)$$

where

G = gravity force on the liquid node (N),

τ_i = interfacial shear stress between the liquid and the vapor (N/m^2),

P_i = interfacial perimeter over which τ_i acts (m),

τ_w = shear stress due to wall friction (N/m^2),

P_w = wetted perimeter over which τ_w acts (m),

Δz = axial length of the node (m),

$(\dot{m}V)_{out}$ = momentum flux out of the node (N), and

$(\dot{m}V)_{in}$ = momentum flux into the node (N).

When the appropriate expressions for each term, derived

in Section 3, are substituted into Equation (D.1), the result for node n is

$$\rho_\ell g \pi D \delta_n \Delta z - f_{w,g}\left(1 + 300 \frac{\delta_n}{D_e}\right) \frac{\rho_g}{2} (u_g - v_n)^2 [\pi (D + 2\delta_n) \Delta z] \tag{D.2}$$

$$- \frac{f_\ell \rho_\ell v_n^2}{2} \pi D \Delta z = \rho_\ell \pi D \delta_n v_n^2 - \begin{cases} \rho_\ell A_{fail} V_0^2 & (n = 1) \\ \rho_\ell \pi D \delta_{n-1} v_{n-1}^2 & (n \neq 1) \end{cases} = 0$$

where

ρ_ℓ = density of alloy (kg/m^3),

ρ_g = density of gas (kg/m^3),

D = outer rod diameter (m),

δ_n = film thickness of node (m),

Δz = axial length of node (m),

u_g = gas velocity (m/s),

v_n = liquid film velocity of node n (m/s),

$f_{w,g}$ = gas friction factor if no film were present,

f_ℓ = liquid film friction factor,

A_{fail} = size of control rod failure (m^2),

V_0 = velocity of breach in control rod (m/s), and

D_e = equivalent diameter of flow channel (m).

For laminar flow,

$$f_{\ell} = 16/Re \qquad (D.3)$$

Hence, Equation (D.2) becomes

$$- f_{w,g}\left(1 + 300 \frac{\delta_n}{D_e}\right) \frac{\rho_g}{2} (D + 2\delta_n)\Delta z (u_g - v_n)^2 - \frac{2\mu_\ell D \Delta z}{\delta_n} v_n + \rho_\ell g D \delta_n \Delta z$$

$$- \rho_\ell D \delta_n v_n^2 + \begin{cases} \rho_\ell A_{fail} V_0^2/\pi & (n = 1) \\ \rho_\ell D \delta_{n-1} v_{n-1}^2 & (n \neq 1) \end{cases} = 0 \qquad (D.4)$$

In simpler terms,

$$\alpha (u_g - v_n)^2 + \gamma v_n^2 + \beta v_n + \Delta = 0 \qquad (D.5)$$

where

$$\alpha = - f_{w,g}\left(1 + 300 \frac{\delta_n}{D_e}\right) \frac{\rho_g}{z} (D + 2\delta_n)\Delta z$$

$$\gamma = - \rho_\ell D \delta_n$$

$$\beta = - \frac{2\mu_\ell D \Delta z}{\delta_n}$$

$$\Delta = \rho_\ell g D \delta_n \Delta z + \begin{cases} \rho_\ell A_{fail} V_0^2 / \pi & (n = 1) \\ \rho_\ell D \delta_{n-1} v_{n-1}^2 & (n \neq 1) \end{cases}$$

Equation (D.5) is quadratic of the form

$$Av_n^2 + Bv_n + C \qquad (D.6)$$

where

$$A = \alpha + \gamma$$

$$B = \beta - 2u_g\gamma$$

$$C = \alpha u_g^2 + \delta$$

Thus, the quadratic formula is used to solve for v_n in Equation (D.6).

For turbulent flow, since

$$f_\ell = 0.023/Re_\ell^{0.2} \qquad (D.7)$$

the equation is more complicated. Substituting Equation (D.7) into Equation (D.2) yields

$$- f_{w,g}\left(1 + 300\,\frac{\delta_n}{D_e}\right)\frac{\rho_g}{2}\left(u_g - v_n\right)^2\pi(D + 2\delta_n)\Delta z - \frac{0.046}{\left(\frac{4\rho_\ell v_n \delta_n}{\mu_\ell}\right)^{0.2}}\,\frac{\rho_\ell v_n^2}{2}\,\pi D\Delta z$$

$$+ \pi D\rho_\ell \delta_n g\Delta z = \pi D\rho_\ell v_n^2\delta_n - \begin{cases} \rho_\ell A_{fail} V_0^2 & (n = 1) \\ \rho_\ell \pi D\delta_{n-1} v_{n-1}^2 & (n \neq 1) \end{cases} = 0 \qquad (D.8)$$

Simplifying,

$$\alpha(u_g - v_n)^2 + \beta v_n^{1.8} + \gamma v_n^2 + d = 0 \qquad \text{(D.9)}$$

where

$$\alpha = -f_{w,g}\left(1 + 300\frac{\delta_n}{D_e}\right)(D + 2\delta_n)\frac{\rho_g}{2}\,\Delta z$$

$$\beta = -0.01743\left(\frac{\mu_\ell}{\delta_n}\right)^{0.2}\rho_\ell^{0.8} D\Delta z$$

$$\gamma = -D\rho_\ell\delta_n$$

$$d = D\rho_\ell\delta_n g\Delta z + \begin{cases} \rho_\ell A_{fail} v_0^2/\pi & (n = 1) \\ \rho_\ell D\delta_{n-1} v_{n-1}^2 & (n \neq 1) \end{cases}$$

Equation (D.9) is of the form

$$Av_n^2 + Bv_n^{1.8} + Cv_n + D = 0 \qquad \text{(D.10)}$$

where

$A = \alpha + \gamma$

$B = \beta$

$C = -2u_g\alpha$, and

$D = \alpha u_g^2 + \delta$

For this case, Equation (D.10) is solved using Newton's method to find the velocity at node n, v_n .

APPENDIX E

AEROMAP CODE

The aerosol maps for Ag, Cd and CsI, presented in Section 6, were prepared by comparing the rates of homogeneous and ion-induced nucleation to heterogeneous nucleation. This appendix will describe the algorithm used to produce these maps.

For any given combination of supersaturation and temperature, a comparison of the rates of homogeneous and heterogeneous nucleation will split the supersaturation temperature space into three regimes as shown in Figure E.1. Either

(1) the rate of homogeneous nucleation will greatly exceed the rate of heterogeneous nucleation,

(2) the homgeneous nucleation rate will be substantially less than the heterogeneous nucleation rate, or

(3) both rates will be "roughly" equal.

The borders that delineate each regime are determined by finding the supersaturation, S, that satisfies the equation

Figure E.1

Schematic of Nucleation Regimes

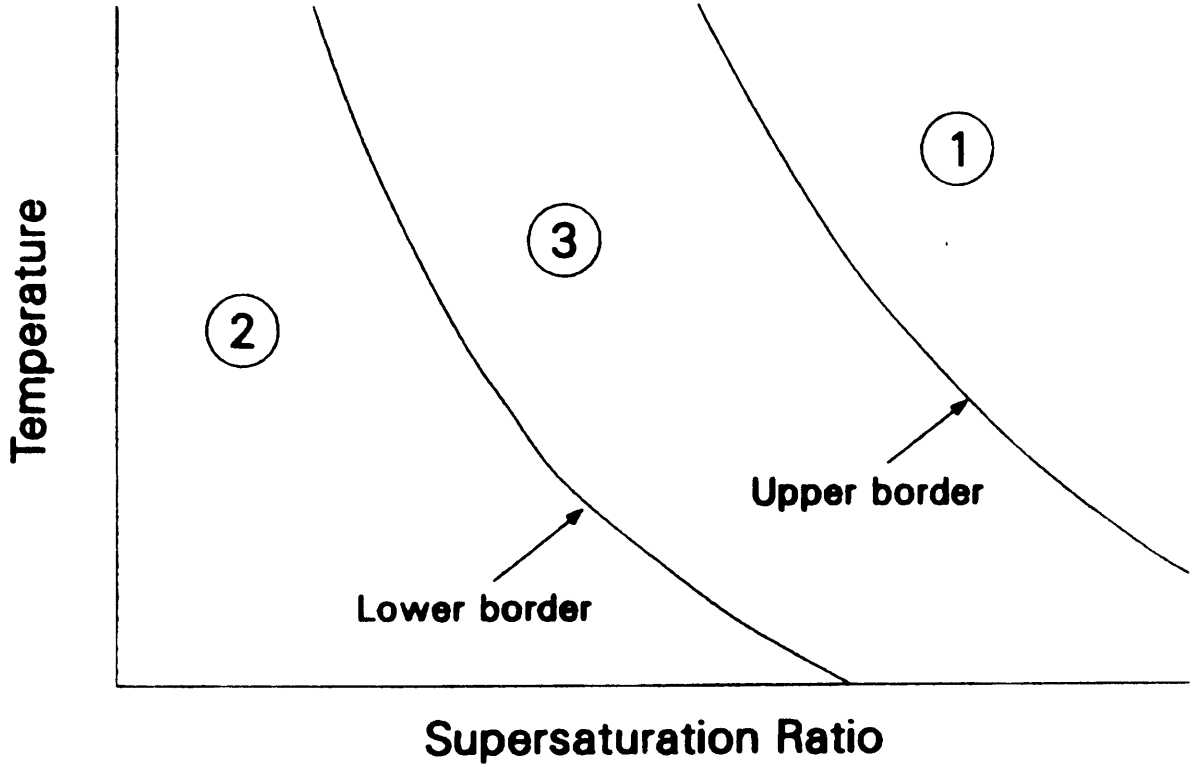

P204-LN85044-11

$$J_{HMG}(S,T) - \alpha J_{HET}(S,T) = 0 \qquad \text{(E.1)}$$

where

J_{HMG} = rate of homogeneous nucleation (kg/m^3s),

J_{HET} = rate of heterogeneous nucleation (kg/m^3s), and

α = border multiplier.

An interval search method is used to determine the supersaturation that is the root to equation E.1.

The aerosol maps are generated using two border multipliers. To determine the transition between regimes 2 and 3, a "lower" border multiplier, α_{low}, is used whereas for the transition between regions 3 and 1, an "upper" border multiplier, α_{up}, is used. The exact values of α_{low} and α_{up} selected in the analysis will determine the size of each regime relative to one another.

For the homogeneous case, values of α equal to 0.02 and 50 were used to calculate the lower and upper borders respectively. Thus, in region 1, the homogeneous nucleation rate is less than 1/50th the rate of heterogeneous nucleation. In regime 2, the rate of homogeneous nucleation is greater than 50 times the rate of heterogeneous nucleation. The rates are within a

factor of 50 of each other in region 3.

This same approach is employed to compare the ion-induced and heterogeneous nucleation rates. Values of 50 and 0.1 were used for the upper and lower border multipliers. (A value of 0.1 was used for the lower multiplier to insure a solution to Equation (E.1).) The overall aerosol map is then obtained by a superposition of the homogeneous/heterogeneous regimes and the ion-induced/heterogeneous regimes. A code termed AEROMAP that determines these nucleation regimes is attached with sample input and output.

```
100         PROGRAM NUCMAP(INPUT,OUTPUT,TAPE5=INPUT,TAPE6=OUTPUT,TAPE8,TAPE9)
110 C   THIS CODE WILL CALCULATE AN AEROSOL MAP BASED ON NUCLEATION REGIMES
120 C DEFINITION OF VARIABLES
130 C SIGMA = SURFACE TENSION OF SPECIE (N/M)
140 C RHOL = LIQUID DENSITY OF SPECIE (KG/M**3)
150 C XMW = MOLECULAR WEIGHT OF SPECIE (KG/KGMOLE)
160 C TCSP = CRITICAL TEMPERATURE OF SPECIE (K)
170 C VCSP = CRITICAL VOLUME OF SPECIE (M**3/GMOLE)
180 C A,B,C ARE CONSTANTS IN THE VAPOR PRESSURE CORRELATION
190 C TWO FORMS ARE APPLICABLE EITHER PV = 10**(A - B/T) OR
200 C OR PV = EXP(A- B/T - C*LOG10(T)) WHERE T IS TEMPERATURE IN K.
210 C AO,BO AND CO ARE VAPOR PRESSURE CONSTANTS FOR CSI SINCE THE
220 C CORRELATION IS   BROKEN INTO TWO REGIONS DEPENDING ON THE TEMPERATURE
230 C IF A SPLIT CORRELATION IS NOT USED THEN ENTER ZEROES FOR THESE VALUES
240 C XH2O AND XH2 = MOLE FRACTIONS OF STEAM AND HYDROGEN RESPECTIVELY
250 C PTOT = TOTAL PRESSURE (ATM)
260 C DP = MONODISPERSE AEROSOL SIZE (M)
270 C XNDP = NUMBER OF PARTICLES PER UNIT VOLUME OF SIZE DP
280 C VOL = VOLUME OF INTEREST (M**3)
290 C XNIONS = NUMBER OF IONS PER VOLUME (IONS/M**3)
300           READ (8,11) SIGMA,RHOL,XMW
310           READ (8,12) TCSP,VCSP
320           READ (8,11) A,B,C
330           READ (8,11) AO,BO,CO
340           READ (8,11) XH2O,XH2,PTOT
350           READ (8,11) DP,XNDP,VOL
360           READ (8,13) XNIONS
370  11       FORMAT (2X,3(2X,E10.3))
380  12       FORMAT (2X,2(2X,E10.3))
390  13       FORMAT (4X,E10.3)
400 C
410 C ECHO INPUT
420 C
430           WRITE (9,11) SIGMA,RHOL,XMW
440           WRITE (9,12) TCSP,VCSP
450           WRITE (9,11) A,B,C
460           WRITE (9,11) AO,BO,CO
470           WRITE (9,11) XH2O,XH2,PTOT
480           WRITE (9,11) DP,XNDP,VOL
490           WRITE (9,13) XNIONS
500           JEND= 14
510 C SET INITIAL TEMPERATURE TO 600 K AND LOOP OVER
520 C TEMPERATURE UNTIL 200 K IS REACHED (NOTE LOOP IN 100 K INCREMENTS)
530           T = 600
540           DO 10 J= 1,JEND
550               T = T + 100
560 C
570 C INPUT FROM TERMINAL THE UPPER AND LOWER BOUNDS FOR THE HOMOGENEOUS
580 C BORDER ROOT SEARCH
590               WRITE (6,99)
600  99           FORMAT(2X,"INPUT YOUR GUESS OF THE ENDPOINTS OF THE
610      +  HOMOGENEOUS S INTERVAL")
620               READ (5,*) SL,SR
630               SL1=SL
640               SR1=SR
650 C
660 C FIND THE UPPER HOMOGENEOUS BORDER
670 C
680 C UPPER MULTIPLIER IS SET TO 50
```

```
690               XMUL = 50
700               CALL HMBORD(SIGMA,RHOL,XMW,TCSP,VCSP,A,B,C,AO,BO,CO,
710      +                XH2O,XH2,PTOT,DP,XNDP,VOL,XMUL,SL,SR,T)
720 C
730 C FIND THE LOWER HOMOGENEOUS BORDER
740 C
750 C LOWER MULTIPLIER IS SET TO 1/50 TH
760               XMUL = 0.02
770               SL=SL1
780               SR = SR1
790               CALL HMBORD(SIGMA,RHOL,XMW,TCSP,VCSP,A,B,C,AO,BO,CO,
800      +                XH2O,XH2,PTOT,DP,XNDP,VOL,XMUL,SL,SR,T)
810 C
820 C INPUT FROM TERMINAL THE UPPER AND LOWER BOUNDS FOR THE ION BORDER
830 C ROOT SEARCH
840               WRITE (6,47)
850  47           FORMAT(2X,"INPUT YOUR GUESS OF THE ENDPOINTS OF THE
860      +  ION S INTERVAL")
870               READ (5,*) SL,SR
880               SL1=SL
890               SR1=SR
900 C
910 C FIND THE LOWER ION BORDER
920 C
930 C SET LOWER MULTIPLIER TO 1/10 TH
940               XMUL = 0.1
950               CALL IONBORD(SIGMA,RHOL,XMW,TCSP,VCSP,A,B,C,AO,BO,CO,
960      +                XH2O,XH2,PTOT,DP,XNDP,VOL,XMUL,XNIONS,SL,SR,T)
970 C
980 C FIND UPPER ION BORDER
990 C
1000 C SET UPPER MULTIPLIER TO 50
1010              XMUL = 50.
1020              SL=SL1
1030              SR = SR1
1040              CALL IONBORD(SIGMA,RHOL,XMW,TCSP,VCSP,A,B,C,AO,BO,CO,
1050     +                XH2O,XH2,PTOT,DP,XNDP,VOL,XMUL,XNIONS,SL,SR,T)
1060 C
1070 C
1080  10      CONTINUE
1090          STOP
1100          END
1110 C
1120 C
1130          SUBROUTINE HMBORD (SIGMA,RHOL,XMW,TCSP,VCSP,A,B,C,AO,BO,CO,
1140     +         XH2O,XH2,PTOT,DP,XNDP,VOL,XMUL,SL,SR,T)
1150 C
1160 C THIS SUBROUTINE DETERMINE THE HOMOGENEOUS/HETEROGENEOUS NUCLEATION
1170 C BORDER USING AN INTERVAL SEARCH METHOD
1180          KOUNT = 0
1190  29      S1 = SL
1200          S3 = SR
1210          S2 = 0.5*(S3 + S1)
1220  111     PV = PPV(A,B,C,AO,BO,CO,T)
1230 C
1240          CALL HMNUC(SIGMA,RHOL,VOL,XMW,PV,T,S1,XJHMG,RSTAR,XMHMG)
1250          CALL HETERO(SIGMA,RHOL,VOL,XMW,PV,S1,T,XH2,XH2O,PTOT,
1260     +       DP,XNDP,TCSP,VCSP,XJHETER)
1270          Z1= AERO(XJHETER,XMHMG,XMUL)
1280 C
```

```
C
      CALL HMNUC(SIGMA,RHOL,VOL,XMW,PV,T,S2,XJHMG,RSTAR,XMHMG)
      CALL HETERO(SIGMA,RHOL,VOL,XMW,PV,S2,T,XH2,XH2O,PTOT,
     +     DP,XNDP,TCSP,VCSP,XJHETER)
      Z2 = AERO(XJHETER,XMHMG,XMUL)
C
C
      CALL HMNUC(SIGMA,RHOL,VOL,XMW,PV,T,S3,XJHMG,RSTAR,XMHMG)
      CALL HETERO(SIGMA,RHOL,VOL,XMW,PV,S3,T,XH2,XH2O,PTOT,
     +     DP,XNDP,TCSP,VCSP,XJHETER)
      Z3 = AERO(XJHETER,XMHMG,XMUL)
C
C
      TEST = (S3-S1)/S3
      IF ((Z1 .GT. 0.0) .AND. (Z3 .GT. 0.0)) GO TO 200
      IF ((Z1 .LT. 0.0) .AND. (Z3 .LT. 0.0)) GO TO 200
      IF (ABS(TEST) .LT. 0.001) GO TO 235
C
      IF ((Z1 .GT. 0.0) .AND. (Z3 .LT. 0.0)) THEN
         IF (Z2 .GT. 0.0) THEN
            S1=S2
            S2=0.5*(S1+S3)
         ELSE
            S3=S2
            S2=0.5*(S3+S1)
         ENDIF
         GO TO 111
      ENDIF
C
      IF ((Z1 .LT. 0.0) .AND. (Z3 .GT. 0.0)) THEN
        IF (Z2 .GT. 0.0) THEN
         S3=S2
         S2= 0.5*(S1+S3)
        ELSE
         S1=S2
         S2 = 0.5*(S1+S3)
        ENDIF
        GO TO 111
      ENDIF
C
C
 200  SL = SL/2
      SR = SR*2
      IF (KOUNT .EQ. 5) STOP
      WRITE(9,66) SL,SR
 66   FORMAT(2X,"NEW INTERVAL NEEDED IN HOMOGENEOUS SEARCH",2E10.3)
      GO TO 29
 235  IF (XMUL .EQ. 0.02) THEN
          WRITE (9,77) S2,T
      ELSE
          WRITE (9,78) S2,T
      ENDIF
 77   FORMAT (2X,"POINT ON UPPER HOMOGENEOUS BORDER (S,T)="
     +     ,2E10.4)
 78   FORMAT (2X,"POINT ON LOWER HOMOGENEOUS BORDER (S,T)="
     +     ,2E10.4)
      RETURN
      END
C
      FUNCTION AERO(X,Y,XMUL)
```

```
      REAL X,Y,XMUL
      AERO= X - XMUL*Y
      RETURN
      END
C
      SUBROUTINE IONBORD(SIGMA,RHOL,XMW,TCSP,VCSP,A,B,C,AO,BO,CO,
     +     XH2O,XH2,PTOT,DP,XNDP,VOL,XMUL,XNIONS,SL,SR,T)
C THIS SUBROUTINE CALCULATES THE ION/HETEROGENEOUS NUCLEATION BORDER
C USING AN INTERVAL SEARCH METHOD
 29   S1 = SL
      S3 = SR
      S2 = 0.5*(S3 + S1)
 111  PV = PPV(A,B,C,AO,BO,CO,T)
C
C
      CALL IONNUC(SIGMA,RHOL,VOL,XMW,PV,T,S1,XNIONS,XJION,RK,RA,XMION)
      CALL HETERO(SIGMA,RHOL,VOL,XMW,PV,S1,T,XH2,XH2O,PTOT,
     +     DP,XNDP,TCSP,VCSP,XJHETER)
      Z1 = AERO(XJHETER,XMION,XMUL)
C
C
      CALL IONNUC(SIGMA,RHOL,VOL,XMW,PV,T,S2,XNIONS,XJION,RK,RA,XMION)
      CALL HETERO(SIGMA,RHOL,VOL,XMW,PV,S2,T,XH2,XH2O,PTOT,
     +     DP,XNDP,TCSP,VCSP,XJHETER)
      Z2 = AERO(XJHETER,XMION,XMUL)
C
C
      CALL IONNUC(SIGMA,RHOL,VOL,XMW,PV,T,S3,XNIONS,XJION,RK,RA,XMION)
      CALL HETERO(SIGMA,RHOL,VOL,XMW,PV,S3,T,XH2,XH2O,PTOT,
     +     DP,XNDP,TCSP,VCSP,XJHETER)
      Z3 = AERO(XJHETER,XMION,XMUL)
C
C
      TEST = (S3-S1)/S3
      IF ((Z1 .GT. 0.0) .AND. (Z3 .GT. 0.0)) GO TO 200
      IF ((Z1 .LT. 0.0) .AND. (Z3 .LT. 0.0)) GO TO 200
      IF (ABS(TEST) .LT. 0.001) GO TO 235
C
      IF ((Z1 .GT. 0.0) .AND. (Z3 .LT. 0.0)) THEN
         IF (Z2 .GT. 0.0) THEN
            S1=S2
            S2=0.5*(S1+S3)
         ELSE
            S3=S2
            S2=0.5*(S3+S1)
         ENDIF
         GO TO 111
      ENDIF
C
      IF ((Z1 .LT. 0.0) .AND. (Z3 .GT. 0.0)) THEN
        IF (Z2 .GT. 0.0) THEN
          S3=S2
          S2= 0.5*(S1+S3)
        ELSE
          S1=S2
          S2 = 0.5*(S1+S3)
        ENDIF
        GO TO 111
      ENDIF
C
```

```
2490 C
2500 C
2510  200     SL = SL/2
2520          SR = SR*2
2530          GO TO 29
2540  235     IF (XMUL .EQ. 0.02) THEN
2550              WRITE (9,77) S2,T
2560          ELSE
2570              WRITE (9,78) S2,T
2580          ENDIF
2590  77      FORMAT (2X,"POINT ON UPPER ION BORDER (S,T)="
2600     +         ,2E10.4)
2610  78      FORMAT (2X,"POINT ON LOWER ION BORDER (S,T)="
2620     +         ,2E10.4)
2630          RETURN
2640          END
2650 C
2660 C
2670          SUBROUTINE HETERO(SIGMA,RHOL,VOL,WTSP,PV,S,T,XH2,XH2O,
2680     +        PTOT,DP,XNDP,TCSP,VCSP,XJHETER)
2690 C THIS SUBROUTINE CALCULATES THE RATE OF HETEROGENEOUS NUCLEATION
2700 C USING FUCHS MODEL
2710                AVGD = 6.023E+26
2720                BOLTZ= 1.38E-23
2730                XLAMDA = GMFP(T,XH2,XH2O,PTOT)
2740                XKNUD = 2*XLAMDA/DP
2750                ETA = (1 +XKNUD)/(1 + 1.71*XKNUD + 1.33*(XKNUD**2.0))
2760                D = DIFF(T,XH2,XH2O,TCSP,VCSP,WTSP,PTOT)
2770                VM = WTSP/(RHOL*AVGD)
2780                XKELV = EXP(4*SIGMA*VM/(DP*BOLTZ*T))
2790                DELTA = 2*3.14159*DP*D*PV*ETA/(BOLTZ*T)
2800                CONV =XNDP*WTSP/AVGD
2810                XJHETER= DELTA*(S-XKELV)*CONV
2820          RETURN
2830          END
2840 C
2850 C
2860          FUNCTION DIFF(TCOOL,XH2,XH2O,TC,VC,WT,PTOT)
2870          REAL TCOOL,XH2,XH2O,TC,VC,WT,PTOT
2880 C THIS SUBROUTINE CALCULATES PSEUDO CRITICAL PROPERTIES OF THE
2890 C H2/H2O MIXTURE AND BINARY DIFFUSION COEFFICIENTS
2900          DATA WTH2,WTH2O/2.0,18.0/
2910          DATA TCH2,TCH2O,VCH2,VCH2O/33.3,637.38,65,56.7/
2920          IF (TC .EQ. 0.0) THEN
2930 C USE TRAPMELT FORMULATION FOR DIFFUSION COEFFICIENT IF CANNOT FIND
2940 C CRITICAL PROPERTIES OF THE SPECIES CONSIDERED
2950               PRES = PTOT*1.013E+05
2960              DIFF = 9.8E-05*(TCOOL**1.75)/PRES
2970              GO TO 20
2980          ENDIF
2990          TCM = TCH2*XH2 + TCH2O*XH2O
3000          VCM = VCH2*XH2 + VCH2O*XH2O
3010          WTM = WTH2*XH2 + WTH2O*XH2O
3020          SIGMA1 = (5/6.)*(VCM)**(1/3.0)
3030          SIGMA2 = (5/6.)*(VC)**(1/3.0)
3040          SIGMA = 0.5*(SIGMA1 + SIGMA2)
3050          EPK1 = 0.75*TCM
3060          EPK2 = 0.75*TC
3070          A1= 1.06036
3080          B1= 0.15610
```

```
3090          C= 0.193
3100          D= 0.47635
3110          E= 1.03587
3120          F=1.52996
3130          G= 1.76474
3140          H= 3.89411
3150          CONST= 1.85E-03
3160          EPK = SQRT(EPK1*EPK2)
3170          TSTAR=TCOOL/EPK
3180          OMEGA = A1/(TSTAR)**B1 + C*EXP(-D*TSTAR) +
3190         +  E*EXP(-F*TSTAR) + G*EXP(-H*TSTAR)
3200          XMMOL= SQRT((WTM + WT)/(WTM*WT))
3210          DENOM = PTOT*((SIGMA)**2.)*OMEGA
3220          ALPHA= CONST*(TCOOL**(1.5)*XMMOL)/DENOM
3230          DIFF=ALPHA*(1E-04)
3240   20     RETURN
3250          END
3260 C
3270 C
3280 C
3290 C
3300          FUNCTION  VISC(T,XH2,XH2O,WTH2,WTH2O)
3310          REAL T,XH2,XH2O,WTH2,WTH2O
3320 C THIS SUBROUTINE CALCULATES MIXTURE PROPERTIES (RHO,VISC)
3330 C WHICH ARE NEEDED IN FLUID CALCULATIONS
3340 C
3350          VISH2O= (0.407*T - 30.)*(1E-07)
3360          A2= 1.16145
3370          B2= 0.14874
3380          C= 0.52487
3390          D= 0.77320
3400          E= 2.16178
3410          F= 2.43787
3420          SIGMA= 2.827
3430          EPK= 59.7
3440          TSTAR=T/EPK
3450          OMEGA= A2/(TSTAR**B2) +C*EXP(-D*TSTAR) + E*EXP(-F*TSTAR)
3460          VISH2 = (2.6693E-05)*(SQRT(2.016*T))
3470          VISH2=VISH2/((SIGMA**2.)*OMEGA)
3480 C
3490          A21=1+(WTH2/WTH2O)**(0.5)
3500          B21= 1 +SQRT(VISH2/VISH2O)*((WTH2O/WTH2)**(0.25))
3510          PHI21= 0.354*(B21**2)/A21
3520 C
3530          A12= 1 +(WTH2O/WTH2)**(0.5)
3540          B12= 1 +SQRT(VISH2O/VISH2)*((WTH2/WTH2O)**(0.25))
3550          PHI12= 0.354*(B12**2.)/A12
3560          VISC= (VISH2O*XH2O)/(XH2O+XH2*PHI21)
3570         +  +(VISH2*XH2)/(XH2+ XH2O*PHI12)
3580          RETURN
3590          END
3600 C
3610 C
3620          FUNCTION RHOMIX(T,XH2,XH2O,WH2,WH2O,PTOT)
3630          REAL T,XH2,XH2O,WH2,WH2O,PTOT
3640          R=8314
3650          RHOMIX= PTOT*(XH2*WH2 + XH2O*WH2O)*1.013E+05/(R*T)
3660          RETURN
3670          END
3680 C
```

```
C
      FUNCTION GMFP(T,XH2,XH2O,PSYS)
      REAL T,XH2,XH2O,PSYS
      DATA WTH2,WTH2O/2.0,18.0/
      X = RHOMIX(T,XH2,XH2O,WTH2,WTH2O,PSYS)
      Y = VISC(T,XH2,XH2O,WTH2,WTH2O)
      GMFP = (Y/X)*(2.062E-02)*SQRT((WTH2*XH2 + WTH2O*XH2O)/T)
      RETURN
      END
      FUNCTION PPV(A,B,C,AO,BO,CO,T)
           IF (C .EQ. 0.0) THEN
               PPV = 10**(A - B/T)*(1.013E+05/760.)
           ELSE
               IF (T .LT. 886) THEN
                 PPV = EXP(A -B/T - C*LOG10(T))
               ELSE
                 PPV= EXP(AO - BO/T - CO*LOG10(T))
               ENDIF
           ENDIF
      RETURN
      END
C
C
      SUBROUTINE IONNUC(SIGMA,RHOL,VOL,XMW,PV,T,S,XNIONS,
     +    XJION,RK,RA,XMION)
C     THIS SUBROUTINE CALCULATES THE RATE OF AEROSOL NUCLEATION
C     DUE TO IONS
C
C     CONSTANTS NEEDED IN FREE ENERGY CALULATIONS
      BOLTZ=1.38E-23
      E = 1.602E-19
      XK= 8.99E+09
      PI= 3.14159
      AVGN= 6.023E+26
C
C
C
      XMATOM= XMW/AVGN
      VM=XMW/(RHOL*AVGN)
C
C
C     SET UP COEFFICIENTS OF DERIVATIVE OF FRE ENERGY EQUATION
C     TO FIND 2 POSITIVE ROOTS
C
      ALPHA = -BOLTZ*T*LOG(S)
      BETA = 2*SIGMA*VM
      GAMMA = (E**2.0)*XK*VM/(8*PI)
C
C START NEWTON'S METHOD TO FIND FIRST ROOT
C  GUESS FOR NEWTON'S METHOD
      GUESS = -BETA/ALPHA
C SET UP NEWTON'S METHOD
      ROOT1 = 0
      ROOT2 = 0
      IROOT = 1
      CALL NEWTON(ALPHA,BETA,GAMMA,GUESS,ROOT1,ROOT2,IROOT,ICHK)
      IF (ICHK .EQ. 0) THEN
        GUESS = ((0.25*(E**2.0)*XK/(PI*SIGMA))**(0.333))/2.0
        IROOT = 2
        CALL NEWTON(ALPHA,BETA,GAMMA,GUESS,ROOT1,ROOT2,IROOT,ICHK)
```

```
4290            IF (ICHK .EQ. 0) THEN
4300               GO TO 50
4310            ELSE
4320               WRITE(9,101)
4330               STOP
4340            ENDIF
4350          ELSE
4360            WRITE(9,100)
4370            WRITE(9,105) ALPHA,BETA,GAMMA,GUESS,ROOT1
4380            STOP
4390  100       FORMAT(2X,"CANNOT FIND FIRST ROOT")
4400  101       FORMAT(2X,"CANNOT FIND 2ND ROOT")
4410  105       FORMAT(2X,5(2X,E10.3))
4420          ENDIF
4430  50      IF (ROOT2 .GT. ROOT1) THEN
4440             RK=ROOT2
4450             RA=ROOT1
4460          ELSE
4470             RK=ROOT1
4480             RA=ROOT2
4490          ENDIF
4500 C   SET UP CONSTANTS TO DETERMINE FREE ENERGY AND ION NUCLEATION RATE
4510          AA = 4*PI*ALPHA/(3*VM)
4520          BB= 4*PI*SIGMA
4530          CC = 0.5*(E**2.0)*XK
4540          DG = DELTAG(RK,RA,AA,BB,CC)
4550          IF (DG .LT. 0.0) GO TO 97
4560          CONST1 = EXP(-DG/(BOLTZ*T))
4570          XGK= 4*PI*(RK**3.0)/(3*VM)
4580          CONST2 = 4*PI*(RK**2.0)*SIGMA - (E**2.0)*XK/RK
4590          IF (CONST2 .LT. 0.0) GO TO 97
4600          CONST2 = SQRT(CONST2/(9*PI*BOLTZ*T*(XGK**2.0)))
4610          CONST3 = 4*PI*(RK**2.0)/SQRT(2*PI*XMATOM)
4620          CONST4 = CONST1/SQRT(BOLTZ*T)
4630          XJION = S*XNIONS*PV*CONST2*CONST3*CONST4*VOL
4640          XMION = XJION*4*PI*((RK**3.0)-(RA**3.0))*RHOL/3
4650          IF (XJION .LT. 0.0)  XJION = 0.0
4660          GO TO 333
4670 97       XJION = 0.0
4680          XMION = 0.0
4690 333      RETURN
4700          END
4710 C
4720 C
4730          FUNCTION DGDR(A,B,C,R)
4740          REAL A,B,C,R
4750          DGDR= A + B/R - C/(R**4.0)
4760          RETURN
4770          END
4780 C
4790 C
4800          FUNCTION DGDRPR(B,C,R)
4810          REAL B,C,R
4820          DGDRPR = -B/(R**2.0) + 4*C/(R**5.0)
4830          RETURN
4840          END
4850 C
4860 C
4870          FUNCTION DGDR1(A,B,C,R,ROOT1)
4880          REAL A,B,C,R,ROOT1
```

```
4890          DGDR1 = DGDR(A,B,C,R)/(R - ROOT1)
4900          RETURN
4910          END
4920 C
4930 C
4940          FUNCTION DGDRPR1(B,C,R,ROOT1)
4950          REAL B,C,R,ROOT1
4960          DGDRPR1=DGDRPR(B,C,R)/(R - ROOT1)
4970          RETURN
4980          END
4990 C
5000 C
5010          FUNCTION DELTAG(RMAX,RMIN,A,B,C)
5020          REAL RMAX,RMIN,A,B,C
5030          DELTAG = A*((RMAX**3.0) - (RMIN**3.0)) + B*((RMAX**2.0) -
5040         +    (RMIN**2.0)) + C*((1/RMAX) - (1/RMIN))
5050          RETURN
5060          END
5070 C
5080 C
5090          SUBROUTINE NEWTON(A1,B1,C1,G,R1,R2,IROOT,ICHK)
5100          REAL A1,B1,C1,G,R1,R2,TEST,TEMP,TOL
5110          INTEGER ICHK,IROOT
5120 C        SOLUTION BY NEWTON'S METHOD
5130          TOL = 0.000001
5140          KOUNT = 0
5150   10     TEMP = G
5160          KOUNT = KOUNT + 1
5170          IF (IROOT .EQ. 1) THEN
5180            Z = DGDR(A1,B1,C1,G)/DGDRPR(B1,C1,G)
5190          ELSE
5200            Z = DGDR1(A1,B1,C1,G,R1)/DGDRPR1(B1,C1,G,R1)
5210          ENDIF
5220          G = G-Z
5230          TEST = (G - TEMP)/TEMP
5240          IF (KOUNT .GT. 50) GO TO 99
5250          IF (ABS(TEST) .GT. TOL) THEN
5260            GO TO 10
5270          ELSE
5280            IF (G .LT. 0.0) GO TO 99
5290            IF (IROOT .EQ. 1) THEN
5300              R1=G
5310            ELSE
5320              R2=G
5330            ENDIF
5340            ICHK= 0
5350            GO TO 199
5360          ENDIF
5370   99     ICHK= -999
5380   199    RETURN
5390          END
5400 C
5410 C
5420          SUBROUTINE HMNUC(SIGMA,RHOL,VOL,XMW,PV,T,S,XJHMG,RSTAR,XMHMG)
5430 C        THIS SUBROUTINE CALCULATES THE RATE OF HOMOGENEOUS
5440 C        NUCLEATION
5450          REAL SIGMA,RHOL,XMW,PV,T,S,XJHMG,RSTAR,XMHMG
5460 C        CONSTANTS  NEEDED IN THE CALCULATION
5470          BOLTZ= 1.38E-23
5480          R = 8.314E+03
```

```
5490        AVGN= 6.023E+26
5500        PI= 3.14159
5510        RV = R/XMW
5520        RSTAR = 2*SIGMA/(RHOL*RV*T*LOG(S))
5530        E = EXP(-4*PI*SIGMA*(RSTAR**2.0)/(3*BOLTZ*T))
5540        XMATOM= XMW/AVGN
5550        CONST1= SQRT(2*SIGMA*XMATOM/PI)
5560        CONST2= (PV/(BOLTZ*T))**2.0
5570        XJHMG= CONST2*CONST1*E*(S**2.0)*VOL/RHOL
5580        XMHMG = XJHMG*4*PI*(RSTAR**3.0)*RHOL/3
5590        RETURN
5600        END
```

100	6.5E-01	1.0E+04	1.12E+02
110	1.90E+03	2.17E+02	
120	7.99E+00	5.31E+03	0.00E+00
130	0.00E+00	0.00E+00	0.00E+00
140	5.00E-01	5.00E-01	6.80E+01
150	1.00E-08	3.18E+11	1.00E+00
160	1.00E+15		

```
100        .650E+00     .100E+05     .112E+03
110        .190E+04     .217E+03
120        .799E+01     .531E+04     .000E+00
130        .000E+00     .000E+00     .000E+00
140        .500E+00     .500E+00     .680E+02
150        .100E-07     .318E+12     .100E+01
160        .100E+16
170    POINT ON LOWER HOMOGENEOUS BORDER (S,T)=1414.734 700.000
180    POINT ON UPPER HOMOGENEOUS BORDER (S,T)=3622.314 700.000
190    POINT ON LOWER ION BORDER (S,T)= 236.975 700.000
200    POINT ON LOWER ION BORDER (S,T)= 175.793 700.000
210    POINT ON LOWER HOMOGENEOUS BORDER (S,T)= 353.784 800.000
220    POINT ON UPPER HOMOGENEOUS BORDER (S,T)= 757.959 800.000
230    POINT ON LOWER ION BORDER (S,T)= 114.124 800.000
240    POINT ON LOWER ION BORDER (S,T)=  86.218 800.000
250    POINT ON LOWER HOMOGENEOUS BORDER (S,T)= 130.273 900.000
260    NEW INTERVAL NEEDED IN HOMOGENEOUS SEARCH  .200E+02  .400E+03
270    POINT ON UPPER HOMOGENEOUS BORDER (S,T)= 244.604 900.000
280    POINT ON LOWER ION BORDER (S,T)=  64.752 900.000
290    POINT ON LOWER ION BORDER (S,T)=  49.738 900.000
300    POINT ON LOWER HOMOGENEOUS BORDER (S,T)=  61.660 1000.000
310    POINT ON UPPER HOMOGENEOUS BORDER (S,T)= 104.805 1000.000
320    POINT ON LOWER ION BORDER (S,T)=  41.228 1000.000
330    POINT ON LOWER ION BORDER (S,T)=  32.122 1000.000
340    POINT ON LOWER HOMOGENEOUS BORDER (S,T)=  34.639 1100.000
350    POINT ON UPPER HOMOGENEOUS BORDER (S,T)=  54.551 1100.000
360    POINT ON LOWER ION BORDER (S,T)=  28.510 1100.000
370    POINT ON LOWER ION BORDER (S,T)=  22.494 1100.000
380    POINT ON LOWER HOMOGENEOUS BORDER (S,T)=  21.980 1200.000
390    POINT ON UPPER HOMOGENEOUS BORDER (S,T)=  32.568 1200.000
400    POINT ON LOWER ION BORDER (S,T)=  20.993 1200.000
410    POINT ON LOWER ION BORDER (S,T)=  16.755 1200.000
420    POINT ON LOWER HOMOGENEOUS BORDER (S,T)=  15.238 1300.000
430    POINT ON UPPER HOMOGENEOUS BORDER (S,T)=  21.515 1300.000
440    POINT ON LOWER ION BORDER (S,T)=  16.210 1300.000
450    POINT ON LOWER ION BORDER (S,T)=  13.065 1300.000
460    POINT ON LOWER HOMOGENEOUS BORDER (S,T)=  11.294 1400.000
470    POINT ON UPPER HOMOGENEOUS BORDER (S,T)=  15.317 1400.000
480    POINT ON LOWER ION BORDER (S,T)=  12.998 1400.000
490    POINT ON LOWER ION BORDER (S,T)=  10.575 1400.000
500    POINT ON LOWER HOMOGENEOUS BORDER (S,T)=   8.808 1500.000
510    NEW INTERVAL NEEDED IN HOMOGENEOUS SEARCH  .200E+01  .200E+02
520    POINT ON UPPER HOMOGENEOUS BORDER (S,T)=  11.549 1500.000
530    POINT ON LOWER ION BORDER (S,T)=  10.738 1500.000
540    POINT ON LOWER ION BORDER (S,T)=   8.809 1500.000
550    POINT ON LOWER HOMOGENEOUS BORDER (S,T)=   7.139 1600.000
560    POINT ON UPPER HOMOGENEOUS BORDER (S,T)=   9.116 1600.000
570    POINT ON LOWER ION BORDER (S,T)=   9.086 1600.000
580    POINT ON LOWER ION BORDER (S,T)=   7.520 1600.000
590    POINT ON LOWER HOMOGENEOUS BORDER (S,T)=   5.974 1700.000
600    POINT ON UPPER HOMOGENEOUS BORDER (S,T)=   7.451 1700.000
610    POINT ON LOWER ION BORDER (S,T)=   7.843 1700.000
620    POINT ON LOWER ION BORDER (S,T)=   6.539 1700.000
630    POINT ON LOWER HOMOGENEOUS BORDER (S,T)=   5.129 1800.000
640    POINT ON UPPER HOMOGENEOUS BORDER (S,T)=   6.267 1800.000
650    POINT ON LOWER ION BORDER (S,T)=   6.891 1800.000
660    POINT ON LOWER ION BORDER (S,T)=   5.782 1800.000
670    POINT ON LOWER HOMOGENEOUS BORDER (S,T)=   4.490 1900.000
680    POINT ON UPPER HOMOGENEOUS BORDER (S,T)=   5.393 1900.000
```

```
690    POINT ON LOWER ION BORDER (S,T)=    6.134 1900.000
700    POINT ON LOWER ION BORDER (S,T)=    5.180 1900.000
710    POINT ON LOWER HOMOGENEOUS BORDER (S,T)=    4.002 2000.000
720    POINT ON UPPER HOMOGENEOUS BORDER (S,T)=    4.732 2000.000
730    POINT ON LOWER ION BORDER (S,T)=    5.526 2000.000
740    POINT ON LOWER ION BORDER (S,T)=    4.694 2000.000
```

APPENDIX F

RESULTS FROM THE AEROSOL MONITOR CALIBRATION

A series of post-test calibrations of the aerosol monitor were performed using a polydisperse aerosol to obtain particle number concentrations from the transmission data gathered during the SFD 1-4 experiment. This appendix will discuss the results of these calibrations and the effect that uncertainty has on the predicted number concentrations.

Experimental calibrations were obtained by measuring the light attenuation from three known polydisperse lognormal aerosol distributions with mass mean diameters of 0.5, 1.0 and 2.0 microns respectively. Details of the method used to generate these aerosols are given in Reference F.1. The results of these calibrations for both the 4-cm and 1-cm path length instruments are shown in Figures F.1 and F.2. These plots were digitized and the results were fit to a seventh degree polynomial to reproduce the exact shape of the calibration curves. The seventh degree polynomial has no theoretical basis; it is used purely for mathematical ease. Hence,

Figure F.1

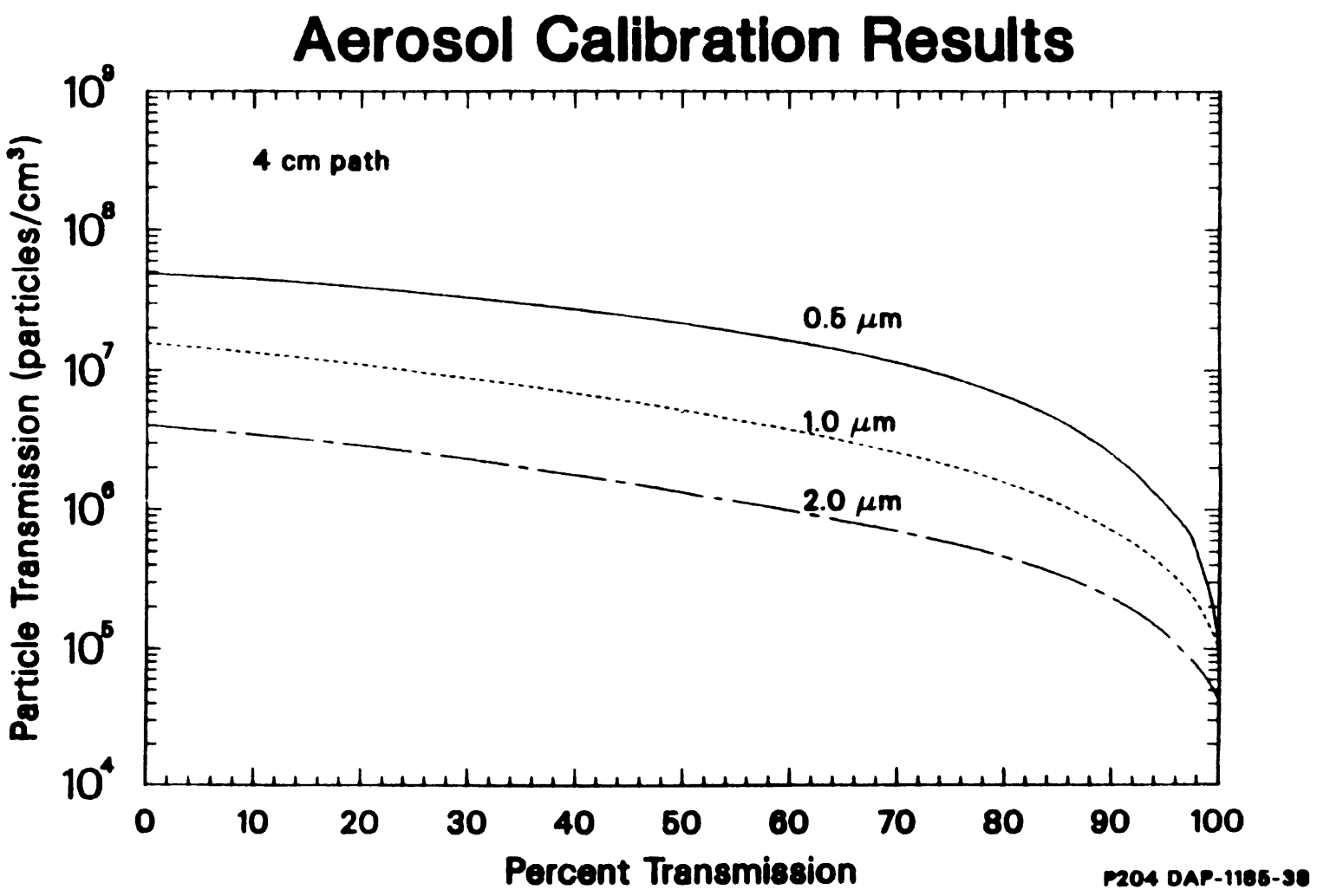
Aerosol Calibration Results
4 cm path
0.5 μm
1.0 μm
2.0 μm
Particle Transmission (particles/cm³)
10⁹
10⁸
10⁷
10⁶
10⁵
10⁴
0
10
20
30
40
50
60
70
80
90
100
Percent Transmission
P204 DAP-1185-38

Figure F.2

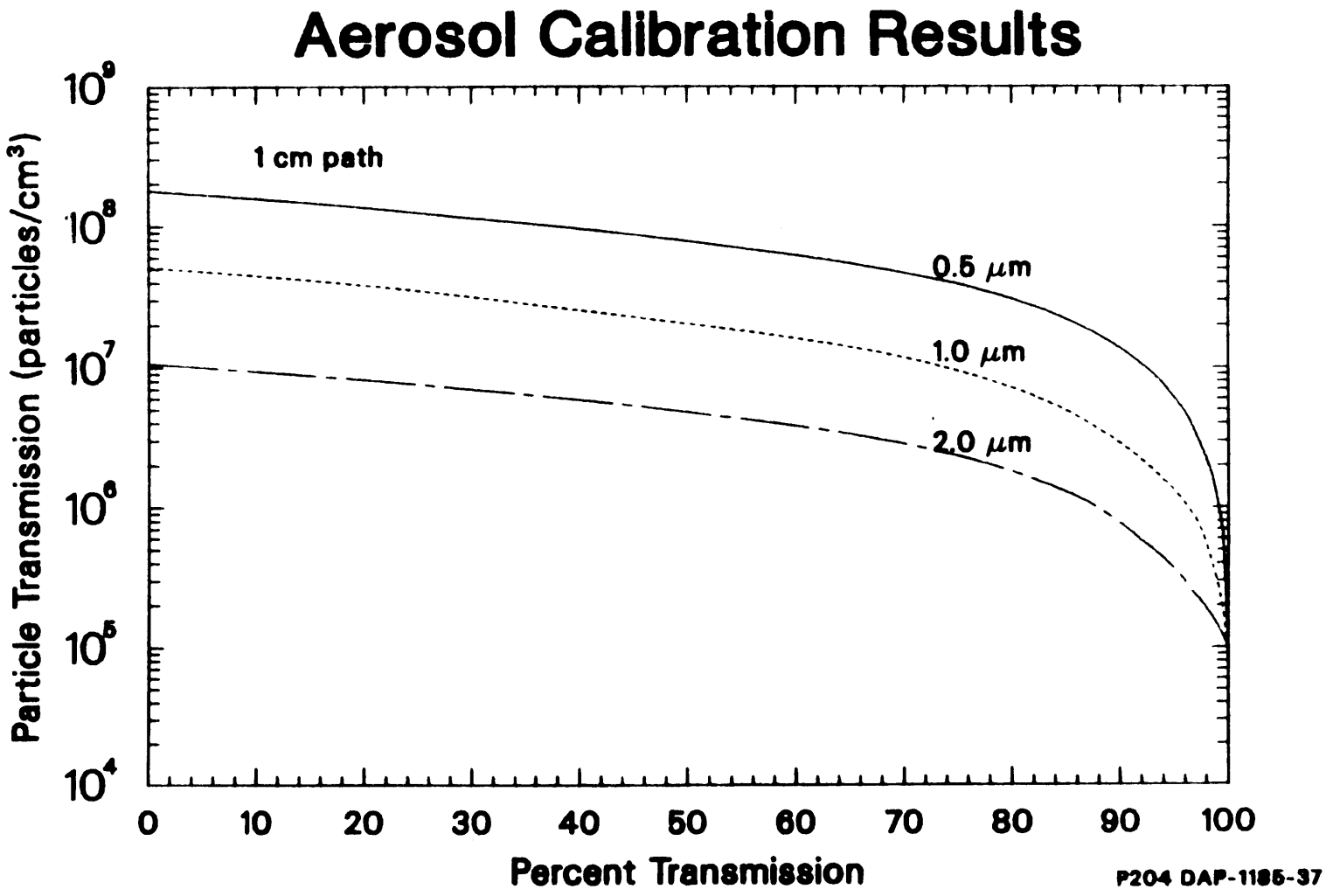
Aerosol Calibration Results
1 cm path
0.5 μm
1.0 μm
2.0 μm
Particle Transmission (particles/cm³)
10⁹
10⁸
10⁷
10⁶
10⁵
10⁴
0
10
20
30
40
50
60
70
80
90
100
Percent Transmission
P204 DAP-1185-37

$$N = a_0 + \sum_i a_i T^i \qquad (F.1)$$

where

N = particle number concentration (particles/cc),

T = measured transmission, and

a_i = fit coeffients.

Values of the fit coefficients are found in Table F.1. Equation (F.1) was used to transform the time dependent transmission data for each instrument into the corresponding number concentrations.

Most of the detail evident in the transmission results (Figures F.3 and F.4) is reproduced in the number concentration predictions shown in Figures F.5 and F.6. However, the non-linear calibration transforms the shape of the original transmission signal. Prior to 1712 seconds, noise caused the aerosol signals to oscillate about 100% transmission indicating that no aerosols were present. This noise was amplified by the conversion to particle number concentration. The amplification is a result of the steep slope in the calibration curve at high transmission percentages. Small changes in the transmission near the 100% level result in large changes in number concentration. Conversely, the sudden drop in aerosol signal between

TABLE F.1
FIT COEFFICIENTS FOR THE AEROSOL CALIBRATION

1 cm path

	0.5 μm	1.0 μm	2.0 μm
a_0	1.911655322e+01[a]	1.783149013e+01	1.618777138e+01
a_1	-9.302690292e-02	-6.547148962e-02	-1.684450546e-02
a_2	1.261712958e-02	8.150866553e-03	7.664469563e-04
a_3	-8.024257348e-04	-5.159145717e-04	-5.599014658e-05
a_4	2.474317285e-05	1.566278372e-05	1.826387617e-06
a_5	-3.957966273e-07	-2.466469613e-07	-3.133223992e-08
a_6	3.155883507e-09	1.940964584e-09	2.720934602e-10
a_7	-9.927869920e-12	-6.055426011e-12	-9.600734414e-13

2 cm path

	0.5 μm	1.0 μm	2.0 μm
a_0	1.776091029e+01	1.658327241e+01	1.522315896e+01
a_1	-4.598902890e-02	-2.939715663e-02	-2.693124946e-02
a_2	5.843491460e-03	2.209108739e-03	1.902870287e-03
a_3	-3.824762735e-04	-1.527027433e-04	-1.285873619e-04
a_4	1.185946904e-05	4.813234921e-06	3.907191531e-06
a_5	-1.905910155e-07	-7.860105095e-08	-6.234663733e-08
a_6	1.527671913e-09	6.410030411e-10	5.049858582e-10
a_7	-4.848041664e-12	-2.076773808e-12	-1.644931937e-12

a. means 1.1911655322×10^1

Figure F.3

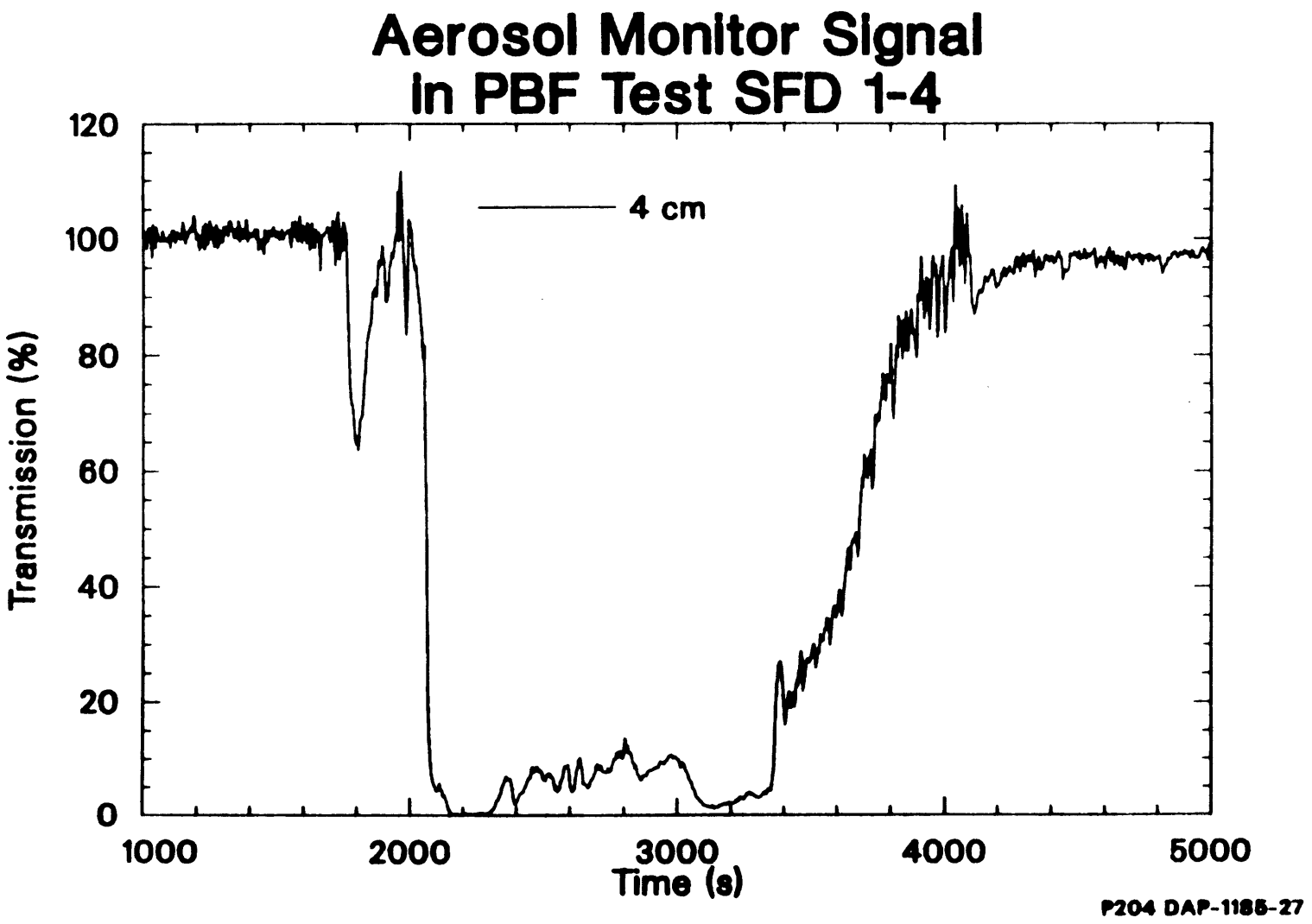
Aerosol Monitor Signal
In PBF Test SFD 1-4
4 cm
Transmission (%)
120
100
80
60
40
20
0
1000
2000
3000
4000
5000
Time (s)
P204 DAP-1185-27

Figure F.4

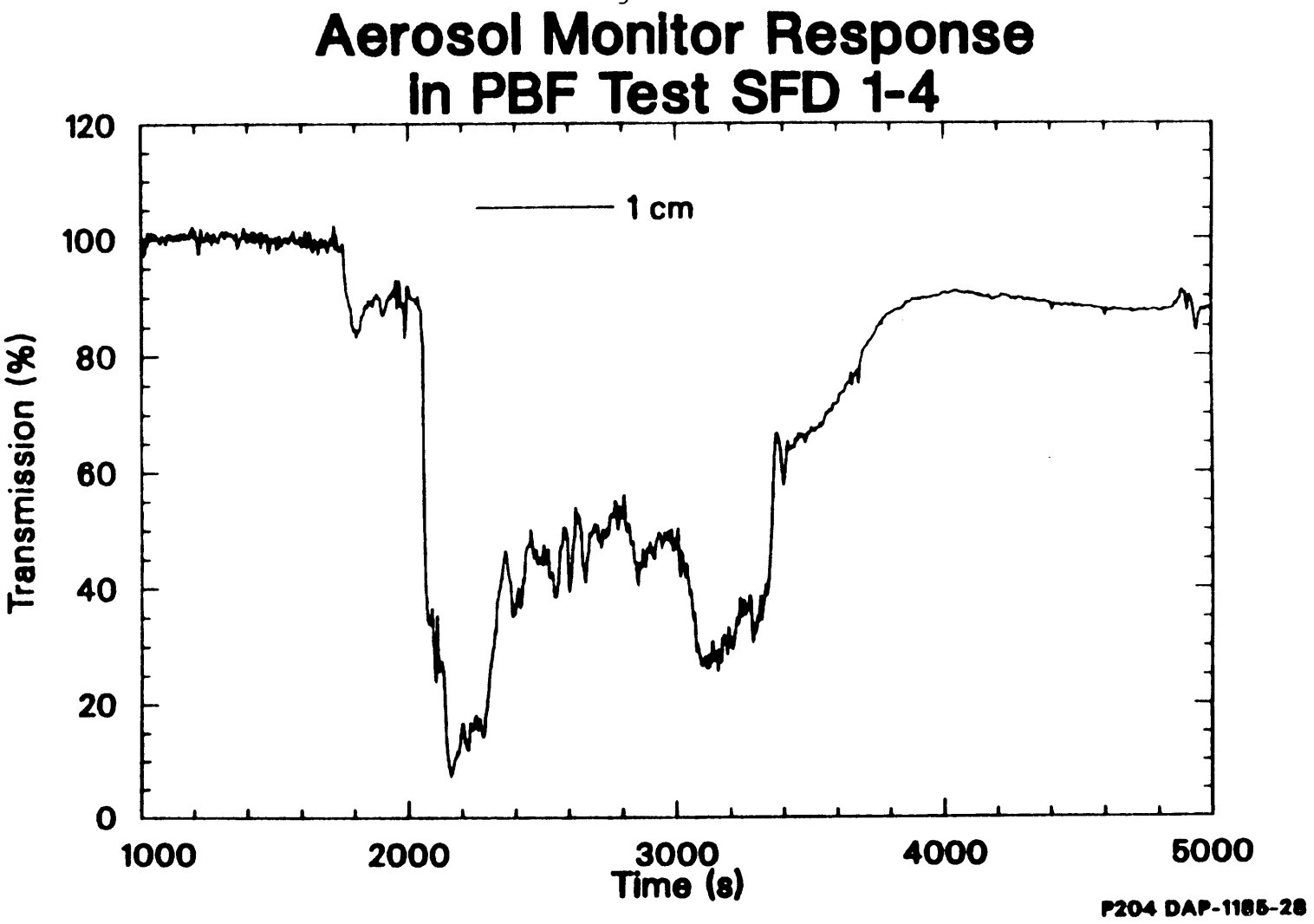
Aerosol Monitor Response
In PBF Test SFD 1-4
1 cm
Transmission (%)
120
100
80
60
40
20
0
1000
2000
3000
4000
5000
Time (s)
P204 DAP-1185-28

Figure F.5

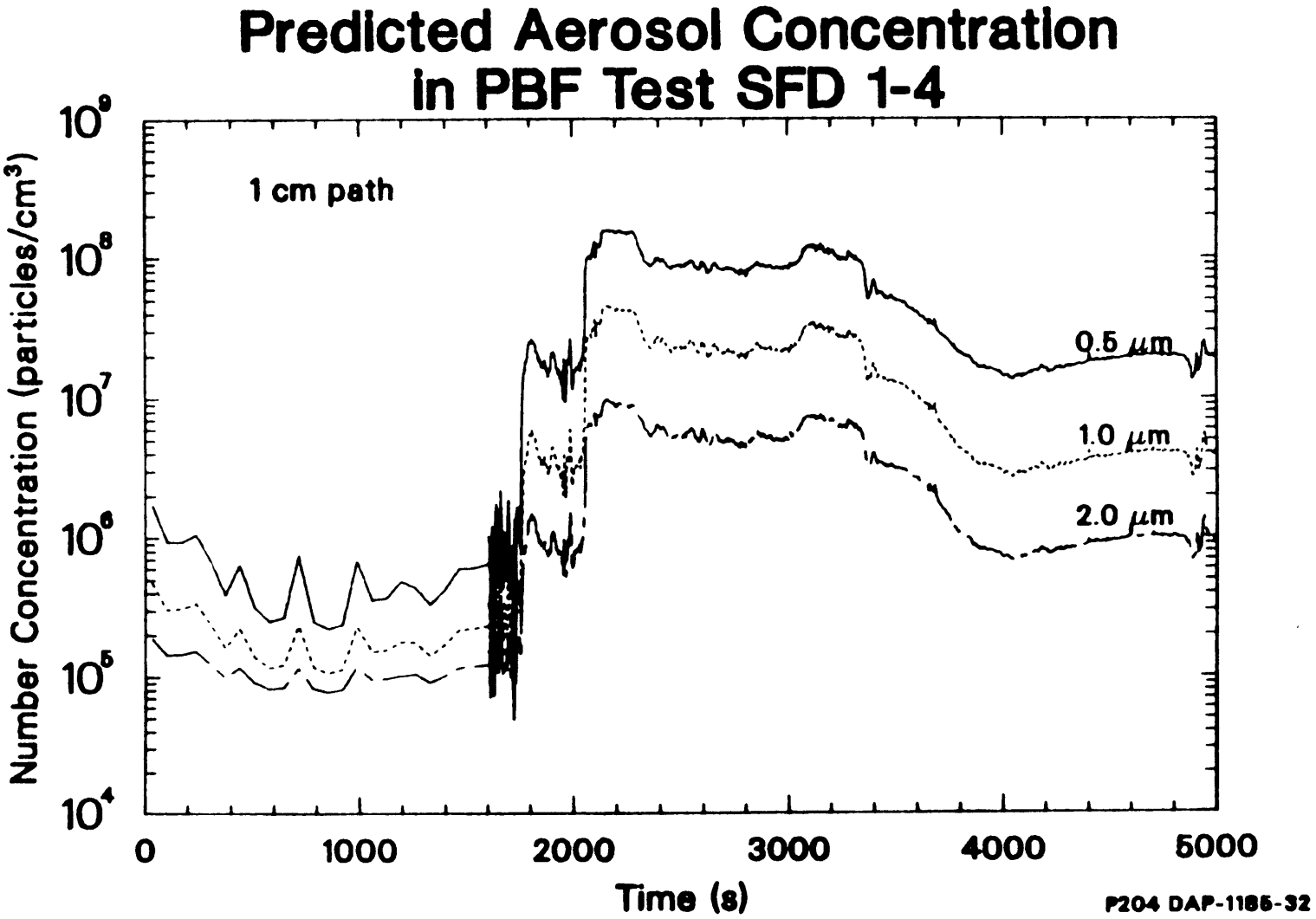
Predicted Aerosol Concentration
in PBF Test SFD 1-4
1 cm path
0.5 μm
1.0 μm
2.0 μm
Number Concentration (particles/cm³)
10⁹
10⁸
10⁷
10⁶
10⁵
10⁴
0
1000
2000
3000
4000
5000
Time (s)
P204 DAP-1185-32

Figure F.6

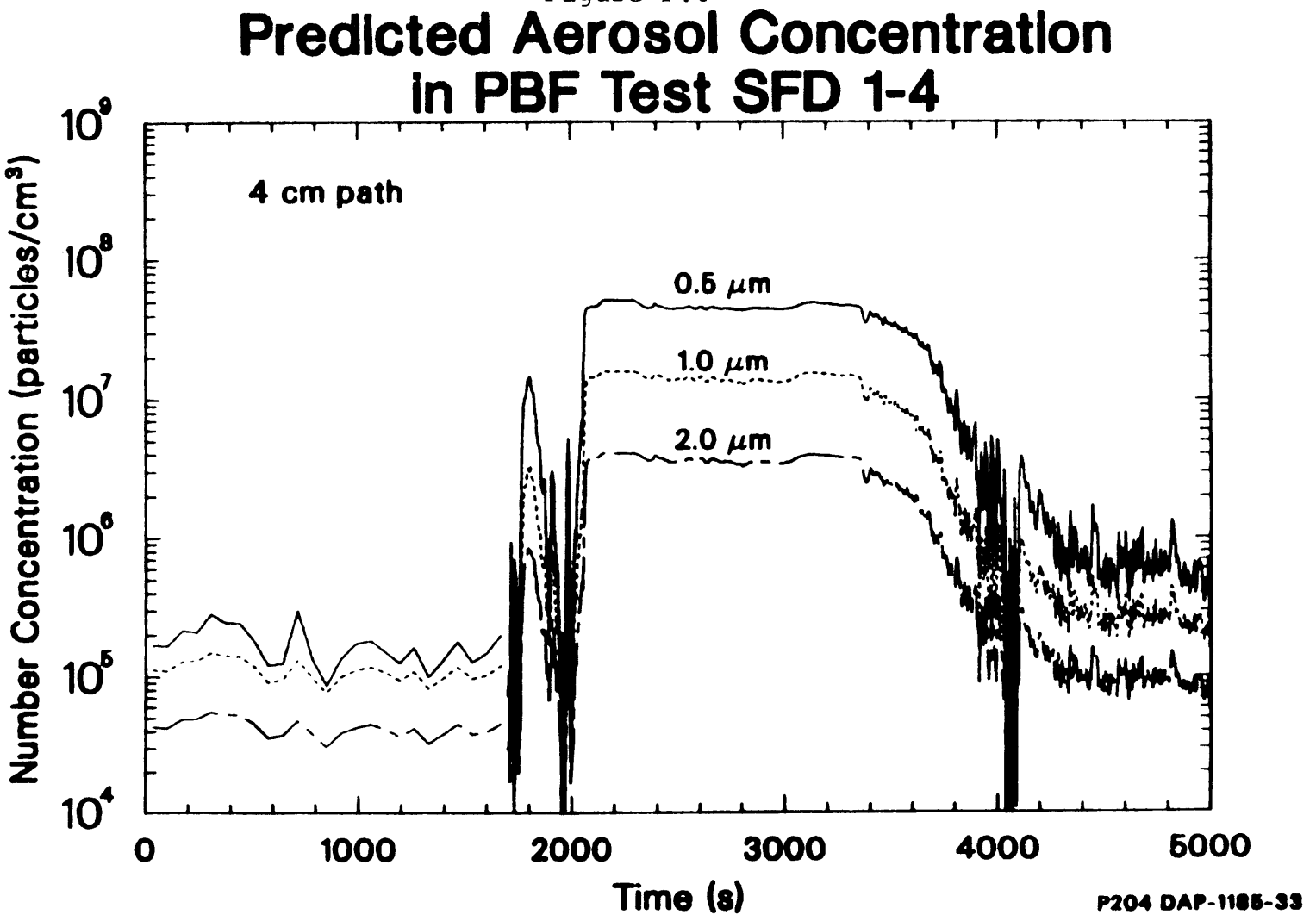
Predicted Aerosol Concentration
in PBF Test SFD 1-4
4 cm path
0.5 μm
1.0 μm
2.0 μm
Number Concentration (particles/cm³)
10⁹
10⁸
10⁷
10⁶
10⁵
10⁴
0
1000
2000
3000
4000
5000
Time (s)
P204 DAP-1185-33

2400 and 3000 seconds is less pronounced when the data is converted to number concentration due to the more gradual change in slope at low transmissions.

Examination of both the particle number concentration curves and the calibration plots indicate that the predicted number concentration is very sensitive to particle size. Except at very low aerosol concentrations, a factor of 4 difference in particle size from 0.5 to 2.0 microns results in a factor of 50 change in number concentration. As a result, an accurate estimate of the particle size is required to have confidence about the predicted number concentration.

Due to the preliminary nature of the transmission data, a formal uncertainty analysis has not been performed. However, an attempt has been made to determine the effect that uncertainty in the transmission signal has on the predicted number concentrations. The transmission data from the 1-cm path length detector have been artifically reduced and increased by 25% to represent an uncertainty of $\pm$ 25%. The value of 25% is artibrary and is intended only to illustrate how uncertainty in the transmission data is propagated in the predicted number concentrations. The results are shown in Figure F.7. As seen in the figure,

Figure F.7

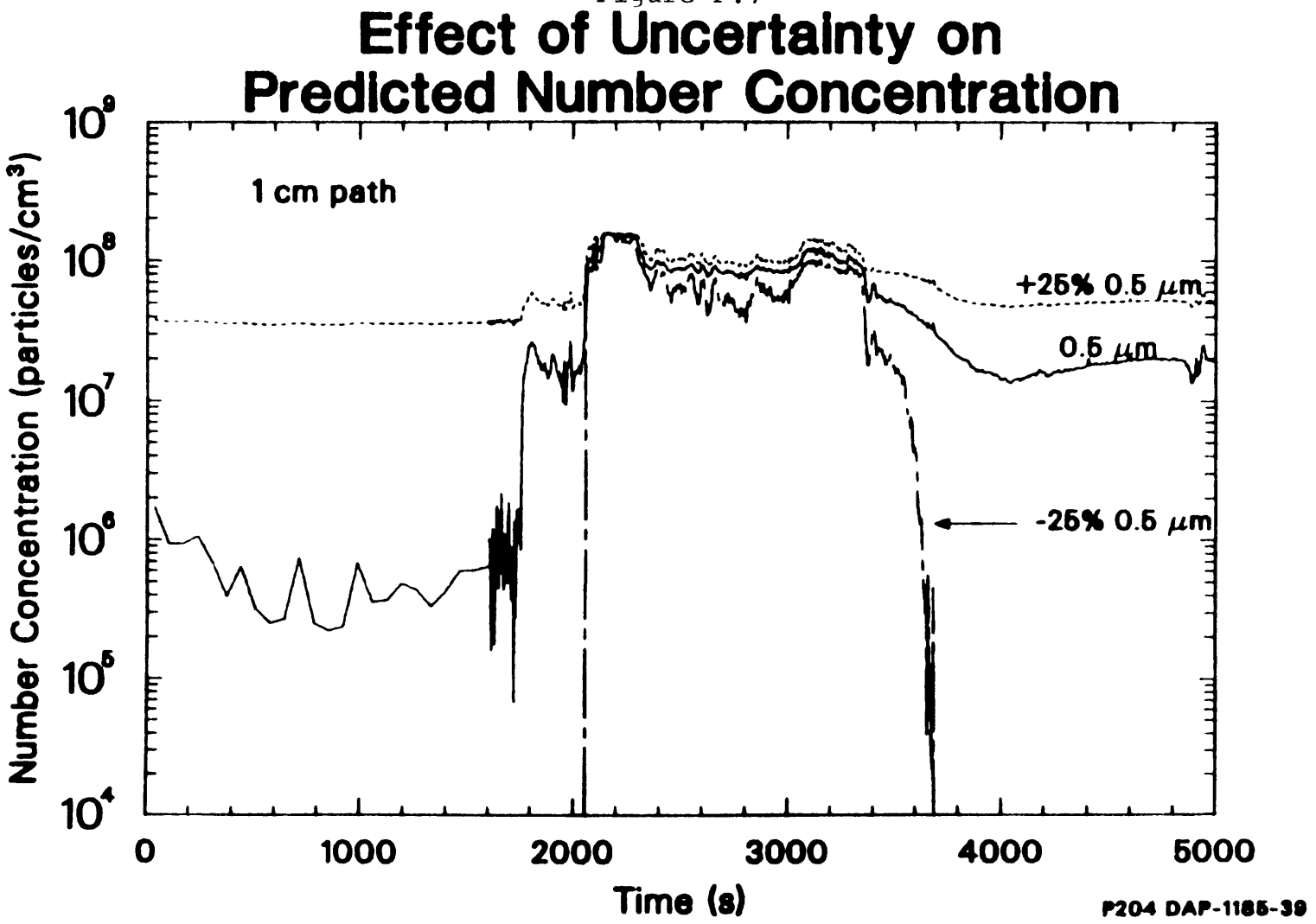
Effect of Uncertainty on
Predicted Number Concentration
1 cm path
+25% 0.5 μm
0.5 μm
-25% 0.5 μm
Number Concentration (particles/cm³)
10⁹
10⁸
10⁷
10⁶
10⁵
10⁴
0
1000
2000
3000
4000
5000
Time (s)
P204 DAP-1185-39

between 2200 and 3500 seconds when light transmissions are low, a 25% uncertainty has a neglible effect on the predicted particle concentration. However, before 2200 seconds and after 3500 seconds, when light transmission is moderate to high, number concentrations are much more sensitive to the change. This behavior can be attributed to the measurement scale of the instrument and once again to the slope of the calibration curve. A 25% uncertainty at 100% transmission corresponds to a range of transmissions between 75 and 125% whereas, at 1% transmission, the same error covers the range between 0.75 and 1.25%. Since the slope of the calibration curve is very steep at high transmissions, the predicted number concentrations vary widely between 75% and 125%. However, at low transmissions, the signal is not very sensitive to uncertainty. The gradual slope of the calibration curve produces number concentrations between 0.75 and 1.25% that are similar in magnitude.

Based on this simple analysis, it is apparent that any effort to reduce the uncertainty in the measured signal at the peak of the transient when aerosol concentrations are high is not warranted. Instead, effort should be concentrated on trying to determine the size characteristics and composition of the aerosol produced during the SFD 1-4 experiment. Since the size

distribution of the aerosol is currently uncertain, the prediction of particle number concentration discussed in Section 8 is based on the results of the 0.5 micron calibration.

REFERENCES

F.1 Novick, V.J., "Light Extinction as a Function of Aerosol Number Concentration", EG&G Idaho letter from V.J. Novick to D.J. Osetek, VJN-01-85, July 8, 1985.